Investigating the mechanism of action of Deep Brain Stimulation using functional magnetic resonance imaging

Thesis submitted for the degree of Doctor of Philosophy

Joshua James Kahan

July 2014

UCL

Sobell Department for Motor Neuroscience and Movement Disorders,

UCL Institute of Neurology,

Queen Square, London

Email: joshua.kahan@ucl.ac.uk

1 Declaration

I, Joshua James Kahan, confirm that the work presented in this thesis is my own. Where information has been derived from other sources, I confirm that this has been indicated in the thesis.

Extracts of this thesis have been published in peer-reviewed journals. Articles include (Kahan and Foltynie, 2013; Kahan et al., 2014, 2012). Information about publications is included at the beginning of relevant chapters.

Signed: _____

Date: _____

2 Abstract

Depleted of dopamine, the dynamics of the Parkinsonian brain impact on both "action" and "resting" motor behaviour. Subthalamic nucleus deep brain stimulation (STN DBS) has become an established means of managing these symptoms, although its mechanisms of action remain unclear. Functional magnetic resonance imaging (fMRI) using the blood oxygen level dependent (BOLD) contrast provides the opportunity to study the human brain *in vivo*, collecting indirect measures of neural activity across the whole brain. To date, technical difficulties and safety concerns have precluded the use of fMRI in DBS patients. Previous work from this department has demonstrated that scanning patients with certain DBS systems and MRI equipment is both safe and feasible.

This thesis explores the neuromodulatory actions of STN DBS on both action and resting motor behaviours in patients with Parkinson's disease (PD) using fMRI. In brief, I present two fMRI studies conducted on STN DBS patients, one task-based, and one resting, collected under a previously approved protocol. I then present experiments exploring the safety of scanning DBS patients using an improved protocol, and then detail two further experiments collected under this new protocol, again one task-based, and one resting.

Specifically, I employ statistical parametric mapping to determine DBS-induced changes in motor evoked responses. Using dynamic causal modelling (DCM) and Bayesian model selection, I compare generative models of cortico-subcortical interactions to explain the observed data, inferring which connections DBS may be affecting, and which modulations predict efficacy. I proceed to use stochastic DCM to model the modulatory effects of DBS on endogenous (resting-state) dynamics.

This work casts DBS in terms of modulating effective connectivity within the cortico-basal ganglia motor loops. I discuss how this may explain its current usage in PD, as well as exploratory uses to treat other pathological brain states.

If you're dumb, surround yourself with smart people. If you're smart, surround yourself with smart people who disagree with you.
Isaac Jaffe in *Sports Night*, written by Aaron Sorkin, 1998.

3 Table of Contents

3.1 List of Tables

3.2 List of Figures

3.3 List of Abbreviations

1.5/3T 1.5/3 Tesla

ACC Anterior cingulate cortex

ACh Acetylcholine

BA Brodmann's area

BG Basal ganglia

BMA Bayesian model averaging

BMS Bayesian model selection

BOLD Blood oxygen level dependent

BPA Bayesian parameter averaging

BUA Background unit activity

DA Dopamine

DAT Dopamine transporter

DBS Deep brain stimulation

DCM Dynamic causal model/modelling

dHb Deoxyhaemoglobin

DLB Dementia with Lewy bodies

DLPFC Dorsolateral prefrontal cortex

DTI Diffusion tensor imaging

ECoG Electrocorticogram

EEG Electroencephalography

FEF Frontal eye fields

FFX Fixed effects assumptions

fMRI Functional MRI

FWE Family-wise error

FWHM Full width half maximum

GABA Gamma-aminobutyric acid

GE EPI Gradient-echo echo-planar

GCM Granger causality modelling

GLM General linear model

GPe Globus pallidus pars externa

GPi Globus pallidus pars interna

HFS High-frequency stimulation

HRF Haemodynamic response function

Hz Hertz

ICA Independent component analysis

IFG Inferior frontal gyrus

IPG Implantable pulse generator

LFP Local field potential

M1 Primary motor cortex

MDD Major Depressive Disorder

MEG Magnetoencephalography

MPTP 1-methyl-4-phenyl-1,2,3,6-tetrahydropyridine

MRI Magnetic resonance imaging

MSNs Medium spiny neurons (cf. SPNs)

MUA Multiple unit activity

NA Noradrenaline (norepinephrine)

NaN Not a number (no data recorded)

NBM Nucleus Basalis of Meynert

OCD Obsessive-compulsive disorder

OFC Orbitofrontal cortex

oHb Oxyhaemoglobin

OHDA 6-hydroxydopamine

PCA Principle component analysis

PD Parkinson's disease

PDD Parkinson's disease dementia

PET Positron emission tomography

PM Lateral premotor area

PPI Psychophysiological interaction

RFX Random effects assumptions

RF Radiofrequency

RSS Residual sum of squares

RT Reaction time

S1 Primary sensory cortex

SAR Specific absorption rate

SEM Structural equation modelling

SMA Supplementary motor area

SNc Substantia nigra pars compacta

SNr Substantia nigra pars reticulate

SNR Signal to noise ratio

SPECT Single photon emission computed tomography

SPNs Spiny projecting neurons (cf. MSNs)

STN Subthalamic nucleus

SVC Small volume corrected

TS Tourette's syndrome

UPDRS Unified Parkinson's Disease Rating Scale

V Volts

Vim Ventralis Intermedius

V_{max} Peak velocity

VOI Volume of interest

ZI Zona Incerta

4 Acknowledgements

Although it is my name that features on the spine of this thesis, this work would not have been possible without a number of people whom I would like to pay tribute to.

First and foremost, thanks must go to my primary supervisor Dr Tom Foltynie, who, for reasons unknown, put me in charge of a wonderful project that he had worked tirelessly to make happen. Luckily, we formed a good team; his pleasant optimism complemented my anxious pessimism nicely. He has been a first-class supervisor and mentor, and I cannot thank him enough for throwing me in the deep end.

Second thanks go to my secondary supervisors, Dr Laura Mancini and Professor Xavier Golay, who somehow translated quantum physics into idiot-proof language that I have (at times) understood. Thanks are also extended to Drs John Thornton, Mark White, Enrico De Vita and Anastasia Papadaki in the Physics team, as well as to Lisa Strykarchzuk and the radiographers for their help with data collection.

Thanks to my "unofficial" supervisor, Professor Karl Friston. Together with Dr Guillaume Flandin, Prof has withstood my unremitting, often specious questions, and I am incredibly grateful for his patience and sense of humour; even when I haven't understood, I've always been entertained. I am proud to say that I no longer have to record and playback conversations I have with him. At least not all the time.

Thanks to Professor Gordon Stewart, Sue Beesley and the UCL MB PhD programme, who have provided me with this unique opportunity, and to my funders, The Rosetrees Trust, The Astor Foundation and The MHMS General Charitable Trust for generously

supporting my work. Thanks also to The Brain Research Trust for funding a lot these experiments.

Thanks to Medtronic and St Jude Medical for providing DBS equipment for my *in vitro* experiments, and for funding travel to academic conferences. Neither company had any role in data collection, analysis or preparation of this work.

Finally, I must thank my wonderful colleagues at the Unit of Functional Neurosurgery at the National Hospital for Neurology and Neurosurgery. Firstly, to our surgeons Professor Marwan Hariz, Mr Ludvic Zrinzo and Mr Harith Akram. Secondly to Professor Patricia Limousin (the most famous person I know) and all the neurology fellows, particularly to Tom's other fellows, Drs Iciar Aviles-Olmos, Zinovia Kefalopoulou, James Gratwicke and Dilan Athauda, and to Professor Marjan Jahanshahi and the neuropsychology fellows. Thanks to Joseph Candelario and Catherine Milabo, our wonderful specialist nurses, Dr Elina Tripoliti and Tim Grover, as well as to Linda, Debbie and Siva.

I am indebted to the heroic patients who took part in this work. Their willingness to have their medication and DBS withdrawn, and be placed in a scanner should not be forgotten.

It goes without saying that I am forever indebted to my parents, grandparents and family for providing me with every opportunity I could have asked for. I can only hope that the *nachas*[1] that this generates has made the past 25 years worthwhile.

Oh, thanks also to Talya, my girlfriend at the time of writing[2].

---

[1] Nachas is a Yiddish word, roughly translating as pride in a relative's achievements. Nachas is typically manifest by bragging relentlessly to the person sitting next to you in Synagogue, or anywhere else that involves you being in close proximity to anyone who may not have heard of, or who may have forgotten about said relative.

[2] I know, I'm in so much trouble.

5 Introduction

> *Before concluding these pages, it may be proper to observe once more, that an important object proposed to be obtained by them is, the leading of the attention of those who humanely employ anatomical examination in detecting the causes and nature of diseases, particularly to this malady. By their benevolent labours its real nature may be ascertained, and appropriate modes of relief, or even of cure, pointed out.*
>
> James Parkinson, An essay on the Shaking Palsy, 1817.

Almost two centuries on from Parkinson's first description of the "shaking palsy", the causes and progression of Parkinson's disease (PD), as well as its treatments, are still being investigated. Deep brain stimulation (DBS) has become an established treatment for advanced PD, and may prove an efficacious therapy for a variety of other neurological and psychiatric diseases. This thesis explores the mechanism underlying the therapeutic effect of DBS, with the ultimate goal of improving the clinical efficacy, and reducing side effects of DBS therapies. Given the extensive evidence for the beneficial effects of subthalamic nucleus (STN) DBS in the treatment of advanced PD, this work specifically addresses STN DBS, which typically improves motor impairment and quality of life substantially.

This thesis details five experiments that were carried out over the past three years; two fMRI studies using a previously safety-tested scanning procedure, one set of experiments confirming the safety of an improved scanning procedure, and two further fMRI studies collected under the new procedure. The fMRI studies explore the physiological repercussions of therapeutic STN DBS in patients with advanced PD, either whilst performing voluntary movements, or whilst lying in the scanner with eyes closed ("at rest").

The findings are duly discussed, and conclusions drawn about the neuromodulatory effect of DBS.

This introduction is in five parts; Section 5.1 rehearses the fundamental principles of brain functional organisation and defines key concepts in neural architecture at the systems level. Section 5.2 discusses Parkinson's disease, the functional anatomy of the basal ganglia and the repercussions of dopamine depletion. Section 5.3 explores the local neuroanatomy and histology of the STN, the surgical procedure and the clinical evidence for STN DBS. Section 5.4 reviews the neural response to DBS, including an in depth review of the neuroimaging literature investigating STN DBS (5.4.2), providing a context for my experiments. Section 5.5 introduces the safety of MRI in patients with implanted DBS devices. I conclude outlining the aims of this body of work (5.6). Introductions to the methods used throughout this thesis are outlined in Chapter 6.

5.1 The functional architecture of the human brain

DBS is an invasive procedure involving the stereotactic placement of an electrode targeting a deep brain structure. Before elaborating on how DBS may be achieving its therapeutic effect, it is important to introduce the fundamental principles of the functional architecture supporting behaviour, which will ultimately frame subsequent questions and experiments.

Since the invention of phrenology by Franz Joseph Gall in the late 18th century, identifying brain regions with specific functions has become a central theme in neuroscience, and has arguably guided neuroimaging and 'brain mapping' over the past few decades. Centuries of scientific exploration have concluded that the functions cannot simply be localised to parts of the brain. Rather, the brain adheres to two fundamental and mutually dependable properties of functional organisation: (1) functional segregation, which states that the

cortical infrastructure supporting a behaviour or function involves multiple components that are specialised in processing task-relevant information, and are often spatially distributed; and (2) functional integration, which states that proper function is dependent upon optimal integration, or communication, of specialised components (Friston, 2011, 1994). The specialisation of a given cortical region is dictated by its functional connections, and vice versa, thus any disturbance in either the viability of a specialised brain region, or the brain's ability to integrate information, will lead to a disturbance of proper function. From a clinical perspective, this could produce signs, symptoms or a clinical phenotype. Early lesion studies and invasive electrical stimulation observations, as well as the more contemporary cartographic neuroimaging literature, has firmly established functional segregation as a principle of brain organisation. However, characterising functional integration, or *connectivity*, has proved more difficult to establish and assess.

5.1.1 Brain connectivity: Concepts and nomenclature

The 100 billion neurons that comprise the human brain do not work in isolation. Anatomically, these neurons form a relatively invariant structural architecture, upon which rests a dynamic, modular and hierarchical functional network, capable of the rich computations that underpin cognition.

The cerebral cortex is organized horizontally into six laminae, each containing characteristic cell types with typical projection patterns. The smallest proposed vertically organised unit, the minicolumn (or microcolumn), typically contains 80-100 neurons (more in the striate cortex). Macrocolumns (or modules) comprise 60-80 minicolumns bound by short-distance (intrinsic) horizontal connections, measuring 300-600 μm in diameter (i.e. 5-10 macrocolumns would be expected in a typical 3mm isotropic voxel). Additionally, intrinsic connections project vertically between laminae within a given macrocolumn. In contrast,

extrinsic connections project to distant macrocolumns either in other cortical areas from layers II/III, or subcortical structures from layers V/VI (Buxhoeveden and Casanova, 2002; Mountcastle, 1997).

The brain can be considered a large and densely connected network, composed of sub-networks, which are themselves comprised of many sub-modules that compute lower-level operations (Buckholtz and Meyer-Lindenberg, 2012; Park and Friston, 2013). This conceptual hierarchy can be extended down to the neural level. The function of a module to is to integrate the computations of its sub-modules. For example, the primary motor cortex (M1) can be considered a sub-module of the motor network, but is comprised of a multitude of cortical columns encoding both low- and high-level kinematic features (Georgopoulos et al., 1986; Sergio et al., 2005). Defining a connection (or *edge*) *in vivo* has traditionally been more complicated than defining a component (or *node*) of a network; nodes are generally simply defined by functional specialisation, i.e. if they show significant changes in activity with the onset of a task/stimulus.

It is thus important to establish a consistent nomenclature when referring to either different *types of connections*, or different *methods of characterising connectivity*. In this thesis, fMRI is the primary mode of data collection and the terms "extrinsic" and "intrinsic" connections are used in an anatomical sense; extrinsic connections are long range connections that connect two distant functional regions (e.g. neurons projecting from M1 to the putamen), usually mediated via white matter projections. In reality of course, each *functional region* is composed of a number of interconnected macrocolumns, which similarly project (to a greater or lesser extent) to a spatially segregated second functional region. Connections within a given *functional region* are referred to as intrinsic connections and are recurrent, and mediated by GABAergic neural populations conferring a self-inhibition, in line with

the known functional anatomy of the neocortex (Bastos et al., 2012; Douglas and Martin, 1991).

I will refer to three characterisations of connectivity that are commonly discussed in the neuroimaging literature:

1. **Structural connectivity** refers to the presence/abundance of physical extrinsic connections via white matter projections, usually inferred noninvasively using diffusion tensor imaging (DTI), which is unable to determine direction or differentiate excitatory or inhibitory connections. For this, some tracing techniques can be employed, but obviously are limited to post-mortem examination.
2. **Functional connectivity** refers broadly to any statistical dependency between the functional time series of distant nodes. This is most commonly, and most simply a correlation between the BOLD signal of two regions (Biswal et al., 1995) or the coherence within a specific frequency band at distant electroencephalography (EEG) sensors. As before, this form of connectivity is symmetrical, and is unable to identify excitatory or inhibitory connections; simply that the functional signature of two regions is correlated. With regard fMRI data, analyses of functional connectivity include seed-voxel correlations, independent component analyses (ICA) & principle component analyses (PCA). This is discussed further in 6.6. Psychophysiological interaction (PPI) analyses (Friston et al., 1997) are examples of context-dependent connectivity, which some regard as effective connectivity given they are regression-based. Others believe they fall somewhere in between functional and effective connectivity given PPIs can be conceptualised as context-dependent *correlations* between BOLD data at distant nodes.

3. **Effective connectivity** is defined as the influence one neural population exerts on another under a particular network model of causal dynamics that is parameterised in some way. In this work, the parameters representing connection strengths are referred to as *coupling parameters.* In contrast to functional connectivity, effective connectivity describes directed connections, which may be context-sensitive, and can be either excitatory or inhibitory. For our purposes, coupling can either be (1) "driving", in other words, the input defines the receptive field of the node, or (2) "modulatory", where the input alters the effectiveness of the drive, without influencing the receptive field (Crick and Koch, 1998; Sherman and Guillery, 1998). This can be conceptualised as a gain modulation of the target. Analyses of effective connectivity include Granger causality modelling (Granger, 1969), structural equation modelling (McLntosh and Gonzalez-Lima, 1994), and dynamic causal modelling – DCM (Friston et al., 2003). The work presented herein employs DCM and PPI, both of which are discussed in detail in 6.5 & 6.6.

Equipped with these definitions and conceptual perspective of brain function, we turn our attention to PD and the repercussions on the motor system and basal ganglia.

5.2 Parkinson's disease, basal ganglia physiology and pathophysiology

> *The first symptoms perceived are, a slight sense of weakness, with a proneness to trembling in some particular part; sometimes in the head, but most commonly in one of the hands and arms.*
> James Parkinson, An essay on the Shaking Palsy, 1817.

5.2.1 Overview and clinical presentation

Idiopathic PD is a progressive neurodegenerative disorder primarily affecting motor control. As the disease advances, *non-motor* symptoms commonly manifest, impacting on domains such as cognition, sleep, and autonomic control. Patients characteristically present with asymmetric motor symptoms, affecting both motor behaviours at rest, as well as motor behaviours on action. The cardinal clinical signs include; (1) "pill rolling" resting tremor of frequency approximately 4-6Hz, (2) akinesia, (3) "lead-pipe" rigidity, i.e. velocity independent increases in muscle tone, and (4) impairment of posture and balance. Akinesia describes many clinical features that can be roughly divided into hypokinesia, and bradykinesia. Hypokinesia describes the reduction in frequency and amplitudes of everyday movements. Examples include reductions in arm swing, stride length, and blinking rate, as well as micrographia and hypomemia. Bradykinesia describes slowness of movements, and fatigability of repetitive movements. In addition, patients commonly display gait and balance impairment, stooped posturing, and hypophonia (Rodriguez-Oroz et al., 2009).

PD is caused by the degeneration of dopaminergic (DA) neurons in the pigmented brainstem nuclei, particularly the substantia nigra pars compacta (SNc). The remaining SNc neurons display distinctive intraneuronal inclusion bodies, known as Lewy bodies, formed of misfolded proteins; specifically, the pre-synaptic protein alpha-synuclein (Braak et al., 2003). Post-mortem examinations reveal that 76% of patients with parkinsonism display this pathology, the remainder showing SN loss without Lewy body deposition (Hughes et al., 1992; Rajput et al., 1991).

Diagnosis is clinical, based largely on a consistent patient history and clinical signs. Dopamine transporter (DAT) scans using the radiopharmaceutical Ioflupane ([^{123}I]FP-CIT) can aid diagnosis. Ioflupane has a strong affinity for pre-synaptic dopamine

transporters and decays to emit gamma radiation, which can be detected using single photon emission tomography (SPECT) imaging. PD patients show characteristic reductions in DAT binding in the striatum, particularly in the putamen secondary to dopaminergic denervation (Scherfler et al., 2013; Tatsch and Poepperl, 2013).

Management of PD patients involves a multidisciplinary team consisting of neurologists, physiotherapists, speech and occupational therapists, and at later stages, urologists, neuropsychologists and neurosurgeons. Initial management is usually some form of pharmacological replacement of DA, either using the DA precursor drug L-dopa, or using agonists of the DA receptors (e.g. ropinirole, pramipexole). A host of other agents are often co-prescribed, either with the intention of reducing the peripheral side effects of, and boosting central DA uptake (e.g. Dopa decarboxylase inhibition using carbidopa; COMT inhibition using entacapone), or reducing DA breakdown (e.g. monoamine oxidase-B inhibition using rasagiline). Other agents such as anti-cholinergics, beta-blockade and amantadine are also often utilised.

Most patients display significant initial improvements with medical therapy, particularly L-dopa; failure to respond should prompt reconsideration of the diagnosis (Cotzias et al., 1967; Hughes et al., 1992; Rascol et al., 2000). However, a large proportion of patients develop long-term motor complications following chronic medical therapy (Ahlskog and Muenter, 2001; Rascol et al., 2000). Specifically, the response to L-dopa becomes progressively more erratic and unpredictable, making it impossible for patients to go about their daily lives, and significantly impairs their quality of life.

Patients with such fluctuations are considered to have advanced disease, and may benefit from neurosurgical intervention, specifically DBS. Before considering the details of DBS, it

is valuable to familiarise oneself with the relevant neuroanatomy, and functional circuits that are routinely targeted.

5.2.2 Functional anatomy of the basal ganglia

The basal ganglia (BG) are a group of subcortical nuclei deep in the cerebrum with no direct sensory inputs, and no direct motor output to the spinal cord (Rothwell, 1994). The major components of the BG include the (1) striatum, which is divided by the internal capsule into the caudate nucleus and putamen, (2) the globus pallidus (GP), which is divided by the medial medullary lamina into internal (GPi) and external (GPe) segments, (3) the STN, and (5) the substantia nigra (SN), which can be roughly divided into a pars reticulata (SNr), and the SNc. In reality, there is dense and reciprocal structural connectivity linking almost all of these nuclei. The following description concentrates on the key pathways discussed in the literature. In humans, the GPi and SNr are considered functionally analogous, both acting as the major outputs of BG circuits.

The striatum acts as the input nucleus of the BG, whose GABAergic medium spiny neurons (MSNs; also known as spiny projection neurons, SPNs) receive divergent and convergent glutamatergic inputs from almost all of the cortical mantle (Kress et al., 2013; Shepherd, 2013). MSNs possess extensive dendritic trees; cortical afferents synapse distally on the dendritic tree, on the tips of dendritic spines. However, MSNs have their excitability regulated by fast-spiking inhibitory interneurons, whose synapses land perisomatically, resulting in very little baseline activity despite the dense glutamatergic drive from the cortex. There are two types of MSNs, differing in electrophysiological properties, projection target and expression of neuropeptides and DA receptors. Five G-protein coupled receptors mediate DA signalling, all of which are expressed in the striatum, but subtypes 1 and 2 are most abundant. MSNs expressing DA receptor subtype 2 (D_2R),

which inhibits intracellular adenyl-cyclase through G-protein signalling, project to the GPe and form the proximal limb of the *indirect pathway*. Those expressing the D_1R, which activates adenyl-cyclase signalling, project to the output nuclei forming the *direct pathway* (Lanciego et al., 2012).

SNc DA neurons project to the striatum and synapse with MSNs at the dendritic spine base, and are thus, morphologically, in a position to modulate the gain of incoming cortical transmission. Nigrostriatal axons innervate both subpopulations of MSNs, producing opposing effects on their activity, as a result of their heterogeneous receptor expression (Surmeier et al., 2007); DA typically reduces the excitability of D_2R MSNs, and increases the excitability of D_1R MSNs (Albin et al., 1989).

MSNs projecting to the GPe synapse on a pool of fast-firing GABAergic neurons, which in turn project to the STN. The GPe is also in receipt of reciprocal connections from both the STN and GPi (Nambu et al., 2000). The anatomy of the STN (and its surroundings) is discussed later. In brief, the STN is the only glutamatergic BG nucleus, and also receives its own cortical afferents via the *hyperdirect pathway*, its name reflecting the relatively faster conduction time to reach the output nuclei compared to the direct or indirect pathways (Nambu, 2005; Nambu et al., 2002). Neurons of the STN project back to the GPe, as well as to the output nuclei - forming the final limb of the indirect pathway.

Like the neurons of the GPe, GPi/SNr neurons are GABAergic. Their major efferent projection is to the VA and VL thalamic nuclei, terminating mainly on thalamo-cortical projection neurons such that electrical stimulation of the output nuclei produces a monosynaptic inhibition of the thalamo-cortical projection neurons. In addition, GPi/SNr neurons project to the centromedian thalamic nucleus, habenula, pedunculopontine

tegmental nucleus, and superior colliculus, as well as contralateral VA/VL thalamic nuclei (Parent and Hazrati, 1995a). The neurons of the VL thalamus in turn project back to the cortex, closing the cortico-striato-thalamo-cortical loop.

It was first proposed that this loop served to integrate diverse cortical inputs, "funnelling" information, via the VL thalamus, specifically to M1 (Kemp and Powell, 1971). However, contemporary understanding is that at least five parallel loops pass through the BG, each with distinct (but overlapping) cortical sources and targets. Each circuit typically has multiple cortical inputs of similar functional specialisation, projecting to the striatum, but only one of them receives the majority of the output from the VL thalamus (Alexander et al., 1986). Functionally, two are thought to involve skeletomotor (M1) and oculomotor areas (FEF) of cortex, and three target non-motor frontal cortex (dorsolateral prefrontal cortex - DLPFC, orbitofrontal cortex - OFC and anterior cingulate cortex - ACC). At each structure in the loop, these circuits are thought to be *partially*[3] anatomically segregated, and somatotopically organised. Regarding the motor circuit, cortical sources include M1, S1, PM and SMA, primarily projecting to the putamen as opposed to the caudate nucleus (Künzle, 1978, 1975) – these initial observations have recently been replicated using DTI (Tziortzi et al., 2014). The cortical target however is primarily thought to be the SMA, which in turn projects to other cortical motor regions, as well as down the pyramidal tract (Alexander et al., 1986). See Figure 5.1 (over-leaf).

[3] *While the circuits are largely segregated, at each point in the circuit activity within the loop can be modulated by the activity of "neighbouring" loops* (Redgrave et al., 2010).

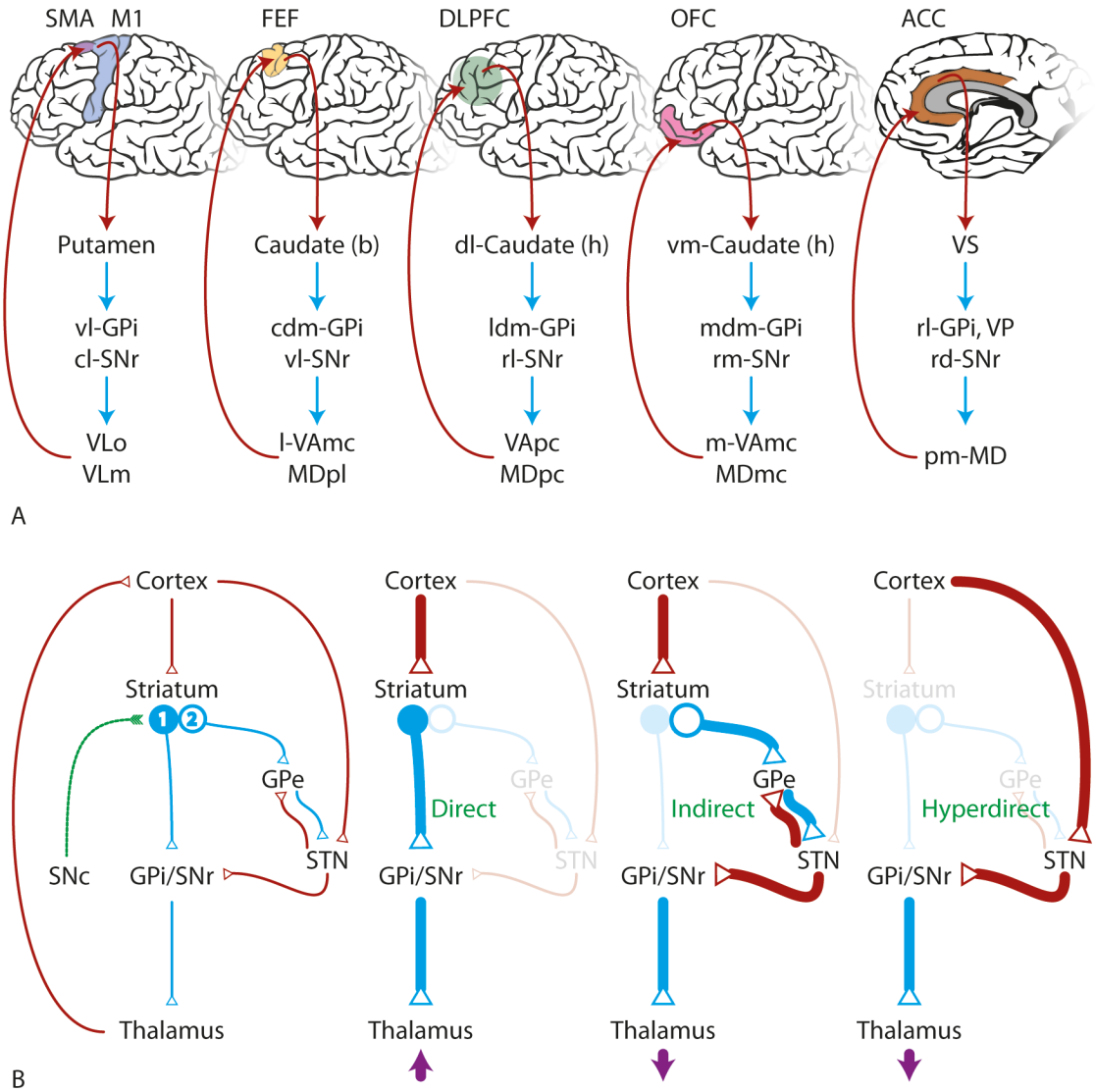

Figure 5.1 The basal ganglia parallel loops & direct and indirect pathways. (A) The five loops of the BG outlined by Alexander et al., 1986; motor, oculomotor, DLPFC, OFC, ACC circuits, including the anatomical portion of the respective striatal, pallidal and thalamic nodes they pass through. Red arrow = glutamatergic projections, Blue arrow = GABAergic projections, Green dotted arrow = DAergic projections. (B) Summary of the three classic pathways from cortex to thalamus. The two pools of MSNs labelled (1) project directly to the GPi, and (2) project polysynaptic to the GPi via the GPe and STN. Purple arrows show the direction of 'activity' in the thalamus following cortical stimulation flowing through the three pathways (according to classic rate based BG models). Abbreviations not used in text body: b = body, h = head, FEF = frontal eye fields, MDpl = medialis dorsalis pars paralamellaris, MDmc = medialis dorsalis pars magnocell ularis, MDpc = medialis dorsalis pars parvocellularis, VAmc: ventralis anterior pars magnocellularis; Vapc: ventralis anterior pars parvocellularis; VLm: ventralis lateralis pars medialis; VLo: ventralis lateralis pars oralis; VP: ventral pallidum; VS = ventral striatum, c1- = caudolateral; cdm- = caudal dorsomedial, dl- = dorsolateral, 1- = lateral, Idm- = lateral dorsomedial, m- = medial, mdm- = medial dorsomedial, pm- = posteromedial, rd- = rostrodorsal, r1- = rostrolateral, rm- = rostromedial, vm- = ventromedial, vl- = ventrolateral.

From a functional perspective, a large and growing literature has mapped aspects of associative learning, goal-directed and habit behaviour control to the cortico-BG system. To summarise, lesion and electrophysiological data from rodents (Yin and Knowlton, 2006) and non-human primates (Miyachi et al., 1997), as well as functional imaging in humans (Lehéricy et al., 2005), have demonstrated that the parts of the striatum in receipt of *associative* projections are necessary for (or show increased activity during) goal-directed control, whereas the *motor* striatum mediates stimulus-response habitual control. The elaborate intrinsic architecture of the circuits, and the qualitative similarity between loops, have led many to suggest the BG serve a generic *selection* function, with associative circuits acting to select the most appropriate from a number of mutually exclusive behaviours (possibly by comparing the utility of predicted outcomes) to yield a goal-directed action, whereas motor loops may select from a host of possible stimulus-response options (Redgrave et al., 2010).

5.2.3 The impact of dopamine depletion

Patients presenting with clinical signs of PD are thought to have already lost ~50% of their SNc neurons, and 80% of their striatal DA (Fearnley and Lees, 1991). PD signs fit well with the early anatomical models of the BG (Albin et al., 1989; DeLong, 1990). Put simply, DA depletion results in under-stimulation of the direct pathway, and over-activity in the STN and GPi, suppressing output to the cortex, producing a lack of movement. However, a number of inconsistencies in the model have since been pointed out, including reports that increased firing in the STN & GP are associated with PD improvements in primate models (Hashimoto et al., 2003), as well as findings that pallidotomies improve dyskinesia (despite theoretically reducing disinhibition of the thalamus), and thalamotomies do not worsen PD (Quiroga-Varela et al., 2013).

Most of our knowledge regarding the neural response to DA depletion either comes either from animal models of PD (primarily the OHDA rat, and MPTP primate[4]), or from recordings either during DBS surgery or from the electrodes themselves before patients receive their implantable pulse generators (IPG). It is important to remember that patients undergoing DBS are those with advanced PD (on average, 14 years post-diagnosis), and thus have extensive DA degeneration. On the other hand, these patients are typically DA-responsive, enabling characterisation of DA-dependent physiology.

Spectral analysis of local field potential (LFP) recordings from the STN of DBS patients reveal highly consistent peaks in beta (13-35Hz) band activity (Little and Brown, 2012), that is most prominent in motor STN territories (Stein and Bar-Gad, 2013), that desynchronises upon administration of DA (Hammond et al., 2007), and is replaced by increased power in the theta (4-7Hz) and gamma (30-70Hz) bands (Brown et al., 2001). These changes have also been recorded in STN single units (Levy et al., 2002), MUA (Weinberger et al., 2006), BUA[5] (Moran et al., 2008), as well as in M1 using EEG (Silberstein et al., 2005) and electrocorticography (ECoG) (N. Mallet et al., 2008). Beta in the STN and cortex desynchronises in preparation of, and during movements, leading some to suggest beta to be a functional signature of promoting "the status quo" at the expense of voluntary movements, potentially due to a loss of computational capacity, or information coding space associated with oscillatory activity (Brittain and Brown, 2014; Brittain et al., 2014).

Human functional imaging using pharmacological manipulations in PD patients, or comparing them to control populations, has provided further insights particularly into the

[4] *See List of Abbreviations for full chemical names of OHDA and MPTP neurotoxins.*
[5] *See section 6.2.2 for description of multiple and background unit activity (MUA and BUA).*

cortical sequelae of DA depletion. A series of papers by David Eidelberg's group have demonstrated a reproducible metabolic profile associated with PD, characterised by increased metabolic activity in the BG, thalamus and cerebellum, and relatively decreased activity in the premotor (SMA/PM) and parietal cortices, correlating with clinical measures of akinesia and rigidity (Spetsieris and Eidelberg, 2011). Furthermore, PD patients show an increased expression of a normal movement related metabolic pattern (i.e. increases in M1, premotor cortices and cerebellum) whilst at rest, but not during movement (Ko et al., 2013).

5.3 STN DBS

Electrical stimulation has long been used as a means of exploring brain function. While reports of the therapeutic effects of stimulation date back as far as the 1960s, it was not until relatively recently that the true value of DBS was realised (Hariz et al., 2010). In 1987, Benabid et al. implanted a series of tremor-dominant PD patients with electrodes targeting the ventralis intermedius nucleus of the thalamus (Vim). They found that chronic 130Hz stimulation reduced tremor in a similar manner to therapeutic thalamotomy (Benabid et al., 1987). Following the discovery of the primate MPTP model of PD (Burns et al., 1983), neurophysiologists began characterising neural firing rates throughout the BG network. This led to the discovery that STN neurons displayed increased firing rates in the Parkinsonian state, and subthalamotomy in these primates produced improvements in all major contralateral motor disturbances (Bergman et al., 1990). It was later shown that similar improvements could be achieved using chronic stimulation, once again demonstrating the similarities between stimulation and ablative procedures (Benazzouz et al., 1993).

Within a few years, these findings began to have implications on clinical practice. In 1995, *The Lancet* published a seminal case series of akinetic-rigid PD patients receiving bilateral STN DBS. Stimulation produced marked improvements in tremor, bradykinesia, and rigidity (Limousin et al., 1995). Since then, STN DBS has been increasingly adopted, and has become an accepted treatment for advanced PD. This section briefly reviews the anatomy, histology, physiology and pharmacology of the STN, and the clinical efficacy of STN DBS.

5.3.1 Neuroanatomy and electrical fields: What are we "stimulating"?

The STN is a *biconvex* (almond-shaped) grey matter nucleus lying in a *double-oblique plane* in the midbrain; its superior pole is both lateral and posterior to its inferior one. From superior to inferior pole, the STN is approximately 10mm. Estimates of volume vary slightly in the literature; limited post-mortem data suggest ≈ 120mm^3 (Hardman et al., 2002), while most others agree a volume of 175 ±20.3 mm^3 (Lambert et al., 2012; Lévesque and Parent, 2005).

One convex surface faces anterior, lateral and inferior (STN_{ali}), whereas the other surface faces posterior, medial, and superior (STN_{pms}). Laterally, the STN_{ali} abuts the crus cerebri superiorly (separating it from the GPi), ansa lenticularis (white matter bundle running from the GPi to the VA/VL thalamus), and SN inferiorly. The STN_{pms} borders the lenticular fasciculus medially, zona incerta (ZI) superiorly (separating it from the thalamic fasciculus and thalamus), and the hypothalamic area inferiorly. The ansa lenticularis and lenticular fasciculus project independently from the GPi before merging into the thalamic fasciculus, terminating in primarily the VLa, VApc, and VM nuclei of the thalamus. The cerebellothalamic fasciculus, which sits inferior to the thalamic fasciculus however, projects from the cerebellar nuclei and targets primarily the VLp nucleus of the thalamus

(equivalent to Vim thalamus in Hassler's nomenclature) (Gallay et al., 2008). If one were to consider brain regions that are either directly within millimetres of the electrode itself, or are in direct receipt of projections carried in white matter bundles passing around the electrode, it is easy to imagine that multiple subcortical nuclei are likely to be directly manipulated, with unknown effects on how those regions process their afferents from distant regions (e.g. the cortex), or whether these effects are reflected in their efferent projection.

Computational models of the electric field generated by therapeutic DBS parameters suggest that current is not purely limited to the body of the STN. Field patterns are dependent on the anisotropy of conductivity tensors of the surrounding anatomy. Using tensors derived from DTI (Tuch et al., 2001), fields were found to extend into the ZI, fields of Forel and internal capsule (McIntyre et al., 2004a). While spreading to the internal capsule can evoke clinically recognisable effects (tonic muscle contractions – usually of the face), it remains unknown what results from stimulating the smaller tracts. One recent study proposes spread to the cerebellothalamic fasciculus may underlie stimulation-induced dysarthria (Aström et al., 2010). Such studies highlight the possibility that some of the adverse effects of DBS may result from *collateral damage*; i.e. modulation of structures neighbouring the target.

The neurons of the STN itself are primarily glutamatergic, with a small GABAergic population accounting for ~7.5% of total neurons (Hamani et al., 2004; Lévesque and Parent, 2005). Primate tracing studies (Carpenter and Strominger, 1967; Haynes and Haber, 2013; Parent and Hazrati, 1995b; Whittier and Mettler, 1949), and recently, high resolution DTI in human subjects (Brunenberg et al., 2012; Forstmann et al., 2012; Keuken et al., 2013; Lambert et al., 2012) have revealed the structural connectivity profile

of the STN. The STN mostly receives projections from the cerebral cortex and GPe. Additionally, the STN receives axons from the centromedial, parafascicular and venteroanterior thalamic nuclei, the substantia nigra, and the pedunculopontine tegmental nucleus, although the functional relevance of these sparser connections remains unknown. Cortical afferents form the hyperdirect pathway (see section 5.2.2), originating from mostly frontal regions including M1, SMA, pre-SMA, FEF, DLPFC, and ACC. Additionally, the STN receives afferents from S1 and the insula cortex. Lambert et al. recently reviewed 130 STN tracing articles published between 1947 and 2011; their results are summarised in the ideogram below (Lambert et al., 2012).

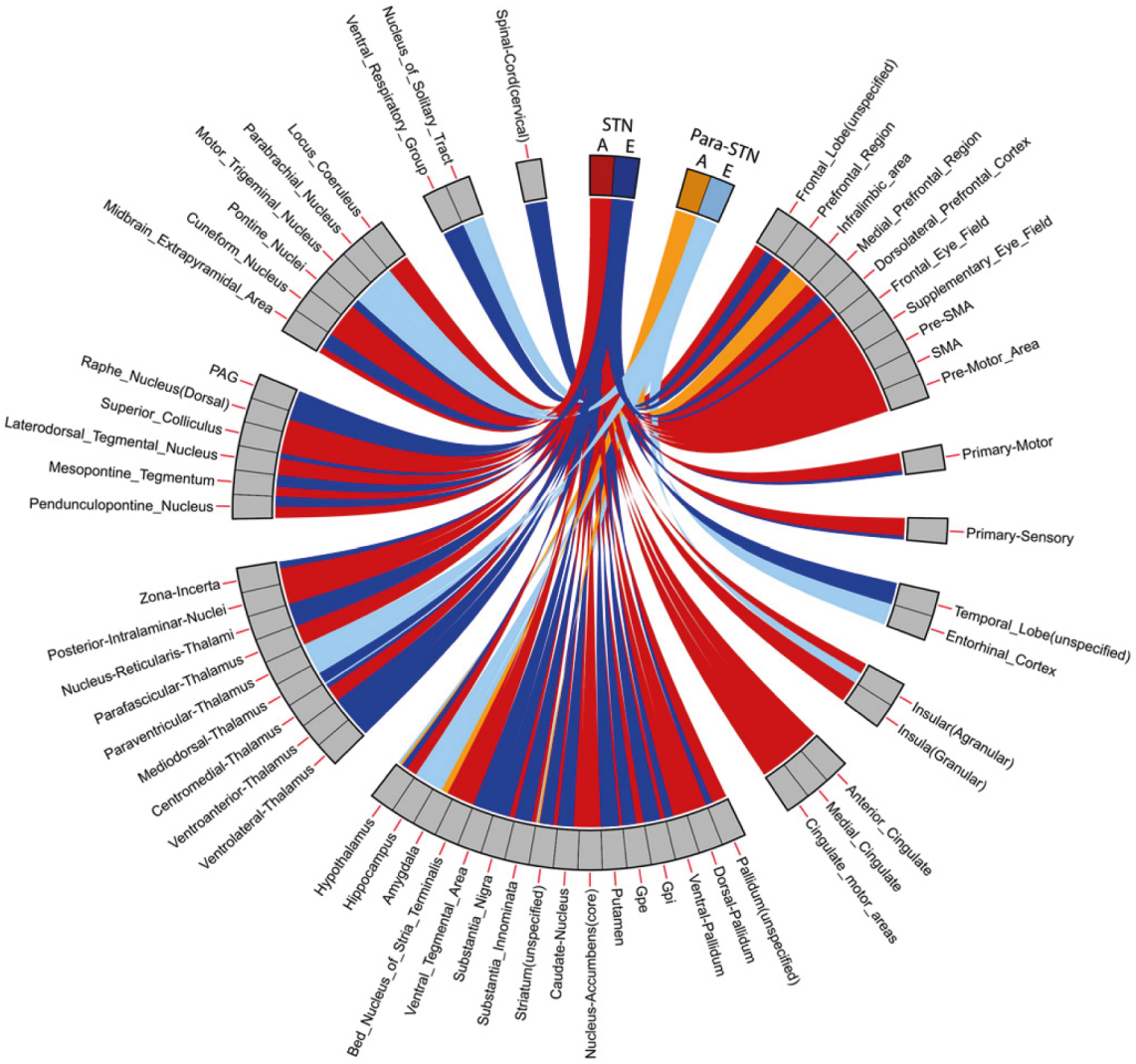

Figure 5.2 Taken from (Lambert et al., 2011). Ideogram of afferent and efferent anatomical connections of the STN reported in the literature between 1947 and 2011. Red represents afferent, blue efferent. Several papers report on a structure called the parasubthalamic nucleus at the STN's medial border; these connections are included separately. The width of the lines represents the normalised proportion (as a percentage) of the respective connections; see (Lambert et al., 2011) for more information.

The structural connectivity signature has led some to suggest that the STN can be parcellated into motor, limbic and associative subdivisions, with greatest clinical efficacy, and minimal side effect risk presumed to be associated with targeting the motor-STN (Haynes and Haber, 2013; Lambert et al., 2012; Parent and Hazrati, 1995b; Welter et al., 2014). As discussed though, the stimulation field is likely to extend beyond the borders of the STN itself, let alone its putative subdivisions. As a result, efforts have been made to

shape the field to avoid limbic and associative domains. Subtle improvements in cognitive-motor dual task performance have been reported using field shaping (Butson et al., 2007; Frankemolle et al., 2010; Mikos et al., 2011).

5.3.2 Surgical procedure and between-centre variability

Surgical procedure varies between centres, and is likely responsible for some between-centre variability in targeting accuracy, risks of haemorrhage and infection, and electrophysiological findings. Typical electrode implantations at the National Hospital for Neurology and Neurosurgery proceed as follows:

1. Pre-operative stereotactic MRI under general anaesthesia to localise the target nuclei.
2. Trajectory planning using commercially available software (Framelink™, Medtronic, Minneapolis, Minnesota).
3. Validation of trajectory using manual calculation from frame fiducials.
4. Trajectory correction based on audited accuracy data.
5. Exposure of the cranium, drilling the burr hole, and coagulation the dural and pial membranes at the calculated stereotactic entry point on one side,
6. Dynamic impedance monitoring using a blunt-tip radiofrequency (RF) electrode along the trajectory to the target, confirming the path does not enter the ventricle, and reaches grey matter.
7. Removal of the RF electrode and 'soft'-passing of a quadripolar DBS electrode along the track created by the RF electrode. Anchoring of electrode to burr hole cover.
8. Steps 5-8 are repeated if electrodes are implanted bilaterally.
9. Post-operative stereotactic MRI to verify electrode location within the target.

The procedure has been highly finessed and employs a number of measures to maximise target accuracy (e.g. trajectory validation and correction, minimising pneumocephalus and CSF leak to reduce brain-shift). Perhaps more importantly, this procedure enables most bilateral implantations to only require two deep brain 'passes' (one for each hemisphere), reducing the risk of haemorrhage. This is in contrast to many centres utilising intra-operative electrophysiology, requiring multiple brain passes to select an appropriate electrode target.

5.3.3 DBS hardware & stimulation parameters

In this centre, patients are typically implanted with Medtronic DBS systems. Each DBS system comprises at least three implanted components; (1) the electrodes ('leads'), (2) an IPG or 'pacemaker', and (3) extension cables connecting the IPG to the electrodes. All components contain some metallic materials including platinum-iridium, stainless steel, titanium and silver as part of the conducting circuit or casing. Four metal contacts lie at the end of each electrode (thus 'quadripolar'), in contact with the target neural tissue. Successful surgery typically results in at least one contact lying within the body of the target nucleus, in the case of the STN, typically two. Following recovery, a voltage is induced either between a contact and the IPG case (monopolar stimulation) or between two adjacent contacts (bipolar stimulation), causing current to flow through the target tissue.

The type of stimulation employed, and the parameters of stimulation determine the properties of the current field produced. Stimulation parameters that are commonly optimised include the amplitude (i.e. the magnitude of the induced voltage, typically 2-3V in STN DBS for PD), frequency (i.e. the rate of pulse delivery, typically 130Hz), and the pulse width (i.e. the length of each stimulation pulse, typically 60μsec).

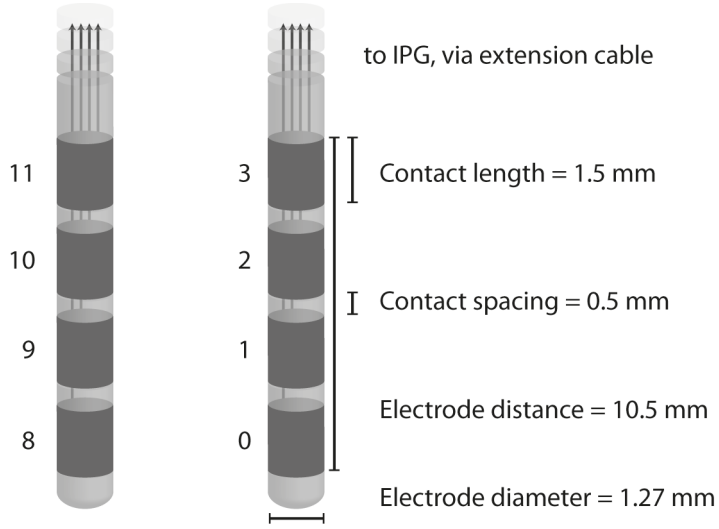

Figure 5.3 The Medtronic 3389 electrode used in DBS patients studied in this thesis. The deepest most distal contacts are 0 and 8.

5.3.4 Clinical efficacy in Parkinson's disease

STN DBS has become an established treatment for patients with advanced PD. Following two case series documenting off-medication improvements (1) in clinical rating scales (Unified Parkinson's Disease Rating Scale; UPDRS), (2) activities of daily living, and (3) reductions in medications at 1 year follow up (Limousin et al., 1998, 1995), continuing to five years (Krack et al., 2003), randomised control trials have demonstrated STN DBS to be superior to medical therapy alone in patients with advanced disease (disease duration ~13 years) and severe motor symptoms (Deuschl et al., 2006). STN DBS is most effective at improving off-medication motor impairment, reducing UPDRS-III (indexing motor impairment) by 54% at five years (Krack et al., 2003). Given its invasive nature, serious adverse effects are more common with STN DBS than medical therapy alone; the key risks of surgery are intracerebral haemorrhage, infection and peri-operative neuropsychiatric disturbances. Stimulation-related side effects can include speech disturbance (many report STN DBS worsens verbal fluency scores (Merola et al., 2013)) dyskinesia, eyelid apraxia, and freezing of gait. Targeting the STN as opposed to GPi produces similar (Follett et al.,

2010), if not superior motor effects (Odekerken et al., 2013). The matter of side effects profile has long been debated, the latest trials suggesting any differences are not statistically significant (Odekerken et al., 2013). STN DBS has recently been shown to be superior to medical therapy alone in PD with early motor complications (i.e. disease durations ~7.5 years), producing similar improvements to those seen in patients with advanced disease (Schuepbach et al., 2013).

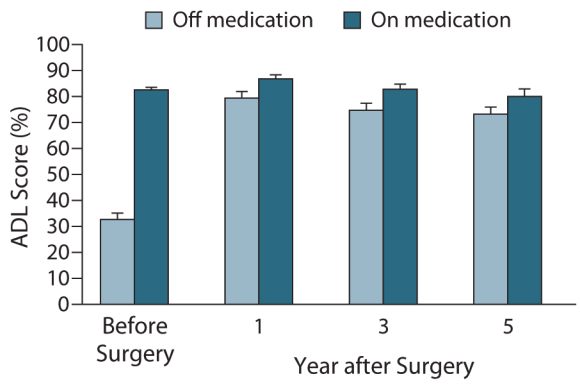

Figure Off-Medication and On-Medication Scores on the Schwab and England Scale for Activities of Daily Living (ADL) at Base Line and One, Three, and Five Years after Surgery.

Data are means ±SD. After surgery, evaluation was performed with bilateral stimulation activated. Scores range from 0 to 100 percent (with a score of 100 percent indicating normal function). A score above 70 percent indicates complete independence in activities of daily living. A score of 70 percent or lower indicates that patients need the help of a caregiver. Off-medication scores were improved at one, three, and five years (P<0.001 for all three comparisons).

Figure 5.4 Clinical efficacy of STN DBS. Plot and caption taken from Krack et al., 2003.

5.4 The neural response to STN DBS

5.4.1 Neuroimaging & DBS: PET, SPECT and fMRI

Neuroimaging offers whole-brain *in vivo* assays of brain function. While these studies sacrifice the rich temporal resolution afforded by electrophysiological techniques and rely on inferences made on indirect measures of neural activity (e.g. regional cerebral blood flow – rCBF; blood oxygen level dependent signal - BOLD), neuroimaging provides a non-invasive measure of global activity. This is an important strength given the likely diffuse effects of electrical stimulation. While it is common practice to use functional magnetic resonance imaging (fMRI) in cognitive neuroscience, most neuroimaging exploring DBS employ either positron emission tomography (PET) or single photon emission tomography (SPECT); both are nuclear medicine techniques requiring intravenous

radiopharmaceuticals. The physiological basis of neuroimaging signals is an expansive topic, and has been discussed at length (Attwell and Iadecola, 2002; Logothetis and Wandell, 2004). For completeness, I provide a brief overview of the techniques relevant to the DBS literature. As the predominant form of data collection in this thesis, fMRI is also discussed in detail in section 6.2.

Both PET and SPECT require injection of a radiopharmaceutical, a waiting period for the pharmaceutical to accumulate in the tissue of interest, and then collection of a signal that is in some way caused by the decay process of the radioactive label. PET detects pairs of gamma rays travelling in opposite directions emitted from the annihilation of an electron and a positron, which is emitted from the radiopharmaceutical as it undergoes beta decay. In contrast, SPECT uses a gamma camera to detect gamma rays directly emitted from the radiopharmaceutical as it undergoes gamma decay. The type of data acquired from these scans thus depends entirely on the radio-labelled ligand used. Typically, the DBS literature employs radioligands that either quantify rCBF, rCGM, dopamine receptor binding potential, or dopamine transporter (DAT) concentration. Table 5.1 summarises the key radiopharmaceuticals used to study the effects of DBS.

Functional MRI differs from the aforementioned methods in a number of important ways. Firstly, fMRI typically does not require the injection of a contrast material, and does not rely on radiation exposure, minimizing any radiation exposure. Secondly, fMRI has significantly improved spatial and temporal resolutions; this is particularly useful when scanning small structures such as the BG, or measuring the response to individual events, as opposed to blocks of events. Thirdly, fMRI is (relatively) widely available, requiring (only) a MRI scanner, and is significantly less expensive, given it does not require the preparation of radiopharmaceuticals.

Name	Quantifies	Description
$H_2[^{15}O]$ PET	rCBF	Radio-labelled water molecule used as a proxy for regional cerebral blood flow. Highly transient signal.
[^{99m}Tc]-ECD SPECT	rCBF	Small lipophilic molecule that crosses the blood brain barrier. Used for as a proxy for regional cerebral blood flow. Highly transient signal.
[^{18}F]DG PET	rCGM	Radiolabelled glucose molecule. Glucose is key for neural metabolism, and is thus used as a proxy for metabolism.
[^{11}C]-Raclopride PET	D_2R binding	Radiolabelled D_2R antagonist with lower affinity to receptor than DA. When DA is released from presynaptic terminals, Raclopride is displaced from D_2R. Therefore, low binding means high DA binding.
[^{123}I]FP-CIT SPECT	DAT concentration	Known commercially as *DaTSCAN*. Has a high binding affinity for presynaptic DA transporters on nigostriatal DA neurons.

Table 5.1: Commonly used nuclear medicine techniques in the DBS literature. rCBF = regional cerebral blood flow; rCGM = regional cerebral glucose metabolism; DAT = dopamine transporter.

5.4.2 Review of the neuroimaging literature

A MEDLINE search was used to identify all neuroimaging studies exploring the effect of *specifically* STN DBS on neural activity published in peer-reviewed journals between 1987 and 1st January 2014 using the following search terms: *("DBS" OR "stimulation" OR "deep brain stimulation") AND ("STN" OR "subthalamic") AND ("fMRI" OR "functional magnetic" OR "PET" OR "positron emission" OR "SPECT" OR "single photon" OR "ASL" OR "arterial spin label*" OR "cerebral activity" OR "blood flow") AND ("1987/01/01"[Date - Publication] : "2014/01/01"[Date - Publication])*. Article abstracts were examined to exclude any non-relevant papers. Reference lists of the remaining articles were searched for any additional relevant papers not found in the initial search. Single case reports were not included unless they concerned STN DBS fMRI.

In summary, 7 studies concerned potential confounds of DBS neuroimaging (peri-operative period, haemodynamic coupling), 8 studies examined the effect of STN DBS on striatal DA, 3 reported results in animal models of STN DBS, and the remainder explored the effect of STN DBS on regional activity. Only 6 human studies used fMRI, the others either PET or SPECT; 37 of which were task-based, and 21 explored endogenous activity. Of the task-based studies, 15 concerned the motor system, the rest studied the effects of STN DBS on cognitive function, which are not reviewed here.

5.4.2.1 Potential confounds: The peri-operative period & microlesion effect of electrode implantation

Following implantation of the electrode, without current passing through the target, patients typically show some peri-operative clinical improvement thought to be related to oedema of the target nucleus (Jech et al., 2012). While inherently confounded by scan order, four studies have explored the so-called "microlesion effect". Comparing preoperative and postoperative 'OFF' FDG uptake at rest in restricted volumes encompassing the STN and GP respectively, one study has reported reductions in rCGM in both regions at six months post-surgery, suggesting implantation has a long-term lesion-like effect. However, these reductions were noted in absence of statistically significant clinical improvement, and analysis was restricted to these regions alone (Hilker et al., 2008). An earlier study conducting a whole brain search did not find any significant differences (Hilker et al., 2004). However, a similar smaller study (n=6) with <3 months follow-up time reported reductions in additional regions including the putamen and VL thalamus, and concomitant increased resting rCGM in sensorimotor and cerebellar cortex. Again though, these findings were in absence of clinical effect of implantation alone (Pourfar et al., 2009). A recent study comparing pre-op fMRI with the first or third

postoperative day both quantified the degree of inflammation, changes in UPDRS-III, and changes in regional BOLD responses in response to visually guided tapping. Patients showed significant increases in both cortical and subcortical oedema and clinical improvement following implantation (postoperative day 3 > postoperative day 1), associated with reductions in BOLD responses in the thalamus, putamen, GP, M1, SMA, cingulate and insula cortex during voluntary movements (Jech et al., 2012).

These findings illustrate (1) the long-term lesion-like effect following implantation – although this does not seem to be clinically manifest, and (2) the potential confound of scanning patients within days of electrode implantation.

5.4.2.2 Potential confounds: The effect of STN DBS on haemodynamic coupling

An important consideration when using neuroimaging methods to explore functional changes associated with an intervention is to confirm that the intervention (usually drug) does not alter the assumed constant haemodynamic coupling between neural activity and blood flow (Iannetti and Wise, 2007). This is particularly relevant to DBS of the STN given reports in rats that microstimulation of neurons in a functionally restricted region of the subthalamus/ZI/Forel's field/prerubral zone elevates rCBF (Glickstein et al., 2001; Golanov et al., 2001), potentially confounding rCBF PET/SPECT and BOLD fMRI. To address this question, Hirano et al., collected rCBF and rCGM at rest in the same patients receiving either a levodopa infusion or active STN DBS, revealing that while levodopa produces flow-metabolism dissociation in BG nuclei (including the putamen, GP, thalamus and brainstem), flow and metabolism remain correlated during STN DBS (Hirano et al., 2008). Another study using functional transcranial Doppler to compare flow velocity in the posterior cerebral artery during visual stimulation (specifically chosen because visual perception is not thought alter under STN DBS) similarly did not find a significant

difference associated with DBS (Azevedo et al., 2010). Thus, at present there is little evidence to suggest DBS alters haemodynamic coupling.

5.4.2.3 The effect of STN DBS on striatal dopamine

Following observations of increased striatal DA release (Benazzouz et al., 2000a), metabolism (Paul et al., 2000), and potential neuroprotective effects of STN DBS in animal models, a number of studies have explored the effect of DBS on striatal dopamine concentrations using either [^{11}C]-Raclopride or [^{18}F]DOPA PET, or *DaTSCAN* SPECT. Five studies (total n=34) have reported no detectable effect of STN DBS on Raclopride displacement, regardless of whether DBS was unilateral (Abosch et al., 2003; Arai et al., 2008), or bilateral (Hilker et al., 2003; Strafella et al., 2003b; Thobois et al., 2003). Similarly, two larger studies (total n=65) exploring the neuroprotective effect of 12 months of STN DBS on DA innervation have reported similar rates of decline to that found in patients treated medically (Hilker et al., 2005; Lokkegaard et al., 2007). One study involving patients with severe wearing off phenomena have reported a stabilisation of raclopride binding associated with therapeutic DBS (i.e. less fluctuation between on and off-drug binding), although only three subjects were studied (Nimura et al., 2005). At present therefore, there is little *in vivo* evidence to support the hypothesis that STN DBS exerts its mechanism of action by DA modulation in the striatum, and might explain why Hirano et al., did not detect any flow-metabolism uncoupling discussed above (Hirano et al., 2008).

5.4.2.4 The effect of STN DBS on endogenous activity

There have been 22 studies exploring changes in rCBF/rCGM induced by STN DBS whilst patients lay at rest, usually with eyes closed. Additionally, a number of other studies have reported contrast results detailing the *main effect of DBS*, averaging across task and

resting sessions. The average (range) cohort age at scanning is 60 (53-65), with disease duration of 13 (7-16) years. The average reported cohort stimulation parameters are a frequency of 159Hz (130-186Hz), amplitude of 3V (1.9-3.65V), and pulse width of 71μs (60-93μs).

Studies either compare, (1) *before vs. after* - a pre-operative resting session to one collected usually after at least 3 months of fully implanted therapeutic DBS, or (2) *ON vs. OFF* - after at least 3 months of fully implanted therapeutic DBS. *Before vs. after* studies usually do not involve having the DBS switched off after it is first initiated, thus truly explore the chronic effect of therapeutic stimulation, and any plastic changes that may entail. In contrast, *ON vs. OFF* studies explore acute changes in manipulating STN DBS, almost always from a state of chronic therapeutic stimulation, to a temporary inactivated state, followed by reactivation; studies vary in how long they wait in each window before scanning (usually switched to the scanning condition about 10-30 minutes before the scan, although some report doing this the day before scanning (Hilker et al., 2004)). Given discontinuation of STN DBS removes >70% of its therapeutic effect within the first 15 minutes, such *ON vs. OFF* manipulations usually capture most of the therapeutic effect[6].

A summary of the findings of each study is presented in Table 5.2; studies are divided into *before vs. after*, *ON vs. OFF*, and task studies reporting *main effects of DBS*. Regarding regions of the BG, most studies report increased activity in the thalamus and STN (Arai et al., 2008; Asanuma et al., 2006; Bradberry et al., 2012; Ceballos-Baumann et al., 1999; Garraux et al., 2011; Geday et al., 2009; Hershey et al., 2003; Herzog et al., 2006; Hilker et al., 2008, 2004; Hill et al., 2013; Karimi et al., 2008; Sestini et al., 2005; Volonté et al., 2012). *Before vs. after* studies also report GP activity increases (Hilker et al., 2008, 2004;

[6] *Indexed using UPDRS-III. Calculated from data presented in Temperli et al., 2003.*

Sestini et al., 2005; Zhao et al., 2004), although the study with the largest cohort (Cilia et al., 2009), and the *ON vs. OFF* studies report metabolic decreases (Arai et al., 2008; Asanuma et al., 2006; Wang et al., 2010). The putamen has similar contradictory results (Asanuma et al., 2006; Bradberry et al., 2012; Hilker et al., 2004; Wang et al., 2010; Zhao et al., 2004), with few (and opposing) reports of caudate nucleus activity changes (Garraux et al., 2011; Le Jeune et al., 2010). The mixed results of the putamen and GP (which are in close proximity, both comprising the lentiform nucleus) are possibly due to the low spatial resolutions achievable with PET/SPECT. Similarly, changes in the cerebellum are mixed and often poorly reported, or not included in the scanning volume.

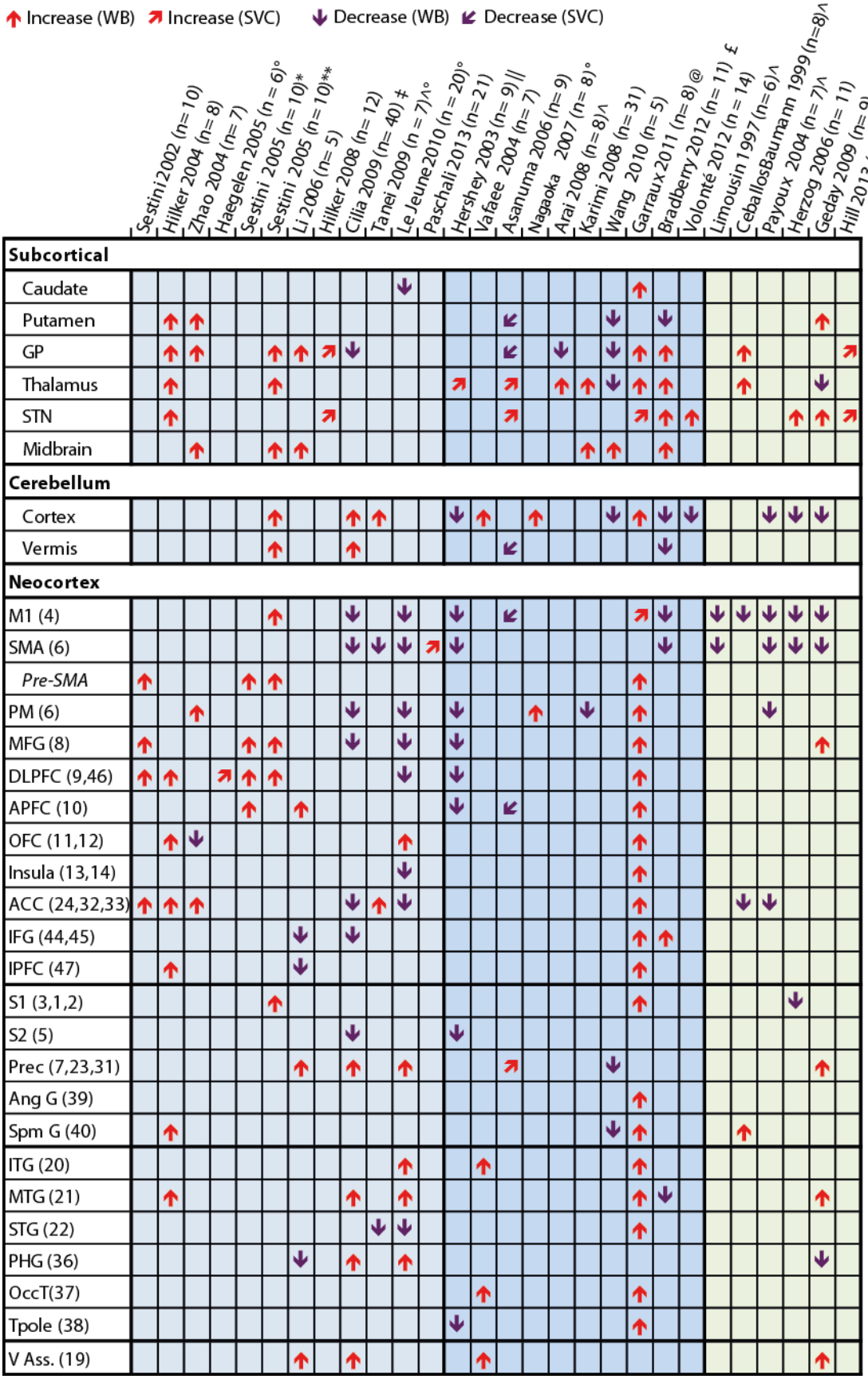

Table 5.2 Literature review: The effect of STN DBS on resting rCBF/rCGM. WB = whole brain corrected statistics, SVC = small volume corrected statistics. Light blue = Before vs. after

studies. Blue = ON vs. OFF studies. Green = Main effects results averaged over task and rest sessions.

$ Hill et al., 2013 compare rCBF in ROIs under two different STN stimulation settings (dorsal vs. ventral); only significant results in both settings included.

£ Bradberry et al., 2012 compared DA to DBS therapy; results of common regions and DBS alone regions included.

@ Garraux et al., 2011 normalised their data according to the standardised uptake value (SUV) after noting a significant difference between SUV during ON and OFF conditions. This normalisation is not used in other studies and may explain why they only report increases in metabolism. Additionally found increases in V2.

°Scanned on medication.

**Sestini et al., 2005 collected data at both 4 months and 42 months post-op; * includes outcome at 4 months, ** includes changes from 4-42 months Additionally found increase in SN.*

^Scanned during unilateral STN DBS.

ǂ Cilia 2009 additionally found increases in the hippocampus.

|| Hershey 2003 addtionally found increases in the red nucleus and decreases in the claustrum

Abbreviations not in text body: BA = Brodmann area, MFG = middle frontal gyrus, APFC = anterer prefrontal cortex, IFG = inferior frontal gyrus, IPFC inferior prefrontal cortex, Prec = precuneus, Ang G = angular gyrus, Spm G = Supramarginal gyrus, ITG = inferior temporal gyrus, MTG = middle temporal gyrus, STG = superior temporal gyrus, PHG = parahippocampal gyrus, OccT = Occipitotemporal junction, Tpol = temporal pole, V. Ass = visual association area.

Regarding cortical modulation, most changes are noted in the frontal lobe, especially the motoric cortices. Ten studies report reductions in activity in M1 (Asanuma et al., 2006; Bradberry et al., 2012; Ceballos-Baumann et al., 1999; Cilia et al., 2009; Geday et al., 2009; Hershey et al., 2003; Herzog et al., 2006; Le Jeune et al., 2010; Limousin et al., 1997; Payoux et al., 2004); only Sestini et al., report any whole-brain corrected increases in M1, and that was only when comparing ON stimulation scans at 4 months to 42 months, potentially showing the DBS effect wearing off (Sestini et al., 2005). Results from the SMA show similar reductions (Bradberry et al., 2012; Ceballos-Baumann et al., 1999; Cilia et al., 2009; Geday et al., 2009; Hershey et al., 2003; Herzog et al., 2006; Le Jeune et al., 2010; Limousin et al., 1997; Payoux et al., 2004; Tanei et al., 2009), however three studies report increased activity in its rostral portion, the pre-SMA (Garraux et al., 2011; Sestini et al., 2005, 2002). The PM shows mixed responses; five studies report reduced flow during DBS (Cilia et al., 2009; Hershey et al., 2003; Karimi et al., 2008; Le Jeune et al., 2010; Payoux et al., 2004), whereas three studies report increased metabolism (Garraux et al., 2011; Nagaoka et al., 2007; Zhao et al., 2004). Prefrontal regions, especially the DLPFC, typically show increases in activity under DBS, although these have been mostly detected in *before vs. after* studies (Garraux et al., 2011; Haegelen et al., 2005; Hilker et al., 2004; Li et al., 2006; Sestini et al., 2005, 2002). There are mixed results regarding the ACC; *before vs. after* studies report increased activity with DBS, although larger studies (Cilia et al., 2009), and task studies reporting main effects (Ceballos-Baumann et al., 1999; Limousin et al., 1997), note decreased activity with DBS.

Changes reported in the parietal, temporal and occipital lobes are more sparse; however, elevated activity in the precuneus/posterior cingulate cortex and middle temporal gyrus activity have been reported under STN DBS at rest (Asanuma et al., 2006; Cilia et al.,

2009; Garraux et al., 2011; Geday et al., 2009; Hilker et al., 2004; Le Jeune et al., 2010; Li et al., 2006).

5.4.2.5 Endogenous activity correlates

Many authors additionally explore correlations between endogenous activity and clinical phenotype. Perhaps unsurprisingly given the changes discussed above, clinical impairment measured with the UPDRS-III has been found to correlate with activity in various parts of motoric cortex. Payoux et al., report correlations in akinesia subscores with endogenous activity in both M1 and the a medial portion of the cerebellum (Payoux et al., 2004), while a longitudinal imaging study scanning at both 5 months and 4 years post-DBS report strong negative correlations between total UPDRS-III and activity in the pre-SMA and PM (Sestini et al., 2005). Similarly, percentage improvements have been found to correlate in both the SMA and ACC (Karimi et al., 2008; Lyoo et al., 2007; Paschali et al., 2013; Volonté et al., 2012), and combined subscores of rigidity and tremor of one hemibody have been found to be positively correlated with activity in the precentral gyrus (Nagaoka et al., 2007; Volonté et al., 2012). One study has additionally found activity within the PPN correlates with improvements in postural stability, although made use of rather liberal statistical practice (Karimi et al., 2008).

Additionally, others have attempted to identify regions correlated with stimulation parameters. One small study conducted on medicated patients found activity in the STN was positively correlated with DBS frequency, whereas M1 and SMA exhibited significant negative correlations (Haslinger et al., 2005).

5.4.2.6 The effect of STN DBS on motor-evoked activity

Only studies examining voluntary limb movements are considered here; a number of other studies employing designs involving other types of movements, e.g. speech (Pinto et al., 2004) are not discussed. The results are summarised in Table 5.3; only *movement x DBS interaction* results are detailed.

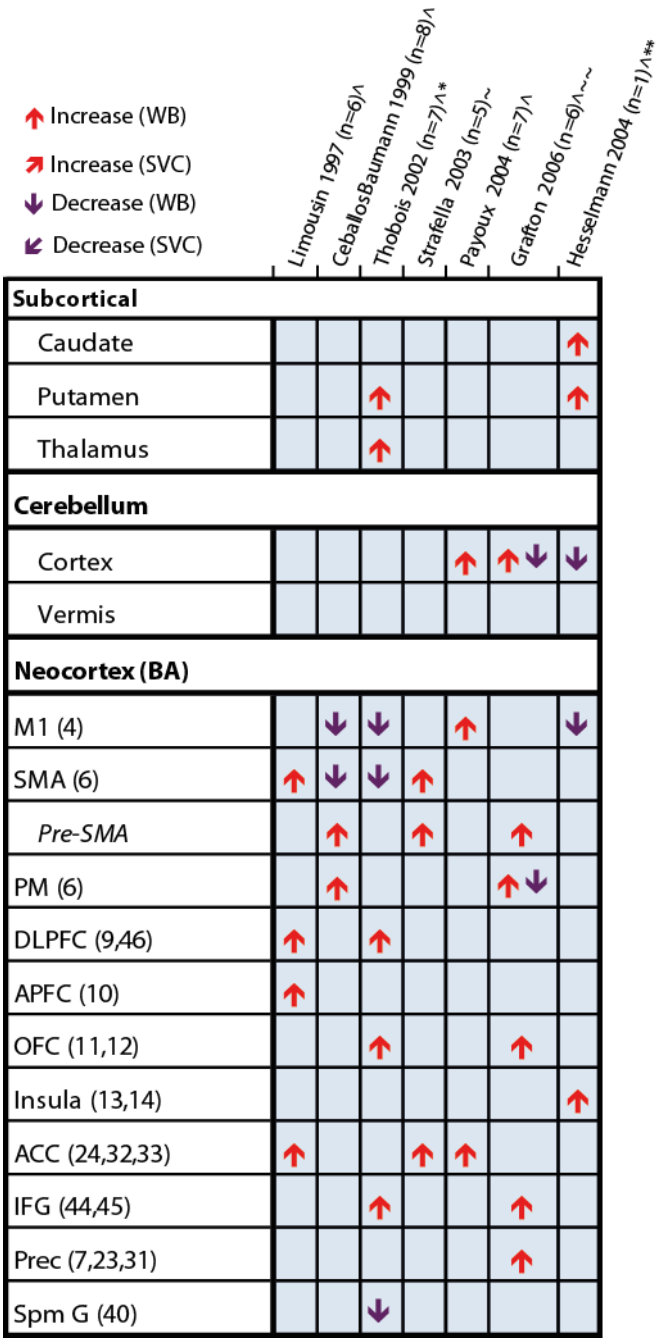

*Table 5.3 Literature review: The effect of STN DBS on motor-evoked activity. *Thobois et al., 2002 used a learned sequential joystick movement task. Only the movementxDBS interaction results are included. ~Strafella et al., 2003 only report the comparison of unilateral vs. bilateral DBS during movement. ~~ Grafton et al., 2006 used a visuo-motor feedback task where the subjects had to adjust their movement speeds according to the visual feedback. Responses were increased by DBS in the posterior cerebellum, but decreased in the anterior cerebellum. Similarly, responses were increased in a lateral portion of PM, but decreased in a medial region. **Hesselamnn et al., 2004 present a case study of intraoperative fMRI whilst a patient performed finger opposition under different STN DBS conditions. ^Scanned during unilateral STN DBS.*

In contrast to the "resting state" studies, those examining the interaction between STN DBS and movement-evoked activity all employ an *ON vs. OFF* design. Six PET/SPECT studies have addressed this question, as well as one intraoperative fMRI case study (discussed in 5.4.2.8). Limousin et al., used an upper limb movement task using a joystick, asking six patients to move in one of four directions when they heard an auditory cue, using their more affected hand. Unilateral STN DBS contralateral to hand movements increased motor-evoked activity in the DLPFC, ACC and SMA. However, the main effect of STN DBS was to reduce activity in M1 and PM (Limousin et al., 1997). An almost identical study in a larger PD cohort reported consistent main effects, additionally reporting activity in the PM, and rostral (or pre-) SMA to increase during movements, and reductions were found in the caudal SMA and M1 (Ceballos-Baumann et al., 1999). During a learned motor sequence task, Thobois et al., detected increases in motor-evoked responses in the thalamus and putamen, as well as in the DLPFC, in response to unilateral STN DBS, and reductions in M1, parietal cortex and the SMA (Thobois et al., 2003). Talairach coordinates reported in this study suggest the reductions occurred in the pre-SMA, contradicting (Ceballos-Baumann et al., 1999); the different tasks may underlie this apparent discrepancy. Another unilateral DBS study simply requiring subjects to perform paced fist clenches, report increases M1, the ACC and cerebellum under DBS, however subsequent analysis revealed these apparent increases were due to reductions in the baseline (i.e. resting) condition in these three regions (Payoux et al., 2004). During a visually guided tracking task, which arguably engages more cerebellar processing than joystick movements, unilateral stimulation increased motor-evoked responses in the SMA (reported coordinates equivalent to the pre-SMA), posterior cerebellum and prefrontal cortex. Reductions were also noted in the anterior cerebellar cortex and parts of the PM (Grafton et al., 2006). The

only study to consider bilateral STN DBS (only reporting results comparing unilateral vs. bilateral) found increased motor-evoked responses in the ACC and SMA (particularly pre-SMA) using the same joystick task discussed previously (Strafella et al., 2003a).

In summary therefore, movement-evoked responses appear to be increased by STN DBS in the prefrontal (DLPFC), cingulate (ACC) and pre-SMA. Only one study has found subcortical changes, and responses in the cerebellum, PM and M1 appear mixed, probably dependent on the motor task employed.

5.4.2.7 Parkinson's disease "covariance patterns" & STN DBS

The PD related pattern (PDRP), first proposed by David Eidelberg (Eidelberg et al., 1994; Spetsieris and Eidelberg, 2011), employs a network approach to the analysis of PET time series, and its expression has been found to correlate with PD severity and striatal DA (Asanuma et al., 2006; Eidelberg et al., 1994). Authors use a PCA-based approach to identify a number of orthogonal principal components amongst an entire cohort, and then define a pattern as PD-related if the amount of variance it explains in PD patient data is significantly different to that of control data. The classic PDRP, as referenced earlier (section 0), shows increased metabolic activity in the BG, thalamus and cerebellum, and relatively decreased activity in the premotor (SMA/PM) and parietal cortices. In addition, a number of other symptom related patterns have since been described including a tremor-related network (PDTP) with co-varying increased activity in the cerebellum, dentate nucleus, putamen and M1 (Mure et al., 2011). Both PDRP and PDTP expression has been shown to reduce during active STN DBS (Asanuma et al., 2006; Wang et al., 2010). Additionally, abnormal expression of normal motor related metabolic patterns that occur at rest in PD, is reduced by DBS (Ko et al., 2013). These analyses are essentially quantifying the expression of modes of functional connectivity, i.e. patterns of functionally connected

brain regions, which are specifically related to disease states. To summarise, this literature suggests STN DBS reduces the expression of pathological modes of functional connectivity.

5.4.2.8 Functional MRI during active DBS in human patients

As discussed above, fMRI has a number of advantages over nuclear neuroimaging techniques. However, the use of fMRI to address DBS questions has been severely limited by concerns regarding the safety of scanning patients with implanted electrodes in contact with neural tissue. Two notable and unfortunate case studies have highlighted the potential dangers of DBS interacting with MRI scanning when safe operating conditions are not observed (Henderson et al., 2005; Spiegel et al., 2003). The specific safety concerns regarding MRI-DBS interactions are discussed in detail later (section 5.5.1).

Excluding experiments detailed in this thesis, there have been a handful of reports of the use of fMRI in DBS patients, in addition to a number of studies conducted on sedated animal models of DBS (see 5.4.2.9). Six studies have described fMRI in STN DBS patients, five of which used 1.5T scanners. One study examined the micro-lesion effect and has been discussed above (Jech et al., 2012), the remainder studied effects of DBS on the BOLD signal.

Jech et al., were first to report a series of three patients with unilateral electrodes who had fMRI following electrode implantation, before the electrodes were attached to the IPG. The electrodes were attached to an external pacemaker that was turned on and off every 30 seconds during the fMRI session. Such a design enabled the authors to identify which areas showed changes in response to acute STN DBS. No formal group analysis was performed, but subcortical increases were reported in the GP, thalamus, SN, superior colliculus, as well as cortical increases in one patient in the PM and DLPFC, all ipsilateral to the stimulating

electrode (Jech et al., 2001). Another study reports a patient who showed a good motor response in one hemibody, and emotional disturbances when the contralateral electrode contact was employed. Using the same block design as before in the peri-operative period, the authors describe different patterns of BOLD changes when each electrode was activated, with motor improvements associated with subcortical increases in the thalamus, putamen, and cerebellum, cortical increases in PM, and decreased BOLD response in the SMA. Increases in the insula and temporal cortex, as well as decreases in patietal areas are also reported (Stefurak et al., 2003). Hesselmann et al., performed intra-operative fMRI in a patient performing blocks of self-paced finger opposition, once without stimulation, and then with unilateral STN DBS at three different bipolar configurations. DBS was associated with decreases in contralateral (to hand movements) M1, and ipsilateral cerebellum, regardless of which contacts were stimulated. DBS at different contacts (thus theoretically moving the field of stimulation, changing the structures exposed to DBS) produced different magnitudes of reductions, although these differences are not formally statistically analysed. With one electrode combination, which also produced the greatest magnitude of reductions in the above, contralateral increases were detected in the caudate, putamen and insula cortex (Hesselmann et al., 2004). Another series of five patients were scanned using 3T fMRI using a similar alternating ON-OFF unilateral stimulation block design. Again, while no group analysis was performed, most stimulated hemispheres showed ipsilateral increases in the GP, putamen, thalamus and contra-lateral cerebellum, and some showed ipsilateral increases in DLPFC and insula cortex (Phillips et al., 2006). One final published report examined changes in functional connectivity within motor cortical regions following STN DBS in 13 patients, finding increases in eigenvector

centrality[7] in the left PM, that correlated with contralateral clinical disability (Mueller et al., 2013). While these results are interesting and employ a relatively novel approach that speaks to similar hypotheses of connectivity that are tested in this thesis, they are difficult to discuss in full, as the report is only a brief letter, and provides little detail regarding data collection and analysis[8].

While these studies have successfully overcome the technical challenges of scanning DBS patients, a number of comments about study design should be noted:

1. MRI safety – As discussed later, most *in vivo* studies make reference to on-site thermometry to confirm that MR-induced heating at the electrode tips does not exceed international and local guidelines (see 5.5.1).
2. Peri-operative scanning – All the published fMRI studies have occurred during the peri-operative period. As discussed above, following implantation of the electrodes, oedema itself can have therapeutic effects (Jech et al., 2012), and can alter the neural response to DBS. For example, the patient with emotional responses to peri-opertaive stimulation reported in (Stefurak et al., 2003), did not have the same response 4 weeks post-op to identical stimulation (although it still only produced 'mild' improvements in contralateral symptoms). Furthermore, the patients (who are usually older people) have only recently undergone a general anaesthesia, which may similarly alter responses.

[7] *Eigenvector centrality is a graph theoretical description of the functional connectivity of each voxel in a search volume of interest (ideally the whole brain). Voxels with many, strong correlations with other voxels receive a high eigenvector centrality score* (Lohmann et al., 2010; Mueller et al., 2013).

[8] *The authors are currently preparing a manuscript detailing their findings (personal communication).*

3. Statistics – Given the technical challenges involved in scanning patients either during or just after surgery, one can understand why only a handful of patients have been studied, and thus why statistical thresholding in these reports have been fairly liberal (most do not correct for multiple comparisons, or present any formal second-level statistics).
4. Artefact – Of the six reports (and others detailing similar case studies in Vim DBS patients), all observe a susceptibility dropout artefact surrounding the tips of the electrodes. The use of unilateral stimulation in patients with bilateral electrodes have confirmed that the BOLD signal changes are due to the stimulation, and not simply an artefact produced by the electrodes (Phillips et al., 2006).
5. Therapeutic stimulation – Few studies have reported whether the stimulation parameters they employed during fMRI were actually therapeutic. For example, Hesselmann et al., report certain stimulation parameters produced the greatest BOLD changes, but does not specify if these parameters were eventually chosen for chronic therapy (Hesselmann et al., 2004).
6. Bipolar stimulation – All studies conducted before IPG implantation have employed bipolar stimulation, creating current fields that are more focal to the target structure than monopolar fields, that are commonly used therapeutically.

To summarise, only a handful of patients have been studied with fMRI, all of which within days of electrode implantation, before having had their IPG implanted. The designs have been mostly alternating blocks of ON and OFF stimulation in an attempt to determine the regions displaying acute changes in activity, with only a single study exploring effects of STN DBS on movements. In contrast to the PET/SPECT literature, the fMRI studies have

not investigated the effect of therapeutic stimulation as much as they have mapped the key afferent and/or efferents of the STN.

5.4.2.9 Functional MRI in animal models of STN DBS

Two relatively recent studies have been published using fMRI in animal models of STN DBS. Using 6 second trains of 130Hz, 1V or 2V pulses (pulse widths = 500μs) in anaesthetised pigs, Min et al., report voltage dependent event-related responses in both PM and M1, as well as responses in prefrontal, insula and cingulate cortices, and the striatum (Min et al., 2012). Similarly, a study in healthy rats where the frequency of STN DBS was manipulated in a block design report frequency dependent activity increases in M1, S1 and cingulate cortices, peaking at therapeutic frequencies (100-130Hz) (Lai et al., 2014). Both these studies were conducted on healthy anaesthetised animals, with very different local anatomy, particularly the size of the STN: the authors report that the rat STN is roughly 0.8mm^3, 50mm^3 in the pig, and 240mm^3 in the human[9] (Min et al., 2012), requiring augmented stimulation parameters to avoid an excessively large current field (e.g. both studies used long pulse widths that are not typically used in therapeutic stimulation).

5.4.3 Electrophysiology & STN DBS

A lot of work characterising the changes in firing rates in BG nuclei following STN DBS has been undertaken. Studies from the animal literature have demonstrated frequency dependent reductions in STN firing rates following DBS (Beurrier et al., 2001; Meissner et al., 2005), and similar observations were noted in human single unit recordings (Welter et al., 2004). However, both GABA-mediated inhibition, and excitatory responses have been

[9] *Although this figure for human STN volume is markedly larger than most reports in the literature.*

observed down-stream in the rat SNr during STN DBS, suggesting DBS activates the efferent pathways of the target (Maurice et al., 2003).

As attention has shifted to the spectral changes associated with PD (see 0), many have attempted to map oscillatory activity under DBS. However, capturing electrophysiological data during active DBS has been limited due to the artefacts associated with high frequency stimulation. In an attempt to minimise stimulation artefact, most studies either (1) record at distant downstream sites, e.g. STN DBS reduces GPi beta power (Brown et al., 2004), or (2) record immediately after a period of therapeutic stimulation in patients who show slightly longer responses to stimulation finishing, e.g. DBS reduces local beta power in these patients, correlating with clinical effect (Kühn et al., 2008). Eusebio et al., are the only authors so far to document the effects of DBS on the STN LFP *in vivo*, demonstrating time-locked reductions in beta power – see Figure 5.5, taken from (Eusebio et al., 2011a). Similarly, closed-loop DBS using beta power as a biomarker of pathology has been shown to be superior to standard DBS (Little et al., 2013). Thus, there is growing evidence that DBS suppresses expression of local beta oscillatory activity, that is known to be elevated in the off-drug state (Brown et al., 2001; Eusebio et al., 2012). STN DBS has also been shown to reduce STN beta phase coupling with gamma amplitude in M1, although the precise role of phase amplitude coupling is as yet unknown (de Hemptinne et al., 2013).

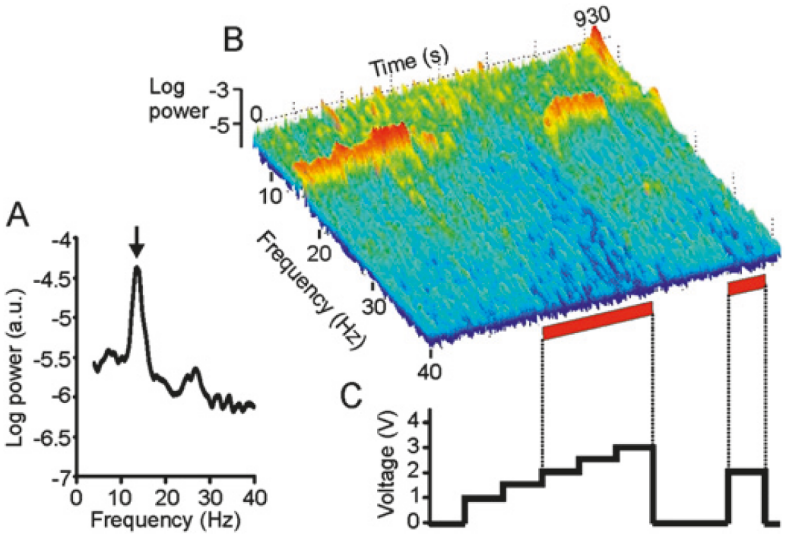

Figure 5.5 Example of beta power suppression during active STN DBS above ~1.5V. (A) power spectrum of the STN LFP recorded off-medication with DBS OFF showing a large peak at 13.6Hz. (B) Time-frequency spectrogram showing the timings of DBS being scaled up over time, turned OFF, and turned back ON again (C). Taken from (Eusebio et al., 2011a).

5.4.4 Conclusions

While much work has been done to characterise the neural response to STN DBS, the neuroimaging literature is plagued with inconsistency. Looking across studies, the direction of modulation in certain regions appears ambiguous. The reason for this can only be speculated. One contributing factor is likely the variability in targeting accuracy and stimulation parameters used, essentially meaning that different centres may be stimulating slightly different parts of the STN and surrounding anatomy. Given the regional anatomy of the target (see section 5.3.1), it is likely that this is an important determinant. Frequency of stimulation is of particular interest given that (1) frequency is an important determinant of clinical efficacy, and (2) this is reflected in neuroimaging signals (Haslinger et al., 2005; Lai et al., 2014). Other factors that could be relevant include patient heterogeneity (including presence of genetic mutations, disease duration, time between implantation and scanning), medication state and whether patients had unilateral or bilateral stimulation. Studies exploring the effect of STN DBS on nigrostriatal DA in humans appear more

consistent. Despite claims from the animal literature, results of the human functional imaging studies fail to evidence any marked changes in DA innervation.

With particular relevance to this thesis, one key conclusion of the literature to date is the paucity of fMRI studies in these patients. This is largely due to the safety concerns of scanning patients with implanted devices. That being said, there have been a handful of studies in DBS patients, using both 1.5T and 3T scanners, with no reported adverse effects of scanning, suggesting that under a safe protocol, fMRI is feasible in these patients. This is discussed further in section 5.5.1.

The literature to date has dealt almost exclusively with questions of functional segregation; in other words, which regions display altered activity under stimulation. However, few have considered the effects of DBS on functional integration, particularly whether and how STN DBS may alter effective connectivity the between regions of the BG and the motor system. It may thus be unsurprising that there remains little mechanistic understanding of what DBS is doing the BG, and how altered brain responses result from stimulation.

5.5 Functional MRI in patients with implanted DBS

5.5.1 Safety

The major, well documented MRI safety concern is rapid temperature increases at the tips of the electrode contacts, due to coupling of the electrical component of radiofrequency (RF) oscillating electromagnetic field excitation pulses applied during MRI to the DBS circuit (known as 'resonant coupling' or 'the antenna effect') (Carmichael et al., 2007; Georgi et al., 2004). The resulting induced currents produce thermal energy elevating tissue temperature to potentially dangerous levels. Furthermore, there is an additional risk that voltages induced in the DBS circuit during MRI could lead to potentially harmful

uncontrolled neural stimulation independent of IPG function. The current UK and international guidelines propose that MRI-induced heating should not cause the temperature within the brain to exceed 38°C, requiring any intra-cerebral heating at the electrodes to be <1°C (HPA, 2008).

Previous *in vitro* studies using various media modelling the thermal and electrical characteristics of neural tissue suggest that electrode heating during MRI is dependent on a number of factors including coiling of the DBS leads (Baker et al., 2005), hardware type and brand (Gleason et al., 1992), scan specific absorption ratio (SAR) (Finelli et al., 2002), field strength (Kainz et al., 2002), as well as the geometry of the RF transmit coil relative to the leads (Rezai et al., 2005). On site thermometry at this centre has previously shown that heating in a Medtronic Kinetra DBS system remains <1°C if scanning is restricted to 1.5T, using a head-transmit/receive coil, and limiting scanner-reported sequence head SAR to less than 0.4W/Kg (Carmichael et al., 2007). Under these restrictions, this centre routinely perform post-implantation electrode placement verification MRI as part of clinical practice (Zrinzo et al., 2011).

As discussed, previous *in vivo* fMRI studies have mostly been done at 1.5T, using a head-transmit/receive coil and low head SAR sequences. However, centres vary regarding how much heating is unacceptable. For example, a 1.5T fMRI DBS study reports to have used a turbo spin echo sequence with head SAR 0.98 W/Kg resulting in 1.1°C of heating (Jech et al., 2012). Another study conducted at 3T reports using a GE-EPI sequence that produced a maximal heating of 1.36°C, quoting guidance from the European Committee for Standardization (EN-45502-1:1997) advising that heating should be kept <2°C (Phillips et al., 2006).

5.5.2 Experimental feasibility

Assuming safe operation can be established, GE-EPI fMRI comparing the BOLD signal 'ON' and 'OFF' DBS stimulation presents an interesting avenue of research.

However, there are a number of potential experimental confounds; the simplest study design would assume that the IPG output is not disrupted by the MR environment. In other words, it is essential that the IPG delivers the intended stimulation during MRI, otherwise the states compared would not relate to the true DBS ON and OFF conditions. In addition, MRI-induced temperature changes could theoretically also confound experimental data physiologically (Boulant, 1998; Guatteo et al., 2005; Kiyatkin, 2007; Travis et al., 1995; Tryba and Ramirez, 2004) potentially altering the assumed constant haemodynamic coupling between blood flow and neural activity. Thirdly, the MRI proton resonant frequency is sensitive to tissue temperature thus local RF-induced temperature increases could cause confounding signal changes during the fMRI experiment independent of activation.

5.5.3 Conclusions

There are a number of variables that affect the safety of scanning patients with implanted DBS systems, and work at this centre has established a protocol that maximises the safety for operated patients (Carmichael et al., 2007). However, this protocol has a number of limiting factors that could be improved if found to be sufficiently safe.

Firstly, from a pragmatic perspective, the current safety studies have only formally tested the Medtronic Kinetra system, a relatively older device that has been all but replaced in the vast majority of patients by the Medtronic ActivaPC™. Thus, it is important to ensure that

scanning patients with newer devices is similarly safe and feasible, so as to maximise the number of patients that could be recruited to have an fMRI.

Secondly, the quality of the data is partly determined by the coils used to collect the data. The rationale for using the head-transmit/receive coil is to restrict RF transmission to the head, in turn theoretically minimising the heating effect at the electrode tips. While this is obviously advantageous, the receive mode of this coil furnishes a lower SNR than that of multi-array head receive coils. It is therefore important to establish whether or not scanning under this optimised arrangement is safe and feasible.

5.6 Aims of this thesis

The overarching aim of this thesis, its *raison d'être*, is to enhance our understanding of the therapeutic mechanisms of STN DBS in patients with advanced PD using fMRI. Specifically, the aims of this thesis are fourfold:

1. Confirm the experimental feasibility of fMRI in patients with advanced disease with implanted STN DBS systems.
2. Identify regions of the brain that are involved in motor control and are modulated by STN DBS in patients with PD, and characterise this modulation.
3. Characterise the neuromodulatory effect on functional integration between cortex and subcortical structures, both during movement, and during rest.
4. Enhance the quality of data acquisition in these patients by using MRI equipment that deliver an improved signal to noise ratio, and confirm the safety of scanning patients under this protocol. This is specifically dealt with in my third experiment.

6 Materials and methods

Parts of the following chapter have been published in Kahan & Foltynie (2013), Neuroimage.

6.1 Summary

In this chapter, I outline the foundations of the key methods employed that are common to most of my experiments. Specifically, I discuss (1) BOLD fMRI, (2) analysis of task-evoked activity using SPM (Friston et al., 1995, 1994a, 1990), and finally (3) dynamic causal modelling of fMRI data (Friston et al., 2003).

The precise methods used in each experiment are outlined in detail in their respective chapters.

6.2 Functional MRI

Magnetic resonance imaging (MRI) is a means of non-invasively imaging three-dimensional volumes, most commonly, various parts of the body. In contrast[10], fMRI is specifically used to detect the magnetic repercussions of changes in blood oxygenation that result from changes of neural activity. The fundamental principles of how this is achieved are discussed below.

6.2.1 The BOLD contrast mechanism

The brain is full of hydrogen atoms, which are essentially single protons with an inherent property (similar to mass or charge) called spin. Protons possess a net spin of 1/2. In the semi-classical vector model, the spins behave like spinning tops and they can be represented by vectors, while in the quantistic representation their behaviour can be described in terms of energy states. The two descriptions are complementary, and help describe different characteristics of the spins. When placed in a strong (static) magnetic field (B0), particles with net spin align themselves in parallel or anti-parallel with B0, in a similar way to how a bar magnet might align itself, with a larger number of spins parallel than anti-parallel to B_0. The resulting net alignment is parallel to B_0 and of a relatively low energy state. Aligned with B0, a particle with net spin can absorb a photon and change to a higher energy state anti-parallel to B_0. The frequency of photon absorbed is dependent on B0, and the gyromagnetic ratio of the particle (for hydrogen 1H = 42.58 MHz / T). This frequency is known as the Larmor frequency. MRI uses static magnetic fields (typically 1.5T or 3T) and electromagnetic waves of radiofrequency (i.e. RF pulses) to manipulate the energy states of hydrogen nuclei within a given volume. Once 'excited' to a higher energy orientation, protons slowly 'relax', i.e. return to the low energy alignment with B0. The relaxation time

[10] *Pun intended*

depends on the tissue types (i.e. it is different in white matter, grey matter, and cerebrospinal fluid). The process of relaxation to the low-energy alignment in physiological tissue can be characterised by changes in two dimensions; (1) longitudinal regrowth - measured by the T1 decay constant, and (2) transverse relaxation - measured by the T2 decay constant (or T2* if local field homogeneities are considered). T2* images are the type of images acquired in fMRI. T2* in a given region is highly dependent on the local homogeneity of the magnetic field (increased inhomogeneity decreases the T2* signal), which in turn is dependent on the composition of the blood in the immediate vicinity, which in turn is dependent on the physiological state of neural tissue. Thus, T2* is an indirect measurement of neural activity, and is herein referred to as the BOLD contrast mechanism (Logothetis and Wandell, 2004).

The BOLD contrast is sensitive to the oxygenation of haemoglobin. The magnetic properties of the ferrous ion buried within the haem group of haemoglobin are dependent on whether it is bound to oxygen or not; deoxyhaemoglobin (dHb) is paramagnetic and disrupts the homogeneity of the field, whereas oxyhaemoglobin (oHb) has a magnetic moment of zero (Pauling and Coryell, 1936). Thus, higher levels of dHb reduce the T2* signal (Ogawa et al., 1990a, 1990b).

Neurons are dependent on a rich oxygen supply to maintain their energetically expensive lifestyles; the brain is responsible for approximately 20% of the body's resting metabolism. The "energy budget" is spent mainly on restoring ion movements generated by postsynaptic currents, uptake of neurotransmitters, and action potentials (Attwell and Laughlin, 2001). These demands scale with the electrical activity of the neural tissue, and thus more oxygen is required in order for neurons to respire aerobically. While there exists heterogeneity across the cortex and between subjects, following a discrete physiological stimulus (e.g. 2

seconds of visual stimulation), the BOLD signal shows a typical response known as the haemodynamic response function (HRF). While neurophysiological responses to such stimuli occur within milliseconds, the HRF is delayed; occurring 1-2 seconds after stimulus onset, rises to a peak within 6-9 seconds, and then returns to baseline; the total time course is typically 10-15 seconds (Kwong et al., 1992). This increase is due to an increase in CBF that (for reasons unknown) over-compensates for any initial oxygen consumption, resulting in a net influx of oHb, known as "functional hyperaemia" (Fox and Raichle, 1986; Fox et al., 1988). This effect is thought to be driven by glutamate released from pre-synaptic terminals, as opposed to a feedback hyperaemia from increased [CO_2] or decreased [O_2] (Attwell et al., 2010a).

Importantly, the BOLD signal is a relative measure. In other words, a control condition is always needed to identify parts of the brain associated with the task condition. For example, if one wants to identify the neural correlates of finger movements, during the length of the scan, the subject must perform finger movements as well as periods of rest.

6.2.2 Electrophysiological correlates of BOLD

Given its latency to stimulus onset, and haemodynamic origins, it is worth briefly considering how the BOLD signal relates to commonly employed electrophysiological characterisations of neural activity. Placing an electrode in the extracellular space permits measurement of the mean extracellular field potential (mEFP); depending on the size (thus impedance) and placement of the electrode tip, the mEFP can detect action potentials of nearby large neurons (Henze et al., 2000), or a combination of dendritic synaptic events and summed action potentials from hundreds of local neurons. The latter can be separated using signal filtering into local synaptic voltages (LFPs, by applying a low pass filter <200Hz), and multiple-unit spiking activity (MUA, by applying high-pass filter >300Hz)

(Logothetis, 2003). In other words, the LFPs measure slower waveforms, thought to reflect synaptic inputs and local intra-cortical processing, whereas MUA measures the output action potentials of the principal neurons (Einevoll et al., 2013). Simultaneous acquisition of mEFP and BOLD data in the primate visual cortex reveal that signal changes following a visual stimulus are best predicted by the marked magnitude changes observed in the LFP signal, suggesting the BOLD signal represents afferents and intra-cortical processing as opposed to spiking output (Friston, 2008; Goense and Logothetis, 2008; Logothetis, 2008; Logothetis et al., 2001). That being said, a number of studies demonstrate a linear relationship between BOLD and spiking rate (Rees et al., 2000), which may not be surprising given spiking is often correlated with responses in the LFP frequencies (Logothetis, 2003).

6.3 Experimental design

6.3.1 Within-subject designs

The four fMRI experiments reported in this thesis employ within-subject designs. In other words, data is collected from same group of subjects both with and without therapeutic DBS. This conforms with the majority of previous studies on DBS. The gold standard for this type of study would be a so-called *double-blind* design, whereby neither the patient nor the experimenter knows whether the DBS is active or not. The striking efficacy of STN DBS in advanced PD (particularly whilst off medication) does complicate this process; especially if the patient is accustomed to what ON and OFF feel like. This is similarly true for the experimenter, most obviously in assessing clinical or behavioural responses to DBS. The method of behavioural task assessment differed between experiments and is discussed in the relevant chapters.

Using a within-subject design does however predispose to carry-over effects such as fatigue or practice effects. To nullify these effects, the order of data collection was randomised across the group; i.e. half of the group were scanned ON DBS and then OFF DBS, and half the group in the reverse order.

6.4 Statistical Parametric Mapping

Throughout this work, analyses of fMRI data were done using the latest version of SPM12b (http://www.fil.ion.ucl.ac.uk/spm/), implemented in MATLAB (The MathWorks, Inc., Natick, MA, USA). Processing and analyses were largely executed in the command line using bespoke looping scripts in an effort to minimise human error. Some of my generic scripts (that call SPM functions) have been made available online for sharing and development. In what follows, I briefly describe the spatial processing that is a pre-requisite to all fMRI data analysis, as well as statistical foundations of the analysis of task-evoked sessions using the general linear modelling (GLM) approach. Throughout this thesis, the term *session* refers to a series of whole-brain images (or *scans*) collected sequentially at a defined inter-scan time interval (also known as *repetition time* - TR). *Scans* refer to individual images within a session; a typical fMRI experiment will run over multiple sessions, each comprised of >5 minutes worth of scans.

6.4.1 Pre-processing

All functional imaging data, regardless of which software suite employed, undergo a series of within-subject spatial pre-processing steps before statistical analysis. All of the imaging data in this thesis underwent the following pre-processing:

1. *Field Map Correction:* EPI datasets are especially vulnerable to geometric distortions caused predominantly by inhomogeneity in the static magnetic field (Jezzard and

Balaban, 1995). These are often most prominent surrounding the petrous portions of the temporal bones, and the frontal sinuses, producing characteristic deformations of the medial temporal lobes and orbitofrontal regions. Following each session, we collected data mapping the magnetic field. Specifically, we measured the change in phase of the MR signal for two images with different echo times. This routine creates a voxel displacement map (VDM) from the field map data, which is used to correct such distortions.

2. *Realignment & Unwarping:* It is almost impossible to keep entirely still throughout the duration of a scanning session. This routine realigns a session of scans from the same subject using the first image as a reference by estimating a 6 parameter spatial transformation, under rigid-body assumptions, i.e. three translations, and three rotations about different axes. The unwarping procedure aims to remove any susceptibility-by-movement interaction that may underlie residual movement-related variance (Andersson et al., 2001). The realignment parameters are then saved and can be subsequently included as covariates in the first-level GLM analysis to further discount any effects of movement during statistical analysis.
3. *Coregistration:* This routine performs within-subject coregistration of functional sessions and anatomical data by maximising mutual information using a rigid-body model. Following this procedure, the registration of functional and structural data was visually inspected using the CHECK REG facility.
4. *Segmentation & Normalisation:* The purpose of this procedure is to warp individual subject data to a standard anatomical space, permitting between-subject comparison using a standardised coordinate system for reporting results. Study specific

templates were not used in the warping procedure, and loss of signal regions were not masked away using lesion masks.

5. *Spatial smoothing:* This step convolves image volumes with a Gaussian full-width half maximum (FWHM) smoothing kernel. Spatial smoothing both reduces any remaining inter-subject difference in gyral anatomy, and boosts the signal-to-noise ratio.

6.4.2 First-level analysis (within-subject)

Questions appealing to functional segregation are best addressed by using a mass-univariate GLM approach (Friston et al., 1995, 1994a). Once the scans and sessions have been aligned (see above), the data from each voxel is treated as individual functional time series of certain anatomical locations. First-level (i.e. within-subject) analyses comprise a model or *design matrix* that defines the experimental setup and the scientific questions to be explored. Each row represents a scan (or time point in the time series), and each column an explanatory variable, of which there are two types; (1) stimulus functions, which are simply the timing onsets of either individual events or the blocks of experimental manipulation of interest, (2) regressors (or covariates), which are known sources of variance orthogonal to the stimulus functions, usually reserved to account for known sources of noise, e.g. head realignment parameters taken from the realignment procedure (see 6.4.1). Prior to modelling, the BOLD signal is high-pass filtered removing any ultra-slow frequency drifts (<0.0078Hz) typically resulting from changes in the ambient temperature in the scanner (known as *scanner drift*).

Under the assumption that the BOLD signal is the output of a linear time-invariant system, (in other words, the response is independent of time, scales linearly with the neural response, and successive responses superpose in a linear fashion,) stimulus functions are

convolved with a canonical HRF, which accounts for the delayed and dispersed nature of the BOLD signal (Henson, 2004).

The GLM approach attempts to model the observed data as a linear combination of explanatory variables. For example, a GLM with two explanatory variables (x_1, x_2) can be expressed as a function of time:

$$y(t) = x_1(t)\beta_1 + x_2(t)\beta_2 + \varepsilon(t)$$

$$\varepsilon(t) \sim N(0, \sigma^2 \xi)$$

In other words, the observed data at a particular time point, $y(t)$, is equal to the linear combination of the explanatory variables, plus an error (or residual) term, which conforms to a zero mean normal distribution with a variance σ^2, multiplied by the noise autocorrelation, ξ. The linear mixture is determined by the regression coefficients (β_1, β_2), which are estimated using an ordinary least squares approach (Friston et al., 1995, 1994a; Kiebel and Holmes, 2004); in other words, in our example, β is optimised based on minimising the discrepancy between y and $x_1\beta_1 + x_2\beta_2$. If the explanatory variables have no predictive capacity of the data, β = 0. An example design matrix is illustrated in Figure 6.1.

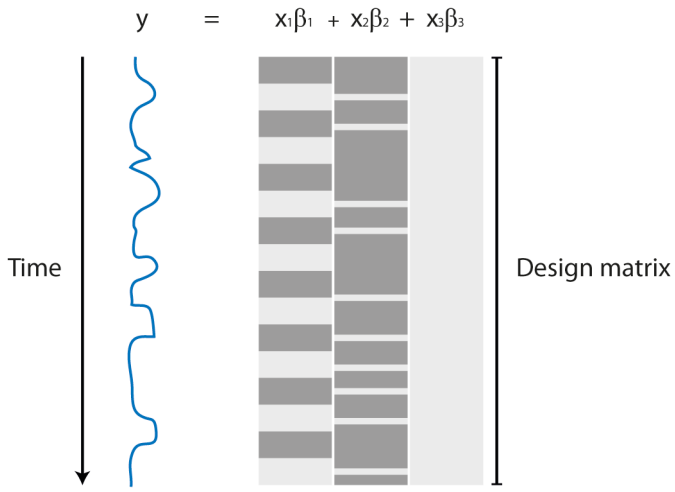

Figure 6.1 Example design matrix for SPM first level analysis. y, the observed BOLD signal recorded from a single voxel over time is equal to the sum of two stimulus functions (convolved with the HRF), multiplied by their beta coefficients, plus a constant (explanatory variable of ones), multiplied by its beta. The design matrix is a scans x explanatory variables matrix. White = high, grey = low.

Statistical inference is conducted through specifying contrasts (simply weighted sums) of β. Returning to our example, the null hypothesis that we may want to disprove is that x_1 has no effect on y, i.e. we wish to test the hypothesis that $\beta_1 > 0$. A contrast weight vector [1 0] is specified and multiplied by our estimate β_1, or $c'\beta$ in vector notation. A T-statistic is calculated according to the formula:

$$T = \frac{c'\beta}{\sqrt{var(c'\beta)}}$$

In other words, the test statistic T is equal to the contrast of β, divided by its variance, which is dependent on both the variance of error term ε, as well as the nature of the contrast and design matrix (e.g. collinearities of explanatory variables). The contrast provides a T statistic for every voxel in the brain, from which P values can be inferred, reflecting the probability that $\beta_1 > 0$ at that voxel is due to chance alone.

Similarly, one may wish to test multiple linear hypotheses at once (e.g. whether x_1 or x_2 significantly explained the observed data). Such inferences appeal to F contrasts, where an F statistic is calculated according to following formula:

$$F \propto \frac{RSS_0 - RSS}{RSS}$$

Put simply, the F statistic is proportional to the normalised difference in the residual sum of squares of the reduced model (RSS_0; i.e. a model that does not include either x_1 or x_2) and the informed model (RSS; i.e. a model including x_1 or x_2).

The result of either contrast analysis is a contrast image containing a test statistic for each voxel. The image is then thresholded to a pre-determined level of significnace creating a SPM. The statistical foundations and derivations of both the T and F tests are discussed at length elsewhere (Friston et al., 1994a; Poline et al., 2004).

6.4.3 Second-level analysis (between-subjects)

First-level inferences from multiple subjects can then be taken to the second level to make between-subject inferences, or put simply, what responses are common/different amongst the cohort. Studies reported in this thesis explore common changes in regional responses upon activating therapeutic DBS. This is pursued using a within-subject design. In other words, each subject is scanned whilst performing a task, with and without therapeutic DBS. Typically, the first level analysis results in a contrast image identifying voxels significantly demonstrating a *task x condition* interaction. Using a summary statistic approach, these contrast images become the data for a second-level analysis, where we test the hypothesis at the group level, taking into account the between subject variability (i.e. a random effects analysis), creating a new group-level SPM.

6.5 Psychophysiological interactions

PPI analyses appeal to questions of functional integration. Specifically, PPIs are an efficient way of searching the brain for voxels exhibiting context-dependent coupling with a source region. Original descriptions of PPIs suggest they are a very simple measure of effective connectivity as they are based on linear regression analyses, which are, by their very nature, directed (Friston et al., 1997), however, some consider them to describe functional connectivity.

The purpose of the PPI is to identify voxels in the brain that demonstrate a context-dependent change in coupling with a source region. In a standard 2 x 2 experimental design (i.e. two experimental effects, each with two conditions; e.g. attention – high vs. low, and visual stimulus – static vs. motion), the observed data can be summarised by the following linear model:

$$y = \left(Att_{high} - Att_{low}\right)\beta_1 + \left(Vis_{motion} - Vis_{static}\right)\beta_2 + \left(Att_{high} - Att_{low}\right)\left(Vis_{motion} - Vis_{static}\right)\beta_3 + G\beta_4 + \varepsilon$$

Where β are regression coefficients for the following; β_1 = main effect of attention, β_2 = main effect of visual stimulus, β_3 = attention x motion interaction, β_4 = covariates, and ε = error. Replacing one of the experimental effects with a region of the brain (V1) would produce the following:

$$y = \left(Att_{high} - Att_{low}\right)\beta_1 + V1\beta_2 + \left(Att_{high} - Att_{low}\right)V1\beta_3 + G\beta_4 + \varepsilon$$

Using this formulation, β_2 = main effect of V1, and β_3 represents the PPI between activity in V1 and attention. Placing a simple T contrast [0 0 1 0] would thus identify voxels that show an attention dependent coupling with V1. In other words, the regression slope

between the source activity and the target will be significantly different under a high attention setting.

Unfortunately, interpretation of PPIs can be somewhat confusing, due to two potential explanations of the observed interaction. Specifically, a significant PPI between region A, condition U, and region B, could either mean that (1) condition U modulates the effective connectivity from A to B, or (2) activity in region A modulates the sensitivity of region B to input U. This is represented in graphical form in Figure 6.2.

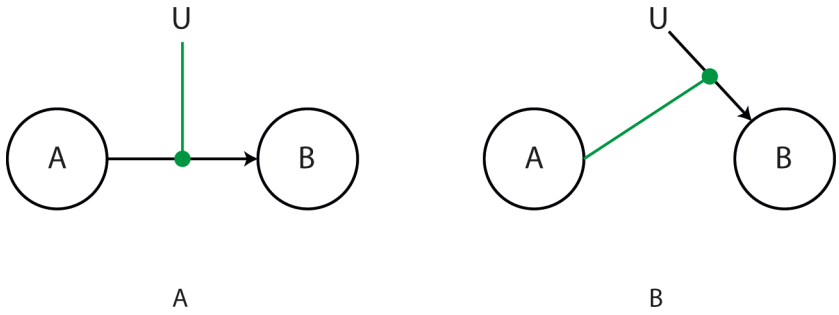

Figure 6.2 Two possible interpretations of a PPI. A PPI created using BOLD signal from region A, and the psychological condition U, finds region B to be significantly modulated. This could mean that either (A) input U modulates the effective connection from A to B, or (B) region A modulates the sensitivity of B to inputs from U. Modulatory effects always in green with solid circle arrow.

6.6 Dynamic Causal Modelling

> *"A Bayesian is one who, vaguely expecting a horse and catching a glimpse of a donkey, strongly concludes he has seen a mule"*
>
> Stephen Senn, 1997

Dynamic causal modelling is a method used to fit differential equation models of a group of interacting regions (or *nodes*) to neuroimaging data using Bayesian inference, yielding estimates of the (context dependent) coupling (or effective connectivity) within and between nodes (Friston et al., 2003). Using a fictitious example, I will briefly outline the

method, as well as extensions that are employed in this thesis. I will conclude with a brief discussion of why I chose DCM and not other methods.

In the case of fMRI, one could consider the BOLD signal a dependent, *measurable* (or observed) variable (y) of the underlying neural activity (z) that cannot be measured with fMRI (thus, the neural activity is an example of a "hidden state variable"). This concept has been used in all GLM-based analysis of fMRI data, and is identical in DCM with one key difference (see footnote[11]).

In a fictitious visual perception experiment, imagine a subject is placed in an MRI scanner and presented with a visual stimulus periodically (Figure 6.3). The timings of stimulus-presentations are used to create an explanatory variable of the whole-brain BOLD data, and we find three clusters (that is, groups of voxels) are significantly explained by this explanatory variable (i.e. regions that show an altered response). Now imagine one knew the functional architecture of the highlighted brain regions; that is, how information propagates through these connected and functionally specialised regions to produce the observed results.

One such architecture could be as depicted in Figure 6.3b. In this example, presentation of the visual stimulus u_1 may cause a change in the neural activity (z) of region 1 (z_1), which in

[11] *Standard GLM analyses rely on convolving a stimulus function (representing onsets and durations of stimuli – an assumed neural model) with a HRF to produce an explanatory variable (an exogenous input) that is used to identify brain regions related to the stimuli. This essentially treats voxels as isolated regions, testing to see which voxels are sensitive to the input. DCM also uses convolution models, with two key differences: Firstly, neural states (z) causing BOLD data (y) in DCM are sensitive to both exogenous inputs (as in GLM analyses) and afferents from other regions. Secondly, the convolution model implicit in DCM is nonlinear due to some mild nonlinearities in the haemodynamic response, dealt with in GLM analyses by including basis functions of the HRF* (Friston, 2002; Friston et al., 2003). *In short, DCM is simply a generalisation of the convolution models used in all GLM analyses, the only important difference is that DCM allows the experimenter to additionally consider the effects of other regions on a their neural model.*

turn causes a change in the measurable BOLD signal (y) of region 1 (y_1). Z_1 then causes an effect on z_2, mediated by the extrinsic connection from 1 to 2 ($a_{2,1}$). Likewise, z_2 in turn causes an effect on z_3. In addition, these regions contain some self-inhibitory properties, mediated by intrinsic connections, e.g. $a_{1,1}$, preventing runaway outbursts of neural activity. Note that this chain of events only occurs with presentation of our visual stimulus, thus the model only explains the network dynamics in that instance. It does not tell us the dynamics when the stimulus is not present (e.g. at rest) or when the visual stimulus changes (to say, an emotional face). Obviously, this functional architecture is only one possible model of how our visual perception data are generated; there are a number of other equally plausible models that could underlie this network.

Measures of effective connectivity in DCM consider the rate of change of neural activity with respect to time ($\dot{z}$) in response to some incoming signal (be it from another brain region or an exogenous environmental stimulus). Most (possibly all) connections that exist in the brain are reciprocal, thus in order to mathematically dissect the effect of one region on another, we must consider that the impact of one region onto another is delayed in time (utilising the principles of *dynamical systems theory*) (Daunizeau et al. 2011).

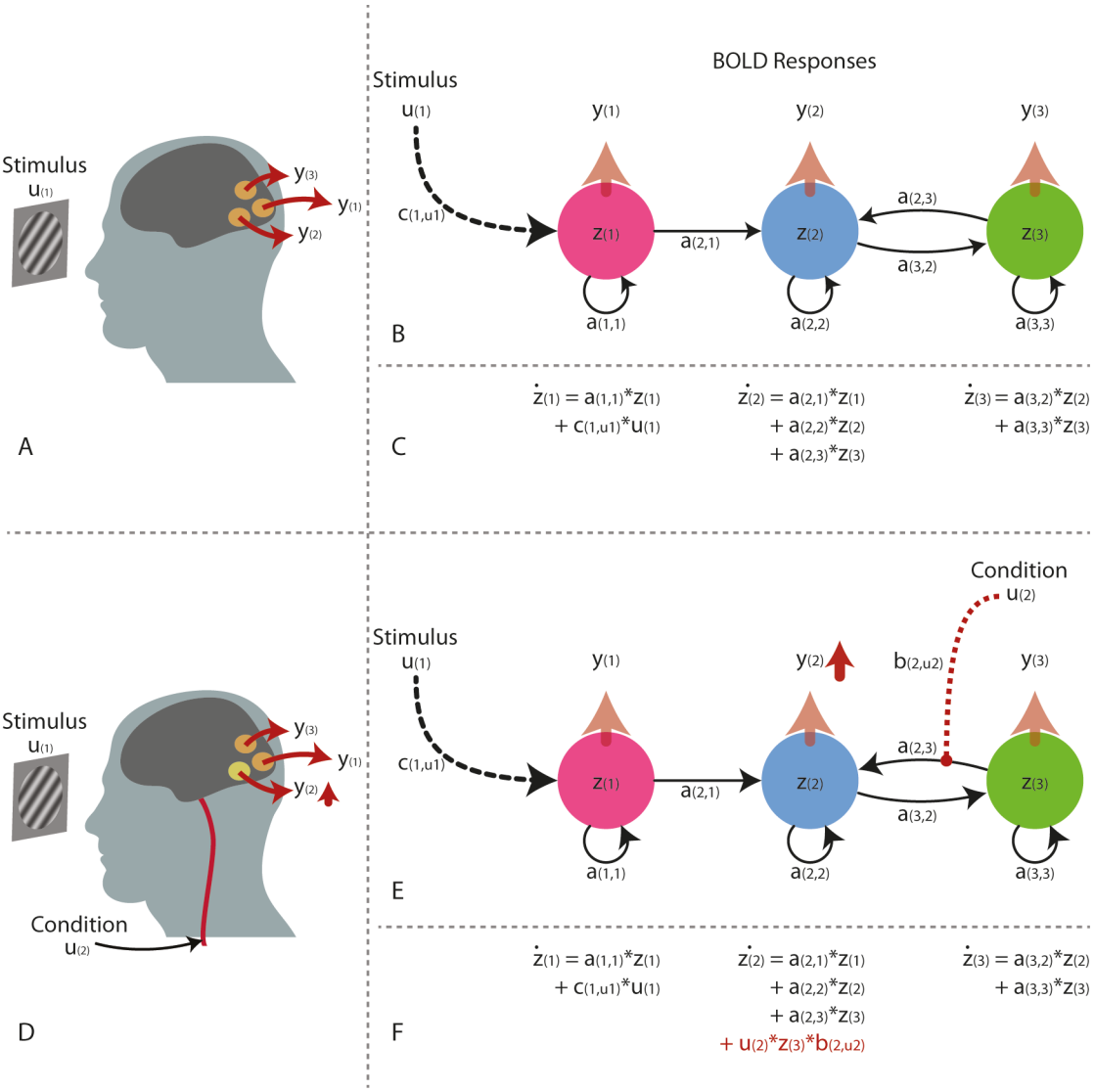

*Figure 6.3 Our fictitious visual perception fMRI experiment. This experiment consists of two experimental manipulations or 'inputs' (u); $u_{(1)}$ = visual stimulus input, $u_{(2)}$ = drug input. Coupling parameters denoted by $a_{(k,j)}$ represents the effective connectivity from node j to k, in the context of stimulus $u_{(1)}$. Parameters labelled $c_{(k,u)}$ denote the effect of the input on target node k. Parameters labelled $b_{(k,u)}$ denote the modulatory effect of the input on target connection. When the subject views the stimuli in the control state (**A**), three brain regions are shown to be related to the onset of the stimuli. The BOLD signal from each of these regions is represented by $y_{(1)}$, $y_{(2)}$ and $y_{(3)}$. (**B**) The BOLD signal from a single region is produced by a change in its underlying neural activity z, which has not been measured during the experiment. The underlying neural activity of region 1 has an effect on the underlying neural activity of region 2 (an extrinsic connection); the strength of this effect is determined by the value $a_{(2,1)}$. The underlying activity of region 1 also has some self-inhibitory dynamics (intrinsic connection), determined by the value $a_{(1,1)}$. The equations of motion (**C**) show the rate of change of each of the regions' underlying neural activity, ż. During the drug condition, an interaction is found in region 2 (**D**). This is modelled as a modulatory drug input having an effect on the strength of the extrinsic connection $a_{(2,3)}$ (**E**). The strength of this effect is determined by the value $b_{(2,u2)}$. (**F**) The equations of motion have thus changed to accommodate this additional modulatory input.*

In order to quantify effective connectivity, one must create a plausible model of how the observed BOLD signal y may be generated by these influences (this is known as a "generative model"), just as was done in Figure 6.3b. This departure from analysing y, to considering how y is generated is an important distinction to understand. When we model data it is important to consider we are rarely able to fully explain how observed data are generated by complex systems – the aim of modelling is really to provide a parsimonious and plausible mechanism with which to better understand such systems.

DCM has become the method of choice for modelling causal interactions in neuroimaging data. The most common implementation of DCM (standard/deterministic DCM) assumes that the system modelled is fully deterministic, meaning that the evolution of hidden neural activity over time in a given region ($\dot{z}$) is purely due to its afferent (incoming) connections and experimental inputs (as described in Figure 6.3c). Note the distinction between an afferent and an input. An afferent arrives from a node (distant or self), whereas an input is introduced by the experimenter (for example visual input from the retina, via the lateral geniculate nuclei – neither of these neural populations are themselves included in the model, rather it is assumed that they convey the convolved stimulus function coding visual input to a region). Theoretically therefore, if all the afferents and inputs to a region (including intrinsic connections) were removed, the rate of change of neural activity z ($\dot{z}$), would be zero, thus activity would remain constant. Such assumptions may not always be ideal as they forgo autonomous dynamics that may characterise certain brain regions (e.g. SN neurons), or periods where there are no experimental inputs (such as resting state fMRI), or regions not showing experimentally evoked effects.

The effect an afferent has on the dynamics of the node depends on the connection strength (or "coupling parameter" – e.g. the size of value $a_{2,1}$) and the activity at the source of the

afferent. This is similarly true of inputs; the influence of an experimental input is determined by the value of $c_{1,u1}$.

6.6.1 Bilinear effects

Now imagine the visual experiment is repeated in the same subject, this time after they have received a drug infusion (for pure theoretical perfection, imagine that this drug had no effect on neurovascular coupling, and had very slow pharmacokinetics) Figure 6.3. New fictitious findings now show the same regions to be active again, and the BOLD signal y_1 and y_3 remains unchanged. However, an interaction between visual stimulation and drug was noted in the observed responses of region 2; under drug, y_2 consistently increases.

Now, returning to our generative model, we can say that because the observed y_1 and y_3 are unaffected by the drug, it is likely that z_1 and z_3 have also remained largely unaffected. The changes noted in y_2 can only be explained by changes in z_2, and – under deterministic assumptions – this must be explained by a change in one (or more) of the coupling parameters of its afferents. In order to explain interactions, separate experimental inputs can enter the model as modulatory effects on a connection, as shown in Figure 6.3e. In our example, the effect of drug (u_2) is modulating the connection $a_{2,3}$, according to the strength of the modulatory effect, $b_{2,u2}$, culminating in changes in $\dot{z}_2$. Notice that these are changes to a rate of change ($\dot{z}_2$), thus are called "second order" or "bilinear effects". This is because the modulatory input and the afferent input interact to affect the rate of change of neuronal activity. The astute reader will notice that changes in $\dot{z}_2$ could have been caused by modulatory effects on any of the other afferents into node 2 ($a_{2,1}$ or $a_{2,2}$ or both). This highlights the problem of competing hypotheses (explanations) in data modelling and will be discussed later.

6.6.2 DCMs estimate the coupling parameters given the structure of the model, the experimental inputs, and the observed data

The purpose of a DCM analysis is to estimate the coupling parameters of a model (the *a, b* and *c* values), and evaluate how well a particular model explains the observed data. This allows the experimenter to make inferences about the structure of the network, as well as/or quantify the coupling strength and direction of coupling between regions. Importantly, neither of these questions can be answered by looking at correlation strengths as in functional connectivity.

6.6.3 The evolution equations

In our example, we have three equations that define $\dot{z}$ for each of our nodes (under deterministic assumptions); these are known as the *equations of motion* (or *evolution equation*) because they described the motion or rate of change of the hidden neuronal states (displayed in Figure 6.3C & F). Equations of motion in DCM generally take the form:

$$\frac{dz}{dt} = \dot{z} = F(z, u, \theta)$$

In bilinear DCM, *F*, in a DCM with *m* inputs, is specifically:

$$\dot{z} = Az + \sum_{j=1}^{m} u_j B_j z + Cu$$

In other words, the rate of change of the hidden neural activity in a given region is a nonlinear function of the current hidden state at a distant region times the strength of the endogenous coupling between the two nodes (*A*), plus any bilinear effects of the inputs on any afferent coupling (*B*), plus any driving inputs arriving at the node multiplied by the coupling of the exogenous input (*C*).

6.6.4 Model estimation

DCM uses an expectation maximisation (EM) algorithm to produce probabilistic estimates of the expected value of each parameter, in addition to its variance (under the assumption that the parameter values conform to Gaussian assumptions, i.e. the parameter values are normally distributed). These values (or *posterior estimates*) are conditional on the model structure, thus models with a different architecture, will have different posterior estimates. In other words, posterior estimates are the most likely parameters, given a particular model and data. The aim of the estimation process is to refine the model parameters, so that the model produces a predicted signal that is as close as possible to the observed BOLD data.

In order to do this, one would need to understand the relationship between the z values for each node and the observed BOLD signal y. The relationship between neuronal state and observed signal can be modelled as a series of nonlinear biological processes depending on the neuroimaging modality utilised. For fMRI data, this originates with neuronal activity, causing an increase in the vasodilatory signal. This results in a proportional increase in flow into the region with concomitant changes in blood volume and deoxyhaemoglobin content, causing the observed change in BOLD response (Friston et al. 2000; Buxton et al. 1998). This is called the *haemodynamic forward model* or the *observation model*, mapping the hidden state to the observed data. This mapping is dependent on a number of haemodynamic parameters that, like the coupling parameters, require estimation.

EM tunes the coupling and haemodynamic parameters so as to maximise the concordance between predicted and observed BOLD signal in a way that avoids using unlikely parameters (large parameters that render the model unstable or those that deviate substantially from prior assumptions on both coupling and haemodynamic parameters – the latter based on those obtained in (Friston 2002)).

6.6.5 Model evidence

The estimation procedure additionally scores the model in terms of how well it explains the data. It is important to note that this scoring is corrected for how many free parameters were estimated; mathematically, a model that has modulatory effects at two connections has the potential to explain the data better (i.e. it could be more accurate) than a model with modulatory effects on one connection. This would introduce a bias towards complex, "over–parameterised" models guilty of "over-fitting"; models that capture noise and over-fit data are less generalizable, thus have limited mechanistic value. This scoring is in terms of *model evidence* (or more accurately, the *Free energy*, which is an approximation of the model evidence), and is a compromise between model accuracy and model complexity, avoiding bias towards over-parameterised models.

6.6.6 Bayesian model selection

The model evidence can subsequently be used to compare a series of models to assess which of a number of plausible models is the most likely to have generated the observed data. This necessitates the investigator to have a series of equally likely competing hypotheses of the underlying functional architecture (or *model space*) to test *a priori*.

Differences in relative *log-evidences* (the logarithm of model evidence) can then be summarised as a conditional probability for each competing model, representing the probability of that model, given the observed data. This process of comparing the evidence for different models is known as Bayesian model selection (BMS) and has been extended to compare models in group studies, and compare different families of similar models (Penny et al. 2004; Stephan, Penny, et al. 2009; Penny et al. 2010).

6.6.7 Extensions: Two-state DCM for fMRI

Two-state DCM for fMRI incorporate an excitatory and inhibitory state per region (Marreiros et al., 2008). Under default settings, all extrinsic projections are between excitatory states, meaning extrinsic connections are always excitatory, which may be more biologically plausible when dealing with long-range cortico-cortical projections. In contrast to standard DCMs where the intrinsic dynamics are simply represented by the intrinsic coupling parameter, in two-state DCM intrinsic dynamics are mediated via four intrinsic coupling parameters, of which only one is free to vary during model estimation. This extension is useful for a number of reasons. I have chosen to make use of this extension in my later chapters because of its ability to incorporate prior beliefs regarding the nature of extrinsic coupling. By default, an extrinsic connection projects from the excitatory subpopulation of one node to the same subpopulation in another, rendering the coupling excitatory. By the same logic, inhibitory coupling can be enforced by simply 'rewiring' the extrinsic connection to project to the inhibitory subpopulation (see Figure 6.4).

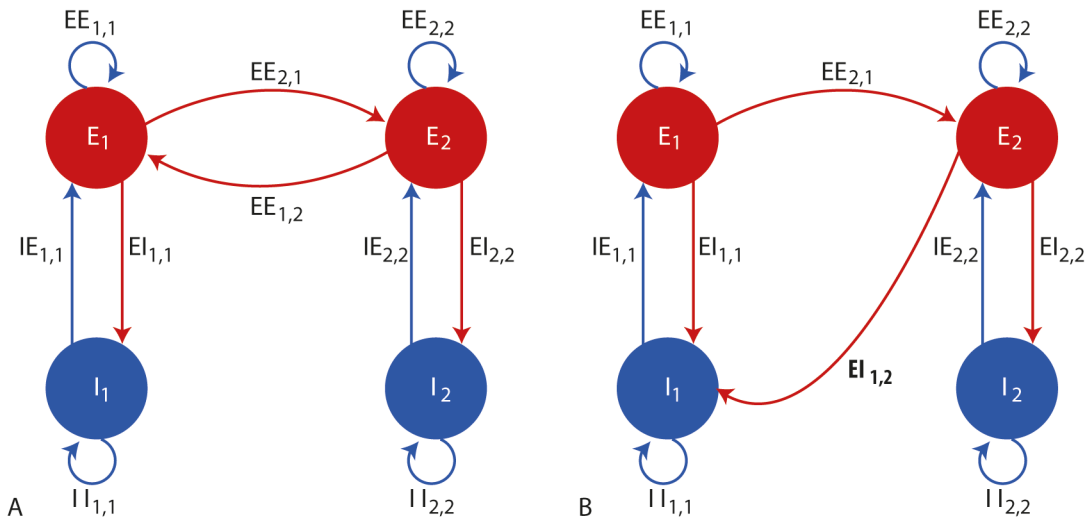

Figure 6.4 'Rewiring' two-state DCM for fMRI to produce inhibitory coupling. Red and blue circles represent excitatory and inhibitory subpopulations respectively.

6.6.8 Extensions: Stochastic DCM for fMRI

In stochastic DCM, we no longer rely on deterministic assumptions and include endogenous (stochastic) fluctuations in the evolution of regional activity. These fluctuations can be conceptualised as autonomous dynamics that are not caused by exogenous inputs, sometimes referred to as *state noise* (Li et al., 2011). In the case of stochastic DCM for fMRI:

$$\dot{z} = F(z, u, \theta) + \varpi$$

Here, ϖ represents stochastic inputs that drive each node in addition to any other exogenous input. Stochastic DCM estimates the hidden states, coupling parameters and haemodynamic parameters, as well as the stochastic inputs (sometimes referred to as *hidden causes* in the literature) using a variational Bayesian generalised filtering scheme that is discussed in detail in a series of technical papers (Friston et al., 2010; Li et al., 2011). This extension has previously been face and construct validated for fMRI data with both high and low levels of physiological noise (Li et al., 2011). Recently, stochastic DCM has been used to model periods of no experimental stimulation, i.e. subjects in the 'resting' state (Urner et al. 2013).

6.6.9 Criticisms of DCM for fMRI

Since its introduction in 2003, DCM has been used to answer a multitude of neurobiological questions, usually comparing competing hypotheses of underlying functional architecture using BMS. There have been a number of papers voicing their concerns for the method, the most notable being (Lohmann et al., 2012). Lohmann et al., highlighted two key issues:

1. *The combinatorial explosion* – The authors point out that models containing a large number of nodes contain large numbers of edges, and if the point of your research question is to ascertain the presence of edges, or whether inputs act upon them, there are very large numbers of potential competing hypotheses. Furthermore, using a common DCM dataset, the authors demonstrate that if the reported winning model is compared to a series of biologically implausible models, BMS identifies the implausible models as more likely generators of the data.
2. *Model fits* – The authors then highlight that while BMS reports which of a series of models is the best, reporting of absolute model fits are often not included in DCM studies. Specifically, they highlight especially poor model fits for subcortical regions (e.g. the lateral geniculate nucleus) with R^2 values in the range of 0.002 – 0.044, which they argue brings the validity of the inferences into doubt.

In response, Friston et al., suggest that (Friston et al., 2013a):

1. The combinatorial explosion is primarily a problem of network discovery, not necessarily if you are comparing a series of *a priori* competing hypotheses. Furthermore, if one were to use family analysis to compare plausible vs. implausible models, one would likely find that the plausible ones are more likely generators of the data.
2. To address the issue of model fit in the lateral geniculate nucleus, the authors suggest that different parts of the brain can have different levels of noise – this could simply be a greater level of observation noise at the subcortical nodes. Furthermore, model selection purely based on model fit would bias selection towards complex models that may be over-fitting the data.

Daunizeau et al., have similarly critically reviewed DCM (Daunizeau et al., 2011). They report that criticisms generally either question the (1) plausibility of the biophysical model, (2) robustness of statistical inference, or (3) pragmatics of implementation. With regard to plausibility, DCM for fMRI employs a relatively simplistic generative model of neural activity that does not rigorously model the complex canonical cortical circuits in the way electrophysiological DCMs do. Ultimately, this limitation is common to all inferences made from fMRI, that is, the neural signal is observed through the haemodynamic response (essentially temporally smoothing the data). This results in a relatively poor temporal data structure in comparison to MEG/LFP acquisition. Thus, arguably, the plausibility of the observer model is of greater importance. In this regard, while DCM for fMRI estimates haemodynamic parameters for each node individually, the model could be better informed by including (1) how inhibitory activity impacts on the haemodynamic response, or (2) how synaptic activity causes vasodilation, with particular reference to glia (Attwell et al., 2010b). That being said, validation plays an important role in DCM development, each DCM undergoing face and construct validity (Friston et al., 2003; Moran et al., 2009), and notably predictive validity in the case of both deterministic and stochastic DCM for fMRI (Daunizeau et al., 2012a; David et al., 2008).

Criticisms of the statistical robustness include (1) the vulnerability of free energy optimisation (e.g. models converge at a local minima, rather than the global minimum of the free energy landscape), and (2) the potential overconfidence of posterior estimates of variational Bayesian schemes. Pragmatic issues raised include optimal experimental design and model space definition, however both point are common to any scientific inquiry. Detailed discussion of these points can be found in (Daunizeau et al., 2011), who conclude that "*the DCM approach must strike at a compromise between biophysical realism and model*

identifiability; both are required to answer difficult questions about brain function". In sum, both informing the models with a greater biophysical plausibility, and advancing the statistical inferential machinery will be required to enhance implementations of DCM, but currently, the method offers a compromise to deliver a mechanistic insight into brain function. That being said, these critiques have highlighted that users should not proceed without thorough understanding of the underlying assumptions.

6.6.10 Alternatives to DCM

Finally, it is worth briefly discussing other established analyses of effective connectivity, namely structural equation modelling - SEM - (Büchel and Friston, 1997; McIntosh and Gonzalez-Lima, 1994), or granger causality modelling - GCM - (Roebroeck et al., 2005).

GCM was first introduced within econometrics (Granger, 1969), and later to neurophysiology (Bernasconi and König, 1999). The method emphasises the role of temporal precedence in causality. Specifically, A 'Granger causes' B if A helps predict the future of B, better than information already in the past of B (Friston et al., 2013b). Application to fMRI data has only taken off relatively recently (Goebel et al., 2003), and is more controversial given the slow dynamics and regional variability of the HRF (dealt with in DCM by estimating region-specific haemodynamic parameters). Importantly it is worth emphasising that GC models dependency amongst observed data, whilst DCM models coupling amongst hidden neural states. One recent study using Human Connectome data has found that regions close to large veins and sinuses display the largest Granger causality lags (Taylor Webb et al., 2013), i.e. regions effecting other regions tend to map to arteries, and receiving regions tend to map to veins and sinuses, suggesting GCM is overly biased by non-neural artefact (i.e. blood flow).

SEM was also imported from econometrics to determine task dependent changes in path coefficients, under the assumption that nodes are driven by stochastic processes (in other words, there is no designed perturbation of the dynamics by experimental stimuli like in DCM). Parameters are estimated by minimizing the difference between the observed nodal covariances, and those implied by a structural model specified *a priori* (Büchel and Friston, 1997). Like GCM, SEM is also performed at the level of the observed signal.

7 The effect of STN DBS on voluntary movement-evoked neural activity

Parts of the following chapter have been published in Kahan et al., (2012) PLoS ONE.

7.1 Summary

In this chapter, I present the results of my first fMRI experiment in 10 PD patients with STN DBS whilst they performed voluntary joystick movements, once with DBS ON, and once OFF. Data was collected under a previously approved scanning protocol. Despite the technical demands associated with the safe acquisition of fMRI data from patients with implanted hardware, movement x DBS (ON>OFF) interactions were detected in the insula cortex and thalamus using small-volume corrected (SVC) statistics.

I then asked whether these observed changes were simply caused by modulation of *intrinsic* coupling, or whether STN DBS had modulatory effects on *extrinsic* coupling between the cortex and thalamus. As a proof of concept, competing deterministic DCMs consisting of a thalamic and cortical node (insula cortex in this case given the observed interaction) were estimated, and BMS was used to identify the most likely generator of the data. Results suggest unequivocal evidence for the modulation of reciprocal extrinsic connections.

My conclusions are twofold: Firstly, fMRI is feasible in a cohort of patients with chronically implanted DBS, although technically challenging. Secondly, in a simple model of cortico-thalamic coupling, STN DBS has modulatory effects on reciprocal cortico-thalamic effective connectivity.

7.2 Introduction

As outlined in Chapter 5, STN DBS is now a recognized treatment for patients experiencing the motor complications of PD (Fasano et al., 2010; Foltynie and Hariz, 2010; Krack et al., 2003). However, its mechanisms of action remain unclear. High frequency stimulation has been found to both inhibit and excite different neurons within the target nucleus, having different effects on different neural elements (Hammond et al., 2008). Evidence exists for both orthodromic stimulation of STN efferents, as well as for antidromic stimulation of STN afferents (Gradinaru et al., 2009; McIntyre et al., 2004b). In addition, abnormal *patterns* of synchronized firing in the STN observed in PD patients are suppressed by STN DBS (Hammond et al., 2007; Litvak et al., 2011).

As reviewed in section 5.4.2, PET and SPECT studies have reported changes in regional activity in response to STN DBS, although the results are sometimes conflicting. Regarding movement-related activity, studies have reported DBS increasing activity in the supplementary motor area (SMA), anterior cingulate cortex (ACC) and dorsolateral prefrontal cortex (DLPFC) (Ceballos-Baumann et al., 1999; Limousin et al., 1997; Strafella et al., 2003a; Thobois et al., 2002). Additional changes have been noted in the cerebellum (Grafton et al., 2006; Payoux et al., 2004), as well as within the subcortical structures comprising the BG (Hesselmann et al., 2004; Thobois et al., 2002).

While altered regional responses have been explored, relatively little is known about the effect of DBS on connectivity amongst functional brain networks. Neural processing is dependent upon functional integration, that is, finely tuned collaboration between functionally specialized regions (Friston, 2009). Increased functional connectivity in frontal-temporal-parietal-striatal-thalamic networks has been reported in response to DBS

of the fornix in patients with Alzheimer's disease, and of the external pallidum (GPe) in patients with Huntington's disease (Ligot et al., 2011; Smith et al., 2012). One study has reported changes in effective connectivity under STN DBS during a response inhibition task; Thobois et al., used a PPI analysis to show altered output from the GPi to the cortex under STN DBS (Thobois et al., 2007), however did not explore reciprocal cortico-subcortical coupling, and the PPI could be ambiguous (see section 6.5 & Figure 6.2).

As discussed in section 5.4.2.8, fMRI has advantages over tracer-based imaging including a superior spatial resolution as well as valuable data modelling methods, but its use in DBS patients has been limited by safety concerns. As a result, only a handful of DBS patients have been evaluated using fMRI, all during the peri-operative period, without internalized neuro-pacemakers (IPGs), that is, before therapeutic stimulation had been established. However our own *on-site* studies have now confirmed that fMRI can be safely performed during active DBS with a completely internalized system, provided strict procedures are followed (Carmichael et al., 2007).

7.2.1 Aims

The aims of this study were threefold:

1. Confirm the technical feasibility of fMRI during therapeutic STN DBS in patients with PD, and identify potential improvements to the protocol.
2. Identify regions displaying a *movement x DBS interaction* (either ON>OFF or OFF>ON).
3. Model the cortico-thalamic effective connectivity, and how it is modulated by STN DBS; specifically, is there evidence for altered cortico-thalamic coupling.

7.3 Materials and methods

7.3.1 Ethics Statement

This study was approved by the National Hospital and Institute of Neurology Joint Ethics committee (approval number 09/H0716/51). All participants provided written informed consent.

7.3.2 Patients

Ten PD patients took part in this study Table 7.1. All patients had PD meeting UK brain bank criteria, and had received bilateral STN DBS for at least 6 months. Surgery had been performed using stereotactic MRI for both preoperative targeting and immediate postoperative verification of lead location prior to implantation of the extension cables and the IPG (Foltynie and Hariz, 2010; Holl et al., 2010).

7.3.3 Stimulation Equipment

All patients had bilateral STN electrodes (model 3389, Medtronic, Minneapolis) and a dual channel IPG (*Kinetra*, Medtronic, Minneapolis) implanted. Stimulation parameters had been previously optimised according to clinical response. Inclusion in this study was restricted to those patients who:

1. Could tolerate lying flat while being *both* off medication and off stimulation
2. Exhibited minimal head tremor
3. Demonstrated an immediate >35% improvement in UPDRS part 3 (UPDRS-III) off-medication score when stimulation was switched ON compared with OFF.

Medication was withdrawn for 10-12 hours (overnight) before the scanning session. Before scanning, (1) UPDRS-III motor scores were documented both ON and OFF stimulation

(OFF was scored approximately 10 minutes after stimulation was stopped), (2) stimulation parameters and system impedance were recorded, and (3) IPG counters were reset.

Participants wore MRI compatible isolating headphones and held an MRI compatible joystick in one hand (Cambridge Research Systems, Kent, England: model No: HH-JOY-4. Angular range: 30 degrees (+/-15 degrees), Grip: 11.5 x 3 cm). The position of the joystick in time and space was recorded at a sampling rate of 20Hz. During the task, participants were instructed to move the joystick consistently in response to auditory stimuli and to avoid excessively fast or large movements[12]. Their heads were securely supported using a vacuum moulded cushion to dampen any head movement. Patients held an alarm in their non-moving hand to alert the clinical team if they experienced any discomfort during the scan. Patients were asked to keep their eyes closed throughout scanning.

The task was performed both with therapeutic stimulation active (ON), and again when their stimulation was inactivated (OFF). During each stimulation condition, the task was performed twice, once with each hand. In other words, every patient performed a right and left hand movement task while stimulation was ON and OFF. The order of stimulation (ON versus OFF) and the movement (right versus left) were randomised over subjects. DBS was switched ON or OFF using the patients' own *Access™* controller, which we ensured functioned normally within the MRI environment.

7.3.4 MRI data acquisition

All scans were performed with a Siemens Avanto 1.5T MRI scanner (Siemens, Erlangen, Germany) using a Siemens-supplied head-transmit/receive coil, similar to the one that

[12] *In piloting this task, we found that such movements resulted in the joystick handle falling off.*

detailed tissue-equivalent test-object thermometry experiments had been performed with in the on-site safety study (Carmichael et al., 2007). The specific absorption ratio (SAR) in the head was limited to under 0.1W/Kg.

Acquisition parameters were as follows:

1. T1 weighted magnetization-prepared rapid gradient-echo (MPRAGE) structural scan (repetition time TR=1590ms, echo time TE=3.3ms, inversion time TI=1100ms, flip angle=15°, field of view FOV=250x250mm^2, matrix size=192x192, 144 sagittal slices 1.3mm thick, for a spatial resolution of 1.3mm isotropic) lasting approximately 10 minutes. This scan, and an additional 8 minute resting scan (reported in Chapter 8), allowed a constant period of equilibrium to follow each patient's stimulation adjustment.
2. GE-EPI Movement session, Hand 1: (TR=3695ms, TE=40ms, flip angle=90°, FOV=192x192mm^2, matrix size=64x64, 49 axial slices 2.5mm thick, gap between slices of 0.5mm, for a spatial resolution of 3x3x3mm^3, 96 volumes, acquisition time=6 minutes). The fMRI task paradigm consisted of 12 blocks lasting ~30 seconds each. During each block, a series of 15 audio stimuli (*beeps*) were sounded through the headphones. The time between *beeps* was randomised to between 1-3 seconds. The blocks alternated between a "rest" and a "go". At the beginning of each "rest" block the participant heard the word "rest" and was instructed to rest their hand on the joystick, ignore the beeps and keep still. At the beginning of each "go" block the participant heard the word "go" and was instructed to move the joystick in one of four random directions of their choice, and then return the manipulandum back to the central resting position. A single movement was defined

as moving the joystick from its position of equilibrium and then returning the joystick back to this position. The exact timings of the beeps were also recorded.

3. GE-EPI Movement session, Hand 2: The joystick was then moved to the opposite hand, and acquisition 2 was repeated.

Additionally, field maps were acquired to correct for field inhomogeneity. Patients then had their stimulation switched to the opposite condition. The joystick was returned to the hand that had first performed the task and the aforementioned acquisitions were repeated.

At the end of the session, DBS was switched back ON if OFF during the second session, and the patient was examined (including a repeat evaluation of UPDRS-III). The DBS system was interrogated to check the settings and impedance, and to check for additional activations. The patients were given their regular PD medication and had a final clinical assessment after their medication had started to take effect to confirm they had returned to their baseline level of Parkinsonian disability before leaving the department.

Each participant completed the session with four movement task sessions, one for each hand during each stimulation condition. This corresponds to a factorial design with three factors; task (movement versus no movement); laterality (right versus left) and stimulation (ON versus OFF). The whole session took approximately 90 minutes. The connection between the electrode lead and the extension cable, commonly sited above the left parietal bone caused a loss of signal artefact resulting in data not being acquired in left hemispheric sensorimotor areas. Given these regions were *a priori* regions of interest, particularly when examining right hand movements, we elected only to analyse the left hand movement data. This resulted in a factorial design with two factors; task and stimulation.

Movement durations and reaction times were extracted from the joystick dataset by manual examination of the position over time. Paired *t* tests were used to judge significant changes in joystick movements comparing ON and OFF stimulation periods.

7.3.5 Image processing

Data were pre-processed and analysed using the SPM12 (Wellcome Trust Centre for Neuroimaging, London, UK; http://www.fil.ion.ucl.ac.uk); for effective connectivity analyses, DCM12 was used. The SPM Anatomy toolbox (Eickhoff et al., 2005) was used to translate *peak* MNI coordinates into anatomical and functional regions based on probabilistic cytoarchitectonic maps.

Data were spatially pre-processed as outlined in section 6.4.1. In brief, data were first corrected using the acquired field maps, then realigned, and normalised to MNI space. Data were then visually inspected to confirm they had been correctly normalised given the artefact created by the DBS hardware, and were finally smoothed using an 8mm Gaussian kernel. Data were high-pass filtered set to the standard threshold (128-s).

When field maps were examined, the extent and amplitude of the expected distortions caused by the DBS hardware on the skull were approximately the same as the extent and amplitude of the distortions caused by the presence of the sinuses. This suggests that the DBS hardware causes no more distortion than the sinuses do, and the field maps are sufficient to correct for them.

7.3.6 Analysis of regional responses

Standard SPM (whole brain) statistical analysis then ensued. An epoch-related design, where each activation epoch (block) was defined as the time period from the beginning of the first movement in a "go" block, to the end of the last movement in that block. Each

movement session thus consisted of six motor epochs, corresponding to the six "go" blocks. The resulting boxcar stimulus function was then convolved with a canonical haemodynamic response function to form expansionary variables or regressors that constitute the design matrix. Both (ON and OFF) movement sessions, for each participant, were analysed in one design matrix. Six nuisance regressors were included for each session modelling the confounding effects of head motion in the design matrix.

A standard random effects analysis was performed by first computing contrasts of effects at the first level, and then analysing these summary statistics at the second level using one sample t-tests. Intrinsic masking was used to exclude voxels affected by DBS hardware-related artefact.

A T contrast corresponding to the main effect of movement was specified to (1) ensure that this could be detected in the DBS setup with a suitable degree of sensitivity and anatomical precision, and (2) to define a network of brain regions engaged by the motor task. Further T contrasts were specified defining the interaction between task and stimulation. This resulted in two contrasts (*Main Effect of Movement* – Left hand, *Movement x DBS interaction* – Left hand), and ensuing statistical parametric maps (SPMs).

All 10 subjects' normalised structural T1 scans (taken during ON) were combined to create a group structural T1 normalised to MNI space. One-sample t-tests were performed on group data separately for each of the contrasts to produce SPMs that were then superimposed on the group structural image. Second level tests on the main effect of movement contrast were adjusted for handedness and UPDRS-III ON score by including mean-centred confounds in the second level design matrix (multiple linear regression model). This accounts for confounding effects due to inter-subject variability in

Parkinsonian disability. In the same manner, second level tests on interaction contrasts were corrected for handedness and percentage improvement in UPDRS-III score when going from OFF to ON.

The main effect of movement contrast served to define the network of brain regions related to voluntary movement. The fifteen peak voxels of clusters larger than 5 voxels with the highest z statistics (range: 4.87–3.81) were defined as 'nodes' of the motor network. Any clusters consisting of purely white matter voxels were omitted.

A restricted volume analysis was then performed to assess the interaction between movement and stimulation within the nodes of the aforementioned network. Restricted volumes (8mm radius spheres) were centred on the peak voxel of each node. A statistical threshold of $p<0.05$ (FWE corrected, with a cluster threshold of 5 voxels) was used to assess significance. Regions surviving this threshold were considered to show significant interactions between movement and stimulation.

Given that extensive PET imaging studies have previously proposed a network of areas involved in the therapeutic response to STN DBS and that this is the first report of fMRI activations and their modulation by therapeutic DBS, interaction contrasts were explored at lower uncorrected thresholds ($p<0.005$, cluster size of 5 voxels) in an exploratory fashion. The results of this analysis are not formally reported, but regions were considered of interest for future study.

7.3.7 DCM

Results of the SPM revealed two regions (one cortical, one subcortical) displaying significant *movement x DBS interaction*s. The design matrix was rotated for the DCM analysis; ON and OFF scans were concatenated into a single session with a single

movement stimulus function. Parametric modulators were used to model the *movement x DBS interaction*. The main effect of DBS was modelled as a boxcar, with values of one during stimulation ON and zero otherwise.

Subject-specific peak coordinates of the regional interactions were used to identify nodes or regions in the DCM. Data was extracted from spheres (r = 4mm) centred on peak voxels ($p<0.05$ uncorrected threshold) within 16mm of the second level peak in each of the two regions. Three subjects failed to show significant peaks in both regions and were excluded from DCM analysis.

The model space compared 16 equally plausible generative models of the two node DCMs. The main effect of movement entered the model as a driving input to the cortical node. The two nodes were reciprocally connected (A-matrix). DBS entered the model as modulatory effect on a subset of connections, including the two intrinsic connections, and the reciprocal extrinsic connections, resulting in (2^4 =) 16 different DCMs per subject, and thus (16 DCMs x 7 subjects =) 112 DCMs in total. The model space is presented diagrammatically in Figure 7.3. Models were estimated using deterministic DCM.

BMS (using fixed-effects assumptions) was used to select which of the 16 models had the greatest evidence, given the data (Penny et al., 2004; Stephan et al., 2010). Fixed-effects model comparison was chosen because subjects were recruited under the assumption they have the same functional architecture and that DBS had consistent effects within this anatomy. For quantitative interpretation, the coupling parameters of the DCMs were averaged using Bayesian Model Averaging (BMA), in which parameter estimates are weighted by the model evidence (Stephan et al., 2010).

Correlations between the connectivity parameters and the UPDRS-III scores and UPDRS-III improvements were performed for predictive validity

7.4 Results

7.4.1 Clinical response and motor task data

Clinical responses as measured by the UPDRS-III scores are shown in Table 7.1. The mean improvement was 27.5 points (56.7% improvement, $p<10^{-6}$). Similar improvements were also seen when the task data was analysed. Left hand movement durations and reaction times were decreased in the ON condition by an average of 28.87% (p=0.002), and 20.33% (p=0.025) respectively. The mean movement duration during ON and OFF were 0.82s and 1.27s respectively. The mean reaction times during ON and OFF were 0.63s and 0.83s respectively. Post-operative MRI – employing fine cuts through the STN – confirmed that each electrode contact lay within or overlapped the anatomical border of the STN in both axial and coronal views.

Scanning proceeded with no adverse events or change in post-scan UPDRS-III scores. Re-introduction of PD medications led to restoration of baseline motor function. Post-scan inspection of the IPG revealed DBS stimulation parameters and circuit impedance were unchanged.

Sub	**Age**	**H**	**Post-op**	**UPDRS-III**			**Move duration (s)**			**RT (s)**		
				OFF	ON	%	OFF	ON	%	OFF	ON	%
1	65	L	20	53	21	60.4	1.1	1.3	12.8	0.8	1.0	27.3
2	72	R	53	47	29	38.3	2.4	0.7	-70.6	1.0	0.6	-44.0
3	54	R	9	33	10	69.7	0.8	0.6	-26.3	0.6	0.5	-12.5
4	65	R	67	60	20	66.7	1.0	0.7	-29.6	0.6	0.4	-23.6
5	50	L	102	51	17	66.7	1.3	0.8	-34.1	0.6	0.5	-21.0
6	63	R	29	46	19	58.7	0.6	0.5	-19.4	1.1	0.6	-44.6
7	54	R	19	45	26	42.2	1.0	0.8	-17.0	0.8	0.8	0
8	56	L	30	52	19	63.5	2.4	1.2	-48.5	1.3	0.6	-52.0
9	43	L	48	51	23	54.9	0.9	0.6	-31.9	0.7	0.6	-6.1
10	61	R	8	46	25	45.6	1.1	0.9	-24.1	0.9	0.7	-26.9
Mean	*58.3*		*38.5*	*48.4*	*20.9*	*56.7*	*1.3*	*0.8*	*-28.9*	*0.8*	*0.6*	*-20.3*
SD	*8.51*		*29.5*	*7.03*	*5.32*	*11.1*	*0.6*	*0.3*	*21.5*	*0.2*	*0.2*	*23.9*

*Table 7.1 Summary of patient demographics and response to STN DBS. All assessments took place off medication. Age and post-op refer to the age of the patient and months since implantation. % refers to the percentage change from OFF to ON, i.e. (OFF-ON)*100/OFF. H refers to dominant hand; left (L) or right (R).*

7.4.2 Hardware-related Artefact

All GE-EPI scans suffered dropout artefact thought to be caused by the subgaleal connectors between the leads and extension cables sited over the left parietal bone (see Figure 7.1).

7.4.3 Analysis of regional responses

The main effect of movement was in accordance with previously published accounts (Limousin et al., 1997). The purpose of this contrast was to establish a network of functionally specialised nodes associated with task performance in our cohort. A summary rendered SPM of the network is displayed in Figure 7.1.

Adjustment for clinical response to stimulation did not affect the regions that demonstrated highest levels of peak level BOLD response.

Our initial restricted volume analysis of the interaction (movement x stimulation) revealed increases in BOLD responses in the right insula cortex, and right thalamus ($p<0.05$, FWE corrected) (i.e. contralateral to left hand movements) when DBS was active Figure 7.1e/f.

Subsequent exploratory whole brain analysis of the interaction contrasts at uncorrected thresholds ($p<0.0005$) revealed increases in the left superior frontal gyrus (Premotor area, PM, BA 6) and middle frontal gyrus (BA 10/46, DLPFC), right intra-parietal sulcus (hIP1), and inferior frontal gyrus pars triangularis (BA 45). See Table 7.2.

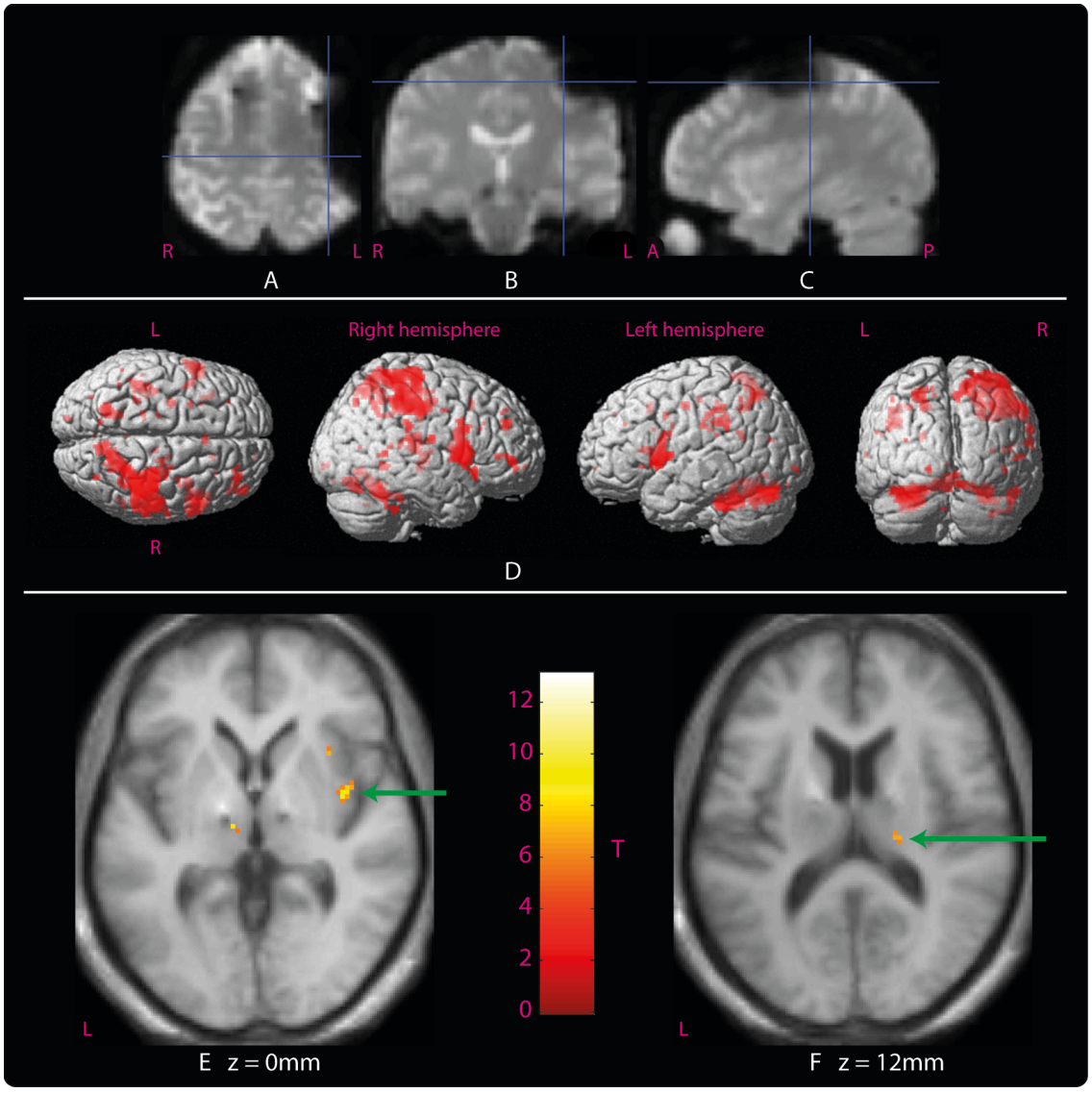

Figure 7.1 Imaging results. A typical drop-out artefact in a single subject's GE-EPI acquisition viewed from (a) axial, (b) coronal, and (c) sagittal sections; cross-hair position = -34.8, -21.5, 53.3mm (MNI coordinates). SPMs in (d) summarize the movement network on a rendered MNI brain ($p<0.001$ uncorrected). Clusters representing BOLD signal increases in the insula cortex (e, green arrow), and thalamus (f, green arrow).

Size (vx)	**T**	**Z**	**P(unc)**	**P(SVC)**	**MNI coordinates**			**Anatomy**		**BA**
					x	y	z			
20	13.1	4.6	1.8E-6	-	-24	-2	62	L	SFG	6
6	10.1	4.3	9.8E-6	-	-40	42	20	L	MFG	47
49	**9.2**	**4.1**	**1.9E-5**	**0.005**	**38**	**-2**	**0**	**R**	**Insula**	
19	8.9	4.1	2.2E-5	-	38	30	16	R	IFG	45
6	8.9	4.1	2.3E-5	-	-24	-14	16	L	Putamen	
7	**8.6**	**4.0**	**2.8E-5**	**0.017**	**18**	**-24**	**10**	**R**	**Thalamus**	
12	8.4	4.0	3.4E-5	-	20	-36	56	R	Postcentral	3
23	8.3	4.0	3.5E-5	-	38	-40	34	R	IPS	
5	8.2	4.0	3.8E-5	-	-10	-16	0	L	Thalamus	
7	8.0	3.9	4.4E-5	-	-30	-22	40	L	Postcentral	3
9	7.6	3.8	6.4E-5	-	32	14	4	R	Insula	
20	13.1	4.6	1.8E-6	-	-24	-2	62	L	SFG	6

*Table 7.2 Results of Movement x DBS (ON>OFF) interaction contrast at second level. Thresholded at whole brain peak voxel p<0.0005 (uncorrected), Cluster size>5 voxels (vx). Regions in **bold** were identified in the restricted volume analysis to the motor network described in the text (p<0.05, FWE corrected). The remaining regions are reported in view of strong support of their involvement from previous publications. BA = Brodmann's area.*

7.4.4 DCM

The relative log-evidences across all models for all participants are shown in Figure 7.2. Model 15 was found to be the most likely architecture (posterior probability > 95%), followed by 3 and 1. The difference in relative log-evidences, ΔF, were 3.77 and 8.25 respectively, indicating that there is strong evidence in favour of model 15 (Kass and Raftery, 1995). Model 15 incorporated modulatory effects on both intrinsic cortical and thalamic coupling, as well as reciprocal extrinsic cortico-thalamic coupling. BMA estimates of coupling are reported in Figure 7.3.

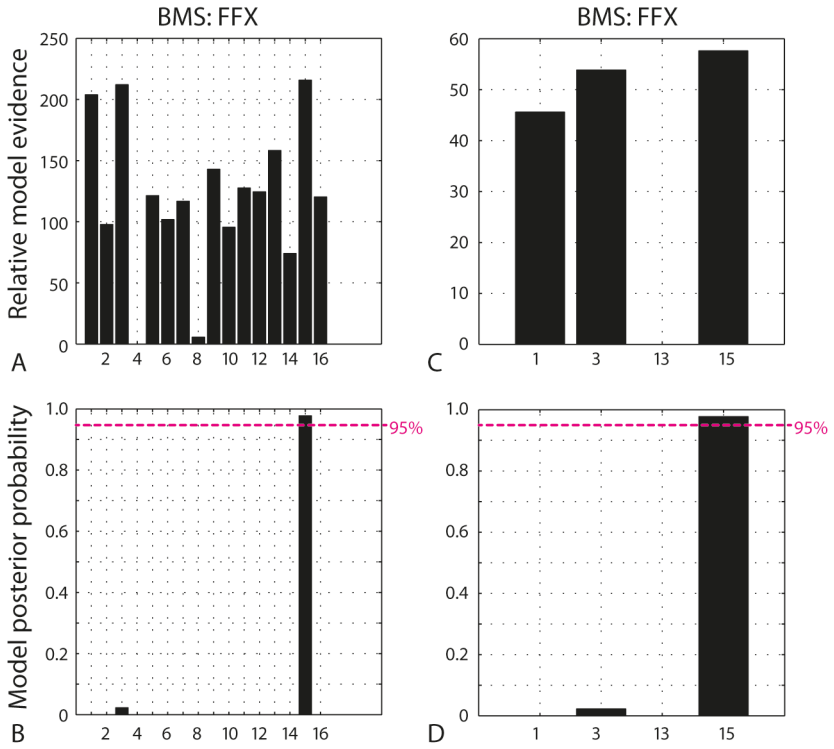

Figure 7.2 BMS results. FFX = Fixed Effects Assumptions. (a) The relative log-evidences across all 16 specified models with model 3 showing the highest log-evidence. (b) Given the observed data and the models specified, one can be >95% certain that model 15 is the data generator. (c, d) This is more clearly illustrated by just including the 4 most likely models.

7.4.5 Predictive validity

There was no significant correlation between cortico-thalamic connectivity parameters and the clinical scores ($P<0.05$) to suggest a direct linear relationship between these indices.

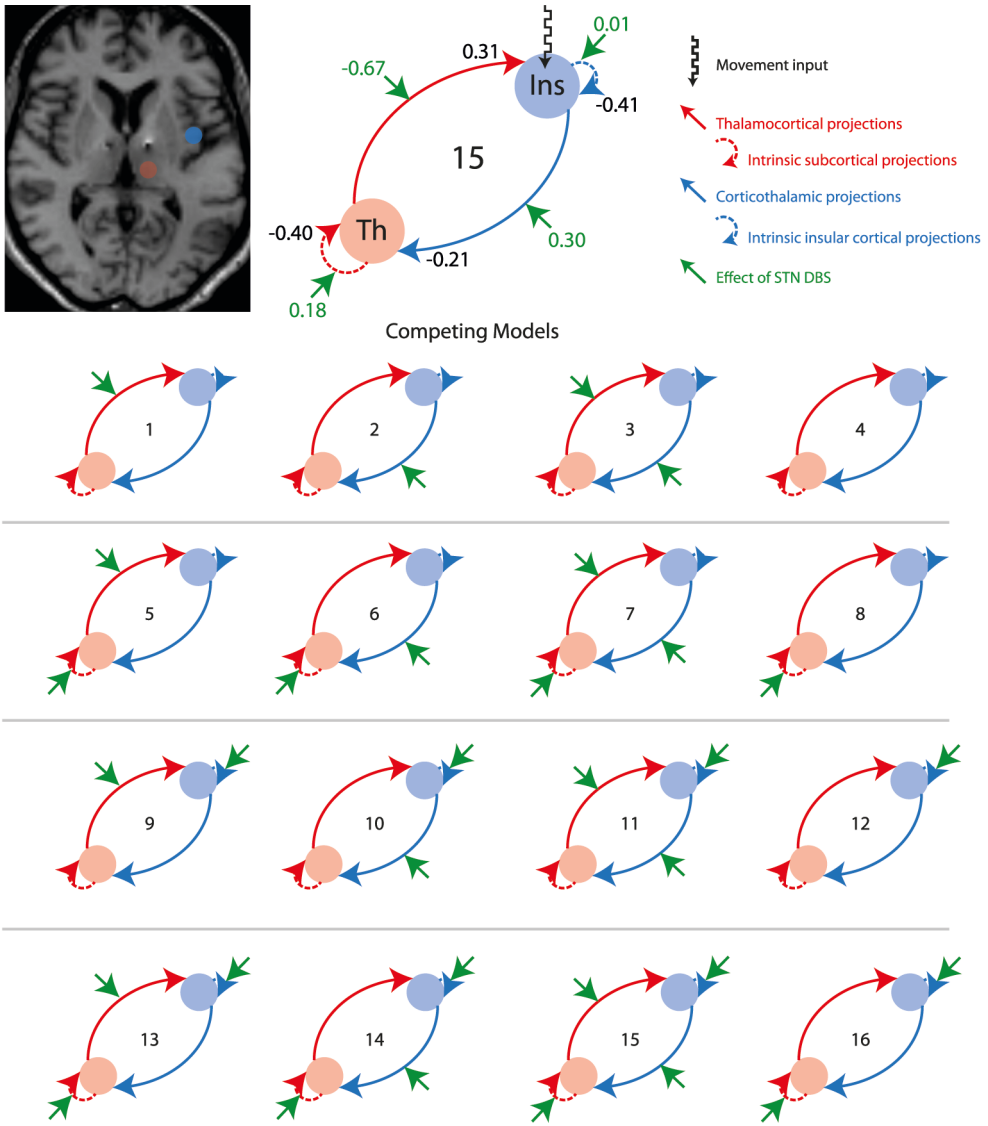

Figure 7.3 Model space, winning model, and BMA estimates. Model 15 – the winning model – is shown enlarged. The blue node represents the right insula cortex, and red node, the right thalamus. Green arrows indicate the connection/s that DBS modulates. The 'movement input' is likely made up of both motor inputs arriving from M1, PM and SMA, as well as sensory inputs elicited by on-going movements. Average DCM parameters are included on the enlarged model 15, units are in Hertz (Hz). Positive A-matrix parameters represent an excitatory effect on the target, whereas negative values indicate an inhibition of the target area. Positive B-matrix parameters (value in green) represent an increased target response to input (i.e. an increased gain), whereas negative values indicate a decreased target response to input (i.e. a reduced gain). The coupling during movements with DBS is equal the sum of the A and B value on that connection, e.g. during movements with DBS, the cortico-thalamic drive switches from -0.21 Hz to (-0.21 + 0.30)= 0.09 Hz, i.e. it switches from an inhibitory to an excitatory drive.

7.5 Discussion

The results of this experiment shed light on both the methodological and neurobiological issues set out in its aims:

7.5.1 Technical significance

Firstly, this experiment demonstrated that fMRI can be used to study the effects of therapeutic STN DBS on brain activity without compromising patient safety or DBS function. All sequences used were informed by the existing safety protocol, which was established following rigorous on site *in vitro* experimentation. It is important to stress the importance of performing *on-site* assessments given the variability in scanner configurations (Carmichael et al., 2007; Zrinzo et al., 2011).

Furthermore, the functional data, at least the movement-evoked activity, appeared consistent with the published literature. In the analysis of regional responses, the *main effects of movement* contrast was specifically examined for two reasons. Firstly, pertaining to the technical feasibility, to assess the reliability of fMRI in these patients, i.e. whether regions specialized for task performance that were in accordance with the literature (Limousin et al., 1997). Secondly, the contrast helped produce a mask within which to search for voxels demonstrating an interaction.

7.5.1.1 DBS hardware related artefact

However, by far the biggest challenge faced with these patients was the artefact produced by the interface between the extension cable and the electrodes. The issue was exacerbated by non-uniformity in the hardware geometry amongst the cohort. In other words, the position of the connector between the extension cable and electrodes varied between subjects, largely

staying over the left parietal bone laterally, but sometimes placed more anteriorly or medially.

The connector resulted in a drop out susceptibility artefact on GE-EPI acquisitions, partially obscuring left sensorimotor regions. While these artefacts were destructive during first level analysis, their effects were more marked in the second level analyses due to the additive nature of the artefact across the group. The same was true with regards the artefact present at the electrode tip. Whilst this artefact was much smaller (in terms of size), the additive nature likely made it impossible to detect any BOLD signal in the STN, possibly extending into the thalamus.

That being said, there was no evidence to suggest that BOLD signal from the remaining brain was affected. This is in line with previous studies involving implanted electrodes have confirmed that similar artefacts do not significantly impair the functional data (Vulliemoz et al., 2011).

As a result of the artefact, data from right hand movements were not formally analysed. We included a covariate for hand dominance to minimize variability vis-à-vis laterality of function. Other studies investigating motor control generally use right hand movements, complicating comparisons with other studies, but this was unavoidable given our standard surgical practice of placing the connector to electrode extension cables subcutaneously over the left parietal bone. Future fMRI studies in patients implanted at this centre (and thus routinely have their artefact over the left hemisphere) should only concentrate on a left sided motor task.

7.5.1.2 Selection criteria

Our selection criteria were set such that the cohort studied (1) responded well to STN DBS acutely, maximising the difference in clinical phenotype between DBS conditions (the minimum UPDRS-III improvement in our sample was 38.5%), and (2) had received DBS for at least 6 months, meaning any post-operative oedema had almost certainly subsided.

While this permitted novel investigation of the modulatory effects of *confirmed therapeutic* stimulation, our conclusions can only be applied to patients who have shown such improvements. Similarly, constraining our selection to only patients with good response (and a small sample size) implicitly reduced the variance of clinical responses, which may explain why none of the correlations between coupling and UPDRS-III scores were significant.

Given the comments made above (section 7.5.1.1) regarding the artefact, in future studies it may be worth selecting patients who have more consistent patterns of artefact. This is obviously difficult to ensure, but future selection should involve reviewing the patient's surgical report for any mention of the position of the subgaleal wiring.

7.5.2 Neurobiological significance: Regional responses

7.5.2.1 Increased motor-evoked responses in the insula

Increased activity in the insula under DBS is a difficult finding to interpret given the vast number of functional properties ascribed to this region. Functional MRI meta analysis has revealed the insula cortex is activated by a range of stimuli including *emotional recall/induction*, *empathy* (as elicited by judging emotional faces), *olfaction*, *gustation*, *interoception* (e.g. listening to one's heartbeat or suppressing the need to void), *somatosensation*, and *motor processing* (Kurth et al., 2010). This suggests the insula is an

extremely non-selectively activated region, thus employing reverse inference to suggest possible relevance would be troublesome (Poldrack, 2006). It is tempting to suggest the changes under DBS are motor related (especially given the contrast searches for regions changed during the movement blocks). However, while reaction times and movement durations were recorded and did change, there are a number of other behavioural variables that were not recorded that feasibly could have changed under stimulation to satisfy similar reverse inferences.

DBS has previously been found to modulate insula activity, both in patients (Garraux et al., 2011; Hesselmann et al., 2004), and in animal models of STN DBS (Min et al., 2012). Similarly, previous reports demonstrate that PD patients show reduced insula cortex activation during self-generated movements (Jahanshahi et al., 1995). Tractography has identified pathways connecting the insula cortex to the STN (Lambert et al., 2012), consistent with reports of posterior insula lesions resulting in hemiballismus (Etgen et al., 2003).

7.5.2.2 Increased motor-evoked responses in the thalamus

While previous studies have suffered from limited spatial resolution making subcortical structures difficult to examine, thalamic modulation at rest has been widely reported (Arai et al., 2008; Asanuma et al., 2006; Hershey et al., 2003; Hilker et al., 2004; Karimi et al., 2008; Sestini et al., 2005) – see . Similarly, one study employing a learned joystick task has reported *movement x DBS interaction* (Thobois et al., 2002). Given that the orthodromic output of the STN ultimately projects to the thalamus, increased thalamic BOLD response is in-keeping with electrophysiologically established orthodromic effects of STN stimulation on the thalamus (Benazzouz et al., 2000b; Dorval et al., 2008; Xu et al., 2008).

7.5.2.3 Exploratory findings at uncorrected whole-brain thresholds

Additional interactions were found in the intra-parietal sulcus, IFG, PM and DLFPC ($p<0.0005$, uncorrected). While these changes did not survive FWE correction, their detection at stringent uncorrected thresholds, high z-scores, and accordance with previous literature (Ceballos-Baumann et al., 1999; Limousin et al., 1997), merit inclusion in this report.

7.5.3 Neurobiological significance: Cortico-thalamic coupling

As a simple proof of concept, I modelled the potential neuromodulatory effects of STN DBS that could have produced the *movement x DBS interaction*s in the cortex and thalamus. The model tested is obviously a simplification, specified in order to make first inferences on whether DBS alters cortico-subcortical coupling. Importantly, DCM does not distinguish between monosynaptic or polysynaptic connections; the BMS was not to test nature of direct insula-thalamic connectivity. Rather the insula served as a summary for a cortical region modulated by DBS, that sends efferents to the thalamus via BG nuclei, and receives thalamic afferents either directly, or more plausibly, via other cortical nodes. The winning model included cortico-thalamic, thalamo-cortical, and intrinsic modulation of both cortex and thalamus.

The nature of the coupling and neuromodulation is less significant in this experiment, the key finding here is where DBS is acting. Although BMA estimates of the coupling suggest that during movements with DBS OFF, the insula has an inhibitory influence on the thalamus. DBS was found to reverse this, as well as reduce the intrinsic self-inhibition. Precise interpretation of the BMA estimates is complicated by the simplified model structure. One can speculate that given the thalamic response to cortical excitation depends on the pathway through which the signal is propagated (the hyperdirect and indirect

pathways cause an excitation of the GPi/SNr - resulting in thalamic inhibition, whereas transmission via the direct pathway disinhibits thalamic neurons), the reported shift from predominant inhibition to excitation of the thalamus may suggest that DBS biases the thalamus towards the direct pathway afferents. This is somewhat of a leap, and more anatomically detailed DCMs are required to test this hypothesis formally (this is undertaken in Chapters 8, 10 & 11).

Modulation at the level of the cortex may be explained by the hyperdirect tract between the STN and insula cortex. This supports recent claims from the animal literature that antidromic stimulation of axons projecting to the STN produces complex activations of cortical circuits (Li et al., 2007), which might also be responsible for the clinical effect of DBS (Gradinaru et al., 2009). Further studies employing electrophysiological techniques may be required to provide deeper insights into the synaptic mechanisms involved.

7.5.4 Limitations and reflection

I believe that while the results of this experiment do contribute to the neurobiological understanding of DBS, there are a number of limitations that should be addressed in later experiments.

Firstly, in the analysis of regional responses, our results were only significant using SVC statistics. While a lot of the previous neuroimaging work has also reported within these constraints, I was disappointed that results were not significant at the whole brain level using robust correction for multiple comparisons. On reflection, this could be due to the quality of the collected data from both a hardware perspective (e.g. the use of head-transmit/receive coils), and at the patient level (e.g. patient movement during scanning).

That being said, we did our best to minimise head movements (securing the head, realign and unwarp, and inclusion of head motion parameters in the first level GLMs).

Finally, more plausible models of the cortico-thalamic BG loop are required to draw informative inferences regarding the modulation of specific pathways. The speculation I put forward above requires formal investigation. Furthermore, more plausible models might help produce more clinically meaningful estimates of effective connectivity.

7.5.5 Conclusions

My conclusions are twofold: Firstly, fMRI is feasible in a cohort of patients with chronically implanted DBS, although technically challenging. Secondly, in a simple model of cortico-thalamic coupling, STN DBS has modulatory effects on reciprocal cortico-thalamic effective connectivity.

8 The effect of STN DBS on endogenous coupling in the basal ganglia motor loop

Parts of the following chapter have been published in Kahan et al., (2014), Brain.

8.1 Summary

In this chapter, I present the results of my second fMRI experiment conducted on 12 PD patients (10 of which were analysed in Chapter 7) with STN DBS as they lay in the scanner at rest with their eyes closed. As discussed, non-invasive characterisations of induced brain responses, and the effective connectivity underlying them, generally appeals to DCM. When the brain is at rest however, this sort of characterisation has been limited to correlations. Using stochastic DCM, I modelled the effective connectivity underlying BOLD fluctuations in the resting Parkinsonian BG motor loop, and the modulatory effect of DBS.

Results demonstrate that STN DBS modulates all the major components of the motor cortico-striato-thalamo-cortical loop, including the cortico-striatal, thalamo-cortical, direct and indirect basal ganglia pathways, and the hyperdirect STN projections. The strength of effective STN afferents and efferents were reduced by stimulation, whereas cortico-striatal, thalamo-cortical and direct pathways were strengthened. Regression analysis revealed predictive validity of coupling parameters on clinical status and response to DBS.

I conclude that (1) anatomically plausible DCMs of the BG architecture can capture the distributed modulatory effects of DBS, (2) STN DBS increases direct, cortico-striatal and

thalamo-cortical pathways, but reduces coupling of STN afferents and efferents, (3) coupling and neuromodulatory effect in the STN afferents and direct pathway predict clinical status and therapeutic effect of DBS.

8.2 Introduction

As outlined in section 5.2, progressive asymmetric degeneration of nigrostriatal dopaminergic innervation is a primary hallmark of PD. Clinically, this typically produces asymmetric motor symptoms that impact on behaviours both 'during action' and 'at rest'. Of this latter group, rigidity and resting tremor are most common. STN DBS has become an established therapy for managing these symptoms – when dopaminergic medications alone are no longer sufficient (Krack et al., 2003; Limousin et al., 1995). While most conventional therapeutics aim to restore dopamine concentrations to physiological levels, the mechanism of action of STN DBS is less clear. Since the effect of DBS mimics that of ablative lesions, it was suggested that DBS 'inhibits activity' in the target, which accorded with rate-based models of basal ganglia (BG) circuits (Albin et al., 1989; Beurrier et al., 2001; DeLong, 1990; Meissner et al., 2005). However, the literature – ranging from animal to computational models – suggests that stimulation has a myriad of effects on various neural elements in and around the STN, culminating in clinical improvement (Deniau et al., 2010; McIntyre and Hahn, 2010; Perlmutter and Mink, 2006; Vedam-Mai et al., 2012).

BOLD fMRI signal recorded while the subject lies at rest with eyes closed could represent an important tool for clinical diagnosis and understanding brain disorders (Biswal et al., 1995; Deco et al., 2011; Fox and Greicius, 2010). Brain regions of similar functional specialisation have been shown to display functional connectivity during rest (e.g. motor and visual networks respectively (Biswal et al., 1995; Lowe et al., 1998)). Parkinsonian patients off medication have been shown to display reduced BOLD functional connectivity amongst the pre/motor cortex and putamen (Esposito et al., 2013; Wu et al., 2009), increased connectivity between M1 and cerebellum (Wu et al., 2009), reduced striato-

thalamic connectivity (Hacker et al., 2012) as well as increased M1-STN connectivity (Baudrexel et al., 2011). Electrophysiological studies report similar changes in coherence between the STN and motor cortical areas in resting Parkinsonian patients (Shimamoto et al., 2013) that can be restored by dopaminergic medication (Litvak et al., 2011). Thus, there is a wealth of evidence implicating dopamine's neuromodulatory role in resting cortico-subcortical circuits.

As reviewed in detail in section 5.4.2.4, when investigating neuromodulatory effects of DBS *at rest*, previous human imaging studies have largely used either PET or SPECT. These studies have demonstrated STN DBS-induced changes in both blood flow and glucose metabolism at rest in key constituents of the motor network including M1, putamen, and thalamus (Asanuma et al., 2006; Boertien et al., 2011; Ceballos-Baumann et al., 1999; Cilia et al., 2009; Geday et al., 2009; Grafton et al., 2006; Haslinger et al., 2005; Hershey et al., 2003; Hilker et al., 2008; Jech et al., 2001; Karimi et al., 2008; Limousin et al., 1997; Payoux et al., 2004; Stefurak et al., 2003). Imaging in animal models has yielded similar results (Lai et al., 2014; Min et al., 2012). One short report described increased functional connectivity among premotor regions in response to STN DBS (Mueller et al., 2013); however, fMRI has been limited in these patients due to safety concerns. This centre has conducted on site safety studies, demonstrating that any risk to the patient can be minimised under a strict acquisition protocol (Carmichael et al., 2007) – as used in Chapter 7.

Resting state fMRI data does not possess any exogenous (driving) inputs as in task-based studies. Thus the evolution of activity in a given region must be driven by endogenous fluctuations. Stochastic DCM accounts for this by including stochastic fluctuations in the differential state equations and uses Bayesian filtering to estimate the hidden neuronal

states, coupling parameters and the precision of observation noise (Daunizeau et al., 2012a, 2012b; Friston et al., 2011; Li et al., 2011) – see section 6.6.8.

In this experiment, I deconstruct the basal ganglia motor loop using stochastic DCM of fMRI data acquired while human patients lay at rest, and examine the effect of therapeutic STN DBS on the underlying effective connectivity. Methodological issues pertaining to region selection in resting state studies is finessed, permitting analysis of data that is both functionally verified and anatomically localised.

8.2.1 Aims

Having demonstrated STN DBS has modulatory effects on extrinsic reciprocal cortico-thalamic coupling (see Chapter 7), and given the clear clinical response of these patients to DBS *at rest*, I hypothesised that clinical improvement could be explained by changes in the way neural populations within the motor loop impact upon one another; in other words, DBS has modulatory effects on extrinsic effective connectivity.

Building on results from Chapter 7, this experiment specifically sought to answer whether the effect was precisely related to particular pathways of the cortico-basal ganglia-cortical loop, or whether there was a diffuse effect on all connections. Furthermore, I explored whether clinical measures of PD impairment could be explained by differences in extrinsic effective connectivity, within the BG motor loop.

The aims were thus threefold:

1. Build anatomically informed models of BG motor loop that allow effects on specific pathways to be tested.
2. Characterise how STN DBS modulates these pathways.
3. Test whether coupling predicts clinical phenotype or improvement.

8.3 Materials and methods

8.3.1 Ethics

This study was approved by the National Hospital and Institute of Neurology Joint Ethics committee (09/H0716/51). All participants provided written informed consent.

8.3.2 Patients

Twelve patients who met UK brain bank criteria for idiopathic Parkinson's disease – were studied (Table 8.1). Selection criteria were as stated in 7.3.2, except there was no minimum improvement criteria as in Chapter 7. Medication was withdrawn for 10-12 hours (overnight) before scanning.

UPDRS-III scores were recorded both ON and OFF stimulation before scanning. Additionally, stimulation parameters and system impedance were noted, and IPG counters were reset[13].

Sub	**Age**	**Hand**	**Post-op**	**UPDRS-III**		**Right electrode**			**Left electrode**		
				OFF	ON	V	P (μs)	F (Hz)	V	P (μs)	F (Hz)
1	65	R	20	53	21	0.5	60	180	3.3	90	180
2	72	R	53	47	29	3.3	60	130	2.3	60	130
3	54	R	9	33	10	2.4	60	130	2.4	60	130
4	65	R	67	60	20	3.7	60	130	3.45	90	130
5	50	L	102	51	17	3.8	60	185	3.6	60	185
6	63	R	29	46	19	2.5	60	130	2.5	60	130
7	54	R	19	45	26	2.4	60	130	2.3	60	130
8	56	L	30	52	19	3.6	90	145	3.3	90	145
9	43	L	48	51	23	5.4	60	80	4.1	60	80
10	61	R	8	46	25	3.2	60	130	2.9	60	130
11	56	R	28	44	42	3.7	60	130	4.1	60	130
12	45	R	48	53	44	2.45	60	130	3.15	60	130
Mean	57.0		38.4	48.4	24.6	3.1	62.5	135.8	3.1	67.5	135.8
SD	8.6		27.0	6.6	9.9	1.2	8.7	26.7	0.6	13.6	26.7

Table 8.1 Patient information. Hand = dominant hand, P = pulse width, Freq = frequency. Post-op = months since electrode implantation. All UPDRS-III scores were conducted off medication. Subjects 11 and 12 were the additional subjects not included in Chapter 7.

[13] *The pacemaker monitors how many times it has been switched ON/OFF. The counters were reset before scanning, and checked the counter after scanning to ensure the pacemaker had not turned ON/OFF during scanning.*

8.3.3 MRI data acquisition

Scanning was performed in a Siemens Avanto 1.5T MRI scanner (Siemens, Erlangen, Germany) using a transmit-receive (Tx/Rx) head coil. The specific absorption ratio (SAR) in the head was limited to <0.1W/Kg, as in Chapter 7.

Subjects received three fMRI scans during each stimulation condition:

1. Resting state with eyes closed (TR=2420ms; TE=40ms; Flip angle=90°; FOV=192x192mm^2; Matrix size=64x64; 32 axial slices 3.5mm thick, gap between slices of 0.7mm; Spatial resolution= 3x3x4.2mm^3; Duration=8 minutes; 200 scans),
2. Motor task (right hand).
3. Motor task (left hand).

A vacuum moulded cushion was used to securely support the head, and limit head movement. Patients had an alarm if they experienced discomfort. Details of the motor task have been presented in Chapter 7. In brief, subjects lay in the scanner with a joystick in one hand and were instructed to move the joystick in a random direction in response to auditory tones during 'go' blocks, and to ignore the tones and rest their hand on the joystick during 'rest' blocks. The task was repeated for both hands, serving as functional localisers (one for each hemisphere) for subsequent resting state analysis.

Patients were scanned both ON and OFF. The scanning order was counterbalanced across subjects. Thus, two resting state sessions were collected per patient, one for each stimulation condition, in addition to two field map scans, an anatomical T1-weighted magnetization-prepared rapid gradient-echo structural scan, and the aforementioned functional (motor) localisers.

Following scanning, active stimulation was restored, normal medication was administered, and a UPDRS-III examination was repeated to confirm patients had returned to their clinical baseline. The settings, counters and impedance of the DBS system were recorded to confirm there were no additional activations induced by the scanner.

8.3.4 Dynamic causal modelling of resting state fMRI data

In this experiment, a series of models were specified of the BG motor loop consisting of M1, putamen, motor thalamus, and STN **in a single hemisphere**. The model space (for each hemisphere of each subject) consisted of models differing in terms of which connections were modulated by DBS.

The artefact caused by the electrode precluded the acquisition of precise BOLD data from the STN region – and this loss of precision was included in our model. This means the STN node can be regarded as 'hidden' from measurement and is referred to as a 'hidden node' (David et al., 2011).

The processing stream is summarised in Figure 8.1. Processing and analysis was performed using SPM12 and DCM12. Anatomical masks of the precentral gyrus from each hemisphere were created using the Harvard-Oxford cortical structural atlas, as available in the FSL suite (http://fsl.fmrib.ox.ac.uk/). Masks from each hemisphere of the motor putamen and motor thalamus were created using probabilistic white matter connectivity atlases thresholded at 50% probability (Behrens et al., 2003; Tziortzi et al., 2014), constraining our analysis to regions that exhibit strong structural connectivity at a population level. For the purpose of this experiment, both hemispheres were considered independently, given (i) Parkinson's disease causes asymmetric degeneration of the

substantia nigra pars compacta, (ii) severity of motor symptoms are usually asymmetric, (iii) DBS settings are often asymmetric.

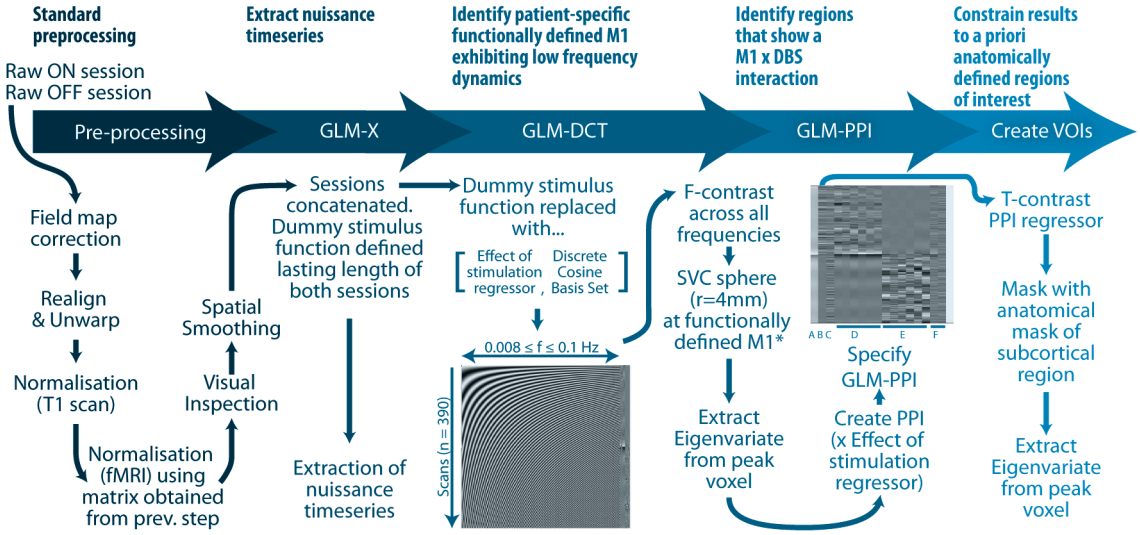

*Figure 8.1 Processing and analysis stream used to define resting BOLD time series for each VOI. Processing can be split into five key steps. The GLM-DCT contained a series of cosine functions with frequencies (f) characteristic of resting state dynamics. Columns in the GLM-PPI were as follows. (A) Main effect of DBS, a boxcar stimulus function with a single epoch lasting the entire on session. (B) M1xDBS PPI. (C) M1 BOLD signal (main effect of M1). (D and E) Head movement nuisance regressors. (F) Nuisance regressors from extra-cerebral compartments. *Functionally defined M1 coordinate was defined using an independent functional localizing motor task.*

8.3.4.1 Functional localisation of subject-specific M1

Using the task data, a contrast defining the main effect of movement for each hand was specified, and the peak voxel of this contrast (constrained by an anatomical mask of the precentral gyrus contralateral to hand movement) was selected as the hemisphere's M1 coordinate. Analysis of the task data is discussed in Chapter 7. Given DCM is ultimately a single subject analysis repeated on many subjects, problems of overlapping loss-of-signal artefact produced by the DBS hardware were avoided (see section 7.5.1.1).

8.3.4.2 Pre-processing

The first 5 scans of each resting state session were removed and data were corrected for field inhomogeneity using the field maps. Data were then realigned, coregistered, anatomical images were normalised to MNI space, the resultant normalisation matrix was then used to normalise the functional data. Finally, the data were visually inspected and spatially smoothed using an 8mm Gaussian kernel. This specific pre-processing routine was employed to ensure that any artefacts produced by the DBS hardware did not impact normalisation to MNI space. The ON and OFF sessions were concatenated to produce a single 390 scan time series. Ultra-low frequency fluctuations were removed in the usual way using a high-pass filter (1/128s ≈ 0.0078Hz). Confound time series were extracted from predefined coordinates of extra-cerebral compartments (the lateral ventricle and eye globe).

8.3.4.3 General linear model of resting state dynamics

Data exhibiting physiologically-relevant resting state (i.e. low frequency) dynamics were modelled using a GLM with a discrete cosine basis set (GLM-DCT) consisting of 189 functions with frequencies characteristic of resting state dynamics (0.0078-0.1Hz) (Biswal et al., 1995; Deco et al., 2011; Fox and Raichle, 2007; Fransson, 2005), a regressor encoding the effect of DBS, six nuisance regressors from each session capturing head motion, and the confound time series from the extra-cerebral compartments. The regional BOLD signal was summarised with the principal eigenvariate (adjusted for confounds - head movements and extra-cerebral compartments[14]) of voxels within 4 mm of the subject's M1 coordinate – as identified using an SPM of motor sessions.

[14] *This was achieved by using an F-contrast including the effect of DBS regressor, as well as the discrete cosine set modelling the resting state.*

A PPI analysis was used to identify voxels within the subcortical nuclei that were sensitive to DBS. The corresponding GLM-PPI included the *main effects of DBS* regressor, the BOLD activity from M1 and the PPI. An SPM of a T contrast testing for the PPI was masked first with the putamen mask, and then the thalamus mask (of the same hemisphere). The BOLD signal (corrected for the same confounds as above) was extracted from a sphere (radius 4mm) centred on the peak T-value within each mask, producing three VOIs per hemisphere and subject (M1, putamen, thalamus). Here, the putamen and thalamus VOIs exhibit a PPI with M1 and DBS. BOLD data from the STN could not be considered due to its small size and loss-of-signal artefact caused by the DBS electrode.

8.3.4.4 Model space and comparison

VOIs from each hemisphere were used to construct a series of 32 DCMs representing different hypothetical architectures. Two-state stochastic DCM for fMRI was used, endowing each node with excitatory and inhibitory subpopulations in receipt of noisy fluctuating inputs or endogenous activity. The STN was included as a hidden node, whose noise precision (given the electrode artefact) was effectively zero, permitting estimation of its hidden states and coupling parameters in the normal way. This reflects a strength of DCM; the Bayesian inversion of these models solves the complex problem of estimating hidden or latent variables. In DCM all parameters of interest are hidden and their expression in data serves to estimate these latent variables, regardless of whether their effects on the data are local or distributed. This has been capitalised on in electrophysiological DCMs (David et al., 2011; Marreiros et al., 2012; Moran et al., 2011a) and is exploited here in DCM for fMRI.

The GPi and GPe were not included in our models; rather it was assumed that thalamic afferents arrived via GABAergic projections from the GPi. In other words, striatal

GABAergic medium spiny neurons projecting directly to the GPi (constituting the direct pathway) were modelled with a net excitatory effect on the thalamus, whereas the glutamatergic STN-thalamic inputs had a net inhibitory effect (Figure 8.2). Striatal afferents to the STN summarise the polysynaptic putamen-GPe-STN connection that produces a net excitatory effect on the STN in accordance with electrophysiological findings (Albin et al., 1989; DeLong, 1990; Gradinaru et al., 2009; Kitai and Deniau, 1981; Kravitz et al., 2010; Nambu et al., 1996, 2000; Rouzaire-Dubois and Scarnati, 1985). The direct pathway was thus defined as the striato-thalamic excitatory connection, and the indirect pathway thus consisted of both the striato-STN and STN-thalamic connections. Finally, the hyperdirect pathway was defined as the M1-STN connection. The effect of DBS entered the models by modulating a subset of connections.

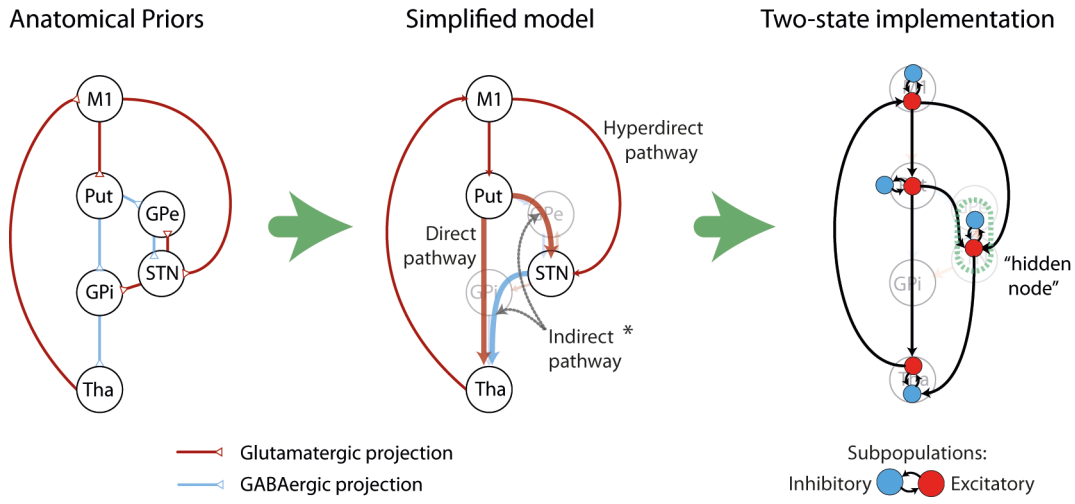

*Figure 8.2 The literature-based anatomical model of the motor cortico-striato-thalamic loop was further simplified by removing the pallidal nodes and summarizing polysynaptic connections (thick arrows joining the putamen, STN and thalamus). Red arrows constitute excitatory coupling, blue arrows inhibitory coupling. Placing priors on the direction of coupling was achieved using two-state DCM as displayed in the left-hand panel. *The indirect pathway comprised of two connections; the striato-STN and STN-thalamus connections (pointed to with the dashed grey arrows).*

The model space compared DCMs that included modulatory effects on the direct, indirect, hyperdirect, cortico-striatal, or thalamo-cortical pathways, or combinations of those five pathways (comprising six connections), resulting in (2^5) 32 models per hemisphere (Figure 8.3).

Models were inverted using generalised filtering[15] (Friston et al., 2010; Li et al., 2011), providing an estimate of the coupling parameters and model evidence. The 32 models from each of the 24 hemispheres entered a BMS procedure (fixed effects assumptions) that computed the posterior probabilities over competing models (Penny et al., 2004; Stephan et al., 2009a). Models were subsequently grouped into families depending on whether they expressed modulatory effects on the five pathways discussed above. A post-hoc BMS family analysis was used to evaluate the posterior probabilities of a modulatory effect on each (set) of the pathways.

[15] *Generalised filtering is a Bayesian filtering scheme for nonlinear state-space models in continuous time, i.e. dynamic causal models (see Friston et al., 2010).*

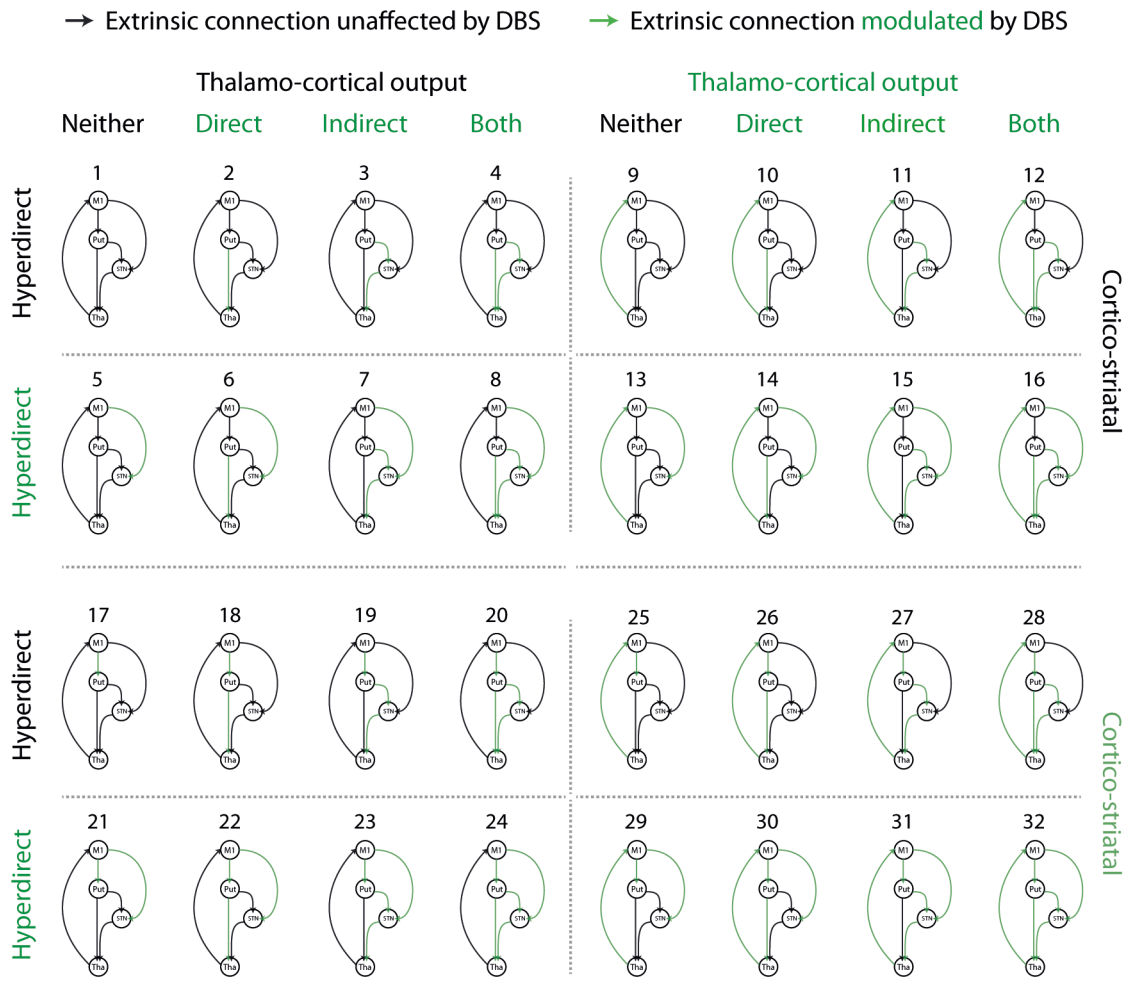

Figure 8.3 Model space. Thirty-two models from each hemisphere were specified with DBS modulating a combination of five pathways. Green colouring represents a target connection for modulatory DBS effects. Put = putamen; Tha = thalamus.

8.3.4.5 Relationship between winning DCM and clinical response to DBS

To quantify and validate the effective connectivity estimates generated, classical regression models were then used to test for the effect of DBS at the between subject level and as predictors of clinical status and therapeutic response to DBS. The model with the greatest log-evidence at a group level (i.e. across hemispheres) was considered the winning model. Extrinsic connectivity values (and their DBS dependent modulation) from the six connections comprising the five pathways of interest were taken from the winning model of each hemisphere. The ON coupling for each parameter was calculated using the OFF

coupling (DCM A-matrix values), and the DBS modulatory effects (DCM B-matrix)[16]. Paired *t*-tests were then used to compare coupling parameters in the ON vs. OFF conditions.

The coupling parameters were subsequently entered into a multiple linear regression model, as independent variables, with the contralateral UPDRS-III score (excluding axial score) as the dependent variable. This was performed separately for the ON and OFF conditions. The direction of the coupling (i.e. excitatory or inhibitory) was not considered in the model, simply whether the strength of the coupling predicted impairment. Additionally, the DBS-induced modulation was calculated for each connection (i.e. exp(DCM.Ep.B)), thus modulations >1 denoted DBS increased the coupling, regardless of whether the connection targeted excitatory or inhibitory subpopulations. These DBS effects entered a final stepwise regression model (employing backwards elimination) as independent variables, predicting the percentage improvement in clinical phenotype (i.e. the larger the percentage, the greater the clinical efficacy).

8.4 Results

8.4.1 Patients

Scanning proceeded with no adverse effects or change in post-scan UPDRS-III scores, IPG function, unexpected IPG activations or change in circuit impedance. Re-introduction of medication led to restoration of baseline motor function. Detailed patient and DBS parameter information can be found in Table 8.1. The mean clinical improvement to DBS off medication was 23.8 points (95% CI: 16.9-37.8, $P < 0.0001$). When considered by

[16] *See section 8.6.2 for details of parameterisation.*

hemisphere, and ignoring axial sub-scores, DBS improved contralateral signs in the limbs by 8.9 points (95% CI: 6.8-11.0, P < 0.000001).

8.4.2 Model fit

Models from two hemispheres (from two separate subjects) failed to fully converge during DCM's model inversion procedure. The time series from these problematic analyses were scaled down by a factor of 2 to suppress high amplitude 'spikes'. Following this, all 32 models across the 24 individual hemispheres were inverted successfully, furnishing predicted BOLD time series for each of the VOIs. These were pleasingly similar to the observed signal. A representative plot showing the observed and predicted data from one model is provided in Figure 8.4.

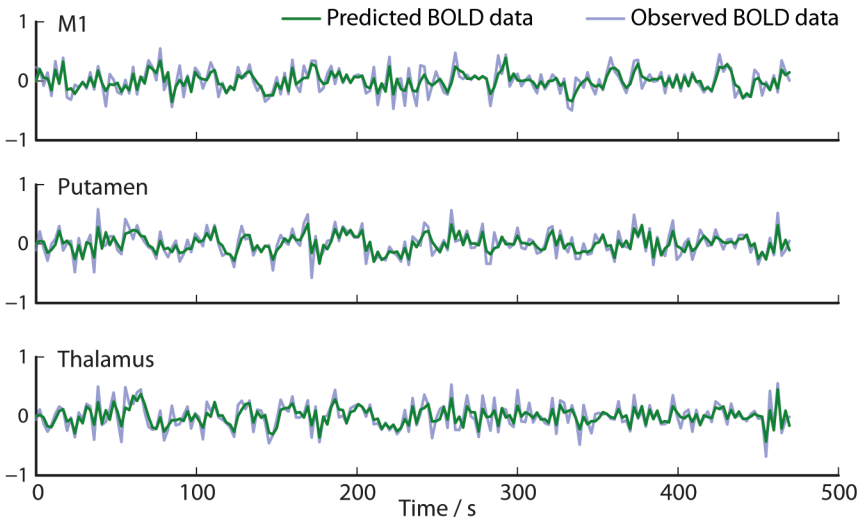

Figure 8.4 Example of model fit; observed and predicted time series from single hemisphere. Stochastic DCM produced predicted BOLD data that closely matched the observed BOLD data.

8.4.3 Bayesian model selection

Fixed effects BMS across 24 hemispheres revealed that model 32 was the most likely to generate the data (posterior probability > 99%). Model 32 included modulatory effects on all five of the pathways explored. Subsequent family analysis – where models were grouped

by the presence of modulatory effects on the five pathways – confirmed that all 5 pathways were >99% likely to be modulated by DBS Figure 8.5. For details of why fixed effects BMS was chosen, see section 8.6.3.

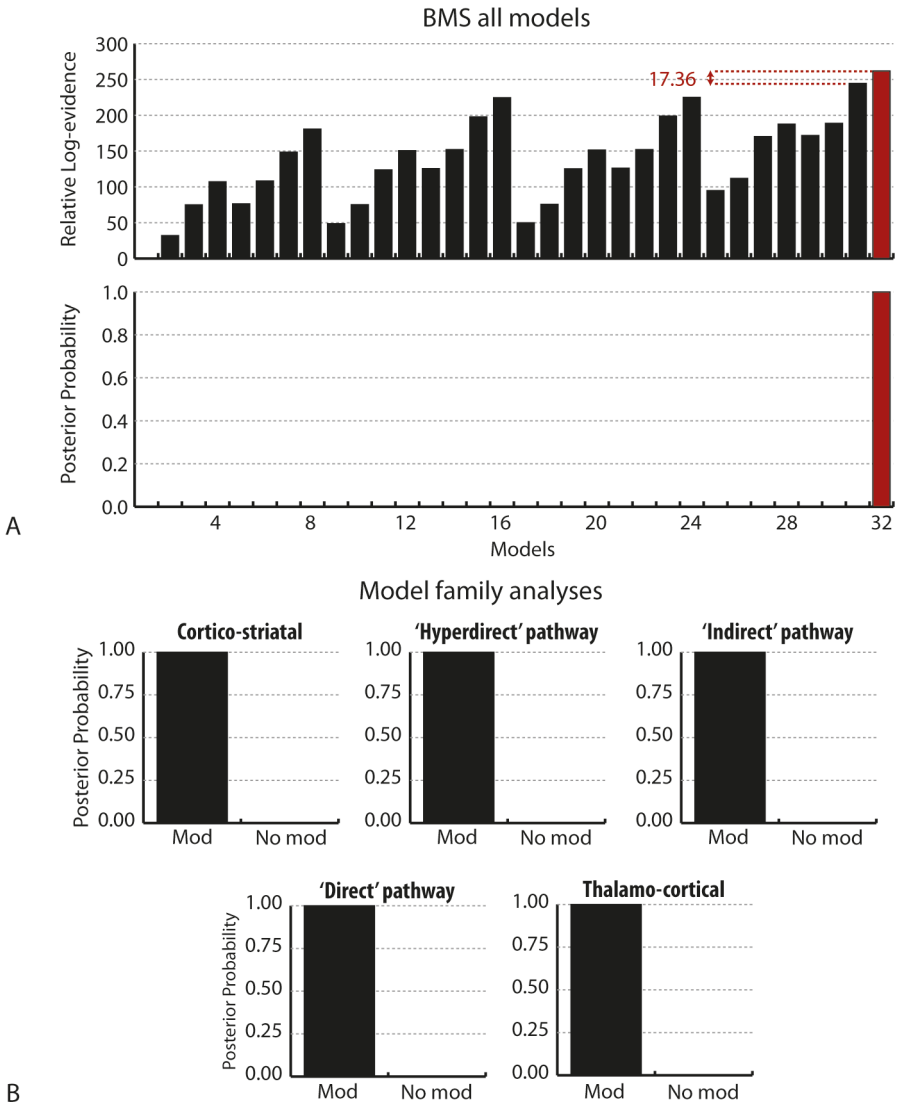

Figure 8.5 BMS results. (A) The relative log-evidence across all models, across all 24 hemispheres, found Model 32 outperformed all other competing models, with a posterior probability of >99%. Model 32 exhibited modulatory effects on all five pathways of interest. (B) This was confirmed using post hoc family analysis; posterior probability of modulatory effects on each of the five pathways was >99%.

8.4.4 Direction of neuromodulatory effect

Estimated coupling parameters from the six extrinsic connections were extracted from model 32 of each hemisphere. Paired t-tests were used to compare the means of the

connection strengths ON and OFF DBS. Stimulation increased the strength of the cortico-striatal (95% CI: 0.01-0.06Hz, P<0.05), direct (95% CI: 0.03-0.07Hz, P<0.001), and thalamo-cortical pathways (95% CI: 0.03-0.07Hz, P<0.001). In contradistinction, STN DBS reduced the strength of all STN afferents and efferents; the hyperdirect (95% CI: -0.0011 - -0.0008Hz, P<0.001), striatal afferents (95% CI: -0.0010 - -0.0006Hz, P<0.001), and STN-thalamic (95% CI: -0.0008 - -0.0005, P<0.001) connections. See Figure 8.6.

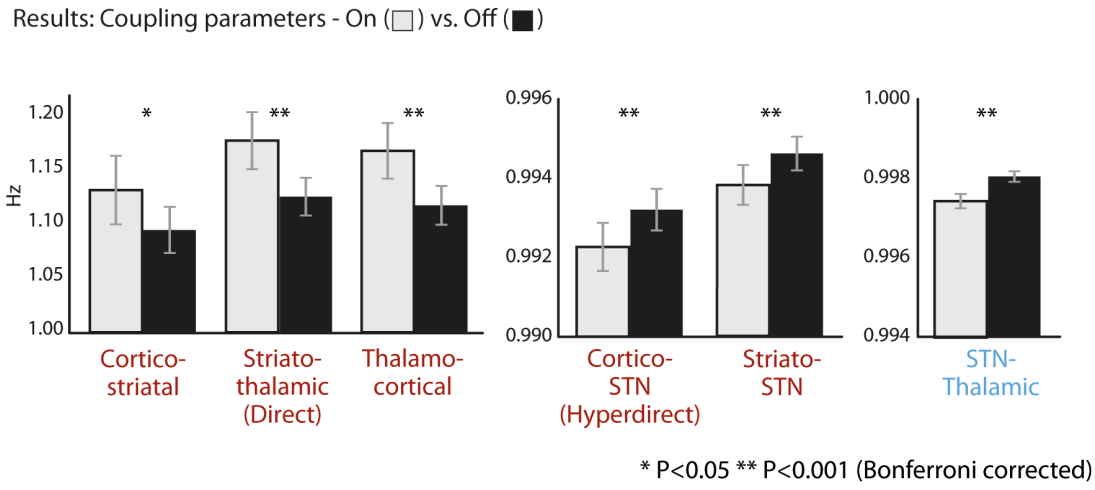

*Figure 8.6 Comparison of coupling strength on and off DBS. Paired t-tests revealed significant difference between extrinsic coupling on and off stimulation. *P <0.05, **P <0.001 (both corrected for multiple comparisons; Bonferroni procedure). (A) Cortico-striatal, direct pathway, and thalamo-cortical connections were potentiated by DBS, whereas (B) STN afferents and efferents were reduced. Note the difference in scale between A and B, is because of the fact that the STN was modelled as a 'hidden node'. See Chapter Appendix (section 8.6.2) for details of calculating ON and OFF coupling.*

The magnitudes of changes to connections involving the STN (i.e. connections constituting the hyperdirect and indirect pathways), although highly significant, were markedly smaller than the other modulatory effects discovered. This was due to the fact that the STN was estimated as a hidden region (see Materials and methods). All *p*-values are corrected for multiple comparisons using the Bonferroni procedure. See Figure 8.6.

8.4.5 Connection strengths predict clinical impairment

Separate ON and OFF multiple linear regression analyses revealed consistent results with regards to the direction of the regression coefficient for each connection. Three connections showed significant predictive capability in both stimulation conditions; the hyperdirect, direct, and striatal-STN connections. As the strength of the direct pathway increased, clinical impairment was reduced. Surprisingly, the same was true of the hyperdirect pathway, despite STN DBS reducing the strength of this connection. The reverse was true of the striato-STN pathway; the stronger this pathway, the more disabled the patient. See Figure 8.7a.

8.4.6 Change in connection strengths predict clinical efficacy

The three connections described above were the only connections of the original six that were included in the most parsimonious (after backwards elimination) regression model (Fig. 7). DBS scaling of coupling parameters were coded such that scaling >1 conferred increased coupling, whereas <1 conferred reduced coupling; thus as scaling increased numerically, the coupling got stronger. Consistent with the previous regression, increased scaling of the direct pathway predicted increased efficacy ($P<0.05$). Increased scaling of the hyperdirect pathway also predicted increased efficacy ($P<0.05$), whereas increased scaling of the basal ganglia afferents predicted reduced efficacy (although this was only trend significant, $P=0.067$). See Figure 8.7b

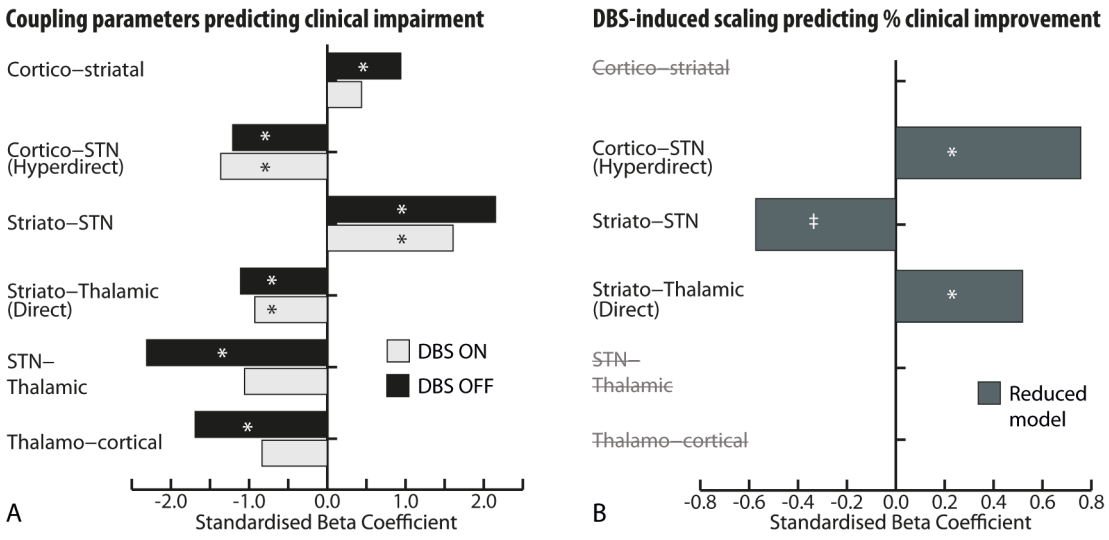

*Figure 8.7 Predictive validity. (A) Coupling parameters on and off stimulation were entered as independent variables to predict contralateral severity. *P <0.05. Direction of regression coefficients were consistent across conditions; however, only the connections in bold were significant predictors in both conditions. (B) DBS-induced scaling of each parameter was entered into a separate multiple linear regression model using stepwise backwards elimination to predict percentage clinical improve- ment. *P <0.05, ‡P <0.10 (trend significant). The hyperdirect, striato-STN and direct pathways remained in the parsimonious model.*

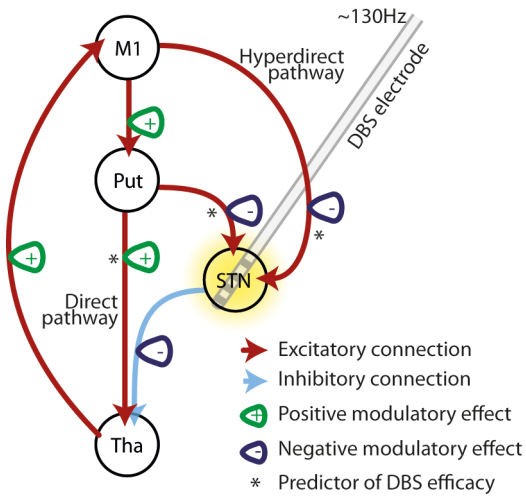

Figure 8.8 Summary of the modulatory effects of STN DBS on the BG motor loop.

8.5 Discussion

The results of this experiment speak to both its neurobiological aims, and the pragmatics of modelling resting state fMRI sessions. Building on the weaknesses of Chapter 7, I used a well-established (if simplified) model of the functional architecture of the motor cortico-striato-thalamic loop and estimated which connections, or combinations of connections, are modulated by STN DBS to produce the observed BOLD signal recorded at rest. The architecture specifically enabled questions to be posed regarding individual pathways, as set out in the experiment's aims. Chapter 7 concluded with speculation regarding the sensitivity of the thalamus to either direct or indirect pathway afferents; this experiment thus permitted formal investigation of this hypothesis in the "resting state".

8.5.1 Widespread neuromodulation

Results of the BMS demonstrate that a model with DBS-related modulatory effects on the extrinsic direct, indirect, hyperdirect, thalamo-cortical, as well as cortico-striatal pathways, consistently outperforms other (plausible) models. Analysis of the connection strength parameters revealed significant differences between active and inactive STN DBS in the six extrinsic connections investigated. The relevance of extrinsic coupling parameters to clinical phenotype was subsequently demonstrated using two orthogonal regression models; extrinsic coupling predicted clinical phenotype, and changes in extrinsic coupling predicted DBS-related clinical improvements (see Figure 8.7).

8.5.1.1 Cortico-striatal coupling & DBS

STN DBS was found to increase the sensitivity of the putamen to cortical afferents. This is interesting given PD patients show reduced MSN dendritic spine density and impairments in cortico-striatal glutamatergic transmission (Garcia et al., 2010). Furthermore, computational approaches have suggested DA potentiates cortico-striatal synaptic strength

(Leblois et al., 2006), and neuroimaging studies have demonstrated increased metabolism in the striatum under STN DBS (Geday et al., 2009; Hilker et al., 2002). Animal models of STN DBS have suggested stimulation normalises cortico-striatal glutamatergic synaptic densities and distributions in 6OHDA-lesioned rats (Walker et al., 2012), and regularises striatal discharge patterns in the resting MPTP-lesioned macaque (Santaniello et al., 2012). It remains possible that such enhancements could contribute to clinical improvements; however, the modulation of this connection was excluded from our parsimonious model of stimulation efficacy.

8.5.1.2 Thalamo-cortical coupling

Similarly, cortical sensitivity to thalamic afferents showed even greater, highly significant enhancements. PET and SPECT functional imaging in STN DBS patients have previously documented reduced perfusion and/or metabolism in the resting motor cortex during stimulation, and several authors have suggested this is caused either by restoration of pallidal inhibition of thalamic outflow or reduced synchronized oscillatory activity between motor cortex and basal ganglia (Ceballos-Baumann et al., 1999; Cilia et al., 2009; Geday et al., 2009; Grafton et al., 2006; Haslinger et al., 2005; Hershey et al., 2003; Limousin et al., 1997; Payoux et al., 2004). Our results are not necessarily in disagreement; increased effective connectivity between the thalamus and cortex does not necessarily confer greater metabolic activity at the target, rather it suggests that during stimulation, while at rest, the cortex may respond more efficiently to afferents from thalamus. Nevertheless, changes in this connection similarly failed to predict clinical efficacy, thus this effect may not be key to the immediate therapeutic mechanism of STN DBS.

8.5.1.3 Sensitizing the thalamus to the direct pathway

STN DBS increased the effective connectivity of the direct pathway, summarised here as a net excitatory connection from the putamen to the thalamus. Additionally, the strength of this connection predicted clinical severity in both ON DBS and OFF DBS states, and its scaling predicted clinical improvement; stronger direct pathway effective connectivity diminished Parkinson's disease impairments. This finding is highly concordant with early rate-based models of BG function that propose dopamine depletion results in an underactive direct pathway, and an overactive indirect pathway, culminating in thalamic inhibition (Albin et al., 1989; DeLong, 1990). Optogenetic investigation in 6OHDA-lesioned rats has lent further evidence to the beneficial effects of enhancing the direct pathway (Kravitz et al., 2010). The mechanism underlying this proposed gain tuning cannot be discerned here; our models do not include the GPi, thus I am unable to confirm whether modulation takes place further upstream of the thalamus. However, MPTP-lesioned monkeys receiving STN DBS display a more regular pattern of neuronal firing in the pallidal-receiving thalamic nuclei (Xu et al., 2008), and reduced neuronal entropy (Dorval et al., 2008), suggesting that STN DBS has downstream effects as far as the thalamus.

8.5.1.4 Desensitising the STN to hyperdirect drive

Coupling of both STN afferents (from the indirect pathway and hyperdirect pathway) was reduced by DBS. The hyperdirect pathway has been previously implicated in the generation of beta oscillations:

Firstly, simultaneous STN LFP and M1 electrocorticography suggest an exaggerated phase-amplitude coupling between cortical beta-phase and broadband gamma-amplitudes in PD. Importantly, cortical gamma was shown to precede STN beta, potentially suggesting

hyperdirect drive maintains STN beta. This altered coupling was reduced by STN DBS (de Hemptinne et al., 2013). Furthermore, single-unit recordings in 6OHDA-lesioned rats receiving STN DBS have shown antidromic hyperdirect activation of M1 layer V neurons, modifying their firing probability, and suppressing beta-synchrony at a population level (Li et al., 2012). STN LFP and cortical MEG have similarly shown that cortico-STN coherence is predominantly cortex leading (Litvak et al., 2011), and optogenetic stimulation of the hyperdirect pathway in 6OHDA-lesioned rats has been shown to ameliorate Parkinsonian symptoms, supporting the idea that interrupting hyperdirect cortico-STN transmission is therapeutic (Gradinaru et al., 2009).

Secondly, DCMs of LFP data in 6OHDA-lesioned rats (Moran et al., 2011a) and human patients (Marreiros et al., 2012) suggest that Parkinsonian spectral patterns at beta frequencies can be explained by increased effective connectivity of the hyperdirect pathway. Both these results support the hypothesis that STN beta oscillations are caused (in part) by increased effective drive from the cortex – something that I found DBS to decrease. Notably, in these studies, DCM was employed to explain observed increased β-band power at the nodes interrogated, whereas BOLD data (such as in this experiment) are not known to possess a reliable correlate of this electrophysiological biomarker.

From a technical DCM perspective, concurrent results from stochastic DCM for fMRI data are encouraging (and rather remarkable), and suggest DCM is able to furnish similar underlying functional architectures from datasets with markedly different temporal structures. This is potentially valuable, especially when considering the non-invasive nature of fMRI.

The relationship between hyperdirect coupling strength and clinical severity is particularly interesting. Comparing coupling ON and OFF stimulation reveal results that are in line with previous studies of effective connectivity, i.e., stronger coupling is associated with Parkinsonian phenotypes (Marreiros et al., 2012; Moran et al., 2011a). However, when all six connections are considered in a regression model predicting impairment including tremor, rigidity and bradykinesia, as rated by the UPDRS-III in humans, stronger effective hyperdirect coupling is beneficial to patient symptoms. This finding should be replicated in an independent dataset; however, considering hemibody scores may provide a more comprehensive evaluation of clinical effects that have not previously been captured by animal models or simple ON vs. OFF comparisons.

Taken together, the results of this experiment suggest that most of the beneficial effects of stimulation on the resting motor system appear to be explained by strengthening the effective coupling along the direct pathway, and not reducing coupling along the hyperdirect pathway.

Of course, this study cannot address whether the amelioration of the hyperdirect pathway is predictive of unwanted effects (or improvements) that are not indexed by the UPDRS-III score, and this issue could be the subject of further investigation. Disruption of the hyperdirect pathway has previously been used to explain increased impulsivity observed in STN DBS patients during high-conflict decision making tasks (Frank et al., 2007); however, this has been studied with medial prefrontal projections as opposed to M1 efferents (Cavanagh et al., 2011). This work suggests that disruption to hyperdirect effective connectivity may not be limited to prefrontal projections, at least during the resting state. Further work would be required to establish whether disruption to the hyperdirect pathway depends on the cortical source, or behavioural context.

8.5.1.5 Desensitising the STN and thalamus to indirect pathway afferents

DBS reduced the effective connectivity of STN afferents arising from the striatum, and efferents to the thalamus. These connections summarise the known polysynaptic connections between these structures (via the GPe for STN afferents, and GPi for STN efferents respectively), although they do not preclude a direct influence. It is difficult to compare this finding to the existing literature on the STN afferents from the GPe, especially as these two nuclei possess dense reciprocal connections (Marreiros et al., 2012; Moran et al., 2011a), although it does suggest that indirect pathway afferents are an important determinant of clinical severity. Unlike the hyperdirect pathway though, this scaling was in agreement with the direction of neuromodulation induced by stimulation.

Given the wealth of evidence for more global changes in brain activity under STN DBS (e.g. dorsolateral prefrontal cortex - Cilia et al., 2009; supplementary motor area and parietal cortex - Hershey et al., 2003; anterior cingulate cortex - Limousin et al., 1997), it is possible that our findings may generalise to other loops of the basal ganglia (interestingly, mostly reducing their cortical metabolic signatures at rest in PET/SPECT studies). Additionally, higher order afferents to the motor cortex (e.g. premotor and prefrontal input) could also be subject to modulation, as well as other subcortical nuclei (Asanuma et al., 2006). However, finding any behavioural correlates of changes within these circuits at rest may be more difficult.

8.5.2 Limitations and model assumptions

The model makes a number of simplifying assumptions, most notably the independence of the right and left hemisphere BG motor loops. As discussed above, this was motivated by the inherent clinical asymmetry observed in patients. However, there is evidence to suggest that components of the loops are functionally connected across hemispheres (de Solages et

al., 2010). Furthermore, this analysis assumes that DBS of one hemisphere is no more effective than DBS of another (i.e. there is no STN-dominant hemisphere).

Another simplifying assumption is the lack of pallidal nodes in our network. As discussed, DCM does not necessarily quantify monosynaptic coupling, thus not all nodes are required to estimate effective connectivity. Exclusion of GP dynamics is discussed in section 12.5.3, as this is common to the remainder of my experiments.

Similarly, the inclusion of the STN as a hidden node is also discussed there. The construct validity of this extension is presented briefly in the Appendix to this chapter – see section 8.6.1.

The range of clinical severity was also fairly small. This was due to the inherent limitation of using DBS patients and placing them in MRI scanners; mildly affected Parkinson's disease patients do not receive DBS, and those who have severe symptoms during OFF (both medication and stimulation) periods are less likely to engage in MRI research. Furthermore, I did not consider axial symptoms in our regression models as they are intrinsically difficult to lateralise.

8.5.3 Conclusions

These findings highlight the distributed effects of DBS on the Parkinsonian resting motor network in human patients in a non-invasive manner, and are largely in agreement with invasive animal experiments. The integration of clinical data, (in contrast to the animal literature,) suggests that the hyperdirect, direct, and STN afferents arising from the striatum are the most important predictors of clinical improvement. Sensitising the thalamus to direct pathway afferents, while simultaneously desensitising the STN to its afferents appear to increase stimulation efficacy. Intriguingly, STN DBS appears to achieve

these effects on the direct and striato-STN pathways, but actually has the reverse effect on the hyperdirect pathway, potentially subverting its therapeutic potential. It is tempting to hypothesise that sparing this pathway of modulatory effects would improve the efficacy of STN DBS; potentially ameliorating unwanted effects of stimulation.

While previous work has focused on statistical dependencies (functional connectivity) between regions of the brain, and how these change with onset of disease/therapy (Deco et al., 2011), this study uses validated modelling to derive effective connectivity between regions; that is, how neural populations impact on one another (Daunizeau et al., 2012a; David et al., 2008). From a methodological standpoint, this work is an example of how researchers can use DCM to provide mechanistic insights into neurological/psychiatric diseases and their therapies – in a non-invasive manner using fMRI data acquired in the resting state.

8.6 Appendices

8.6.1 Modelling a hidden node in DCM for fMRI

In this Chapter, I used stochastic DCM for fMRI to estimate the effect of DBS on extrinsic effective connectivity within the BG motor network. As discussed, classic implementations of DCM for fMRI require the user to extract summaries of the BOLD signal from a series of regions of interest, and an accompanying model structure, so that the hidden parameters governing the underlying dynamics can be estimated. Implanted hardware in our patients rendered it impossible to collect BOLD data from the vicinity of the STN, an important node in our network of interest. To solve this problem, a simple method that has previously been used in electrophysiological DCMs (David et al., 2011; Marreiros et al., 2012; Moran et al., 2011a) was translated to DCM for fMRI allowing inclusion of the STN as a 'hidden'

node in the graph, and only used the observed data collected from the remaining nodes to fit the models. In this appendix, I demonstrate that the resulting estimates provide qualitatively identical results, but quantitatively under-estimate the raw effect size. In other words, conclusions about the direction, standardised effect size, and cross-subject stability remain consistent, but these DCMs furnish lower raw values for the coupling.

To test the construct, I inverted two two-state, stochastic DCMs for fMRI per hemisphere per subject comprising three nodes; M1, the putamen and the thalamus. VOIs were defined as detailed in 8.3.4.3. The two DCMs possessed identical endogenous connections (M1→Putamen, Putamen→Thalamus, Thalamus→M1, see Figure 8.9a) and DBS entered the model as modulatory inputs on all three extrinsic connections. The models differed with regard to how the putamen was modelled; one used the observed putamen data, and one treated it as a hidden node with noise precision effectively zero. The DCMs were inverted and the posterior estimates for the extrinsic connections of the A- and B-matrices were extracted, and two multivariate one-sample Hotelling's T-square tests were used to test that these parameters were different from 0. Post-hoc one-sample two-sided t-tests were then conducted on individual extrinsic coupling estimates. The posterior estimates were plotted to demonstrate qualitative and quantitative difference in the estimates (Figure 8.9b,c). It is important to note that all values estimated in two-state DCM are log-transformed, this is not the case in deterministic DCM for fMRI.

8.6.1.1 Estimates of endogenous coupling (A-matrix)

Across 24 hemispheres, regardless of the model used, all estimates of extrinsic endogenous coupling were significantly different from 0 ($P<0.05$). Post-hoc one-sample t-tests confirmed this was true across all estimates ($P<0.05$). The estimates were numerically larger when the real data was used to fit the model, as opposed to the hidden model. The greatest

underestimation occurred at the afferent to the hidden node. That being said, the generalised effect sizes as measured with the T-statistic were just as large, indicative that although the mean was smaller, the cross-subject variability was also smaller. Furthermore, all values were larger than 0, conferring a coupling of >1Hz.

8.6.1.2 Estimates of DBS-induced scaling (B-matrix)

Once more, across 24 hemispheres, all estimates were significantly different from 0 ($P<0.05$), and post-hoc one-sample t-tests confirmed this was true across all estimates ($P<0.05$). Importantly, because the *direction* of modulatory effect is of particular interest (i.e. does DBS make the connection stronger or weaker, regardless of whether it is excitatory or inhibitory), it is noteworthy that the *direction* of modulatory effect is entirely consistent when using the hidden model. In other words, regardless of model used, I conclude that DBS strengthens the extrinsic connections of this network.

8.6.1.3 Conclusions

DCMs including hidden nodes produce qualitatively similar posterior estimates to DCMs fitted with real data from that region; both the direction and cross-subject consistency are unchanged. The magnitudes of the estimates are affected, believed to be due to the loss of region-specific parameters that would have normally been estimated (e.g. haemodynamic parameters).

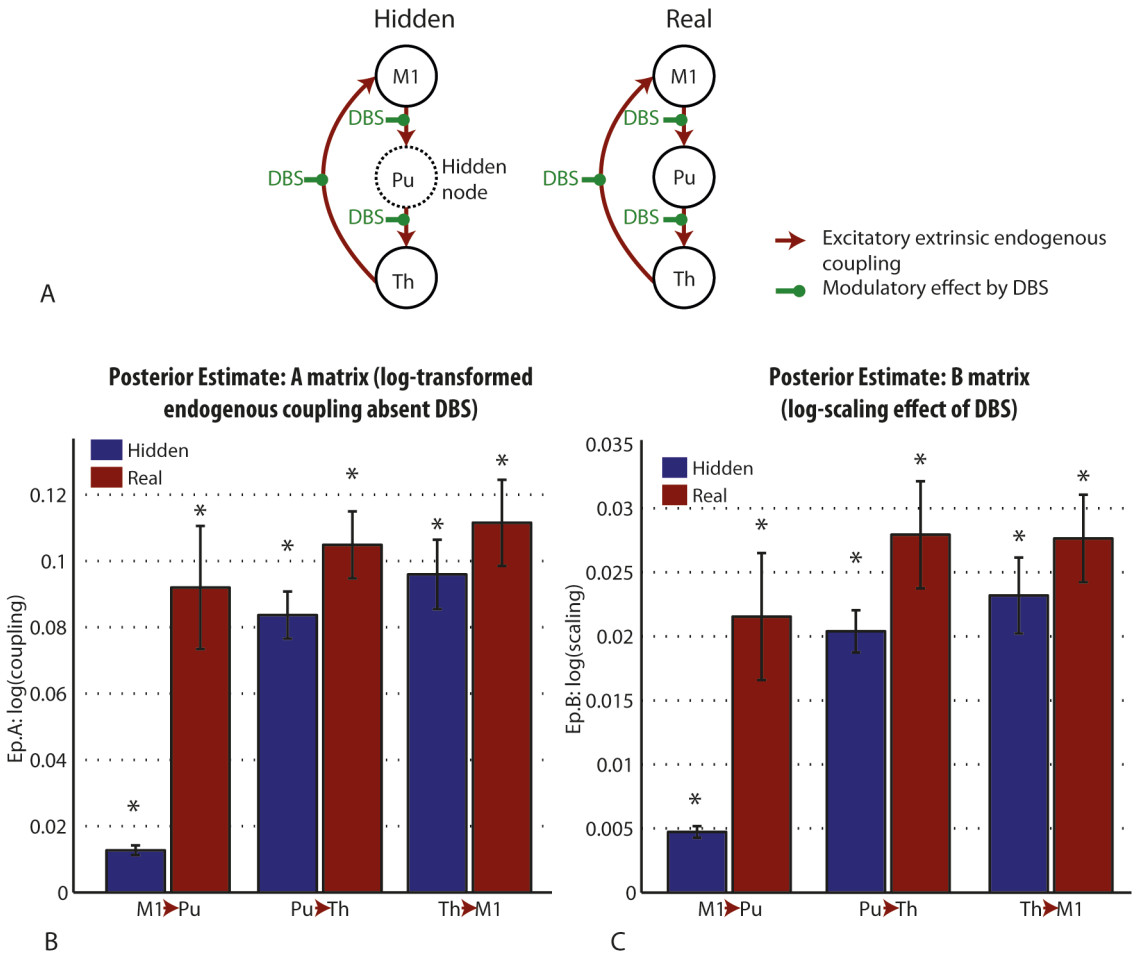

Figure 8.9 Comparison of DCM posterior estimates; 'hidden' putamen vs. real putamen data. (A) Posterior expectations of the log-transformed extrinsic coupling parameters (i.e. DCM.Ep.A matrix) across 24 hemispheres. Blue = hidden DCM, Red = real data DCM. Error bars represent standard error of the mean. All values were significantly different from 0, but the hidden DCM underestimates the parameters, particularly the afferent to the putamen. Although the magnitude of estimate was smaller, the narrower error bars suggest a similarly large standardised effect size. (B) Posterior expectations of the log-transformed scaling (i.e. DCM.Ep.B matrix) across 24 hemispheres.

8.6.2 Calculating ON and OFF coupling

The values of the DCM A-matrix typically reflect the endogenous coupling (in the absence of DBS in our case), whereas the B-matrix values estimate the effect of the modulatory input (DBS in our case) on the endogenous coupling (Friston et al., 2003). In two-state DCM for fMRI, the posterior estimates of these matrices are log-transformed, thus the A-matrix (DCM.Ep.A) reports log(coupling) values. Furthermore, the B-matrix reports

log(scaling) values, such that the coupling under the effect of DBS could be calculated by multiplying values of the A- and B-matrices. Thus, to transform to values in Hertz commonly reported in DCM studies, OFF = exp(Ep.A), and ON = exp(Ep.A)*exp(Ep.B) = exp(Ep.A+Ep.B). This reconfiguration was chosen to simplify things for people not familiar with the particular parameterisation of this DCM.

With regard the regression exploring the predictive capacity DBS-induced modulation, the value of the ratio ON / OFF = exp(Ep.A+Ep.B) / exp(Ep.A) = exp(Ep.B). In other words, the DBS-induced modulation is formally identical to the values of the B matrix in Hertz.

8.6.3 Bayesian model selection with fixed effect assumptions

When using fixed effects model assumptions, one assumes the model structure or connectivity is the same for each subject, but the strength of the coupling (or its modulation) can show random inter-subject variations. In other words, I implicitly assume that DBS modulated the same connections in each subject, but to varying degrees. In line with this, I used paired t-tests to explore the effect of DBS in relation to random effects on the parameters over subjects. For completeness, I also performed a random effects BMS, which produced consistent results; model 32 clearly outperformed the competing hypotheses (model exceedance probability > 99%).

8.6.4 Extracting M1 VOIs given the artefact

Figure 8.10 details the spatial location of the centre of the M1 VOI, relative to the artefact patterns on the functional (GE-EPI) images. A mask of the precentral gyrus taken from the Harvard-Oxford Cortical Atlas (in the FSL software suite) is overlaid (in transparent green) on the 50th acquisition from each subject. The cross-hairs demarcate the centre of the M1 VOI extracted. The z represents the level of the axial slice in millimetres (MNI space).

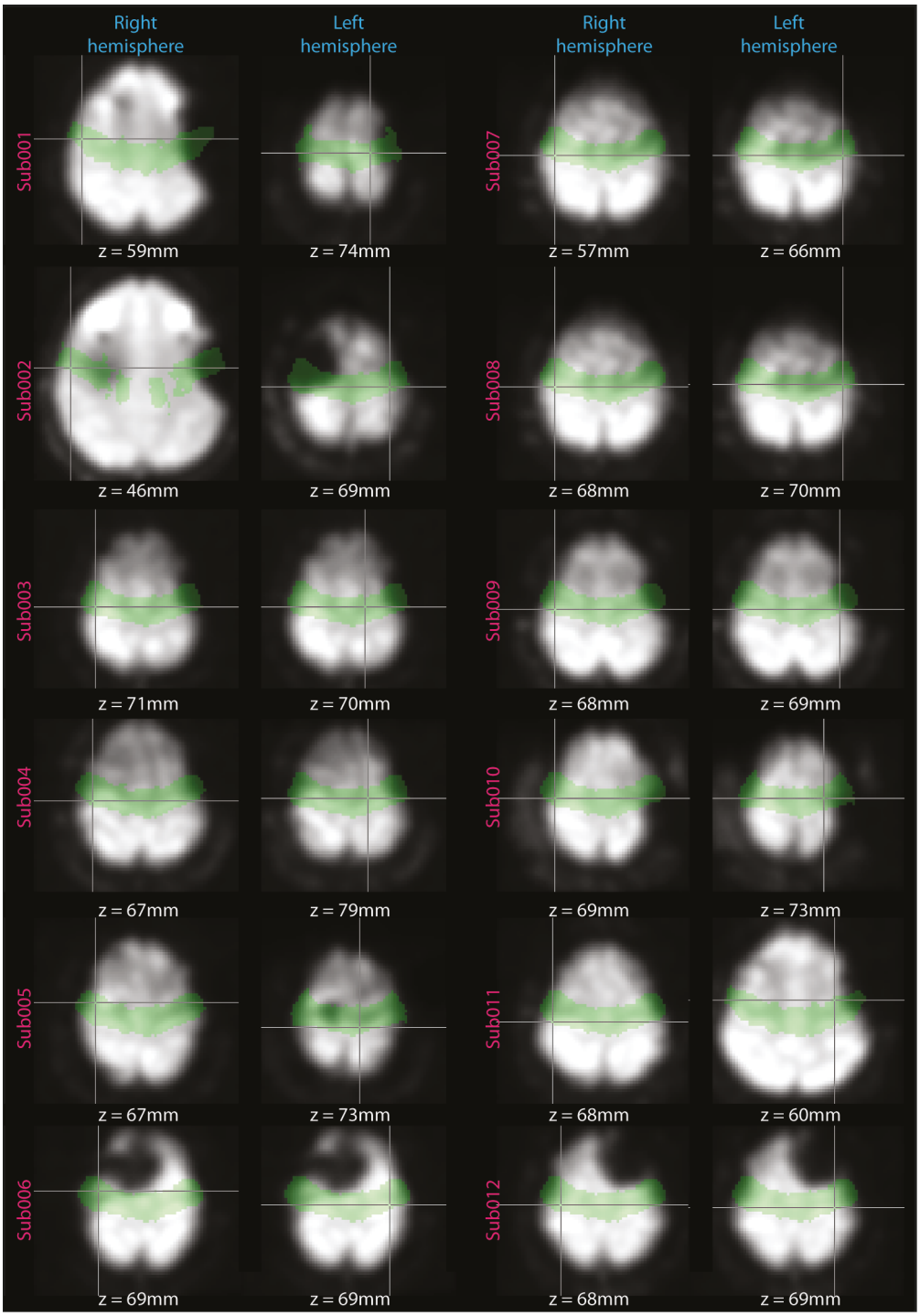

Figure 8.10 Spatial location of the centre of the M1 VOI, relative to the artefact patterns on the functional (GE-EPI) images. A mask of the precentral gyrus taken from the Harvard-Oxford Cortical Atlas is overlaid (in transparent green) on the 50th acquisition from each subject. The cross-hairs demarcate the centre of the M1 VOI extracted. The z represents the level of the axial slice in millimetres (MNI space).

9 The safety of using body-transmit MRI in patients with implanted STN DBS

Parts of the following chapter have been submitted for publication.

9.1 Summary

In this chapter, I present a series of *in vitro* experiments aimed at (1) improving the quality of collected fMRI data, and (2) widening the potential pool of subjects to recruit from. As discussed, the main safety concern with MRI in DBS patients is heating at the electrode tips (see section 5.5.1). Previous onsite investigation has shown that heating can be minimised with strict adherence to a supervised acquisition protocol using a head-transmit/receive coil at 1.5T (Carmichael et al., 2007).

MRI using the body-transmit coil with a multi-channel receive head coil has a number of potential advantages including an improved SNR. Furthermore, previous safety studies have used old DBS systems that are being used less, thus it was important to confirm the MRI safety of newer systems. Therefore, I compared the safety of MRI in an *in vitro* model of bilateral DBS using head-transmit and body-transmit coils respectively, at both 1.5T and 3T. Additionally, I investigated the effect of transmit coil choice on DBS stimulus delivery during MRI.

Changing from head- to body-transmit coil increased the electrode tip temperature at both field strengths, and the position of the phantom relative to the body coil significantly was

an important determinant of heating at 1.5T. However, the worst-case at 1.5T remained <1°C.

I conclude that (1) body-transmit cranial MRI at 1.5T, with our specific hardware and protocol (head SAR ≤0.2W/Kg), does not produce heating exceeding international guidelines, even in cases of exaggerated patient misplacement (2) cranial MRI at 3T produces unacceptable heating, (3) patients with ActivaPC™ Medtronic systems are safe to be recruited to further fMRI experiments, and (4) ON vs. OFF DBS fMRI studies are not confounded by inappropriate stimulus delivery or discrepant heating.

9.2 Introduction

As discussed (see sections 5.4.2.8 & 5.5), the paucity of fMRI studies in DBS patients has been largely due to safety concerns with regards to scanning patients with implanted systems (Rezai et al., 2005). Two notable and unfortunate case studies have highlighted the potential dangers of DBS interacting with MRI scanning when safe operating conditions are not observed (Henderson et al., 2005; Spiegel et al., 2003). Thus it is important to establish MRI protocols that both minimise risk to the patient, while maximising the quality of the resulting clinical or research data. To date, safety considerations have led to some compromise in the quality of fMRI data attainable with DBS apparatus *in situ*, particularly the specification of a head-only RF transmit coil effectively precluding the image-quality advantages of multi-channel receive coil technology. Furthermore, the contemporary gold standard for fMRI in the cognitive neuroscience literature is to use body-transmit MR with multi-array receive coils (usually 16 or 32 channels), thus we aimed to bring DBS fMRI in line with best practice.

In addition it was also important to test the safety of scanning patients with the latest systems. Only older generation DBS systems have been rigorously safety tested, thus recruitment has been limited to the few patients who still have Medtronic Kinetra systems[17].

To address these limitations, I investigated the safety of MRI in an *in vitro* model of a DBS patient using a body RF transmit coil. I compared the results with those obtained using a head-transmit coil in accordance with our established clinical and research practice, with

[17] *Patients routinely have their IPGs replaced every 5 years or so. The Kinetra™ has not been implanted since approximately 2011, so even if some patients at this centre originally received a Kinetra™, only a few of them still have one implanted.*

the purpose of improving the quality and versatility of research and clinical MRI in patients with DBS.

Finally, it was important to establish whether the MR environment confounded fMRI data collection with the new devices/coil combinations. Specifically, I compared whether there were any differences in induced heating under different stimulation conditions, and whether scanning impacted on IPG output.

9.2.1 Aims

Through *in vitro* testing, the aims of these experiments were to:

1. Confirm head-transmit/receive coil MRI is safe using the currently implanted DBS hardware.
2. Compare the MRI-induced heating obtained using the body-transmit coil to that with the head-transmit coil under both 1.5T and 3T field strengths.
3. Compare the MRI-induced heating between DBS 'ON' and 'OFF' stimulation conditions.
4. Confirm that fMRI sequences using the body-transmit coil do not impair IPG function.

9.3 Materials and methods

Standard radiological orientation is used throughout this report. A poly-methyl-methacrylate phantom with dimensions resembling a human torso was filled to a depth of 10cm with a gel of poly-acrylic acid partial sodium salt (8 g/L), sodium chloride (0.70 g/L), and distilled water (Carmichael et al., 2007; Rezai et al., 2002). At room temperature, this gel has been demonstrated to possess electrical and thermal characteristics similar to those of human tissue (Carmichael et al., 2007; Park et al., 2003). See Figure 9.1.

A Medtronic ActivaPC™ DBS system (Medtronic Inc, Minneapolis, MN, USA) was positioned within the phantom in a configuration resembling that in a patient with fully implanted hardware. The IPG (Model 37601) was partially submerged in the left 'pectoral' region of the phantom such that the outer casing was in contact with the gel. Two 18mm diameter burrholes were drilled into the superior edge of the phantom, representing the superior cranium, and burr-hole caps were fixed into position.

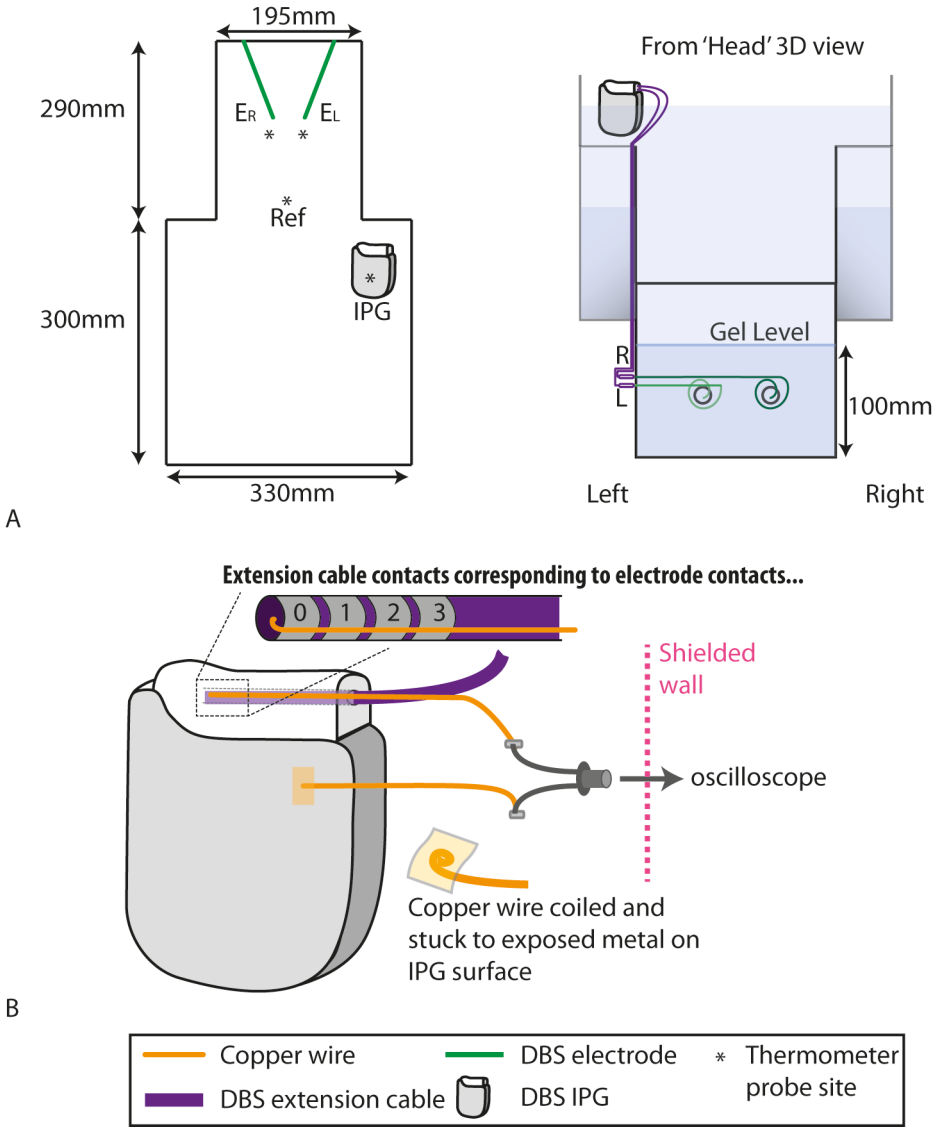

*Figure 9.1 In vitro model of DBS patient implanted at this centre. (A) Phantom dimensions. * = thermometer recording site, IPG = Implantable pulse generator. (B) Recording the voltage output of the IPG. E_L = left electrode, E_R = right electrode.*

The simulated target nuclei positions were established at fixed locations analogous to the positions of the subthalamic nuclei (STN) relative to the burr-holes in a human (based on measurements from STN-DBS implantation surgeries). Two electrodes (model 3389, Medtronic Inc, Minneapolis, MN, USA), one on each side, were fixed to the burrhole caps, and their ends were positioned in the target 'nuclei' regions. Suture silk and a plastic frame were used to maintain the path of the electrode leads through the gel. Excess lead was coiled around the burrhole 2-3 times on the external surface of the phantom, in an arrangement similar to our clinical practice. The leads were connected to the IPG using two DBS extension cables (Model 37085) routed along the external surface of the phantom.

9.3.1 MRI scanning

Measurements were performed in Siemens MAGNETOM Avanto (1.5T) and TIM Trio (3T) MRI systems, both operating at Siemens software level VB17. The phantom was placed head first, supine within the bore of the scanner, with the tips of the electrodes at the magnet isocentre (i.e. using the tips of the electrodes as a central landmark for image-volume prescription). The scanner calculated predicted SAR values assuming the phantom was a 75 kg, 44 year old male. Imaging was performed with either the respective manufacturer-supplied head transmit-receive coil, or using the system body-transmit coil with a 12-channel head receive coil. To provide temperature changes of sufficient magnitude to assess reliably while minimizing the risk of damaging the DBS equipment, turbo-spin echo (TSE) sequences (repetition time (TR) 4000ms; echo time (TE) 111ms; bandwidth (BW) 100Hz/pixel; field of view (FOV) 22x25cm; matrix 320x320; echo-train length 12, 4 slices; slice thickness (ST) 2mm; 4 averages; scan time 6 minutes 14 seconds)

with scanner-reported head SAR 0.2W/kg were used as a 'worst-case' test[18]. Measurements were performed twice for each coil combination used, and twice for each DBS stimulation condition. The head SAR calculated by the scanner was recorded for each scan.

Additionally, at 1.5T it was important to examine the effect of changing the phantom position relative to the body-transmit coil on electrode heating, in this case with the IPG set to 'OFF' for all measurements. This was explored to ensure that cranial MRI with the body-transmit coil was safe even when patients were misplaced in the scanner. The tips of the electrodes were initially positioned at a reference site at the magnet isocentre. The phantom was then displaced 150mm *into* (negative displacement) the scanner and scanned using the TSE sequence. This was subsequently replicated at six further successive displacements relative to the magnet isocentre (-100mm, -50mm, 0mm, +50mm, +100mm, and +150mm).

To confirm the safety of a typical research fMRI acquisition compared to our worst-case test TSE protocols, I performed 1.5T thermometry, with the electrode tips at the magnet isocentre, during a gradient-echo echo-planar (GE-EPI) acquisition (TR 3700ms; TE 40ms; BW 2298Hz/pixel; FOV 19.2cm; matrix 64x64; 49 slices; ST 2.5mm; 96 measurements 1 average; scan time 6 minutes). The effect of phantom position within the scanner was not explored with this sequence.

9.3.2 IPG settings

Scanning was performed with the IPG active ('ON') and inactive ('OFF'). During ON scans, the IPG was programmed to deliver stimulation typical of that employed in STN DBS for PD (Frequency: 130Hz; Amplitude: 3.5V; Pulse width: 60μs). Unipolar

[18] *At isocentre, scanner reported body SAR = 0.064 W/Kg.*

stimulation settings were used so that current flowed from the case to the distal (the deepest) contacts of each electrode (RHS = contact 0, LHS = contact 4).

9.3.3 Fibre-optic thermometry

The temperature was recorded simultaneously from four loci in the phantom using a 4 channel fibre-optic temperature thermometer (Neoptix ReFlex – Neoptix, Québec, Canada) based on gallium arsenide (GaAs) semiconductor crystal technology (sampling rate = 1Hz). Temperature probes were located at the distal electrode contacts (one for each electrode lead – see Figure 9.2), the IPG case, and the centre of the phantom 'head' region, remote from the electrode contacts, providing a control recording of background temperature changes (Figure 9.1a).

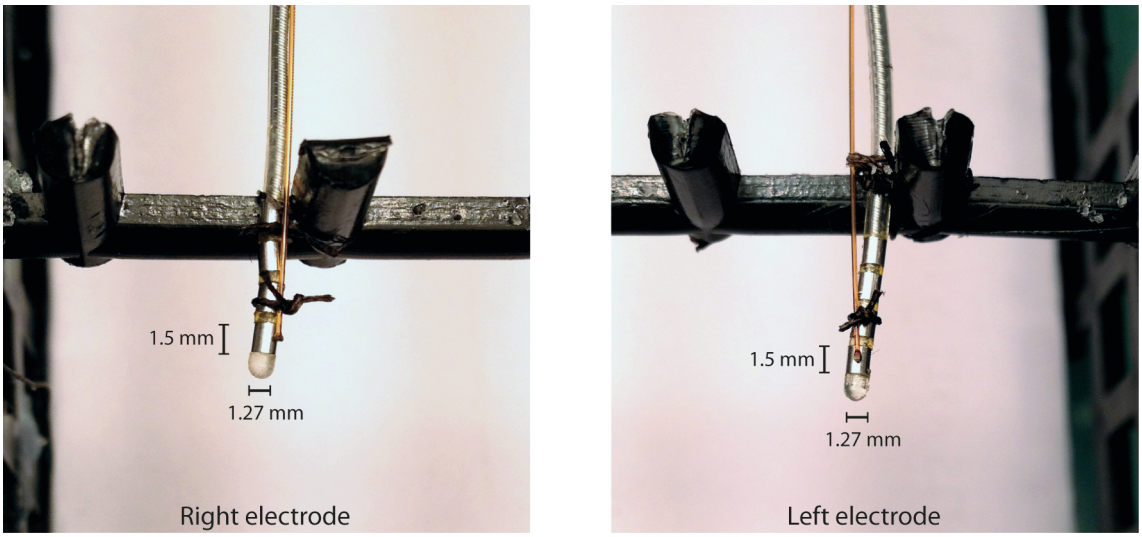

Figure 9.2 Positioning the fibre-optic probes at the distal electrode contact. The fine golden probes are the temperature probes, whereas the grey probes with 4 metal contacts on the end are the DBS electrodes. Suture silk was used to ensure that the thermometer probes were opposed to the distal electrode contacts, believed to be the site of the greatest MRI induced heating. This was fiddly.

9.3.4 Pacemaker voltage output in during typical fMRI sequences

To confirm that the fMRI sequences did not disturb IPG function, the voltage between contact 0 (i.e., the most distal contact on the quadripolar lead) and the IPG case was

measured whilst the phantom was exposed to the typical fMRI sequence. Fine enamelled copper wire (Diameter: 0.15mm; Gauge: 40swg) was threaded into the extension cable socket in the IPG, such that the end of the wire was in electrical contact with the distal electrode contact. A separate wire was in electrical contact with the IPG case. The wires were attached to an oscilloscope probe made of gold-plated and nickel-plated brass that was firmly secured to the external wall of the phantom. This was in turn connected via a coaxial extension cable (Impedance: 50Ω), which passed through a shielded wall into the MRI control room, to a digitizing oscilloscope (WaveJet 354A, Teledyne LeCroy - Bandwidth = 500 MHz) (Figure 9.1b). The voltage was recorded both with and without an active IPG output before scanning sessions to confirm the captured signals were in accordance with the voltage and frequency that the IPG had been programmed to deliver. Temperature data were not collected during these scans as the additional wiring involved may have confounded heating estimates.

9.3.5 Data Analysis

9.3.5.1 Maximum heating estimates

Data were analysed using MATLAB (The MathWorks, Inc., Natick, MA, USA). Fifteen pre-scan temperature measurements from each probe were averaged to provide a probe-specific baseline temperature. Temperature change (ΔT) was calculated by subtraction of this baseline value for each time-point during the scan and for up to 1 minute post-scan to allow time for the temperature to stabilise. To remove occasional instrumentally generated temperature recording point instabilities a threshold was applied to remove any implausibly extreme values (mode +/- 80°C), before a second threshold was applied to prevent implausibly large changes in temperature between data points (i.e. the first differential w.r.t time was calculated and data points that increased/decreased > 1.9°C/sec were removed).

These thresholds were optimised on pilot data collected in the 3T scanner with the body-transmit coil displaying the greatest and fastest increases in temperatures, and were then applied to all data sets.

Pilot thermometry measurements demonstrated a characteristic exponential increase in temperature at the electrode tips, asymptotically approaching a plateau phase towards the scan end, with the most extreme heating occurring at the left electrode tip, consistent with previous findings (Carmichael et al., 2007). In light of this time-course, a 20 second epoch was extracted at the end of each scan (i.e. during the plateau phase, whilst the electrode was at its highest temperature) to represent the maximum temperature in each case. Thus there were 20 data points for each MRI scan; each scan sequence was tested twice, thus there were 40 data points per coil combination per stimulation condition. Using the left electrode data as the worst-case temperature rise estimate, paired T tests were used to compare MRI-induced ΔT produced by the head-transmit and the body-transmit coils respectively (collapsing across stimulation conditions). Additionally, ΔT was similarly compared across stimulation conditions (collapsing across coil conditions).

9.3.5.2 The effect of position relative to the body-transmit coil

Linear regression analysis was used to analyse the effect of phantom position within the body transmit coil. The electrode tip position at the isocentre was defined as 0cm; displacement *into* the scanner (i.e., equivalent to *pushing* a subject's feet further into the scanner) was coded as a negative displacement, whereas displacement *out of* the scanner (i.e., equivalent to *pulling* a subject's feet out of the scanner) was coded as positive displacement. Mean ΔT at the left electrode tip during the final 20 second epoch at each position was considered the dependent variable, with position the independent variable.

9.3.5.3 IPG output during MRI scanning

Voltage waveforms before and during a GE-EPI fMRI sequence were captured with the digital storage oscilloscope and transferred electronically into MATLAB for plotting and analysis. The DBS pulse period was calculated by averaging the time between voltage excursions greater than 2.5V. The DBS frequency was calculated as the inverse of the period, i.e. $f = 1 / T$.

9.4 Results

Baseline temperatures before the measurements commenced were between 18-20°C. At the electrode tips, the TSE sequences produced a ΔT of <1°C and <2°C at 1.5T and 3T respectively, regardless of coil used. Any temperature increases at the IPG body were <0.2°C in all cases. The reference probe confirmed that gel temperature changes distant from any DBS hardware remained within the range of the thermometer sensitivity (±0.1°C). In accordance with previous work (Carmichael et al., 2007), the left electrode consistently displayed greater heating than the right. Regardless of coil or stimulation setting, ΔT plots followed a similar pattern (Figure 9.3); an initial rapid increase in temperature resembling a logarithmic plot lasting approximately 50 seconds, followed by a curve resembling an exponential recovery eventually tending towards a plateau at a maximum temperature at the end of the MRI pulse sequence. When the scan ended, temperatures rapidly returned to baseline.

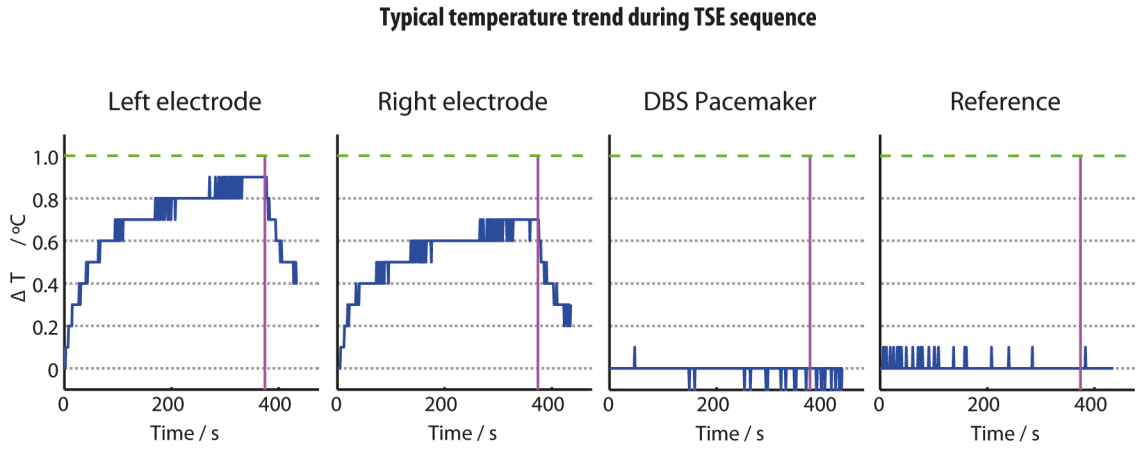

Figure 9.3 Typical temperature trend observed during a TSE sequence at the 4 thermometer sites using the body-transmit coil. Green line is the safety limit (1°C). Pink line indicates the end of the scan.

Exposure to MRI at both 1.5T and 3T had no effect on the IPG's ability to turn on/off and communicate with the DBS patient controller. With the phantom positioned at the

magnet isocentre, the scanner-reported head SAR remained at 0.2 W/Kg for the prescribed TSE sequence, and was 0.1 W/Kg for the GE-EPI sequence, regardless of coil used.

9.4.1 Pre-scan induced heating

It is important to note that prior to commencement of the imaging acquisitions, following changes in phantom position the scanners automatically perform a 'pre-scan' calibration procedure lasting approximately 30 seconds. Scanner-induced ΔT were also observed during this pre-scan period, specifically during the 3D shim-field estimation. At 1.5T, pre-scan ΔT were similar to the maximum values observed during the TSE image-data acquisitions, regardless of coil used. At 3T, pre-scan ΔT using the head-transmit coil were similar to the TSE scan heating. However using the body-transmit coil at 3T, heating at the left electrode approached 10°C during the pre-scan procedure, far above the maximum temperatures observed during the scans themselves (see Figure 9.4).

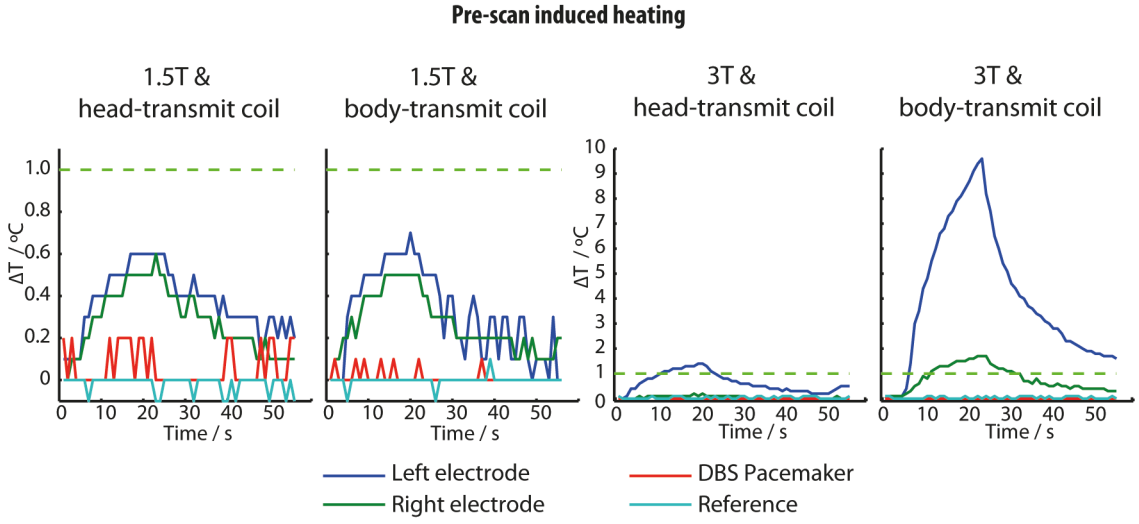

Figure 9.4 Heating at the 4 thermometer sites during the 'pre-scan' period, potentially coinciding with the shimfield estimation produced. Note the change in scale for the 3T plots.

9.4.2 Effect of body-transmit coil on electrode heating

Changing from head- to body-transmit coil produced small but significant increases in the observed electrode tip maximum ΔT during TSE scans from a mean of 0.45°C to 0.79°C ($p < 0.001$, 95% CI: 0.29-0.39°C) at 1.5T, and from 1.25°C to 1.44°C ($p < 0.001$, 95% CI: 0.13-0.25°C) at 3T (see Figure 9.5). When this comparison was repeated with the GE-EPI sequences at 1.5T, this effect was not observed ($p = 0.652$).

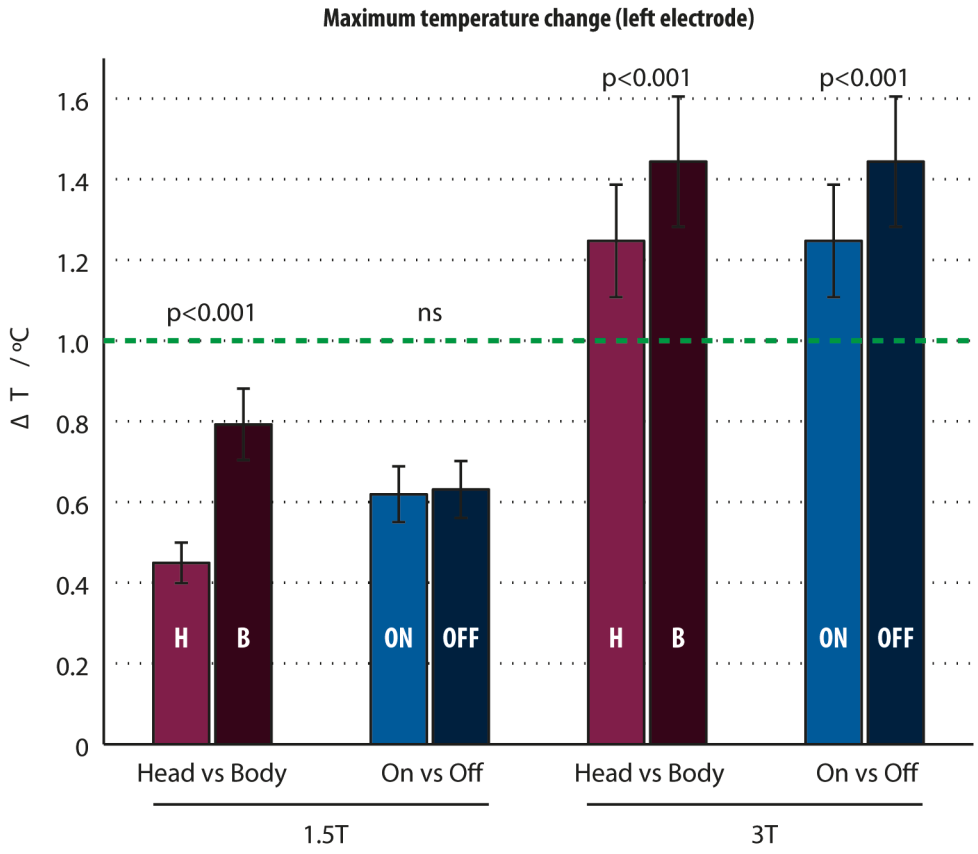

Figure 9.5 Maximum temperature change induced by the TSE sequence.

9.4.3 Effect of stimulation setting on electrode heating

I did not observe an effect of IPG stimulation setting ($p = 0.42$) upon ΔT at 1.5T during TSE sequences. However at 3T, ΔT was greater when the stimulator was switched off, increasing from a mean of 1.24°C to 1.44°C ($p < 0.001$, 95% CI: 0.14-0.26°C) (see Figure 9.5).

When this was repeated with GE-EPI sequences at 1.5T, active stimulation increased electrode ΔT from a mean of 0.43 to 0.51°C ($p < 0.0072$, 95% CI: 0.02-0.14°C), roughly an increase of 0.08°C, which falls within the measurement accuracy of our thermometer (±0.1°C).

9.4.4 Effect of position within the body-coil on electrode heating

Position within the body coil impacted significantly on electrode heating for the same MRI acquisition sequence and parameters. Linear regression revealed a significant effect of position (beta = -0.02, T = -6.87, $p < 0.001$), indicating that the further the phantom was *into* the scanner, the greater the observed heating at the electrode tips. Worst-case ΔT (0.9°C) occurred when the phantom was displaced 15cm *into* the scanner (Figure 9.6). Scanner-reported SAR values varied with phantom position and are presented for completeness (Figure 9.6). *Head SAR* was a maximum (0.2 W/Kg) at 0 displacement, but reduced to 0.16 W/Kg at larger displacements in either direction. Both scanner-reported *body SAR* (max = 0.16 W/Kg, min = 0.03 W/Kg) and scanner-reported *exposed SAR* (max = 0.10 W/Kg, min = 0.06 W/Kg) reduced as the displacement out of the bore (i.e. +ve displacement) increased.

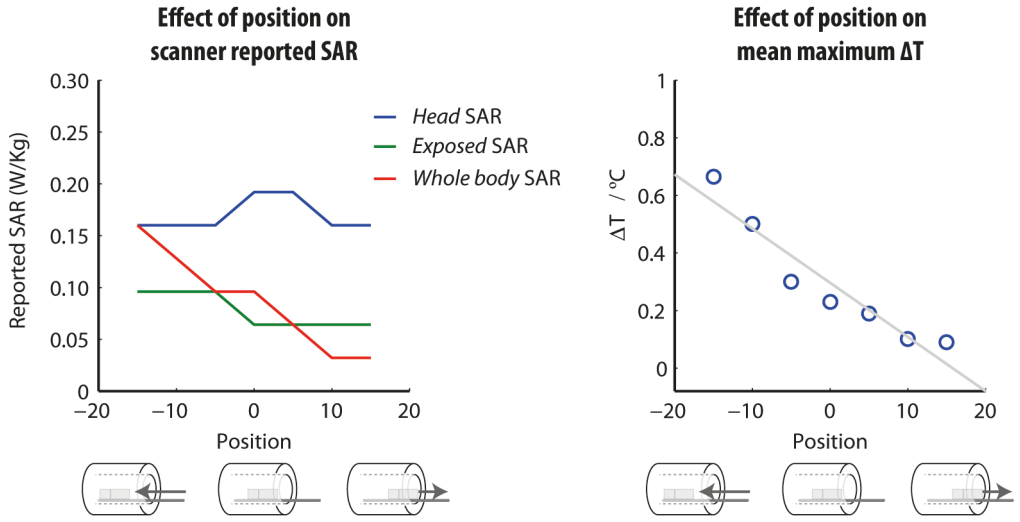

Figure 9.6 The effect of position of the phantom within the body-transmit coil on the resultant temperature increase.

9.4.5 Effect of fMRI sequences on IPG output at 1.5T

The voltage output of the IPG recorded outside of the scanner revealed regular discharges with frequency and amplitudes matching the programmed settings (estimated to be 130.9Hz), confirming our recording circuit functioned as expected. Example plots of the voltage between one active electrode contact and the IPG body captured during scanning using the body-transmit coil are displayed in Figure 9.7. As previously observed with the head transmission (Carmichael et al., 2007), GE-EPI sequences produced high frequency (i.e. exceeding the oscilloscope Nyquist sampling frequency) signals due to the sequence RF pulses, and lower frequency signals (~1000 Hz) arising from the switching magnetic field gradients. The RF excitation pulse induced a large amplitude component (peak amplitude <2V), whereas the fat saturation pulse produced a lower amplitude (<0.5V) component. The IPG pulse amplitude and frequency appeared superimposed upon and independent of the MRI-induced signals components. Similar results (data not presented) were obtained using the head-transmit coil.

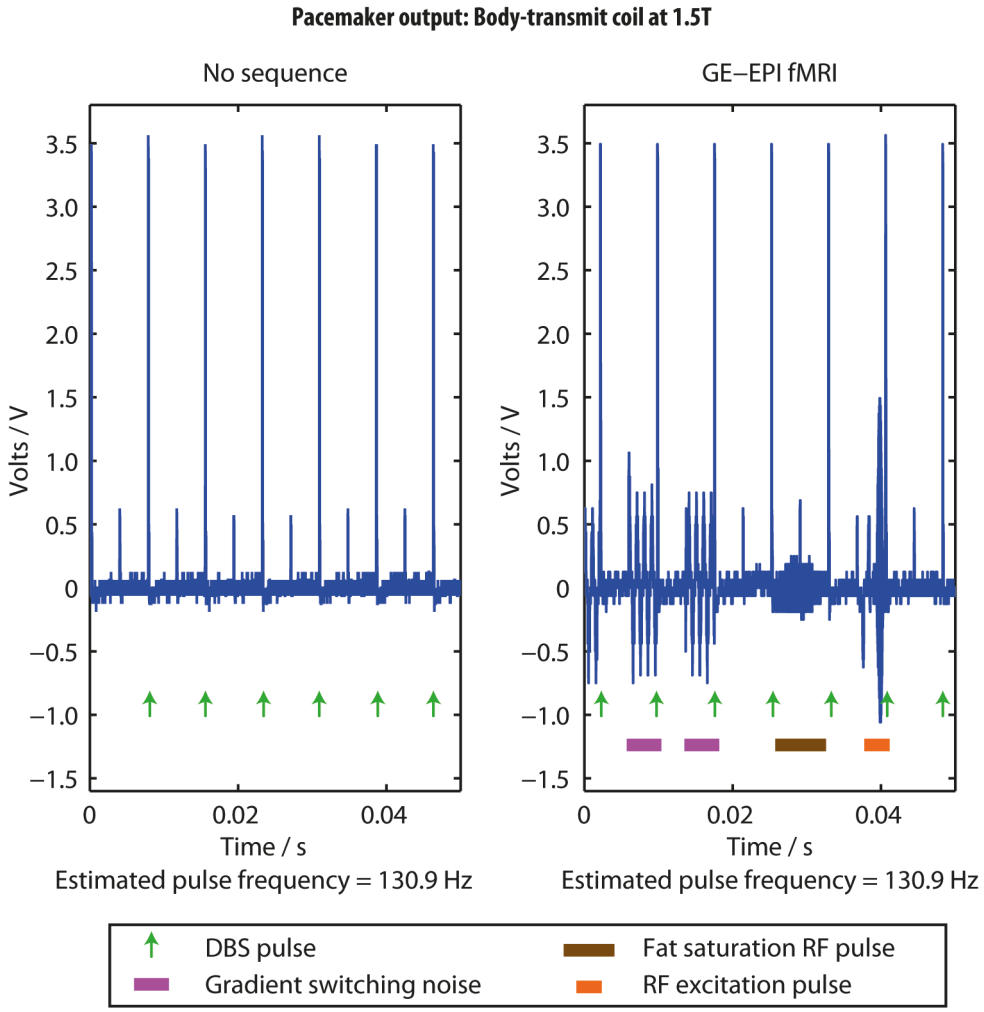

Figure 9.7 The voltage output during a typical GE-EPI fMRI sequence.

9.5 Discussion

This series of experiments provide evidence that cranial MRI at 1.5T using the body-transmit coil in patients with new DBS systems can be collected without harm to the patient, provided a restricted SAR threshold is adopted. Herein, I discuss how this relates to current safety data on implanted DBS devices. I additionally discuss how these results do not suggest that scanning under this protocol confound fMRI data.

9.5.1 The safety of active DBS during fMRI using the body-transmit coil

9.5.1.1 Guidelines

The current UK and international guidelines impose that MRI-induced heating should not cause the temperature within the brain to exceed 38°C, requiring any intra-cerebral heating at the electrodes to be ≤1°C (HPA, 2008). Results of this experiment propose that this can be safely achieved during 1.5T cranial MRI with a Medtronic ActivaPC™ system, regardless of transmit coil used, providing the head SAR is limited to ≤0.2 W/Kg. This SAR limit exceeds that currently recommended by the device manufacturer (Medtronic, 2010) and it is important to state that MRI of patients with implanted hardware outside of the manufacturer's instructions should only be performed following a comprehensive local risk assessment specific to the MRI system and particular DBS hardware under supervision from MRI experts (in our case, the MRI physics team at the National Hospital).

9.5.1.2 Experimental design

MRI-induced heating was measured in the vicinity of the electrode tips, as these regions are in direct contact with neural tissue *in vivo*, and have previously been identified as regions that show the greatest MRI-induced ΔT (Baker et al., 2006; Bhidayasiri et al., 2005; Carmichael et al., 2007; Georgi et al., 2004; Kainz et al., 2002; Rezai et al., 2002; Sharan et al., 2003; Tronnier et al., 1999). Heat dissipation in these regions occurs primarily via

thermal conduction and convection within the gel; it should be noted that, despite similar thermal properties, the *in vitro* gel measurements conservatively over-estimate MRI-induced heating obtained *in vivo*. In the latter case, heating would be reduced by cerebral blood flow (Collins et al., 2004; Salcman et al., 1989).

TSE sequences with a relatively high SAR were deliberately chosen so as to generate ΔT sufficient for accurate measurement given the sensitivity of the thermometry. Heating was consistently largest at the electrode tips, with the left electrode displaying the greatest ΔT. Such asymmetry has been reported elsewhere and is believed to be due to asymmetry in the DBS circuit with respect to scanner field orientation (Baker et al., 2004; Bhidayasiri et al., 2005; Carmichael et al., 2007), combined with asymmetries in the scanner B1 transmit field at 3T due to similar permittivity boundary conditions as seen in human scanning. It was unlikely that local conditions in the gel caused this asymmetry as this was observed consistently throughout all measurements, including separate temperature recordings and multiple gel preparations.

9.5.1.3 Effect of coil at 1.5T

Using the head-transmit coil at 1.5T, average maximum ΔT was 0.45°C, compared to 0.79°C using the body-transmit coil. With the electrode tips positioned at the scanner isocentre, scanner-calculated head SAR remained constant (0.2 W/Kg) for both coil arrangements, suggesting ΔT differences were not due to varying RF pulse power calibration. The different ΔT are most likely explicable by differences in the area of the DBS circuit exposed to the RF B_1-field in each case, changing the conditions for electrical coupling according to Maxwell's equations (Georgi et al., 2004). A similar mechanism presumably underlies our subsequent finding that ΔT is also dependent upon position of

the phantom within the body-transmit coil. Furthermore, differences in the design of the RF coils (and hence the associated electric fields) may also play a role.

9.5.1.4 Position in the scanner during body-transmit MRI at 1.5T

It was important to ensure that cranial MRI was safe, even when patients were accidentally misplaced in the scanner[19]. Heating produced by body-transmit MRI at 1.5T was significantly predicted by the position of the phantom in the scanner. ΔT increased the further into the scanner the phantom was moved, consistent with more of the DBS circuit being exposed to the RF field, increasing the magnitude of the induced currents. The pulse sequence parameters were held constant between positions; interestingly, the scanner-reported *head* SAR did not directly explain the temperature change. Rather, in a separate regression, the *whole body* SAR significantly predicted the observed ΔT ($P < 0.05$). This suggests that the *whole body* SAR is a better means of confirming safety when using the body-transmit coil, and may provide a more meaningful metric for defining maximum safe RF exposure. Analogous experiments using the head-transmit coil did not need to be undertaken given the position of the patient (and hence DBS circuit) remains fixed relative to the transmit coil.

9.5.1.5 Regardless of coil, 3T confers too great a risk

Scanning at 3T produced ΔT >1°C suggesting an increased thermal risk compared with similar acquisitions at 1.5T. Although relatively modest when using the head-transmit/receive coil (<2°C), heating exceeded the HPA 2008 recommendations. Since there is limited published evidence on what temperature changes are safe in this context, I

[19] *Scanning with the patient displaced +150mm from isocentre would be equivalent to their heads being almost outside the scanner. This would be a rather extreme case of patient misplacement, however was collected for completeness.*

(under the supervision of the MRI physics team at the hospital) have chosen to adhere to these recommendations in our current practice.

9.5.1.6 Pre-scan heating

The instance of 10°C heating observed during the pre-scan procedure at 3T with the body-transmit coil is a cause for concern and further investigations are required to determine the precise origins of this unexpected ΔT. In any case this observation highlights the importance of considering the effects of RF deposition during the pre-scan phase of MRI acquisitions as well as during play-out of the main imaging sequence. Throughout the data collection process, magnitudes of pre-scan heating at 1.5T remained in keeping with that associated with the TSE sequence.

9.5.1.7 The safety of induced electrical components in the DBS circuit

Voltage recordings faithfully captured the expected qualitative characteristics of voltage signals produced by the DBS equipment, and those induced by the MRI scanner operation. Sequences produced intermittent (1) RF and (2) low-frequency gradient-switching signals in the DBS circuit, consistent with previous reports (Carmichael et al., 2007; Georgi et al., 2004). The safety of induced voltages is dependent on both the:

1. Frequency, which determines the risk of depolarisation and direct neural stimulation. The frequency of the RF pulse-induced signals at 1.5T exceed 60MHz, and are thus too high to cause neuronal stimulation. The observed induced signals related to gradient-switching were significantly lower in frequency (≈1kHz), however still exceed any stimulation frequencies known to have therapeutic potential. In any case, scanner internal safety checks limit gradient switching rates

such that induced tissue currents are outside the range causing direct peripheral nerve, and presumably also cerebral neuronal stimulation.

2. Amplitude, which in combination with the frequency determines the electrode temperature increase. The induced voltage peak-to-peak amplitudes remained less than 1.5V, i.e. approximately half of the therapeutic DBS pulse amplitude, and therefore presumed to be safe.

9.5.2 Potential confounds of fMRI in DBS patients

9.5.2.1 IPG delivers programmed DBS during fMRI

Typical fMRI sequences did not produce any changes to DBS frequency, pulse width or amplitude, or general function. Previous studies with older DBS systems have reported spontaneous switching on/off of the IPG (Rezai et al., 1999). Carmichael et al. reported that, for a different DBS device, approximately 10% of DBS pulses following a 90° RF pulse had extended inter-pulse intervals. This was not detected using the ActivaPC™ system, which may reflect advances in IPG design. As discussed above, the MRI-induced low frequency signals observed are outside the frequency range of therapeutic DBS. Furthermore, they appeared during both 'ON' and 'OFF' stimulation conditions suggesting they do not confound any comparisons of the BOLD response between conditions.

9.5.2.2 Temperature should not confound ON vs. OFF comparisons

As mentioned above, local brain temperature differences due to ON and OFF stimulation states could complicate any fMRI study comparing the two conditions. During the TSE sequences, DBS was not found to alter heating, however a significant effect of active DBS was detected during GE-EPI, increasing the temperature by an average of 0.08°C. However, this small difference is comparable with the sensitivity of our thermometry

system and I conclude that any effect is of negligible practical importance. This is discussed further in section 12.2.2.

9.5.3 Limitations

There are a number of important caveats to the presented findings, centred on the generalizability of these results to other settings.

Firstly, electrode heating appears to be dependent on the specific geometry of the exposed circuit. This study report results from an arrangement simulating a (single) IPG situated in the pectoral region, receiving cranial MRI. Further research is required to confirm the safety of scanning patients with abdominal and or multiple IPGs, or scanning other parts of the body (e.g. spine, abdomen).

Furthermore, the phantom was intended to model a typical DBS arrangement for patients that have been operated at our centre. Different lead coiling configurations or geometric orientations of the DBS components may impact on electrode heating.

Importantly, these results are based upon scans limited to a scanner-reported head SAR in all scans to ≤0.2W/Kg, as obtained on our specific MRI systems. The effect of head SAR magnitude on induced heating has been previously explored (Finelli et al., 2002), however it is important to note that the modelling used to calculate scanner-reported SARs depend upon the scanner and software level, and thus may vary between centres.

Therefore, whilst this experiment was fundamental to improving the fMRI data in DBS patients, it is difficult to generalise these results to other centres. It remains important to perform local risk assessments and *in vitro* measurements to confirm safety before proceeding with examinations that do not conform with device manufacturer's instructions-for-use.

9.5.4 Conclusions

I conclude that (1) body-transmit cranial MRI at 1.5T, with our specific hardware and protocol (head SAR ≤0.2W/Kg), does not produce heating exceeding international guidelines, (2) cranial MRI at 3T produces unacceptable heating, (3) patients with ActivaPC™ Medtronic systems are safe to be recruited to further fMRI experiments, and (4) ON vs. OFF DBS fMRI studies are not confounded by inappropriate stimulus delivery or discrepant heating.

10 The effect of STN DBS on motor-evoked neural activity & coupling

10.1 Summary

In this chapter, I present the results of a third fMRI experiment, conducted in an independent cohort of eleven PD patients with implanted STN DBS. This experiment is almost identical to my first experiment in Chapter 7, the key difference being an improved acquisition protocol and recruitment procedure, as well as extending the time spent performing the movement task.

To summarise, BOLD data was collected whilst patients performed blocks of cued voluntary joystick movements, in a direction of their choice. Patients performed this task off medication, once with their DBS OFF, and once with it set to deliver therapeutic stimulation. SPM was used to determine regions showing a *movement x DBS interaction* at a whole brain level.

Results demonstrate two clusters surviving whole brain correction for multiple comparisons, indicating that both M1 and a midline cerebellar region show increased activity during voluntary movements under therapeutic stimulation. No decreases were detected. Increases in the insula cortex and thalamus were only detected at uncorrected thresholds.

A model space of 256 DCMs per subject was then constructed, including the BG motor loop (exactly as specified in Chapter 8), as well as the cerebellum. The model space asked which combination of pathways was modulated by DBS, as well as whether integration of the cortico-BG and cortico-cerebellar loops occurred at the cortex or thalamus.

Results propose models with integration at the cortex were more likely to generate the data, with DBS modulating all the BG connections, as well as the cortico-cerebellar pathway. Estimates of effective connection strength from the winning model across the group were significantly changed by DBS, however did not predict motor performance or clinical impairment.

I conclude that: (1) under an improved data collection protocol fMRI reveals robust increases in M1 and cerebellar activity during voluntary movement, (2) changes in M1 are caused by increased thalamo-cortical coupling, (3) similar effects on BG pathways to those reported during rest are present during movement, (4) changes in cerebellar activity are caused by increased cortico-cerebellar effective connectivity.

10.2 Introduction

In Chapter 7, data from 10 patients with advanced PD treated with STN DBS is presented. Patients underwent BOLD fMRI whilst they performed voluntary movements, once with their stimulation ON, and again OFF. Analysis of regional responses at the group level identified two clusters that were significant at SVC statistical thresholds; one in the cortex (insula), and one in the thalamus. A number of other regions previously reported in the literature were detected at uncorrected thresholds.

Given the extensive PET literature demonstrating marked cortical changes following therapeutic stimulation (although many do only report at SVC or uncorrected thresholds), we replicated the data collection, this time under an improved protocol, in an attempt to detect unequivocal changes in regional BOLD signal. The following improvements were thus implemented:

10.2.1 Reducing the variability of hardware artefact patterns

Firstly, my Chapter 7 highlighted the impact of hardware-related artefact on GE EPI data. This was typically manifest as loss of signal artefact primarily surrounding the connection between the extension cable and the DBS lead, as well as at the tips of each electrode. For the purposes of subject-level SPM analyses, and data extraction for DCM VOIs, these artefacts were destructive, but were restricted to only that subject's individual artefact pattern. For example, despite spatially varying artefacts, it was possible to extract data from each node from each subject used for the DCM analyses in the experiments presented in Chapters 7 & 8. However, group-level SPM analyses were more severely affected due to the additive nature of the artefact across the group. In other words, SPM can only compute

statistics on voxels from which data was collected in all subjects[20]. This effectively masked out large portions of cortex and subthalamic area bilaterally. In order to combat this, only patients with IPGs implanted in their left pectoral region were recruited, as these subjects all have their extension cable connector over the left hemisphere.

10.2.2 Optimising data collection

Secondly, in Chapter 9, I presented *in vitro* data confirming that (1) MR-induced heating at the electrode tips using the body-transmit MRI at 1.5T does not exceed 1°C, bringing it in line with current safety guidelines, and (2) the MR environment does not impair or confound IPG output. Given the improved SNR yielded by the multi-array head-receive coil used in this protocol, I elected to use this new coil arrangement to optimise data collection. As a result, only patients with Medtronic ActivaPC™ systems could be recruited to this study. This implicitly meant all subjects had been operated on in the last 3 years, which incidentally coincided with greater standardisation in the surgical positioning of the extension cable connector to just superior and posterior to the left ear. This serendipitously aided point 10.2.1.

Additionally, given the data from the left hemisphere was so severely affected by the artefact, subjects no longer performed the task with their right hands. Instead, subjects only performed the task once using their left hand, during each stimulation condition. Due to the time saved in removing the right hand task, we increased the task length from 6 to 8.5 minutes. Finally, patients practiced the task before scanning, and were instructed more clearly to plan their next movement in between *beeps*.

---

[20] *This could be done using toolboxes such as GLM Flex (http://mrtools.mgh.harvard.edu/index.php/GLM_Flex#What_is_GLM_Flex.3F).*

10.2.3 Aims

The aim of this study was thus to:

1. Re-examine the effect of STN DBS on movement-induced BOLD responses under this new protocol.
2. Build plausible models of underlying dynamics causing any observed *movement x DBS interaction*s as realised in Chapter 8.

10.3 Materials and methods

10.3.1 Ethics statement

This study was approved by the National Hospital and Institute of Neurology Joint Ethics committee (09/H0716/51). All participants provided written informed consent.

10.3.2 Patients

Eleven patients who met UK brain bank criteria for idiopathic PD were studied (Table 10.1). Patients had received chronic bilateral STN DBS for >3 months. Electrode implantation was performed using stereotactic MRI – for both preoperative targeting and immediate postoperative verification (Foltynie et al., 2011), ensuring electrode contacts were well-sited within the STN. All patients received bilateral electrodes (Model 3389, Medtronic, Minneapolis) and a dual channel pacemaker IPG (ActivaPC™, Medtronic, Minneapolis) implanted. Only patients with IPGs implanted in their left subclavicular area were recruited, so as to minimise the dropout artefact from impacting on functional data from the right hemisphere. Stimulation parameters were set to produce optimal clinical responses. Medication was withdrawn for 10-12 hours (overnight) before scanning. Inclusion was limited to those patients who could tolerate lying flat with minimal head tremor, while being both off medication and off stimulation.

As previously, UPDRS-III scores were recorded both ON and OFF stimulation before scanning. Additionally, stimulation parameters and system impedance were noted. UPDRS-III scores were broken down into; (1) hemi-body scores, which was the sum of all lateralised items in the scale, including rigidity, bradykinesia and tremor, (2) rigidity, (3) bradykinesia and (4) tremor scores.

Sub	**Age**	**Hand**	**Post-op**	**LED**	**L hemibody**		**R hemibody**		**Total**	
					OFF	ON	OFF	ON	OFF	ON
1	60	R	24	598.75	11	5	12	10	38	21
2	64	R	22	632.00	22	7	18	10	61	29
3	34	R	24	1190.00	29	12	24	11	69	30
4	43	R	5	825.00	11	7	5	1	26	12
5	50	R	28	72.00	21	11	18	8	55	28
6	43	R	7	600.00	21	13	16	11	52	31
7	49	R	37	882.00	26	14	24	15	75	45
8	52	L	25	460.00	17	2	17	7	45	12
9	58	R	12	370.00	23	8	19	7	54	22
10	61	R	9	1731.75	17	12	14	7	43	25
11	65	R	3	948.00	10	3	10	2	32	8
Mean	53		18	755.41	19	9	16	8	50	24
SD	9.7		11.2	443.50	6.3	4.1	5.7	4.0	15.1	10.6

Table 10.1 Patient information. LED = daily levodopa equivalent dose, L = left, R = right. All UPDRS-III scores were conducted off medication. SD = standard deviation. Post-op = months since DBS implantation. R + L hemibody scores do not equal total score because there are additional points for axial signs that are not detailed in this table.

10.3.3 MRI data acquisition

Following onsite tissue-equivalent test-object thermometry experiments confirming that (under strict protocol) sequences used in fMRI studies posed no risk to the patient (see Chapter 9), scanning was performed in a Siemens Avanto 1.5T MRI scanner (Siemens, Erlangen, Germany) using the body-transmit coil and a 12-channel receive-only head coil. This differs from previous studies using a head-transmit/receive coil (i.e. experiments in Chapters 7 & 8). The decision to modify our protocol was motivated by results in previous studies that failed to reach statistical significance at a whole-brain level. The new protocol

has subsequently been shown to keep any electrode heating to <1°C (see section 9.5.1.3). The SAR in the head was limited to <0.4W/Kg.

Patients were scanned with their stimulation ON and OFF, the order of which was randomised. Patients received three scans in each stimulation condition in addition to standard localiser and field map scans:

1. Anatomical T1 MPRAGE (TR=1900ms; TE=3.14ms; TI=900ms; Flip angle=9°; FOV=256x256mm^2; 176 sagittal slices 1mm thick; Spatial resolution= 1x1x1mm^3; Duration=7min 24sec).
2. Resting state fMRI with eyes closed (TR=2420ms; TE=40ms; Flip angle=90°; FOV=192x192mm^2; 32 axial slices 3.7mm thick, gap between slices of 0.52mm; Spatial resolution= 3x3x3.7mm^3; Duration=6min 21sec; 155 scans) – reported in Chapter 11.
3. Movement task fMRI (TR=3650ms; TE=40ms; Flip angle=90°; FOV=192x192mm^2; 49 axial slices 2.5mm thick, gap between slices of 0.5mm; Spatial resolution= 3x3x3mm^3; Duration=8min 53sec; 145 scans).

Patients entered the scanner with their DBS ON, and were either switched OFF or left ON before the scans started, resulting in a ~15 minute latency between DBS manipulation and starting the task fMRI. The task was based on one used previously, and is discussed in detail elsewhere (see section 7.3.4). In brief, patients heard an audio stimulus (*beep*) every 1-3 seconds throughout the session, in addition to audio commands alternating between "rest" and "go" every 30 seconds. During "go" blocks, patients were instructed to perform a joystick movement as fast as possible, each time they heard a *beep*. A movement consisted of displacing the handle from the centre in a direction of their choice, and then returning it

back again. Additionally, patients were instructed to plan their next movement between each *beep*. During "rest" blocks, patients were instructed to rest their hand on the joystick and ignore the *beeps*. Patients were given a practice run before entering the scanner, and were monitored throughout to ensure they were performing the task correctly. There were 9 rest and 8 movement blocks in each session. The couch was then withdrawn from the magnet, keeping the patient's head in the head coil, and their DBS was switched to the opposite condition.

10.3.4 Analysis of task performance

Joystick position (two dimensions, x and y) was recorded at a rate of 20 Hz throughout the scanning sessions. Only data during "go" blocks were analysed. Analysis of task performance was automated, providing unbiased estimates of velocity and RT. Data were first squared and summed over dimensions to ensure movements away from the centre in all directions produced a positive displacement. A window of 3 seconds after each beep was extracted, and the first derivative was calculated, yielding velocity plots for each voluntary movement. The peak velocity (V_{max}) of the movement away from the centre was used as a summary for movement speed, and the latency from stimulus onset to reaching half their V_{max} defined the RT. V_{max} and RT were averaged across trials in each DBS condition in each subject. These summaries were then taken to the group level, where two-tailed paired T tests were used to compare the mean V_{max} and RT in the different stimulation conditions. Significance was set at $p<0.05$.

10.3.5 Analysis of regional responses

Analyses were performed using SPM12 & DCM12 executed in MATLAB R2011b (The MathWorks, Inc., Natick, MA, USA). The first 5 scans of each session were removed and data were corrected for field inhomogeneity using the field maps. Data were then realigned

and unwarped, then coregistered with matching anatomical scans, segmented, normalised to MNI space, spatially smoothed using a Gaussian kernel (8mm full-width half maximum) and visually inspected. Data were subsequently analysed using the GLM framework; each subject's two task sessions (one for each stimulation condition) were entered into a single GLM. Blocked stimulus functions (boxcars) were specified in each session coding the effects of voluntary movement. Due to collinearity between the stimulus functions and head movements, I explicitly did not include head motion regressors in the first level GLMs. While this is not best practice, I did ensure to *realign & unwarp* the data to try and help minimise any head movement induced artefact. Furthermore, subsequent DCM is immune to the instantaneous signal fluctuations related to motion, and instead models the delayed nature of the haemodynamic response. Stimulus functions were convolved with a canonical HRF in the normal way, and the GLMs were then fitted to the data. Three contrasts were specified; (1) the main effect of movement, (2) *movement x DBS interaction* ON>OFF, (3) *movement x DBS interaction* OFF>ON. The resulting T maps from each subject were used for second-level random effects analysis. Clusters surviving a cluster-wide threshold of $p<0.05$ (family wise error corrected for multiple comparisons) at a whole-brain level were considered significant, and peak voxels within those clusters are reported. Contrasts were subsequently examined at lower uncorrected significance thresholds, however, the results of which are not formally reported.

10.3.6 Dynamic causal modelling

Results from second-level analysis of regional responses identified two clusters displaying robust *movement x DBS interaction*s, namely M1 and the cerebellum. Given these findings, and the results of Chapter 8, I embellished our BG DCM (which already included M1 as

its only cortical node), including a cerebellar node ipsilateral to movements, and modelled the effect of STN DBS on movement-related coupling in this patient cohort.

The GLM was rotated to allow the effect of STN DBS to enter the model as a modulatory input. VOIs were extracted using the movement x DBS (ON>OFF) T contrast and corrected for the effects of interest (i.e. the *main effects of movement* and DBS, and the *movement x DBS interaction* regressor) in each subject. The basal ganglia motor loop was modelled using observed data in M1, the putamen and thalamus (all contralateral to the limb moved). In addition, we included the STN as a hidden node (see section 8.6.1). This was achieved by setting the noise precision at that node to effectively zero, permitting estimation of its hidden states and coupling parameters in the normal way (see Chapter 8). Two-state, stochastic DCM was used in this analysis. As previously, pallidal nodes were not included; rather, their connections were collapsed to simplify the circuit. In other words, the direct pathway was summarised as an excitatory connection from the putamen to the thalamus, and indirect pathway as an excitatory putamen-STN connection, and an inhibitory STN-thalamus connection. The cerebellar node received an excitatory M1 afferent (assumedly via the pontine nuclei).

The first question addressed by the model space addressed the architecture of the coupling between cortico-basal ganglia and cortico-cerebellar loops during voluntary movement. Specifically, we examined whether convergence of the two circuits occurs at the thalamus, or at the cortex. Therefore, half of the models specified had cerebellar efferents projecting to the thalamic node (architecture A), and half simply had a reciprocal connection to M1, presumed to be a polysynaptic connection via cerebellar receiving nuclei of the thalamus (architecture B).

This yielded two sets of models, each with 8 extrinsic (between-region) connections. The main effect of movement entered both models as a driving input to M1, and the effect of DBS entered as a modulatory effect on extrinsic connections. The model space compared DCMs that included modulatory effects on the direct, indirect, hyperdirect, cortico-striatal, thalamo-cortical pathways, as well as cortico-cerebellar and cerebellar efferent connections, or combinations of those 7 pathways (comprising eight connections), resulting in (2^7) 128 models per architecture, thus 256 models per subject (see Figure 10.1).

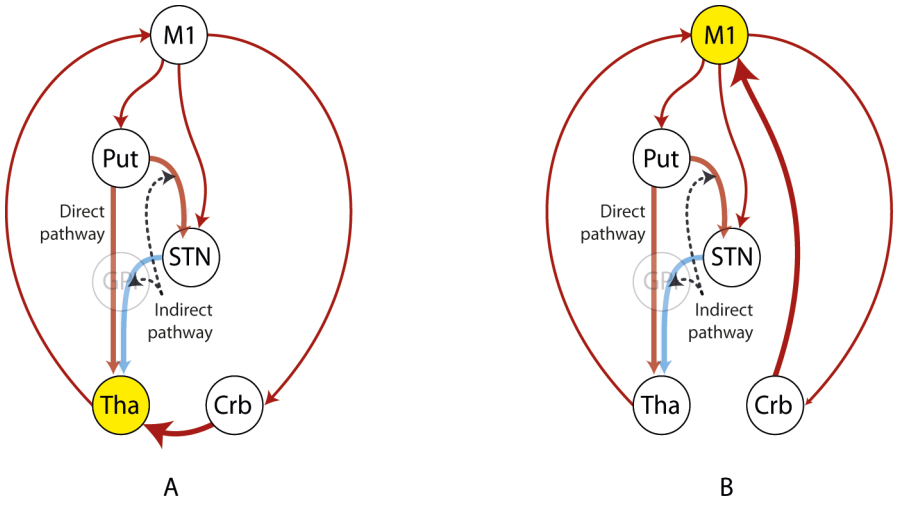

Figure 10.1 Cortico-BG and cortico-cerebellar integration. Architectures (A) and (B). 128 variants of each of the two architectures were compared in the BMS. Models differed by which combination of extrinsic connections were modulated by DBS. Yellow nodes highlights the different sites of integration of the two circuits.

Models were subsequently compared across all subjects using BMS (fixed effects assumptions). Models were subsequently grouped into families depending on whether they expressed modulatory effects on the 7 pathways above. Post-hoc BMS family analyses were used to evaluate the posterior probabilities of (1) models with architecture A compared to architecture B, and (2) models with modulatory effects on each of the 7 pathways. The single model with the greatest log-evidence at the group level was considered the winning model.

Posterior expectations of the extrinsic coupling parameters (from the DCM.Ep.A matrix) and modulatory effects (DCM.Ep.B matrix) from each subject's winning model were extracted and transformed to yield coupling OFF DBS (=exp(DCM.Ep.A)), and ON DBS coupling (=exp(DCM.Ep.A+DCM.Ep.B)), measured in Hertz. Paired T tests were used to compare coupling ON and OFF DBS across the group (Bonferroni corrected for multiple comparisons).

The coupling parameters were subsequently entered into multiple linear regression models, as independent variables, with the dependent variable either the (1) contralateral UPDRS-III score (excluding axial score), (2) percentage improvement in clinical UPDRS-III score. Similar models were specified predicting the ON and OFF behavioural measures (V_{max} or RT), as well as their improvements with DBS.

10.4 Results

10.4.1 Clinical effect of STN DBS

All patients showed significant improvement in clinical PD impairment. UPDRS-III scores reduced from an average (± standard deviation) of 50 (±15.1) OFF DBS, to 23.9 (±10.6) ON DBS, equivalent to a mean improvement of 52.2% (±12.2%) ($p<0.05$). Improvements were observed across all sub-domains, and across both hemi-bodies (Figure 10.2).

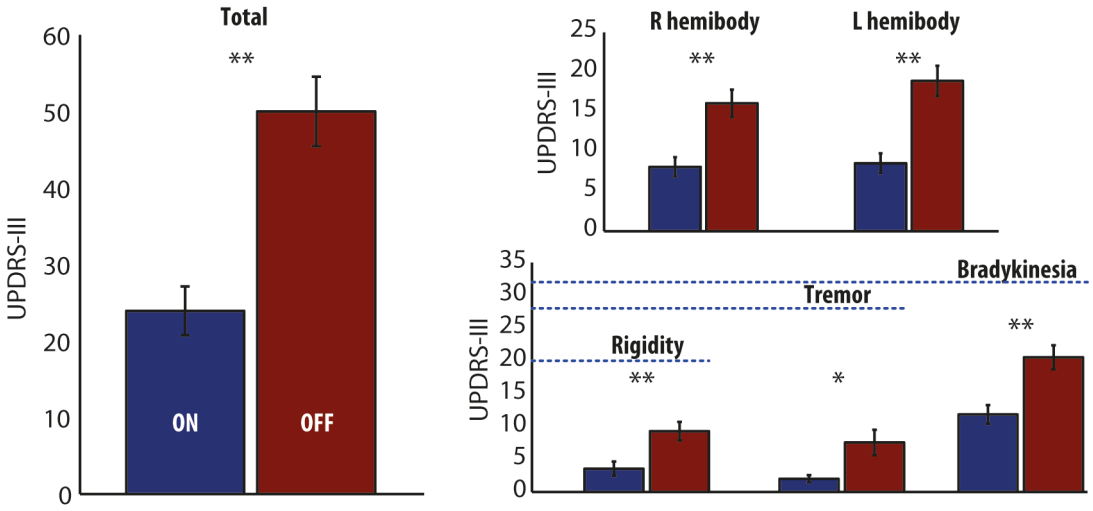

*Figure 10.2 Clinical improvements following STN DBS. All scoring was performed off medication. Higher scores confers greater impairment. Blue dashed line indicates the maximum number of points in the respective sub-scale. * p<0.01 **p<0.001.*

10.4.2 The effect of STN DBS on peak velocity and reaction time

STN DBS significantly increased V_{max} (p = 0.0062), but improvements in RT were only trend significant (p = 0.06). To confirm the validity of the analyses, strong negative correlations were identified between V_{max} and total UPDRS-III (r = -0.56, p = 0.0066), and the bradykinesia subscores (r = -0.64, p = 0.0012).

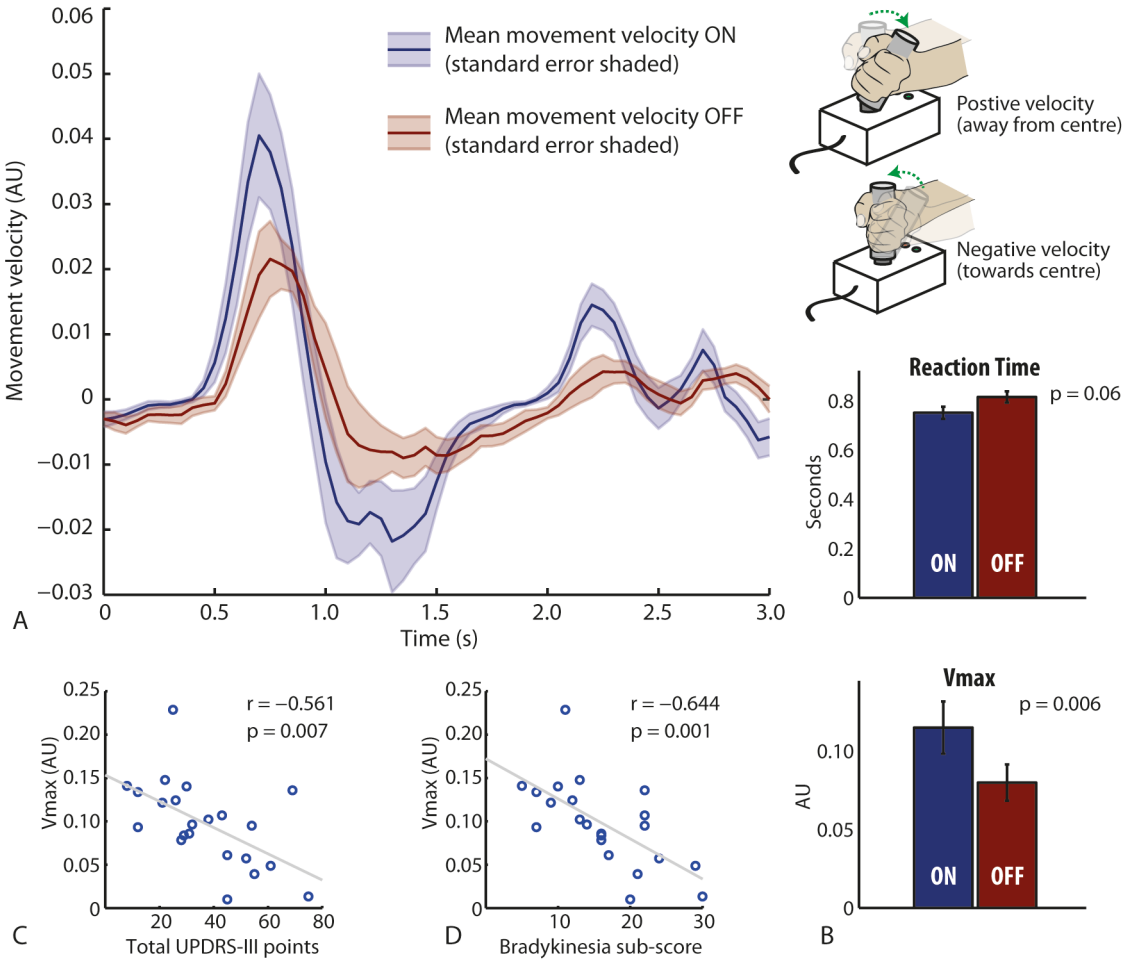

Figure 10.3 The effect of DBS on V_{max} and RT. (A) The mean velocity plot for a single movement trial – ON and OFF compared. Cue sounds at time = 0 with joystick in central position. Positive velocity occurs when subject moves joystick away from central position in their chosen direction, slows to 0 at maximal displacement, then velocity is negative as the handle is returned to the centre position. (B) Mean RT and V_{max} ON and OFF stimulation; RT only trend significant. (C & D) Scatter plots of total UPDRS score, and bradykinesia subscore against V_{max} (both ON and OFF values for each subject included).

10.4.3 The effect of STN DBS on regional BOLD responses

Scanning proceeded with no adverse effects; DBS system impedances were unaffected by scanning, and following administration of medication, patients returned to their pre-scan clinical baseline. The *main effects of movement* contrast at the group level revealed a map of motor cortical regions that are characteristically engaged during voluntary movements, consistent with the PET and fMRI literature that have employed similar tasks. There were not any obvious stigmata of motion artefact (e.g. cortical 'rims' or spurious ventricular

activations), which, in combination with the classical motor regions activated, suggested that the data were not significantly corrupted by motion artefact. Inclusion of covariates for hand dominance and clinical improvement at the second level did not significantly change the results.

The group-level *movement x DBS* ON>OFF contrast revealed two large clusters that survived cluster-wise whole brain correction, located in the precentral gyrus hand area, and cerebellum (see Figure 10.4 & Table 10.2). A cerebellar atlas normalised to MNI space using FLIRT (Diedrichsen et al., 2009) revealed that the cluster encompassed the left crus V, as well as the vermis and right-sided crus V and VI. There were no significant DBS-related reductions in movement-induced regional response using the OFF>ON interaction contrast.

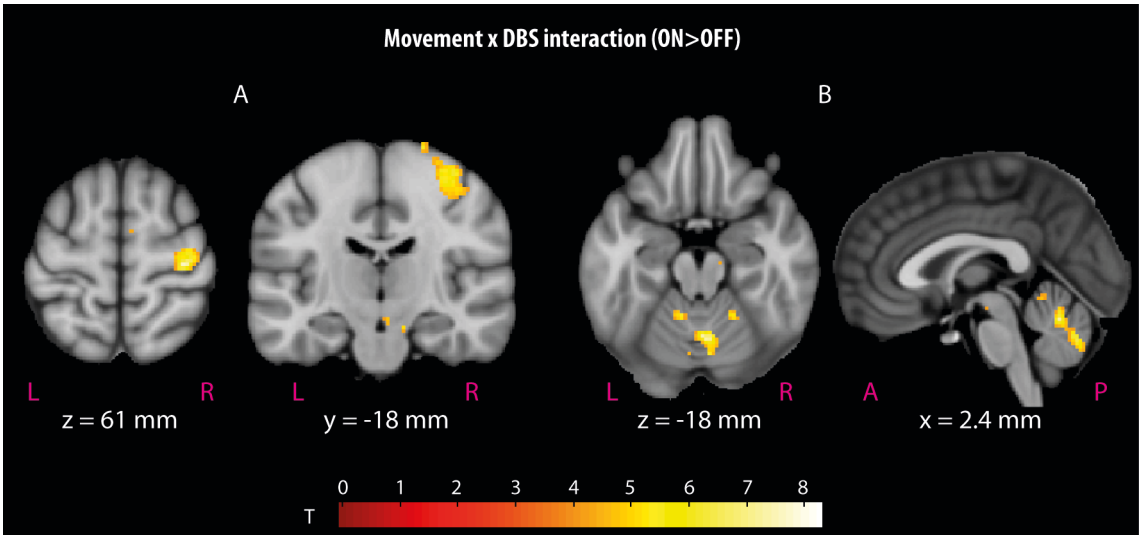

Figure 10.4 Movement x DBS (ON>OFF) interactions. Two clusters were identified as significant in (A) M1 hand area contralateral to movements, and (B) midline cerebellum encompassing left crus V, vermis and right crus V & VI. Second level SPMs overlaid on the MNI brain. SPMs are thresholded at p<0.001 (uncorrected). Additional activations at this threshold can be seen in the SMA and midbrain (A).

Cluster-wise			**Peak-wise**			**MNI coordinates (mm)**		
P_{FWE}	Voxels	P_{unc}	T	Z	P_{unc}	x	y	z
0.00180	245	9.4E-05	8.27	4.44	4.4E-06	6	-60	-18
Cluster B in Figure 10.4			6.46	3.97	3.6E-05	4	-70	-30
			6.36	3.94	4.1E-05	-2	-60	-22
0.00010	369	5.1E-06	7.79	4.33	7.4E-06	34	-22	60
Cluster A in Figure 10.4			6.06	3.84	6.1E-05	42	-14	52
			5.73	3.73	9.5E-05	30	-22	70

Table 10.2 Results of second level whole brain search for movement x DBS interaction. Clusters surviving cluster wise significance (corrected using the family wise error correction for multiple comparisons = P_{FWE}) of $p<0.05$ were considered significant. Peak voxels of clusters are reported. P_{unc} = uncorrected P values.

10.4.4 Bayesian model selection

All 256 models successfully converged. BMS revealed that model 192 was the most likely generator of the data across the group (posterior probability > 99%) - Figure 10.5. This model had parallel basal ganglia and cerebellar loops, converging at the level of the cortex (architecture B). The model encompassed DBS-induced modulatory effects on all the connections within the BG loop, as well as the projection from M1 to the cerebellum. Subsequent family analyses confirmed that (1) models with architecture B were more likely to generate the data than architecture A, and (2) models incorporating modulatory effects on cortico-striatal, direct, indirect, hyperdirect, thalamo-cortical, and cortico-cerebellar connections respectively outperformed sparser models (posterior probabilities > 99%).

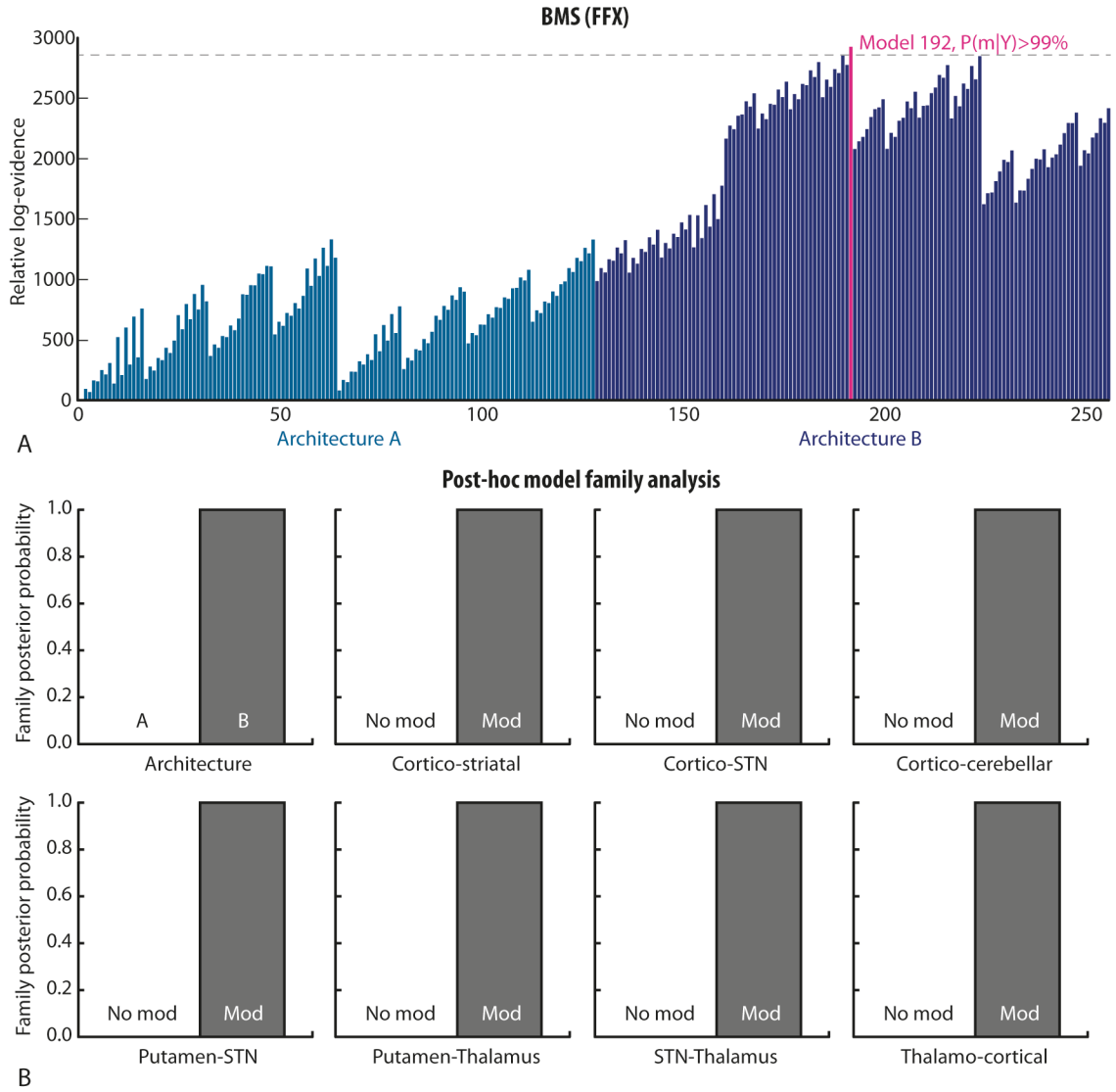

Figure 10.5 Results of (A) BMS and (B) post-hoc family BMS analysis. Looking at (A), it is clear that models with architecture B outperform equivalent models with architecture A. Model 192 has the highest model evidence with posterior probability = P(m|Y) > 99%. Dashed grey line at highest competitor (model 190).

10.4.5 The effect of STN DBS on extrinsic coupling

Posterior coupling estimates extracted from model 192 from each subject revealed significant changes in cortico-striatal, direct, indirect, hyperdirect, thalamo-cortical, and cortico-cerebellar coupling. Cortico-striatal ($p<0.05$, corrected), direct ($p<0.05$, corrected), thalamo-cortical ($p<0.05$, corrected) and cortical-cerebellar ($p<0.05$, uncorrected) coupling increased under therapeutic STN DBS, whereas hyperdirect, striato-STN and STN-

thalamic coupling was reduced during DBS (p<0.05, corrected). The magnitudes of change of coupling involving the STN were smaller than other changes observed (although still highly significant), in line with previous experiments utilising hidden nodes. Multiple linear regression analyses predicting clinical impairment or improvement using the coupling parameters failed to reach statistical significance.

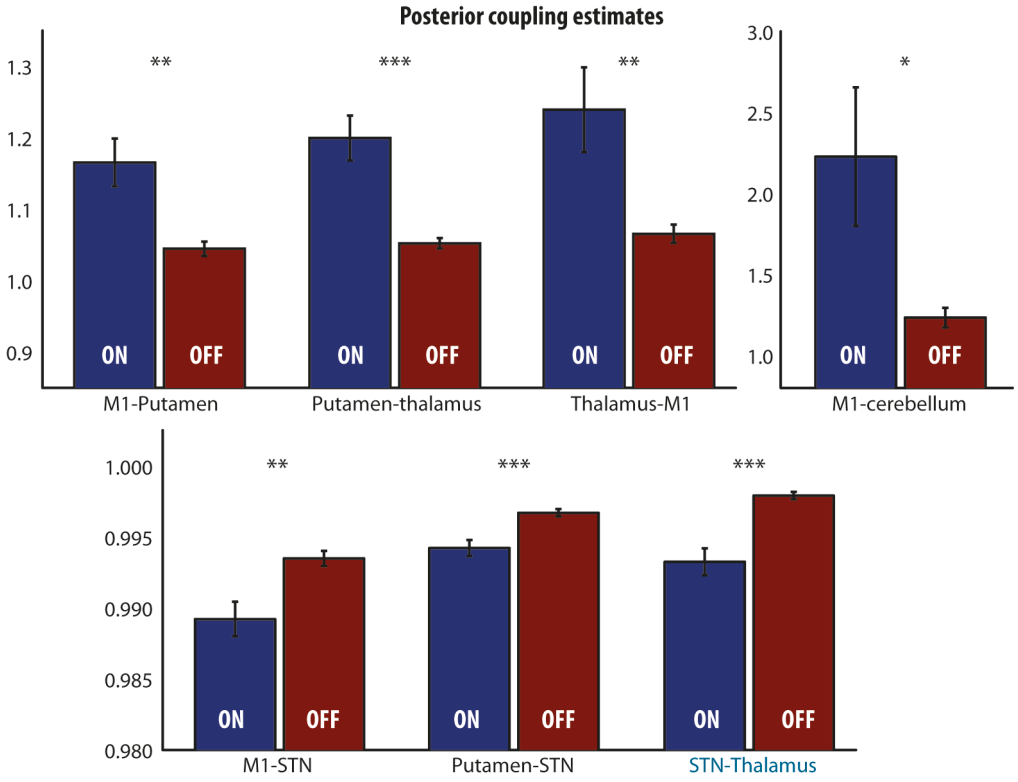

*Figure 10.6 The effect of DBS on posterior estimates of extrinsic coupling. *P<0.05 (uncorrected), **P<0.05 (Bonferroni corrected), ***P<0.001 (Bonferroni corrected). Note the different scale used for M1-cerebellum, and coupling with the STN. STN-thalamus coupling was set to be inhibitory a priori.*

10.5 Discussion

The first part of this experiment was, in essence, a replication of my first experiment under a superior acquisition protocol. Following detection at the second level of robust interactions in M1 and the cerebellum, DCM was used to explore how these results were generated, specifically by developing the BG DCMs conceived in Chapter 8. The results of

this experiment reveal that (1) therapeutic STN DBS significantly increases motor-evoked BOLD responses in M1 and cerebellum, and (2) that the changes observed during movement are most likely caused by modulation of both BG pathways, as well as cortico-cerebellar dynamics.

10.5.1 STN DBS increases motor-evoked responses in M1 & midline cerebellum

Results demonstrate robust interactions (ON>OFF) in both M1 and the cerebellum, both regions richly involved in control of voluntary movement. This is in line with results from a similar $H_2{}^{15}O$ PET study using an almost identical joystick task in unilateral DBS patients (Payoux et al., 2004). In that paper, the interaction was explained by reductions in activity at rest, resulting larger apparent motor-evoked activity (Figure 10.7).

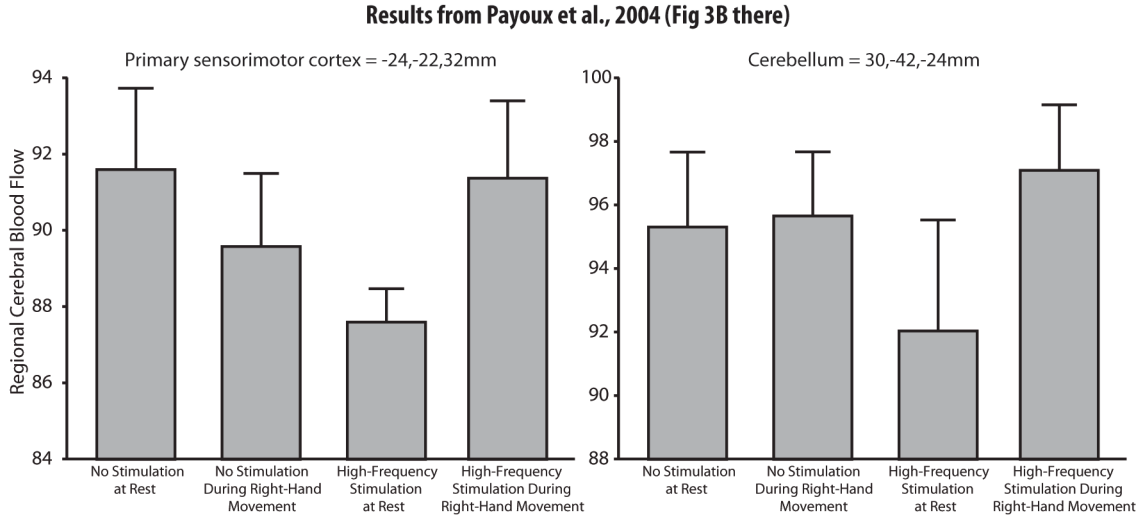

Figure 10.7 Previously reported movement x DBS interaction in M1 thought to be caused by reductions in baseline activity. Taken from Payoux et al., 2004 (Figure 3B in that publication). Coordinates reported in Talairach space.

However, modulation in both M1 and cerebellar cortex have shown mixed results in previous DBS neuroimaging studies (discussed in 5.4.2.6). One early study using unilateral STN DBS patients reported reduced motor-evoked activity in M1, although the cluster (–42, –12, 26 in Talairach space) appears quite low and lateral for it to be the equivalent

hand region reported here (Ceballos-Baumann et al., 1999). Similarly, reductions claimed in (Thobois et al., 2002) appear quite medial, and intriguingly posterior to the central sulcus.

Only one previous paper has reported *movement x DBS interaction*s in the cerebellum. Grafton et al., collected rCBF PET whilst six unilateral DBS patients performed a visuo-motor feedback task, reporting both increased and decreased evoked responses in different parts of the lateral cerebellar cortex (Grafton et al., 2006). In contrast, DBS induced changes in resting cerebellar metabolism have been widely reported, in both the vermis (Asanuma et al., 2006; Bradberry et al., 2012; Cilia et al., 2009; Sestini et al., 2002), and lateral cerebellar cortex (papers demonstrating vermis changes, and Garraux et al., 2011; Hershey et al., 2003; Nagaoka et al., 2007; Tanei et al., 2009; Vafaee et al., 2004; Volonté et al., 2012; Wang et al., 2010).

10.5.2 The integration of cortico-basal ganglia and cortico-cerebellar loops

The first result of the BMS analysis solved what was in fact a question that presented itself during model specification. Given the significant interaction observed in the cerebellum, it was important to integrate cortico-cerebellar dynamics into my model of the BG, thus the question of how these loops were organised required either an *a priori* constraint of some form (i.e. that one architecture is more plausible), or was a simple model selection question. Anatomical studies suggest that the thalamus can be parcellated into discrete pallidal receiving nuclei (VLa, VApc, and VM) and nuclei such as the VLp – equivalent to Vim thalamus in Hassler's nomenclature (Gallay et al., 2008) – that receive afferents from the deep cerebellar nuclei. Thus the anatomical literature would probably support that architecture B is the more plausible generative architecture (Wu and Hallett, 2013). In the end, the decision was made to ask the question empirically, and the BMS results in fact

evidenced anatomical hypotheses, i.e. parallel cortico-BG and cortico-cerebellar loops are integrated at the level of the motor cortex. While not specifically a question set out *a priori*, this finding has not previously been reported in the human neuroimaging literature, thus is of interest to those studying both PD and motor control (under the assumption that the PD architecture is consistent with healthy controls).

10.5.3 Cortical changes are best explained by an increased sensitivity to basal ganglia afferents

Interestingly, model selection suggests that increases in motor-evoked BOLD signal in M1 are better explained by a selective increase in sensitivity to its BG afferents, as opposed to cerebellar afferents. This is in agreement with classic rate-based models of the BG and PD (Albin et al., 1989; DeLong, 1990), and has been much speculated as a possible mechanism for previously observed cortical changes in the PET/SPECT literature (early examples include Ceballos-Baumann et al., 1999; Limousin et al., 1997; etc.), but until now has not been formally tested. Under therapeutic DBS, my results show that M1 shows an afferent specific gain modulation. Put simply, M1 becomes selectively more sensitive to BG afferents, whereas its sensitivity to incoming cerebellar signals remains unchanged.

10.5.4 Therapeutic STN DBS increases thalamic sensitivity to direct pathway afferents during movement

This is in line with the results outlined in my previous fMRI experiment (section 8.5.1.3), which, as discussed there, is in line with a growing wealth of physiological data, as well as early models of BG function and PD (Albin et al., 1989; DeLong, 1990). Similarly, DBS again was shown to reduce the STN and thalamic sensitivity to hyperdirect and indirect afferents, this time during voluntary movement. This combination of findings evidences speculations voiced in the discussion of Chapter 7, i.e. DBS appears to bias the sensitivity

of the thalamus towards its direct pathway afferents, resulting in a greater net excitatory drive during voluntary movements (section 7.5.3).

However, in contrast to findings at rest (Chapter 8), regression models of coupling predicting either clinical status, clinical improvement, or behavioural measures (V_{max} or RT), failed to reach statistical significance. This could be due to a lack of sufficient statistical power; this study only considered 11 hemispheres, Chapter 8 included 24. Furthermore, this study necessarily included seven independent variables in the design matrix, whereas Chapter 8 only included 6 (due to the lack of cerebellar connections). Finally, the models and thus parameters are fundamentally different given the models discussed here include an explanation of cortico-cerebellar dynamics, not previously explored in Chapter 8. Experiments in Chapter 11 explore this in more detail.

10.5.5 The effect of STN DBS on cortico-cerebellar dynamics during movement

BMS and post-hoc comparisons of coupling estimates propose that during voluntary movements, STN DBS increases the effective connectivity from M1 to the cerebellum. In other words, DBS appears to be altering the cerbellum's sensitivity to cortical afferents. As in previous experiments, DBS was modelled as a modulator of effective connectivity, thus these results do not explain how DBS spreads to modulated regions, rather that the result of DBS is that they are modulated. In terms of explaining its biological plausibility, anatomical and histological investigation have demonstrated structural connectivity between the BG (specifically striatum and STN) with the cerebellum and deep cerebellar nuclei (Bostan et al., 2010; Hoshi et al., 2005; Wu and Hallett, 2013). Without a control population, it is difficult to determine whether this increase is some form of normalisation of the dynamics of the motor network. It is tempting to interpret these results as an improvement of distant functional integration in the context of STN DBS; *distant* here

meaning a similarly specialised node that is independent of the BG circuit. This is discussed further in Chapter 11.

Previous studies comparing PD patients to control populations have repeatedly reported increased cerebellar activity during both movement (Catalan et al., 1999; Rascol et al., 1997; Yu et al., 2007), as well as increased resting state functional connectivity amongst M1, PM and cerebellar cortex (Wu et al., 2009). One recent study using multiple PPIs to characterise effective connectivity between regions of the motor system have similarly yielded increased connectivity between these regions in PD cohorts (Wu et al., 2011). Those authors have suggested that this could be explained in terms of compensation for underactive frontal cortical components of the motor network. While such differences between patients and controls have been reported, changes induced by DBS appear to be more ambiguous. These results do not support the compensation hypothesis posed by previous authors, in fact advocate the opposite, namely that DBS results in increased M1-cerebellar effective connectivity.

10.5.6 Limitations

This experiment suffers the same limitations of my modelling studies so far. A general discussion of these limitations is presented in section 12.5.

10.5.6.1 Regional responses: Head movements and motor task

Head movements were explicitly excluded from first level GLMs in this experiment, owing to an observed collinearity with the main effect of movement condition. While this is not best practice, had these not been excluded, the model's ability to estimate *main effects of movement* and interactions would have been compromised. This specific limitation is discussed in the context of findings from Chapter 7 in section 12.2.5.

10.5.6.2 Regional responses: What about the thalamus and the insula?

My first experiment (Chapter 7) identified two *movement x DBS interaction* clusters that were significant at SVC statistical thresholds; one in the insula, and one in the thalamus. Exploring the ON>OFF contrast at uncorrected peak thresholds in this cohort did reveal clusters in bilateral insula cortex (peak voxel $p<0.013$) and thalamus (peak voxel $p<0.012$), but were not significant at whole-brain corrected thresholds. By adopting the same SVC analysis as performed in Chapter 7, I was similarly unable to replicate this result. This failure to replicate findings is discussed in the thesis discussion (section 12.3.2).

10.5.7 Conclusions

This experiment presents robust interactions between movement and DBS in both M1 and the cerebellum, both displaying increased BOLD signal during voluntary movements with active DBS. Results of my DCM and BMS reveal that these interactions are most likely explained by modulatory effects in both the basal ganglia motor loop and cortico-cerebellar dynamics. Interestingly, BOLD increases at M1 are more likely caused by an increased sensitivity to its basal ganglia afferents, as opposed to afferents from cerebellar loops.

I conclude that: (1) under an improved data collection protocol fMRI reveals robust increases in M1 and cerebellar activity during voluntary movement, (2) changes in M1 are caused by increased thalamo-cortical coupling, (3) similar effects on BG pathways to those reported during rest are present during movement, (4) changes in cerebellar activity are caused by increased cortico-cerebellar effective connectivity.

11 The effect of STN DBS on endogenous coupling in BG & cortico-cerebellar loops

11.1 Summary

In this chapter, I present the results of a fifth fMRI experiment, conducted in the same cohort of PD patients as studied in Chapter 10. As in Chapter 8, BOLD data was collected whilst patients lay in the scanner at rest with eyes closed. Patients were scanned off medication, once with their DBS OFF, and once with DBS ON.

Building on results of Chapters 8 & 10, I re-examine the effects of STN DBS on endogenous coupling, this time including cortico-cerebellar dynamics. This experiment aimed to characterise the effects on both cortico-BG and cortico-cerebellar circuits at rest.

A model space of 256 DCMs per subject was constructed, identical to that tested in Chapter 10. The model space asked which combination of pathways was modulated by DBS, as well as whether integration of the cortico-BG and cortico-cerebellar loops occurred at the cortex or thalamus. As in Chapter 10, results propose that models with integration at the cortex were more likely to generate the data. Winning models included DBS modulating all the BG connections, as well as the cerebellar-cortical connection. Estimates of effective connection strengths amongst the BG motor loop across the group were significantly changed by DBS, however, cerebellar-cortical effective connectivity was not found to significantly changed by the intervention. Regressions of coupling estimates and clinical status/improvement did not identify significant predictive relationships.

I conclude that (1) previous findings of modulatory effects on BG effective connectivity under STN DBS whilst patients lay at rest have been partially replicated in an independent patient cohort, and (2) whilst models incorporating modulatory effects on cerebellar-cortical coupling prevail, random effects analysis at the group level does not identify significant differences in cerebellar-cortical coupling under DBS.

11.2 Introduction

Data presented in Chapter 10 demonstrate that STN DBS produces robust increases in M1 and cerebellar activity during voluntary movement. Modelling of how these interactions were generated revealed that STN DBS produced modulatory effects on both BG dynamics, as well as cortico-cerebellar dynamics. Results in the BG were in agreement with the modelling presented in Chapter 8, despite the fact that the patients were performing voluntary movements, and the additional modelling of cortico-cerebellar dynamics.

Given the demonstrated importance of the cortico-cerebellar loops in the generation of voluntary movements, and the modulatory effects DBS has on these dynamics during movement, this experiment asks if similar modulatory effects take place in the resting state as well. In other words, does STN DBS produce identical effects during movement and rest at all parts of the motor circuit, or are there context-dependent effects.

In addition, there is a consensus in the literature that tremors (either resting or postural) in PD are in someway attributable to dysfunction of cortico-thalamo-cerebellar dynamics (Helmich et al., 2011; Mure et al., 2011; Ni et al., 2010). Thus, it was of interest to include cortico-cerebellar dynamics in models of data acquired in the resting state.

Previous neuroimaging studies in the resting state have reported mixed results in the cerebellum. Some report increased activity under DBS (Cilia et al., 2009; Garraux et al., 2011; Nagaoka et al., 2007; Sestini et al., 2005; Tanei et al., 2009; Vafaee et al., 2004) in both lateral cortex and midline vermis, whereas others report decreased activity (Bradberry et al., 2012; Hershey et al., 2003; Volonté et al., 2012; Wang et al., 2010). Thus while the direction of modulation may seem somewhat inconclusive, stimulation-induced changes in the cerebellum's endogenous activity has been widely reported.

The aims of this experiment were to:

1. Determine whether STN DBS produces modulatory effects on cortico-cerebellar dynamics during the resting state.
2. Replicate findings from Chapter 8 in an independent patient cohort, taking into account cerebellar dynamics.

11.3 Materials and methods

11.3.1 Ethics statement

This study was approved by the National Hospital and Institute of Neurology Joint Ethics committee (09/H0716/51). All participants provided written informed consent.

11.3.2 Patients & MRI data acquisition information

The patient cohort used in this study were identical to the cohort used in the previous chapter (see section 10.3.2). Details of the MRI data acquisition protocol are detailed in section 10.3.3. Resting state scanning took place before completion of the motor task in each DBS condition. As a result, the time between switching stimulation setting and scanning was approximately 10-15 minutes, depending on the patient.

11.3.3 Dynamic causal modelling

Given the findings of the movement task data in this cohort (see Chapter 10), namely, that STN DBS increased motor related activity in M1 and the cerebellum, and that DBS had modulatory effects on coupling within both the cortico-basal ganglia, and cortico-cerebellar loops, the cerebellum was included in the DCMs. This permitted specification of an identical model space to that used in Chapter 10. In other words, this experiment mirrors previous analysis of data collected during voluntary movement, however substitutes task fMRI data for resting state data.

Only data from the right hemisphere were considered in this analysis because subjects only performed left hand movement tasks, allowing the right M1 to be functionally defined in each patient. Had we wanted to explore both hemispheres, we would have had to use different VOI extraction methods for each hemisphere, which was suboptimal (e.g. for the left hemisphere we could have extracted from within a sphere centred on the mean of the equivalent VOI in Chapter 8). VOI selection proceeded in a similar manner to as described in Chapter 8 (section 8.3.4). In brief, the coordinates of the peak voxels of the M1 (MNI coordinates: 34, -22, 60mm) and cerebellar (MNI coordinates: 6, -60, -18mm) clusters in the task data second level analysis of the *movement x DBS interaction* contrast (ON>OFF) were used to guide data selection. Masks from right motor putamen and right motor thalamus were created using probabilistic white matter connectivity atlases thresholded at 50% probability (Behrens et al., 2003; Tziortzi et al., 2014), constraining our analysis to regions that exhibit strong structural connectivity at a population level. The first 5 scans of each resting state session were removed and data were corrected for field inhomogeneity using the field maps. Data were then realigned, coregistered, anatomical images were normalised to MNI space, the resultant normalisation matrix was then used to normalise the functional data. Finally, the data were visually inspected and spatially smoothed using an 8mm Gaussian kernel. The ON and OFF sessions were concatenated to produce a single 300 scan time series. Ultra-low frequency fluctuations were removed in the usual way using a high-pass filter (1/128s ≈ 0.0078Hz). Confound time series were extracted from predefined coordinates of extra-cerebral compartments (the lateral ventricle and eye globe).

The resting state was modelled using a GLM-DCT consisting of 145 functions[21] with frequencies characteristic of resting state dynamics (0.0078-0.1Hz) (Biswal et al., 1995; Deco et al., 2011; Fox and Raichle, 2007; Fransson, 2005), a regressor encoding the *main effect of DBS*, six nuisance regressors from each session capturing head motion, and the confound time series from the extra-cerebral compartments. The principal eigenvariate was extracted (adjusted for confounds - head movements and extra-cerebral compartments) of sphere (r = 4 mm) of voxels, centred on the peak voxel of an F contrast spanning the DCT components, within 4 mm of the group M1 coordinate.

A PPI regressor was created using the extracted M1 data and the *main effect of DBS* regressor (Friston et al., 1997). A GLM-PPI was specified including the *main effects of DBS*, the extracted M1 data, and their PPI. A SPM testing for the PPI was masked first with an anatomical putamen mask, and then the thalamus mask, and then a sphere (r = 4 mm) centred on the cerebellar peak voxel from the second level task analysis. The BOLD signal (corrected for the same confounds as above) was extracted from a sphere (radius 4mm) centred on the peak T-value within each mask, producing four volumes of interest (VOIs) per hemisphere and subject (M1, putamen, thalamus, cerebellum). As previously, data from the STN was not extracted, and was instead modelled as a hidden node.

VOIs were used to construct 256 DCMs per subject, each differing according to which connections were modulated by DBS. The model space compared DCMs that included modulatory effects on the direct, indirect, hyperdirect, cortico-striatal, thalamo-cortical

[21] *The number of functions is somewhat arbitrary; the purpose is to include enough components to thoroughly span the frequency domain of interest (0.0078-0.1Hz), while maintaining degrees of freedom for estimation. The reader might have noticed that in section 8.3.4.3, 189 components were used. This is simply because in that GLM, there were more scans (390), thus we could afford to include more components. In reality both GLMs are likely over-specified. However, the purpose of these SPMs is simply to inform the first step of VOI extraction.*

pathways, as well as cortico-cerebellar and cerebellar efferent connections, or combinations of those 7 pathways, as described previously.

Models were subsequently compared across all subjects using BMS (fixed effects assumptions). Models were then grouped into families depending on whether they expressed modulatory effects on the 7 pathways above. Post-hoc BMS family analyses were used to evaluate the posterior probabilities of (1) models with architecture A compared to architecture B, and (2) models with modulatory effects on each of the 7 pathways. The single model with the greatest log-evidence at the group level was considered the winning model.

Posterior expectations of the extrinsic coupling parameters (from the DCM.Ep.A matrix) and modulatory effects (DCM.Ep.B matrix) from each winning model were extracted and transformed to yield coupling OFF DBS (=exp(DCM.Ep.A)), and ON DBS coupling (=exp(DCM.Ep.A+DCM.Ep.B)), measured in Hertz. Paired T tests were used to compare coupling ON and OFF DBS across the group (Bonferroni corrected for multiple comparisons).

Finally, the coupling parameters were subsequently entered into multiple linear regression models, as independent variables, with the dependent variable either the (1) contralateral UPDRS-III score (excluding axial score), (2) percentage improvement in clinical UPDRS-III score.

11.4 Results

11.4.1 Clinical effect of STN DBS

All patients showed significant improvement in clinical PD impairment. UPDRS-III scores reduced from an average (± standard deviation) of 50 (±15.1) OFF DBS, to 23.9 (±10.6) ON DBS, equivalent to a mean improvement of 52.2% (±12.2%) ($p<0.05$). Improvements were observed across all sub-domains, and across both hemi-bodies (Figure 11.1).

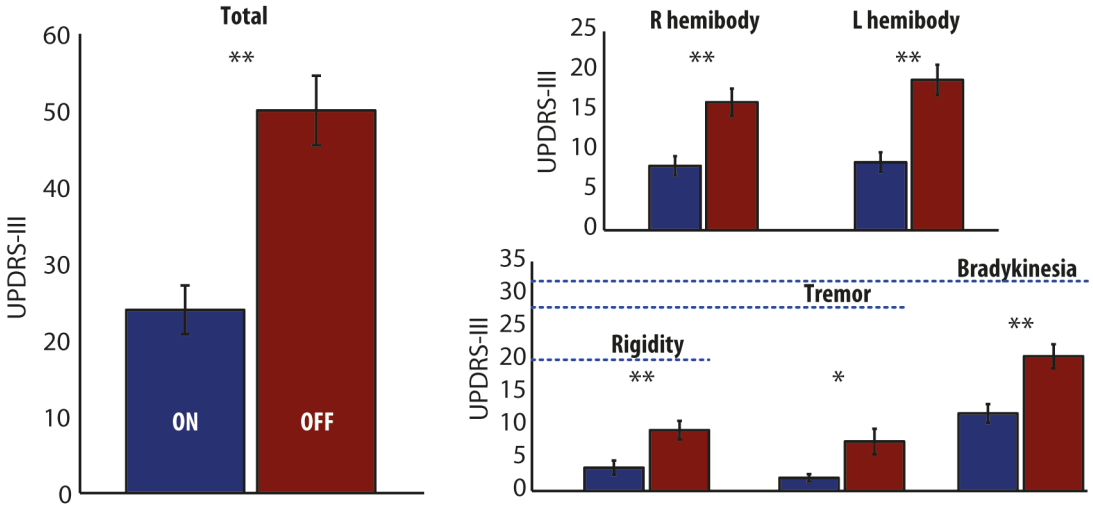

Figure 11.1 The effect of STN DBS on clinical PD impairment. All clinical scoring took place off-medication. This is exactly as in Figure 10.2 for patient demographics, see Table 10.1.

11.4.2 Bayesian model selection

All 256 models successfully converged. BMS under fixed effects assumptions revealed that model 224 was the most likely generator of the data across the group (posterior probability > 99%). In agreement with Chapter 10, this model had architecture B, i.e. parallel BG and cerebellar loops, converging at the level of the cortex. The model encompassed DBS-induced modulatory effects on all the connections within the BG loop, as well as the projection from the cerebellum to M1. Subsequent family analyses confirmed that (1) models with architecture B were more likely to generate the data than architecture A, and (2) models incorporating modulatory inputs on cortico-striatal, direct, indirect,

hyperdirect, thalamo-cortical, and *cerebellar-cortical* connections respectively outperformed sparser models (posterior probabilities > 99%). Results are presented in Figure 11.2.

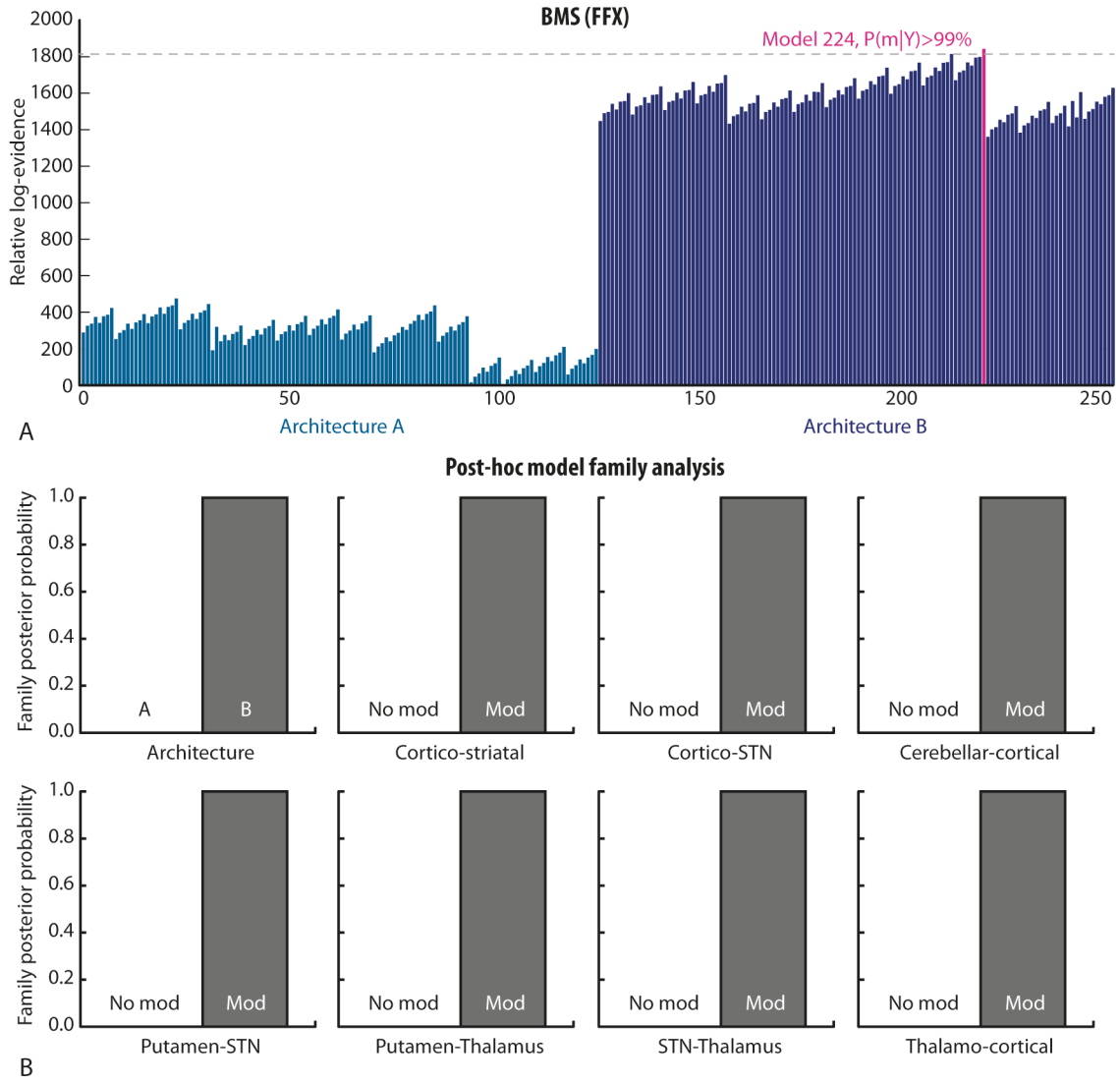

Figure 11.2 Results of BMS (A) across entire model space, (B) post-hoc analyses of model families.

11.4.3 The effect of STN DBS on extrinsic coupling

Posterior coupling estimates extracted from model 224 from each subject revealed significant changes in cortico-striatal, direct, indirect, hyperdirect, thalamo-cortical, and cortico-cerebellar coupling. Cortico-striatal ($p<0.05$, corrected), direct ($p<0.05$, corrected), thalamo-cortical ($p<0.05$, corrected) coupling increased under therapeutic STN DBS,

whereas hyperdirect, striato-STN and STN-thalamic coupling reduced during DBS ($p<0.05$, corrected). As before, the magnitudes of change of coupling involving the STN were smaller than other changes observed (although still highly significant). Importantly, while model selection favoured models with modulatory effects on cerebellar-cortical connections, when examining for changes in the coupling parameters, paired T tests failed to find significant differences between the coupling parameters ON and OFF DBS. Multiple linear regression analyses predicting clinical impairment or improvement using the coupling parameters failed to reach statistical significance ($P>0.5$).

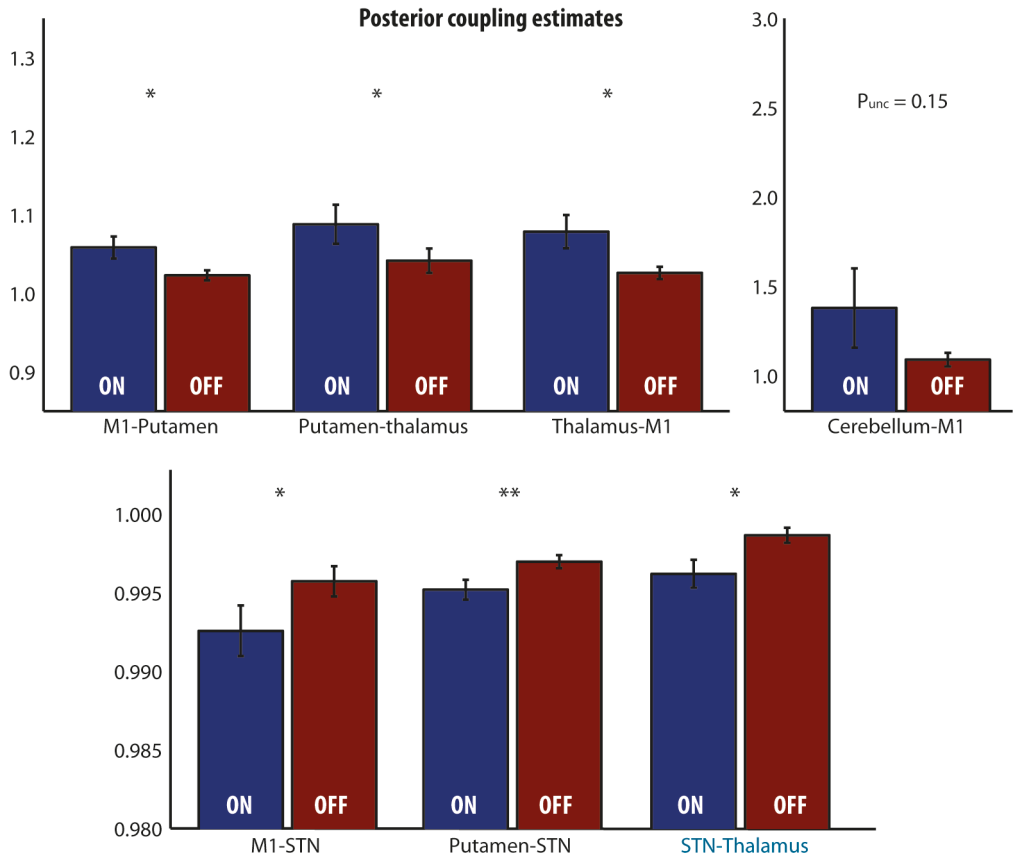

*Figure 11.3 The effect of STN DBS on extrinsic coupling across the group. *P<0.05 (Bonferroni corrected), **P<0.001 (Bonferroni corrected). Same axis scaling used in this plot as in Figure 10.6. There was insufficient evidence to suggest cerebellum-M1 coupling was significantly changed by STN DBS; uncorrected P value reported. Note the different scale used for M1-cerebellum, and coupling with the STN. STN-thalamus coupling was set to be inhibitory a priori.*

11.5 Discussion

In this experiment, the effects of STN DBS on endogenous dynamics within the cortico-basal ganglia motor loop were re-examined, this time including cortico-cerebellar dynamics, given their relevance to improvements in voluntary movements under DBS (see sections 10.4.3 & 10.5.5), as well as their hypothesised role in PD tremor (Helmich et al., 2011). Results demonstrate qualitatively identical modulatory effects within the basal ganglia to those reported in my previous resting state dataset (an independent dataset, collected under a different scanning protocol, excluding cortico-cerebellar dynamics; see Chapter 8), that are also consistent with modulatory effects in the BG reported during movement. DBS-induced coupling differences between the cortex and cerebellum did not survive random effects analysis across the group in the most likely generative model.

11.5.1 Consistent modulatory effects on the basal ganglia motor loop

Results from this experiment suggest that even with the additional modelling of cortico-cerebellar dynamics, the effects of DBS on the BG motor loop appear consistent with sparser models of the resting state (i.e. results from Chapter 8). Once again, results suggest that DBS reduces the effective connectivity of the hyperdirect pathway, indirect afferents to the STN, and indirect afferents to the thalamus, while simultaneously increasing the coupling down the direct pathway, cortico-striatal, and thalamo-cortical projections.

Perhaps of more interest is the consistency of effects on the BG motor loop regardless of behavioural state. In other words, STN DBS appears to be producing qualitatively identical effects on the BG, indiscriminate of whether the patient is engaged in voluntary movements or simply at rest in the scanner. Given the general state-dependence of neural activity and functional integration, the fact that DBS produces certain state independent

effects is rather remarkable, and perhaps makes sense given its therapeutic ability across a range of behavioural states that patients engage in.

Furthermore, this may also help explain negative effects of STN DBS. For example, as discussed previously, authors have reported increased impulsivity in STN DBS patients during high-conflict decision making tasks (Frank et al., 2007). The identical DBS effects on BG dynamics during the two different behavioural states explored in this thesis may generalise to further behavioural states, such as decision making. In which case, the impulsivity deficits reported might result from this common mechanism. With regard decision making, it has been proposed that the disruption of the hyperdirect pathway is specifically responsible (Cavanagh et al., 2011).

However, it is also worth considering the nature of resting state fMRI. The previous discussion is based on there being an obvious difference between motor-task and resting state fMRI. Put simply, just because the patient is not engaged in the motor task, does not necessarily mean the patient is not moving at all during the resting state session. To explore this question further, it may be worth scanning patients performing a completely orthogonal task (e.g. engaging in a cognitive process), and see if there is an effect of state. That being said, it is impossible to not move during any MRI session.

11.5.2 Cortico-cerebellar dynamics during rest

Contrasting the effects of STN DBS on cortico-cerebellar dynamics at rest and during movement is also particularly interesting. Model selection favoured models with modulatory effects on cerebellar-cortical afferents (in contrast to my findings during movement). However, the posterior estimates across the group of the effective connection

strength between cerebellum and cortex were not found to be statistically significantly changed by DBS.

Taken together, results propose that during rest, there does not appear to be significant neuromodulation of cortico-cerebellar coupling, in either direction, whereas during movement, cortico-cerebellar coupling is increased. Thus, while effects on the BG motor loop, the circuit directly targeted by DBS, appear to be context-independent, the integrative abilities of the cortical targets of the BG show context-dependent modulatory effects.

11.5.3 Coupling did not predict clinical impairment

As in Chapter 10, linear regression modelling did not identify coupling in any of the pathways to have significant predictive capacity of either clinical status, or clinical efficacy of DBS. However, as discussed in section 10.5.4, this may be due to the power of the regression analysis to detect effects in such a small cohort with so many explanatory variables. Another possibility is that there was a high degree of posterior covariance amongst the coupling parameters, making them highly correlated, as has been observed in more complex DCMs (Rowe et al., 2010).

11.5.4 Limitations

This experiment suffers the same limitations of the presented modelling studies so far. A general discussion of these limitations is presented in section 12.5.

One notable limitation of the comparison between resting and movement experiments presented in the previous two chapters pertains to how the data were analysed. This is presented in detail in section 12.3.4.

11.5.5 Conclusions

My conclusions are twofold: Firstly, previous findings of modulatory effects on BG effective connectivity under STN DBS whilst patients lay at rest have been partially replicated in an independent patient cohort. Secondly, whilst models incorporating modulatory effects on cerebellar-cortical coupling prevail, random effects analysis at the group level does not identify significant differences in cerebellar-cortical coupling under DBS. This suggests possible behavioural context-independent effects on the BG motor loop.

12Discussion

12.1 Summary

In this chapter, I discuss the results of my five experiments and their significance to our understanding of how STN DBS produces therapeutic effects in patients with PD. My discussion is split into three fundamental questions, followed by a discussion of limitations.

Specifically, I first reflect on the technical aims of this thesis, the safety and feasibility of collecting fMRI in DBS patients. I review what I have achieved and discuss which aspects require further research.

I then discuss the neurobiological significance of my movement fMRI experiments, before turning my attention to effects of STN DBS on endogenous coupling. Discrepancies in results are considered, and limitations of my experiments are critically examined.

12.2 Is DBS fMRI safe & experimentally feasible?

The first aim of this thesis was to assess the experimental feasibility of conducting fMRI research in patients with implanted DBS systems, specifically PD patients with STN DBS. I have included safety issues with this discussion point, as the two are very much related, and is often the first question asked when presenting this work at conferences or talks.

12.2.1 The safety of fMRI in DBS patients

Prior to starting this research, the National Hospital for Neurology and Neurosurgery had in place a specific protocol for MRI scanning patients with implanted DBS hardware based on on-site *in vitro* studies (Carmichael et al., 2007). This protocol was (and still is) employed on a weekly basis to perform anatomical scans following implantation of DBS electrodes to verify targeting precision (that is, before implantation of the IPG). Those studies formed the basis of the protocol used to collect data presented in my first two fMRI experiments (Chapters 7 & 8). However, following some disappointing results in my first experiment, and some concern recruiting patients with newer systems, I felt it was worth trying to improve scanning protocol, which would both boost the quality of the collected data and maximise potential recruitment. Furthermore, the ability to collect higher quality scans has obvious implications on the (admittedly rare[22]) occasions that DBS patients require cranial MRI post-surgery.

12.2.1.1 Functional MRI in DBS patients at 1.5T

Functional MRI data presented in this thesis was collected exclusively in 1.5T MRI scanners, and is the largest known cohort of DBS patients to receive fMRI. Given this, it is important to note that there were no adverse effects of scanning in any of the patients taking part in my experiments. All patients returned to their clinical baseline following re-

[22] *If imaging is required, CT is usually adequate – but on occasion MRI needs to be used.*

administration of their medication, there were no significant changes to the DBS circuit impedances between any contact combinations, and there were no unexpected switching on/off of the IPG whilst in or around the MRI scanner. This was true under both safety protocols used in this thesis.

Safety was determined primarily by assessing the heating produced at the electrode tips given the general agreement within the literature that this represents the foremost danger of scanning (Baker et al., 2006; Georgi et al., 2004; Golombeck et al., 2002; Kainz et al., 2002; Rezai et al., 1999, 2002; Sharan et al., 2003). In addition, I performed several pilot scans with the DBS electrodes taped to my head to confirm to myself that electrode 'migration' really was not a cause for concern[23]. The safety thresholds used in *in vitro* results in Chapter 9 (<1°C) were based on current international guidelines (HPA, 2008), and assume that the heating produced is not dispersed by cerebral blood flow (which it likely is – (Collins et al., 2004; Salcman et al., 1989)). As an illustration of the margins of safety used, it is worth considering that under these recommendations, high fevers (40°C), which are not known to cause neural tissue damage, would be considered too dangerous (Finelli et al., 2002). It is also worth noting that other studies employing fMRI in these patients have not conformed to as strict guidelines: Phillips et al., report using a GE-EPI sequence that produced as much as 1.36°C of heating using a 3T scanner (Phillips et al., 2006), and Jech et al., have used T2-weighed sequences with a SAR as high as 0.98 W/Kg, producing heating of 1.1°C.

My results confirm that both head-transmit MRI is safe in patients in ActivaPC™ systems, and propose that using body-transmit MRI is sufficiently safe at 1.5T, even in extreme

[23] *This was largely done to relax my prior beliefs about strong magnets and metal. It was not formally measured given previous studies have demonstrated that MRI at 1.5T is not associated with electrode movement* (Uitti et al., 2002).

cases of misplacement of the patient (±15cm from iso-centre). This was confirmed following successful safe data collection in Chapters 10 & 11. This technical accomplishment is itself a significant advance to the field. However, like all the literature on the safety of scanning patients with implanted devices, these findings are not immediately generalizable given the inherent between centre differences in scanners, and scanner software versions. Centres looking to perform similar studies must make sure to perform their own on-site *in vitro* experimentation before embarking on *in vivo* investigation.

12.2.1.2 Scanning at 3T

One published study has already scanned patients immediately following electrode implantation at 3T, reporting no temporary or permanent adverse effects (Phillips et al., 2006). While this is promising, the conclusions of this work suggest that as things stand at our centre, scanning at 3T is too dangerous (see section 9.5.1.5). Of particular concern is the heating occurring during the pre-scan process. The MRI physics team at the hospital have contacted Siemens to ask them specifically what occurs during this period that could produce the large temperature changes reported. However, even if the cause is identified, heating during scanning still exceeded acceptable limits, bringing into doubt whether 3T MRI in these patients will ever be feasible.

12.2.2 DBS hardware, fMRI and experimental confounds

In terms of the potential *technical* experimental confounds of performing fMRI in DBS patients, this thesis specifically addressed two: (1) interruption of programmed stimulation by the MR environment, and (2) different heating effects seen during different DBS conditions.

Results from Chapter 9 show that ActivaPC™ devices appear to deliver programmed stimulation during fMRI, regardless of whether head-transmit or body-transmit MRI was employed. Furthermore, this new device did not appear to 'drop' any pulses or deliver additional stimulation, as has been previously reported with older devices (Carmichael et al., 2007; Georgi et al., 2004).

Regarding heating effects across stimulation conditions, my results were somewhat confusing and lacked some consistency across field strengths. The results of the effect of DBS condition (presented in section 9.4.3) are summarised below in Table 12.1:

	TSE sequence	GE-EPI sequence (fMRI)
1.5T	-0.01°C (p =0.420)	+0.08°C (p <0.008)
3T	-0.20°C (p <0.001)	-

Table 12.1 The effect of activating the IPG on maximum heating achieved during different sequences at different field strengths. All values are relative the heating achieved during OFF stimulation. The measurement sensitivity was ±0.1°C.

I have not been able to explain the differences in ΔT observed across sequences and field strengths; clearly more work is required, especially at 3T. Perhaps working with higher energy sequences will enable the effect of stimulation to be better characterised, as heating effects may be exaggerated, which will be useful given the limited sensitivity of the thermometer. At 3T, Phillips et al., have reported different heating effects under different stimulation conditions; in that instance, activating the DBS increased mean heating by 0.08°C, although the comparison was not statistically analysed (Phillips et al., 2006)[24]. One can speculate that if the effect is indeed true, it is likely due to differences in the circuit impedances in the two stimulation conditions.

[24] *That study also used an external pacemaker with externalized extension cables running from the skull to the control room. Thus, there are a number of other factors (geometry of cables) that make those results difficult to compare to these.*

For the purposes of my studies however, these results confirmed that if there is any difference in heating effect between ON and OFF conditions during fMRI, it is sufficiently small (in a model that implicitly over-estimates heating,) that it is within the range of the thermometer sensitivity. Thus, it is assumed that any real heating occurring *in vivo* is likely negligible and does not confound fMRI studies comparing ON and OFF stimulation conditions.

12.2.3 Hardware-related artefact

On reflection, artefact remains one of the key complicating issues in DBS fMRI, one that does question the feasibility of certain experiments, and one that was unfortunately not addressed in this thesis. The two major sources of artefact in fully implanted patients are the (1) connection between extension cable and electrodes, and (2) electrode tips.

The first experiment was short-sighted in this regard, although arguably excusable. At the time of scanning the only published fMRI studies had focused on patients who had yet to receive their IPGs, thus delivered active stimulation using an external stimulator connected to the patients' externalised leads via a long extension cable. The resultant cable geometry was obviously very different to that of an implanted patient, thus it was difficult to predict what the artefact would look like when the patient had their DBS *in situ*. In fact, the experiment in Chapter 7 is, to my knowledge, the first report of performing fMRI in patients with fully implanted systems.

The metal screws that secure the extension cable to the electrodes likely cause the artefact at this junction, and typically produced much larger loss of signal artefacts than the electrodes themselves. This was first noted by Arantes et al., in their fMRI study in externalised patients (Arantes et al., 2006). Regarding the artefact at the electrode tip, previous *in vitro*

experiments have attempted to characterise and optimise sequences to minimise its effect (Pollo et al., 2004). However these experiments have focused on sequences commonly employed for anatomical scans, posing questions like *which sequence is optimal for post-implantation electrode verification scanning?* Two studies have examined the artefact at the lead during GE-EPI sequences, reporting loss of the MR signal in a volume extending as much as 1 cm from the electrode (Georgi et al., 2004; Shrivastava et al., 2012).

These artefacts were especially destructive at second level analysis (again, something that no one else had performed in DBS patients). As voiced in section 7.5.1.1, their effects were more severe in the group analyses due to the additive nature of the artefact across the group. Thus at the second level, even when recruitment was limited to patients known to have their connectors at a relatively fixed location (as in the second cohort), the SPM "whole brain" volume mask excluded a large portion of the left hemisphere (presented in Figure 12.1).

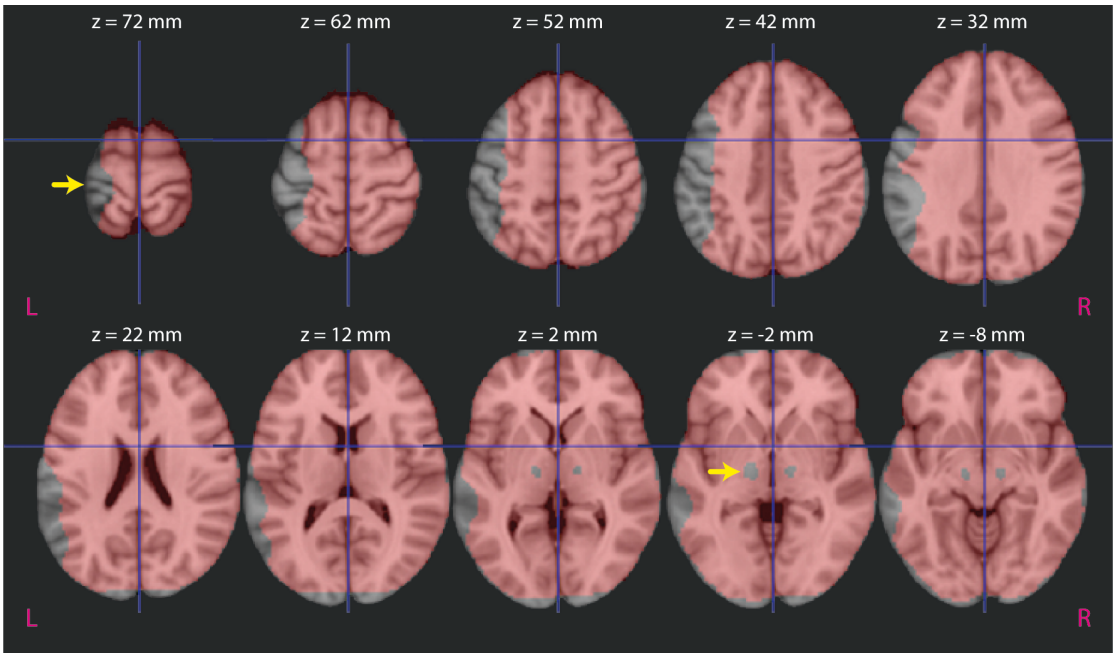

Figure 12.1 The resultant search volume for second level analysis in Chapter 10. The image presented is the MNI brain with the mask.nii image (found in the same directory of the

estimated SPM.mat) overlaid in transparent pink. The blue-grey brain regions are therefore regions not included in the "whole brain" search volume. Yellow arrows highlight regions lost due to the DBS artefact including the left hemisphere cortex and bilateral thalamus area.

So, do these artefacts make fMRI in DBS patients unfeasible? In my opinion, it appears to depend entirely on the scientific question pursued[25]. If the experimenter wants a truly *unbiased* search across *all* regions of the brain to detect some *factor x DBS* interaction in patients with chronically implanted hardware, then yes, unfortunately that is not going to be possible in these patients, in a similar way to how it would not be possible to do an unbiased search in GE-EPI data that had not been corrected for susceptibility artefacts (Devlin et al., 2000; Hutton et al., 2002). For example, analysis of data in temporal or orbitofrontal cortex has long been complicated by identical issues, and can be aided by correcting for field inhomogeneity (Hutton et al., 2002) and/or optimising the EPI parameters (Weiskopf et al., 2006). Therefore, future work should certainly focus on optimising scan parameters to minimise the observed artefact.

Regardless of progress made on that front however, there will likely always be some artefact, and given the small size of the nuclei targeted in DBS operations, it is unlikely that DBS fMRI will be able to inform us about neural activity at the target nucleus[26]. Thus, if the experimenter wants to know whether activity at the STN changes under DBS, then an fMRI study is not suitable as things stand. Similarly, if the experimenter wants to look for *task x DBS* interactions that they believe are likely to occur in the in the left parietal and frontal cortex, the artefact from the connector is likely to render the experiment unfeasible

[25] *…like almost everything in science.*

[26] *In fact, given the size of the STN, it is questionable whether current fMRI can ever really attribute activity to nuclei of these sizes at all, especially considering most authors employ 3 mm isotropic scanning, and then spatially smooth their data. This is forgetting of course that the HRF has a spatial dispersion, as well as a temporal one* (Penny et al., 2005). *For this, lessons might have to be learnt from the growing literature on brainstem fMRI (see section 13.2.2).*

– this may be particularly relevant for those wanting to explore the known adverse effects of STN DBS on verbal fluency (Cilia et al., 2007).[27]

12.2.4 Recruiting patients with advanced PD, severe motor symptoms & DBS

The following points are not entirely specific to DBS fMRI studies, however are worth briefly mentioning because they were important considerations in these studies. Scanning patients presents a number of challenges; both with regard experimental design, and pragmatics.

12.2.4.1 Implications on experimental design

Experiments in Chapters 7 & 10 sought to identify regions displaying *movement x DBS interaction*s and model the underlying functional architecture. Despite one of the key advantages of fMRI over PET being the improved temporal resolution and the ability to perform event-related designs, epoch designs were chosen for two reasons[28]: (1) because that is what had been done previously in the PET literature, and (2) because they are the most efficient at identifying regions engaged in simple tasks such as our own (Henson, 2007).

Efficiency was key because it was necessary to minimise the time spent in the scanner, given the discomfort associated with being off medication, and for half of the session, off stimulation too. The *discomfort factor* is actually an important issue in these types of studies, and certainly (but unavoidably) confounds comparisons between the ON and OFF state. In retrospect, I should have collected survey data post-scanning, and attempted to correct

---

[27] These studies could be possible if the surgeons and patients agree to have their systems wired down their right side. This is equally feasible from a clinical perspective, however the standard surgical practice here is to implant the IPG in the left pectoral area.

[28] On this note, it is worth clarifying that while this thesis has used terms like the "main effect of voluntary movements" or "movement x DBS interactions", "movements" are more accurately blocks of movements including the gap between actual movements.

for levels of discomfort across the group. Furthermore, it implicitly biases recruitment to those patients who can tolerate the discomfort.

12.2.4.2 Washout periods

Related to this is the latencies adopted between de/activating DBS and scanning, as well as the gap between stopping medication and scanning. In an ideal world, both washout periods would have been longer such that scanning really captured the true off/OFF state, as well as the off/ON state. While the vast majority of its clinical effect is delivered within the 10 minute window adopted, the literature reports that delivery (or removal) of *full* efficacy can take hours (80% of efficacy on rigidity and bradykinesia subsides after 30 minutes of DBS OFF – see Figure 12.2 adapted from (Temperli et al., 2003)). Unfortunately, the pragmatics of doing this would be incredibly difficult, and arguably questionable from an ethics perspective.

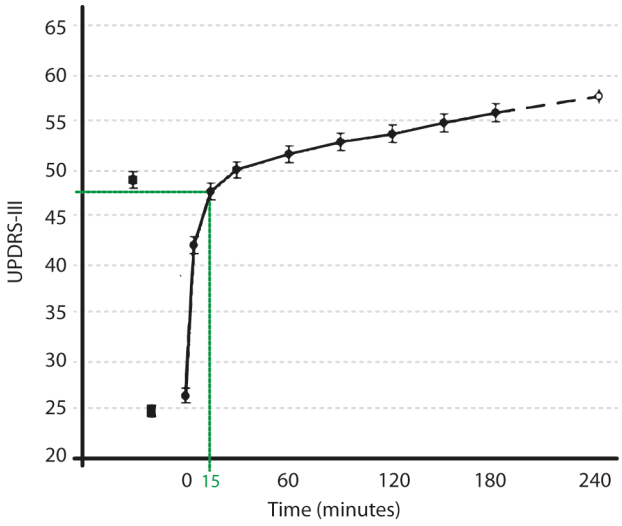

Figure 12.2 The time taken for PD symptoms to return following discontinuation of STN DBS. Adapted from (Temperli et al., 2003)*, Figure E in that paper. Green line estimates the time at which fMRI data acquisition began.*

12.2.4.3 DBS circuit impedance

On the matter of recruitment, all participants in these experiments had their DBS system impedances checked before scanning to ensure there were no potential lead fractures or vulnerable circuit components. This was important because our safety data had been collected in fully functioning systems, and thus the safety of scanning patients with lead fractures was unknown. Theoretically, a loose connection or circuit defect could cause a large voltage across the defect, potentially causing excessive heating or a spark (Georgi et al., 2004). One case report of such an event has been reported with ECG equipment (Kugel et al., 2003).

Additionally, all patients in this study had to tolerate lying flat in the scanner with minimal head tremor in both DBS conditions. The reason for this was based on two factors: (1) head movements reduce the quality of the data (discussed in the next section), and (2) the safety data was collected in a static *in vitro* model and did not study potential currents that could be induced by moving the DBS circuit within the magnetic field. This again biased selection away from patients with a more tremulous phenotype.

All these factors, in addition to only selecting patients with left pectoral IPGs in the latter experiments, complicated patient recruitment. Of the patients that we felt could tolerate scanning based on their clinical history:

- 2 patients could not be scanned due to high system impedances (subclinical),
- 2 patients could not be scanned due to excessive head tremor,
- 1 patients started scanning but could not tolerate being OFF stimulation,
- 1 patients started scanning and could not tolerate being enclosed in the scanner,
- 23 patients successfully completed scanning sessions.

12.2.5 Task fMRI & motion artefacts

> *To most economists the single equation least squares regression model, like an old friend, is tried and true… As with most old friends, however, the longer one knows least squares, the more one learns about it. An admiration for its robustness under departures from many assumptions is sure to grow. The admiration must be tempered, however, by an appreciation of the model's sensitivity to certain other conditions.*
>
> D. E. Farrar and R. R. Glauber, 1967

A prominent source of noise in fMRI is motion of the subject during scanning, producing both spin-history and susceptibility-by-movement artefacts (Andersson et al., 2001; Friston et al., 1996; Wu et al., 1997). As a means of nullifying this, data in these experiments were first realigned and unwarped (see section 6.4.1). Subsequently, data collected in experiments in Chapters 7, 8 & 11 were modelled using GLMs including realignment parameters (i.e. head motion parameters) as nuisance regressors in an attempt to explain away any obvious correlates of head motion.

In the second task fMRI study in Chapter 10, head movement covariates were specifically not included in the first level GLMs, owing to the noted collinearity between stimulus function and head movements (reported in section 10.3.5). A representative example from that experiment can be seen in Figure 12.3. Simply put, the GLM is not well equipped to cope with interdependent (sometimes referred to as correlated, collinear or multicollinear) explanatory variables; the columns of the design matrix are assumed to be controlled elements of a laboratory experiment, where experimental factors are orthogonal with respect one another (Farrar and Glauber, 1967; Friston et al., 1994b)

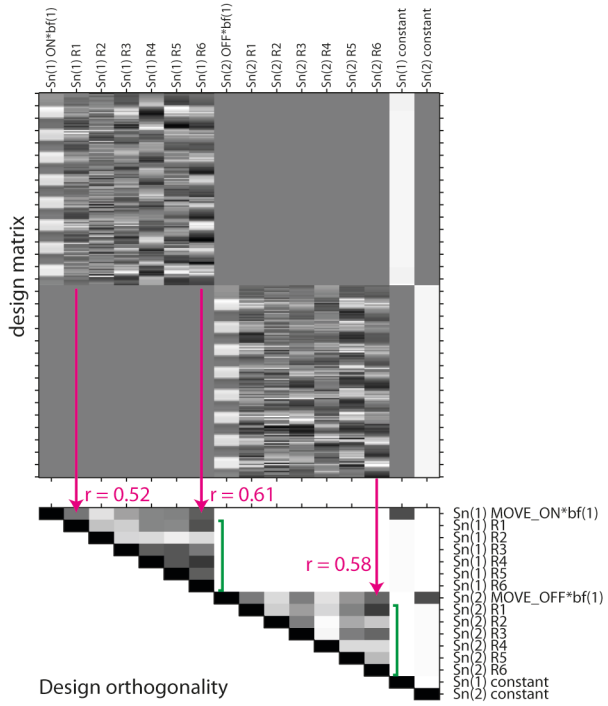

Figure 12.3 Example of non-orthogonality between head motion regressors and the stimulus function. Taken from Sub006 from Chapter 10 with their head motion regressors included in the design matrix. Green brackets highlight motion regressor collinearity. Pink arrows demonstrate shared variance between given head motion regressors and the stimulus function, with correlation coefficient.

As a result, one obvious difference between task experiments in Chapters 7 and 10 is the presence of those covariates in the first level analysis. Thus, it could be that the differences in results could be due to collinearities in those GLMs that were initially missed. To investigate this, the data from Chapter 7 were re-analysed using the same batch pipeline as used in Chapter 10. Results at the second level found no evidence for any *movement x DBS interaction*s surviving SVC or cluster wise whole brain significance thresholds, suggesting that collinearity between hand and head movements was unlikely to be masking true experimental effects.

Addressing a more general issue, head movements are clearly an important source of noise in all fMRI studies, especially in PD patient cohorts. In brief, it is assumed that voxel X corresponds to brain volume Y throughout scanning, and upon head movement, this

assumption is broken. Therefore the variance in the signal from voxel X is going to be a function of both the experimental factors, and the head movement. Head movement variance tends to be more pronounced than experimental variance, and if the movements are collinear with the experimental stimuli (for us, hand movement blocks), identifying experimental effects becomes more difficult (Friston et al., 1996; Wylie et al., 2014).

In studies such as the ones presented herein, when PD patients are scanned in two treatment states, one associated with less tremor, differences in BOLD signal could therefore result from either a biological difference (i.e. a real difference), or a difference in the SNR of the two datasets. To confirm therefore that there was not a significant difference between the motion during ON and OFF, the second cohort's average variance of each of the 6 motion parameters from task sessions during both conditions are presented below (Figure 12.4). These simple comparisons suggest that the ON vs. OFF comparisons presented in Chapter 10 are not significantly confounded by differences in head motion.

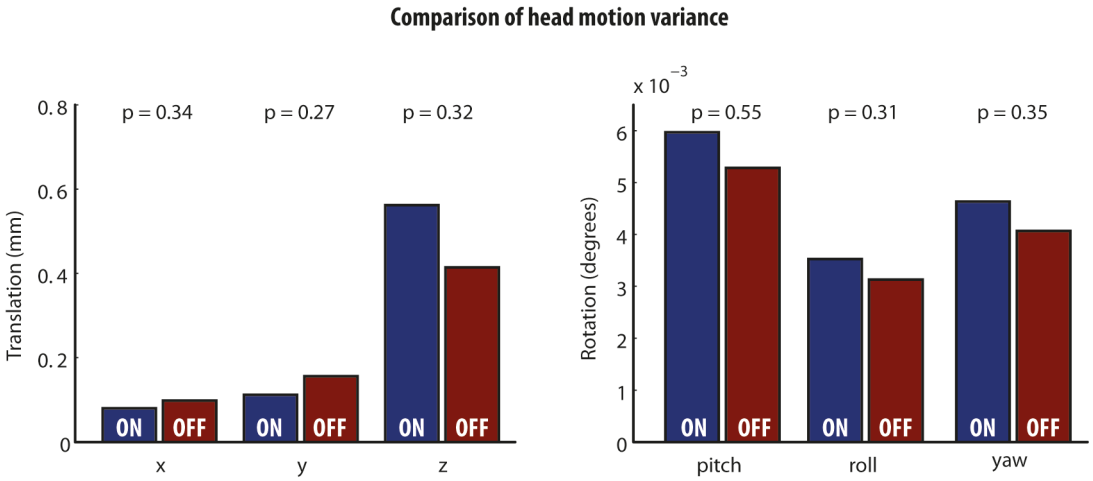

Figure 12.4 Comparing the variance of parameters of head motion during task fMRI sessions ON and OFF DBS (data from Chapter 10). Variance = standard deviation. The mean variances across the group are presented. P values are for the paired T test comparing ON and OFF sessions and are uncorrected for multiple comparisons. There is no evidence to suggest there is an effect of DBS on variability of head motion during scanning.

12.2.6 Conclusions

So, let us return to the question set out in this sub-section, is DBS fMRI safe & experimentally feasible? In my opinion, the answer is yes, but these experiments are certainly more restrictive than fMRI in other patient cohorts, and far more restrictive than fMRI in control cohorts. Undertaking such studies requires careful consideration of:

1. Safety and MRI protocol, including on site in vitro testing.
2. Limitations posed by the hardware-related artefact.
3. Balancing experimental ideals with pragmatic recruitment and patient comfort.
4. Motion artefact in patient cohorts (especially with movement disorder cohorts).

12.3 What does STN DBS do to the PD brain whilst engaged in voluntary movements and whilst "at rest"?

Turning our attention to its neurobiological significance, this thesis presents a series of experiments that examine the effect of STN DBS on neural activity both whilst patients perform blocks of voluntary movements, as well as whilst patients lay in the scanner at rest. To my knowledge, this work is the first fMRI study to examine patients with bilateral STN DBS with fully implanted systems. As a result, all had their DBS parameters optimised over a period of at least 3 months, and had received chronic stimulation at confirmed therapeutic parameters. Any effects of inflammation were likely to have passed by the time patients underwent scanning.

12.3.1 The nature of the voluntary movements studied

It is worth briefly pausing to clarify exactly what is meant by *voluntary movements*. The task used has been employed in a number of previous PET studies (Ceballos-Baumann et al., 1999; Limousin et al., 1997). While movements are cued by the auditory stimuli during

the "go" blocks, the *voluntary* component arises from the choice of direction in which the handle can be moved with each trial. Furthermore, subjects were instructed to plan their next movement between cues. Thus, modelling the movement block additionally includes periods of planning and initiation, as well as the movement themselves.

12.3.2 Where does DBS produce the greatest changes in motor-evoked responses?

Both experiments in Chapters 7 and 10 sought to identify key components of the motor system that demonstrated *movement x DBS interaction*s. Results from Chapter 7 detected two such clusters that were significant at SVC statistical thresholds; in other words, only when the search volume was limited to spheres surrounding key nodes of the motor network (identified using the orthogonal contrast – the *main effect of movement*) were these changes statistically significant. The data were fastidiously interrogated to ensure that analysis had not been confounded; for example, collinearity of experimental effects with head motion (discussed in 12.2.5). At the time of analysis (and subsequent publishing) these data were the best achievable, thus provided the best insight at that time, acknowledging of course that results failed to reach whole brain significance following correction for multiple comparisons. That particular paper concluded with this important limitation (Kahan et al., 2012). However, following collection of the second dataset under an improved protocol (having learnt from previous studies), the two clusters identified were only significant at liberal whole brain uncorrected thresholds, whereas two additional clusters, not detected in Chapter 7, were significant at the whole brain corrected level. larger effect sizes are more likely to be causal to behavioural changes.

Another important finding was the lack of detection of any decreased motor-evoked responses under DBS in either study (i.e. *movement x DBS interaction*s OFF>ON). As

reviewed in 5.4.2.6, studies have previously reported decreases in parts of the precentral gyrus (Ceballos-Baumann et al., 1999; Thobois et al., 2002) and cerebellum (Grafton et al., 2006).

Based on the results of these experiments, I conclude that, in terms of regional responses to blocks of voluntary movements, therapeutic STN DBS produces its most marked effects on M1 and the cerebellar cortex, increasing the activity in both of these well established component nodes of the motor network.

12.3.3 Does STN DBS change cortico-subcortical effective connectivity?

Moving on to address the third aim of this thesis, all four of my fMRI experiments have in some way posed this scientific question, in progressively greater detail. In my first experiment (Chapter 7), given the lack of interaction clusters that survived corrected whole brain statistical thresholds, the insula and thalamus (both clusters that survived SVC) were chosen to summarise the respective cortical and subcortical systems. In DCM, interactions in a given region are typically explained by some modulatory effect of an experimental factor on at least one of the afferents to that region. In the simple reciprocal architecture specified (see Figure 7.2), the observed data could well have been explained by modulatory effects on each node's respective intrinsic afferents, suggesting that modulatory effects on cortex and thalamus are not dependent on the two interacting. However BMS demonstrated that both extrinsic and intrinsic afferents were modulated by STN DBS, suggesting that both the cortex and thalamus experience a gain "tuning", altering their sensitivities to incoming signals from each other. Put simply, the answer to the question in

this sub-section was *most likely*[29], but the nature of this change, its anatomical detail, and significance to clinical efficacy were unclear.

The question then became more specific. Chapters 8, 10 & 11 each asked which of the known pathways coursing through the BG, and subsequently cerebellum, were modulated by DBS.

The BMS results as well as subsequent comparisons of parameter estimates clearly demonstrated that regarding the BG, STN DBS had relatively consistent effects. In each of the datasets studied in Chapters 8, 10 & 11; STN DBS increased cortico-striatal coupling, direct pathway (or more specifically, excitatory striato-thalamic) coupling, and thalamo-cortical coupling. In contradistinction, DBS reduced hyperdirct cortico-STN coupling, as well as STN afferents from the striatum (considered the proximal limb of the indirect pathway), and STN-thalamic (distal limb of the indirect pathway) effective connectivity (presented graphically in Figure 12.5). In other words, STN DBS:

- Increases the putamen's response to cortical afferents;
- Biases thalamic sensitivity towards the direct pathway afferents;
- Reduces the sensitivity of the STN to incoming signals;
- Increases the gain of cortical targets to information arriving from the BG.

The relevance of these findings to the published literature has already been discussed at length in section 8.5.1.

---

[29] *Remember, the answer to all model comparison questions (arguably all statistics for that matter) that select a winning model end in "most likely". This probabilistic estimate is conditional on both the data and the competing models tested. The job of BMS is to allow the experimenter to compare competing plausible hypotheses. The job of the experimenter is to come up with interesting and plausible hypotheses.*

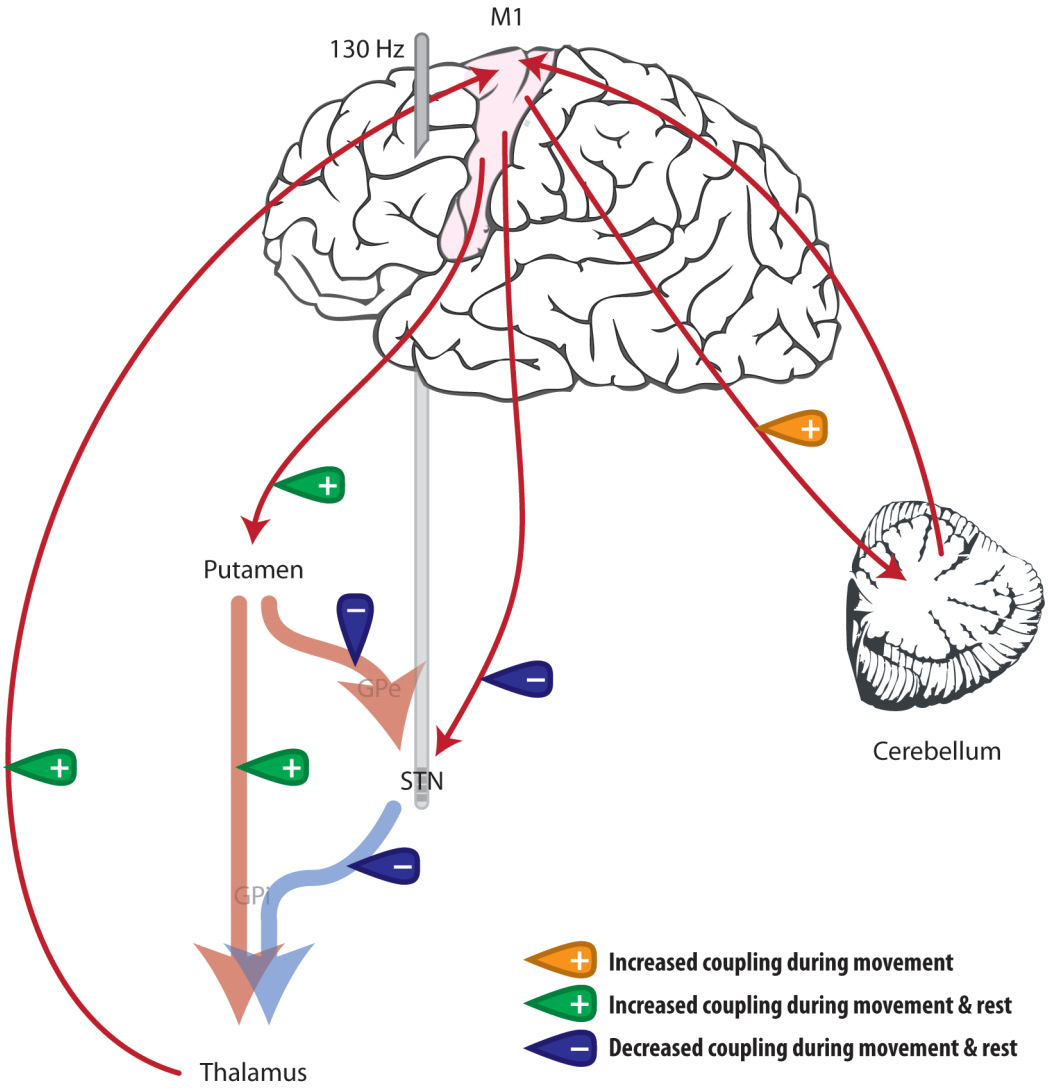

Figure 12.5 Summary of the effects of STN DBS on effective connectivity within the motor system.

12.3.4 Does STN DBS produce state-independent effects on the BG motor loop?

The follow-up question is of particular interest; are the effects of STN DBS dependent on behavioural state? This was briefly addressed in section 11.5.1. To summarise, DCMs of the cortico-BG and cortico-cerebellar dynamics were fitted to data collected in two different behavioural states (voluntary movements and at rest). BMS was then used to select the most likely generative architecture for each state, parameter estimates from the winning model were extracted and paired T tests were used to test for a significant effect of DBS on each connection at the group level. Through qualitative comparison, it was clear that the

direction of modulatory effects on pathways in the BG were consistent across behavioural states. From that, it was inferred that STN DBS produces state-independent neuromodulatory effects on the BG.

This inference however is limited in two keys ways: Firstly, while both experiments model the dynamics of the 5 nodes with identical model spaces and endogenous connections, the data for each region was not extracted from anatomically identical voxels, despite being from the same group of subjects. This is due to discrepant methods used to extract VOIs in the two experiments, and ideally would have been identical.

Secondly, in an ideal analysis, data during movement and rest would have been considered in one large first-level GLM, including *effects of movement blocks* (i.e. the 30-second boxcar functions used in the previous experiment), as well as *main effects of DBS*, and *main effects of context*. That way, all data would have been in one DCM with effects of movement driving M1, and effects of DBS and context modulating connections. This framework would have (1) solved the problem of discrepant VOI extraction methods mentioned above, and (2) allowed quantitative analysis of context x DBS interactions, as opposed to the qualitative (and arguably speculative) comparison presented in this discussion. This unfortunately was not possible given the difference in the sequence parameters between resting state and task fMRI. These differences in sequence parameters (specifically the TR and voxel dimensions) were introduced for pragmatic reasons to do with minimising the time in the scanner, whilst maximising the amount of data that could be collected.

In fact, the current findings could be interpreted in a completely different way, speaking to a more general methodological neuroimaging question. If one were to assume that the effects of intervention are identical in both states (which is what we have found in the BG)

such a comparison could equally be asking which type of dataset is DCM more efficient at estimating modulatory effects in, task data, or "resting state"?

Finally, it is also worth highlighting that not all the effects appear to be context-independent. Our modelling suggests that whilst effects on the BG remain fairly constant between movement and rest, some effects of DBS appear to be task dependent. Specifically, DBS increases the response of midline cerebellar activity to incoming signals from the cortex (see 10.5.5), during movement, but not during rest. It would be interesting to determine whether or not this phenomenon generalises to other functionally specialised motor cortical regions by including these regions in future DCM experiments.

12.3.5 Concluding speculation

If the inference discussed above is valid, this may shed light on the potential generalizability of DBS to other neurological or psychiatric conditions. Put simply, DBS appears to be producing the same local effects on a circuit irrespective of what the circuit is engaged in doing. Specifically DBS is (1) reducing the target's response to incoming signals, and (2) altering the sensitivity of neural populations that are anatomically related to that target to their incoming afferents[30]. Assuming DBS directly produces at least (1), translating its therapeutic potential to brain disorder X would require characterisation of the neural dynamics in condition X, and identification of nodes in that architecture that show increased afferentation in the disease state (as has been shown to occur in PD with the STN - (Marreiros et al., 2012; Moran et al., 2011a)). In order to test this hypothesis, future

[30] It is also interesting to consider whether or not STN DBS is actively doing both of these things, or whether DBS does (1), which then results in (2). This could be investigated by scanning subthalamotomy patients before and after surgery; in theory, subthalamotomy would result in a reduction of the STN's response to its afferents, and its output to the thalamus thus I would hypothesise that this could produce at least (1), with possible modulatory effects on the STN-thalamus coupling. If this also produces all the effects on coupling produced by DBS, it is very possible that DBS is acting similarly.

experiments must both establish that STN DBS is producing consistent effects across different disease populations, as well as characterise the modulatory effect of other DBS therapies in both PD (e.g. GPi DBS), and other diseases. This is discussed further in 13.5.

12.4 Does effective connectivity predict clinical parameters?

Given STN DBS was found to significantly alter extrinsic effective connectivity within the BG motor loop, it was interesting to see if the furnished coupling estimates had some predictive capacity for clinical status, clinical improvement and behavioural performance.

This was attempted in all DCM experiments, but unfortunately, only yielded significant results in Chapter 8 (performed on our first resting state cohort). In that experiment, multiple linear regression analyses were performed (n=24 hemispheres, with 6 explanatory variables), finding:

- Contralateral[31] hemibody clinical score OFF DBS was predicted by a linear combination of all OFF DBS extrinsic coupling in the BG motor loop, each connection providing a statistically significant contribution to the model.
- Contralateral hemibody clinical score ON DBS was predicted by a linear combination of all ON DBS extrinsic coupling in the BG motor loop, but only hyperdirect, striato-STN and direct pathway provided statistically significant contribution to the model.
- Finally, using a stepwise elimination regression to yield the most parsimonious model, percentage improvement in contralateral hemibody clinical score was predicted by a linear combination of the modulatory effect on the hyperdirect,

[31] *Contralateral to hemisphere modeled.*

direct pathway and striato-STN coupling, but the latter variable's contribution was only trend significant ($p<0.1$).

At the time of analysis and subsequent publishing, this provided (1) predictive validity of stochastic DCM parameter estimates, (2) further evidence that coupling was an important determinant of clinical phenotype (or behaviour in general), (3) understanding of which coupling parameters were the *most important* determinant of therapeutic efficacy (i.e. hyperdirect, direct pathway and striato-STN coupling), and (4) the direction of change associated with clinical efficacy. Multiple linear regression analyses were employed specifically because of their ability to simultaneously consider multiple dimensions of the data; in other words, because all parameters were considered to be potential sources of the variance in the clinical response, linear modelling allowed us to consider them all together, and not just do multiple individual parameter correlations (which would then result in another multiple comparisons problem).

Unfortunately, these interesting relationships could not be reproduced in subsequent experiments. This could be due to one of three reasons, either (1) the detected relationships are not true, (2) the analysis was not suitably powerful enough to detect the effect, or (3) the analyses were different, and thus are not true replications. Considering the second option, subsequent experiments included and an extra explanatory variable (because the models included an extra connection, see 12.5.6), and fewer hemispheres (because the task fMRI was only performed using the left hand, in Chapter 10). The statistics literature tends to recommend sample sizes an order of magnitude larger than was possible in our experiments to produce robust estimates in multiple linear regressions; different formulae suggest different sizes, for example, Green suggests $N > 104 + m$ (Green, 1991), whereas Harris' formula proposes a minimum of $N > 10m$ (N being the sample size, and m being

the number of independent variables in the regression) (Harris, 1985). Considering the third option, the parameters included in Chapters 10 & 11 were taken from models that included cortico-cerebellar dynamics, thus these results are not a true replication of the originals[32].

Unfortunately though, despite their biological plausibility (see 8.5.1), it remains possible that there are not strong predictive relationships between coupling and clinical status/efficacy. Further studies with much larger cohorts are required to deliver a more confident verdict on this question. Furthermore, it would be desirable to collect objective measures of clinical features such as rigidity, tremor, and bradykinesia. While the UPDRS-III is the current gold-standard in clinical neurology, objective measures would enhance tracking of disease progression (over years), but could also potentially provide reliable time series data that could be integrated into fMRI designs.

12.5 Limitations

12.5.1 Resting state fMRI

One of the advantages of resting state fMRI is its clinical compatibility; in other words, the only expectation you have of the participant is that they can lie in the scanner and stay still. For obvious reasons, it is also popular amongst the experimenters as well. However, the lack of experimental manipulation brings with it a complete lack of experimental control. In our case, analyses were restricted to regions believed *a priori* to be involved in motor processing, informed either empirically from these experiments, or from the literature. Furthermore, PD patients switching from ON to OFF and vice versa, demonstrate a very obvious change

[32] *It is also worth noting that the priors used by DCM for fMRI were updated in January 2014 by the SPM methods team. Given these priors were the most informed at the time of analysis, the decision was made to adopt these. I did not replicate the experiments with the old priors. This is one of the key strengths and potential weaknesses of working with Bayesian schemes.*

in motor phenotype, even when they lie in the scanner at rest. Thus in some respects, these studies do have an element of experimental control.

However, as most fMRI participants will confess, it is remarkably easy to fall asleep in the scanner, especially over a 5 minute period with eyes closed. Thus, there is a risk that patients may have fallen asleep during these scans, despite our encouragement to stay awake. The important question that emerges is whether there is a change in motor phenotype between sleep and wake in PD patients, the answer to which is yes, although difficult to prove without waking the patient. For example, patients typically do no tremor in their sleep; however assessing rigidity in sleep is almost impossible. Thus it remains plausible that data could have been collected during sleep, in which case, the motor phenotype would not have been as measured in the pre-scan clinical assessment.

Finally, it is also worth noting that it is commonplace in the resting state fMRI literature to correct for physiological parameters such as respiratory and cardiac rates collected during the resting state session. Physiological parameters have been shown to explain significant variance in the spontaneous BOLD signal collected at rest (Birn, 2012; Biswal et al., 1996), and thus they are often included in first level GLMs. The reason these parameters were not collected and included was purely pragmatic; the equipment was not available in our centre, thus did not have the opportunity to explore this in these experiments. That being said, respiratory and cardiac noise are generally most prominent in frequencies >0.1Hz; our analyses used the DCT to direct VOI extracted towards regions demonstrating hypothesised neural fluctuations (0.0078-0.1Hz) (Birn, 2012; Biswal et al., 1996, 1995). That being said, respiratory and cardiac noise can alias to lower frequency bands within the ranges specified by the DCT (Lund, 2001).

12.5.2 Anatomical precision & DCM VOI selection

The DCM studies presented attempt to model the dynamics of the BG motor loop. The components of this circuit are obviously very small relative to cortical regions usually examined in the neuroimaging literature. While extraction of the subcortical VOIs was anatomically informed using thresholded probabilistic tractography atlases (Behrens et al., 2003; Tziortzi et al., 2014), the anatomical precision of the VOIs remains imperfect, especially with regard the thalamus, which is well known to host a number of smaller sub-nuclei. The effective spatial resolution of the GE-EPI data collected in these studies were approximately 3 mm isotropic, this was before the data was spatially smoothed using a Gaussian kernel of 8 mm FWHM. This point, in fact, was what prevented a more detailed modelling of the BG motor loop by including the GPi and GPe (see 12.5.3).

Secondly, Chapter 8 extracted data and modelled the dynamics of both hemispheres, despite the artefacts obscuring parts of the precentral gyrus. As a result, as evident in Appendix 8.6.4 of that chapter, M1 VOIs tended to be extracted from more slightly more medial regions of the precentral gryus than equivalent VOIs from the right hemisphere. That being said, DCM results did not significantly differ between the hemispheres.

Finally, DCMs in Chapters 10 & 11 include a cerebellar node. The peak voxel of the cluster found to show a *movement x DBS interaction* was located in the medial cerebellum, and subsequent VOI extraction in both experiments was based on this medial location. Interactions were detected in the cerebellum bilaterally, however given the peak occurred medially, the decision was taken to use this as the centre-point for searches in first level SPMs. Other studies that have examined the cerebellum in PD typically discuss more lateralised activity.

12.5.3 Pallidal dynamics in PD

As briefly discussed, the pallidal nodes of the BG motor loop were explicitly excluded from our DCMs. Given the effective spatial resolution of the data, the small sizes of the GPe and GPi and their anatomical juxtaposition, it was decided that extracting data that could be confidently attributed to each nucleus would be questionable.

As a result, the pallidal components of the BG motor loop were assumed to function as simple relays to either the thalamus (GPi), or the STN (GPe). On reflection, this assumption is similarly questionable. The reciprocal dynamics of the GPe and STN have been implicated in the generation of beta oscillatory activity in the BG (Marreiros et al., 2012; Moran et al., 2011a). In those DCM papers of LFP data, compared to medicated patients and control animals respectively, patients off medication or 6-OHDA lesioned rodents had increased input to the STN from both the hyperdirect and GPe afferents, as well as stronger coupling from the STN to the GPi[33]. Furthermore, in post-hoc contribution analyses, small changes in the STN-GPe effective connectivity resulted in large fluctuations of beta expression. In addition a number of other authors have used forward models to investigate these dynamics, many of which highlight the central role of the STN–GPe circuit in the elaboration of pathological oscillations (Gillies et al., 2002; Holgado et al., 2010; Terman et al., 2002). Including pallidal dynamics in DCMs of fMRI data will be an important and interesting development, however will only be achievable if the spatial resolution of data improves.

[33] *Note that these results are largely in agreement with the results presented in this thesis, despite the different modality used (allowing for non-invasive characterization), and our sparser model.*

12.5.4 Artefact, the STN & hidden nodes

Due to signal drop-out around the electrode, it was not possible to record BOLD data from the STN itself. Therefore, the STN was modelled as a hidden node, enabling inference on its afferents and efferents based on the influence they exert on nodes from which *precise* recordings were available[34]. This is standard practice in dynamic causal modelling of EEG data, where some sources are hidden or silent because they cannot be 'seen' by scalp electrodes (David et al., 2011; Marreiros et al., 2012). In principle, the hidden node could be any brain region with the connectivity fingerprint specified by the model (i.e. any brain region excited by both M1 and the putamen, and that exerts inhibition on the thalamus). Given the anatomical and electrophysiological literature on the functional anatomy of the BG, our hidden node was attributed to the STN. Including hidden nodes can reduce associated effect sizes (because the parameters of hidden nodes are not informed by empirical data and shrink to their prior expectations of zero). This has been demonstrated empirically in Appendix 8.6.1 of Chapter 8.

12.5.5 Modelling DBS as a modulatory input, not a driving input

It is important to note that DBS was modelled as a modulatory effect on extrinsic coupling, not as a driving input to individual nodes. Thus, this work specifically addresses the effects of DBS on extrinsic coupling; it does not address *how* these changes are mediated or delivered to the therapeutic targets. For example, as discussed, STN DBS has been found to induce antidromic effects on the cortex (Li et al., 2012). While this finding may explain how DBS reaches its target, it does not mean there is a DBS-dependent effective connection from the STN to cortex – the *consequences* of antidromic stimulation would be

[34] *The hidden state work-around essentially suggests that recording a series of NaNs is equivalent to recording a real time series; the only difference is the precision of the data. In other words, no data is the same as some very imprecise data.*

expressed orthodromically in cortical efferents (and afferents) to/from basal ganglia or other regions.

12.5.6 The number of nodes and edges

As discussed, DCM does not assume that edges between nodes are monosynaptic. Thus, complicated chains of connections could be conveniently summarised. One limitation of the modelling experiments presented in this thesis is the exclusion of other cortical motor and frontal territories that are commonly studied in PD. For example, DCM and SEM have previously been used to model the cortical dynamics between M1, SMA, PM, and portions of the PFC, and have been shown to be altered by dopamine in PD patients (Rowe et al., 2002, 2010). While in theory, developments in DCM have permitted estimation of very large models (Seghier and Friston, 2013), including many nodes has its complications. Firstly, especially with stochastic DCM, the time taken for models to converge increases significantly with the number of nodes and edges (although this has improved in the latest implementations). Secondly, inclusion of more nodes (especially cortical) will result in many more edges, given that almost all cortical regions are reciprocally coupled in some way (Friston et al., 2014). This implicitly increases the potential model space, and the potential for posterior covariances among coupling estimates. The added dimensionality of the data would additionally induce a more problematic multiple comparisons problem if post-hoc T tests were used, as were here. Finally, this would also increase the number of explanatory variables in any potential regression analysis, thus requiring a much larger patient cohort if one wanted to predict clinical status from the coupling, as was attempted in this work. Given these factors and the relatively small sample sizes achievable in this patient cohort, M1 was included as the

representative motor cortical node, capturing thalamo-cortical dynamics. Future work should attempt to include other important cortical targets of the BG.

12.5.7 High frequency STN DBS

Finally, it is worth highlighting that all work presented in this thesis and discussions of the mechanism of action of DBS are limited to high frequency DBS (typically 130Hz). While these frequencies are commonplace in the treatment of PD and tremor, experience in this centre suggests that DBS at lower frequencies (80Hz) is clinically useful in certain STN DBS patients, despite not a lot of published evidence supporting this (Sidiropoulos et al., 2013). Furthermore, other forms of DBS utilise much lower stimulation frequencies, for example, clinically effective PPN stimulation is typically programmed to deliver 20-30Hz stimulation (Stefani et al., 2007).

13 Future research

Parts of the following chapter have been published in Kahan & Foltynie (2013), Neuroimage.

13.1 Summary

In this chapter, I discuss the future of DBS fMRI. I outline five key areas of research that would enhance our understanding of both the mechanisms underling DBS, as well PD pathogenesis from a systems level perspective.

Specifically, I discuss (1) optimisation of data collection, (2) integration of fMRI data with multimodal approaches including structural connectivity data and current field mapping, (3) modelling synaptic repercussions of DBS, and finally (4) extending this research beyond STN DBS to address common effects of DBS therapies.

13.2 Optimising data collection

13.2.1 Artefact minimisation

As discussed in 12.2.3, an important goal of future research should be to characterise and minimise the artefact observed at both the electrode tips, and at the junction between the electrodes and extension cable. This should be studied systematically in a spherical phantom head model, examining individual parts of the circuit, and contributors to the signal drop out. In terms of sequence development, it is worth considering the literature on GE EPI in the OFC, a region that suffers from similar drop out artefact due to its proximity to the air/tissue interface created by the frontal sinuses. Tilting the slice angle has produced beneficial results there; Deichmann et al., found that artefact is maximised when the slice is parallel to the surface between tissues with different susceptibility (Deichmann et al., 2003), thus it is worth experimenting with the slice angle in DBS fMRI. Alternatively (and/or additionally,) reducing the slice thickness would also reduce the artefact, however would bring with it reductions in SNR, requiring more data to be collected to be collected (thus more time in the scanner) in order to produce data of similar quality. Given the nature of the cohort, this may be untenable. Finally, it may also be worth considering using spin-echo (SE) fMRI (as opposed to gradient-echo used here). SE BOLD would theoretically both reduce drop out artefacts, as well as increase the potential spatial resolution of the data. However, SE BOLD also has a reduced sensitivity (halving the SNR), requiring four times the data to be collected (Norris, 2012).

Finally, it was inferred that the signal loss near the extension cable was due to the metal screws used to connect the cable to the electrodes. If this inference were true, one obvious solution would be to encourage the manufacturer to use alternative screws, or otherwise consider competitor systems from other manufacturers to see which system delivers the

least artefact. Market pressure may be the optimal (if slow) means of driving changes in this regard, assuming such changes in the hardware do not impact on the clinical efficacy.

13.2.2 Improved segmentation and normalisation

Another important future development that will benefit DBS fMRI will be the finessing of subcortical segmentation and normalisation in SPM. Currently, SPM segments the brain into three canonical tissue types; grey matter, white matter and cerebrospinal fluid. However, it is clear that three tissue types is a significant simplification. Recent work studying the brainstem has employed multiparametric mapping (MPM), specifically using quantitative magnetisation transfer and proton density maps to create tissue probability maps for four tissue types in the brainstem alone. These tissue probability maps correspond well with both post-mortem high resolution MT-T2* data, as well as ex-vivo 9.4T MRI microscopy data, and permit a highly accurate warping of individual data (Lambert et al., 2013). Extensions of this work to include the nuclei of BG and thalamus are in preparation[35], although application to DBS fMRI would have to contend with the artefact produced in the GE EPI sequences. To address this, pre-operative MPM scans may prove beneficial for subsequent post-operative fMRI.

13.2.3 Respiratory and cardiac artefacts

Given the physiological artefacts associated with fMRI, particularly at the level of the brainstem (Brooks et al., 2013), where there are likely interesting effects of DBS that we have yet to detect, one very simple improvement to the current acquisition protocol is to simultaneously collect both heart and respiratory rates using pulse-oximetry and respiratory

[35] *Personal communication with Lambert et al.; Poster presented at OHBM 2014, "Fine Grain Cortical Segmentation using Multiparametric Maps at 3T".*

bellows respectively. These physiological parameters could then aid and potentially bolster results of GLM analyses using methods such as RETROICOR (Glover et al., 2000).

13.3 Integration with structural connectivity & anatomy

The relationship between structural and functional connectivity is an extensive and growing discipline (Bullmore and Sporns, 2009; Sporns, 2014). Of particular relevance to DBS is the potential to map the structural architecture intersected by the active electrode contact. DBS targeting tracts and white matter is gaining increasing interest in the treatment of different diseases (Henderson, 2012), given white matter's greater sensitivity to electrical stimulation than grey matter. In the case of Major Depressive Disorder (MDD) trials of DBS of the subcallosal cingulate region have produced mixed results. Recent work though has suggested that the position of the electrode relative to the subcallosal cingulate white matter (specifically forceps minor, uncinate fasciculus and cingulum bundle) is an important determinant of clinical efficacy (Riva-Posse et al., 2014).

In the same vein, it would be of great interest to determine the relationship between structural and effective connectivity within the BG motor loop, and clinical response. In this centre, patients able to tolerate longer sessions in the scanner are currently receiving high-resolution pre-operative DTI and MPM scans at 3T to learn more about the impact of structural connectivity on clinical status and efficacy of DBS. Additionally, either using indices of structural connectivity to guide VOI extraction on a subject by subject basis, or informing DCM's priors of the network's structural connectivity matrix (Stephan et al., 2009b) could enhance the modelling process. A sub-group of the second DBS cohort reported in Chapters 10 & 11 received these scans, and we are planning to explore these relationships in more detail.

Related to this point, it is also worth considering the subject-specific current field produced by DBS, as opposed to simply assuming DBS is stimulating the same regions at the same intensity regardless of stimulation parameters or the patient's anatomy. This was largely ignored in this thesis, despite growing interest in optimising stimulation settings based on current fields (Butson et al., 2007; Mikos et al., 2011). The relationship between stimulated volume, stimulation settings and resultant effect on effective connectivity in the BG should be explored in future studies.

13.4 Modelling synaptic mechanisms underlying neuromodulation

This subsection specifically addresses more biologically plausible modelling of the finer detail mechanisms underlying the modulatory effects of DBS using electrophysiology, not fMRI.

13.4.1 DCM for EEG/MEG & DBS

Unlike fMRI data, EEG/MEG and LFP datasets have a rich temporal structure allowing much more complicated models of cortical and subcortical function to be employed (David et al. 2005). Electrophysiological DCMs use physiologically plausible neural mass and neural field models, embedding each region with several neuronal subpopulations representing key constituents of grey matter (David et al. 2006; Jansen & Rit 1995). Most include excitatory pyramidal output neurons, inhibitory interneurons, and excitatory spiny input neurons. Intrinsic connections are estimated for each region (in the case of Figure 13.1; reciprocal connections between the pyramidal and inhibitory interneurons, reciprocal connections between the pyramidal and spiny input neurons, and a self-inhibitory connection in the inhibitory population). Extrinsic connections are also subdivided into forward, backward or lateral connections, each arriving as afferents to different

subpopulations in accordance with primate connectivity patterns (Felleman and Van Essen, 1991). The firing rate of each subpopulation is treated as a hidden state, dependent on the average pre-synaptic inputs, post-synaptic membrane potential, and constants summarising the biophysical membrane properties. The forward models used to map the neural activity to the observed data are discussed in depth elsewhere (see review - Moran et al. 2013). Putting aside the elegant mathematics, these DCMs can be used in exactly the same way as we have discussed. Importantly, given the additional complexity of the generative models employed, these DCMs can furnish estimates of much more subtle parameters than those estimated in DCM for fMRI. For example, these DCMs have been applied as a "mathematical microscope" to probe neurotransmitter receptor function (Moran et al. 2011), but can also be used in a similar way to DCM for fMRI to explore extrinsic coupling parameters (Marreiros et al. 2012; Moran et al. 2011). In order to gain insights into the synaptic mechanisms underlying DBS, future studies should make use of developments in DBS electrophysiology that now permit LFP recording during stimulation (Eusebio et al., 2011b; Little et al., 2013), and the more complete modelling offered by electrophysiological DCMs.

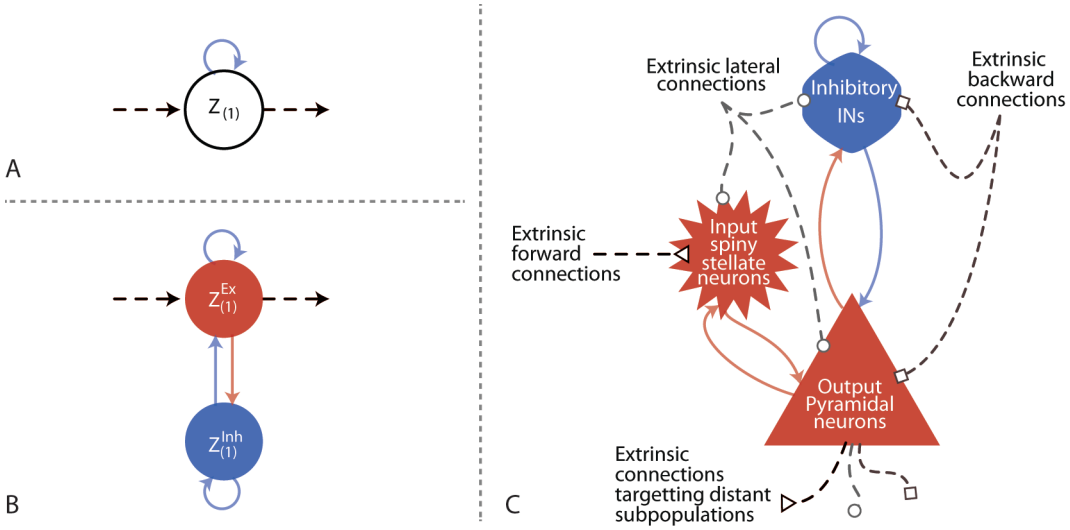

Figure 13.1 The relative complexities of modelling fMRI and EEG/MEG/LFP data. (A) The basic fMRI model, with a single intrinsic connection, and non-specific extrinsic afferents and efferents. (B) The two-state fMRI model containing four intrinsic connections linking the excitatory and inhibitory subpopulation. (C) The convolution based ERP and LFP model – an example of a biophysical model employed in EEG/MEG/LFP data (adapted from Moran et al. 2009) - is relatively more complex. Firstly, three subpopulations are modelled with five intrinsic connections. Additionally, extrinsic afferents are categorised as either forward connections arriving at the input population, backward connections arriving at both the output and interneuron populations, or lateral connections arriving at all three populations. All extrinsic efferents project from the output pyramidal population. Red populations signify glutamatergic cell types, blue populations signify GABAergic cell types. Dashed lines represent extrinsic connections, solid lines represent intrinsic connections. INs = interneurons.

13.4.2 Combining STN LFP and global BOLD

Additionally, although this may be a long term idea, there are newer generation devices coming to market that have the capability of recording LFP data from the DBS target during active stimulation, as well as from additionally implanted cortical sources or even ECoG sheets. Supposing those devices were similarly compatible with fMRI, and the scanner did not significantly impair the recording LFP data, simultaneous neurophysiology and fMRI could enable more detailed modelling of the BG motor loop.

13.5 A common effect?

13.5.1 STN DBS and other BG circuits

One avenue of research that is in fact possible to explore with the current resting state datasets would be the effect of STN DBS on other circuits of the cortico-BG (see section 5.2.2 for introduction on BG loops). For example, STN DBS has been shown to impact on both saccade and smooth pursuit eye movements (Antoniades et al., 2012; Nilsson et al., 2013; Yugeta et al., 2010). Given these findings, it would be interesting to model the dynamics of the BG oculomotor circuit, modulation of which may explain the improvements noted. The oculomotor circuit's cortical target is believed to be the FEF, projecting to the body of the caudate nucleus (as opposed to the posterior putamen modelled in these studies – see Figure 5.1) (Alexander et al., 1986). It would be interesting to see if similar effects are produced by DBS on this circuit, despite specific targeting of the supero-postero-lateral STN believed to house sensorimotor function (Yelnik et al., 2007). Similarly, this could be reproduced with higher-level circuits (DLPFC, OFC and ACC) to see if STN DBS produces generalised effects on these circuits. If this were the case, this would provide further evidence for a generic effect of DBS on a given target region.

13.5.2 STN DBS in other diseases

As voiced in section 12.3.5, it would be similarly interesting to establish whether or not DBS has a common mechanism regardless of which disease is being treated. If the effects on the BG motor loop are independent of the behaviour executed, so long as the target circuit is implicated in the generation of some other symptoms, perhaps its effects are also independent of symptoms exhibited? This hypothesis could be tested by scanning patients who have received STN DBS for reasons other than PD. STN DBS has been trialled in a other conditions, including obsessive-compulsive disorder (OCD) (Chabardès et al., 2012;

L. Mallet et al., 2008), as well as a complicated case study of a patient with PD and Tourette's syndrome (Martinez-Torres et al., 2009).

13.5.3 Different targets, different diseases

Finally, this work should be extended to characterise the effect of DBS of other targets in both patients with PD, as well as other conditions. One obvious cohort to scan would be PD patients with implanted GPi, or even Vim DBS electrodes, and explore the effects on the BG motor loop (and cortico-cerebellar dynamics) as performed in this thesis. Unfortunately, from a pragmatic perspective, both groups would be difficult to scan given GPi DBS is typically reserved for PD patients with dyskinesias, and patients with tremulous PD are given Vim DBS; both cohorts are likely to move more in the OFF condition, thus attention must be paid to the effects of motion on the datasets.

Extending this beyond PD would be similarly fascinating. At this centre, data has already been collected from patients with dystonias receiving GPi DBS[36]; such data would appeal to modelling of the BG motor loop in the manner described in this thesis, or elaboration of the circuit to include the GPi, perhaps as a hidden node. Similarly, this centre is currently running trials of low frequency DBS of the nucleus basalis of Meynert as a treatment for PD dementia and dementia with Lewy bodies (Gratwicke et al., 2013). As part of these clinical trials, patients will be receiving both task[37] and resting state fMRI during each of the blinded stimulation periods, and the current plan is to model the effect of DBS on the cortical visual attention network, as well as the effects on the BG motor loop. In addition, scanning patients partaking in trials examining hypothalamic DBS for the treatment of cluster headache could yield greater insights into its pathogenesis, and DBS's clinical

[36] *Not my data - currently being analysed.*
[37] *Posner's task of visual attention will be the task undertaken in these patients.*

efficacy. A summary of diseases that are currently being treated with DBS, and potential studies are presented in Table 13.1.

Disease	Targets	Circuit dynamics of interest
PD, dystonia & essential tremor (ET)	STN GPi Vim PPN	These diseases are all thought to involve pathology of the BG motor loop, as well as cortico-cerebellar circuitry. Similar modelling to that employed in this study would be of great value in characterising the modulatory effects of DBS on this circuit, and identify any common features.
Obsessive-compulsive disorder (OCD)	STN NAcc IPT AIC	OCD is more complicated than the above, due to the variety of the possible targets. If STN, surgeons have previously targeted the antero-medial STN straddling the limbic and associative portions of the nucleus (L. Mallet et al., 2008). Volumetric imaging and fMRI studies have implicated the OFC and ACC BG loops with the disease, including the ventral striatum/NAcc (Ahmari et al., 2013; Bourne et al., 2012; Lozano and Lipsman, 2013). All four targets are thought to alleviate pathological cortico-striatal coupling. Thus it would be interesting to model the effects of DBS of either target on this circuit.
Tourette's syndrome (TS)	GPi CM-Pf	DBS for TS is another potential avenue of research, similarly thought to involve pathology of the BG. In contrast to OCD however, the GPi or CM thalamus is targeted in these patients. Results from clinical trials suggest some benefit in tic reduction (Ackermans et al., 2011). The circuit dynamics of interest include the prefrontal and ACC BG loops, as well as the motor loop.
PD dementia (PDD) & DLB	NBM	Clinical trials in this centre and others are in the midst of exploring the effect of NBM DBS in patients with dementias. The patients at this centre either have PDD or DLB. Both task and resting fMRI is being collected during both stimulation conditions. Dynamics of interest are diffuse; the theory is that DBS will increase cortical ACh, which has widespread neuromodulatory effects (Gratwicke et al., 2013). Patients suffer lapses in visual attention, thus the task fMRI is a simplified Posner task. In addition, given the proximity of the NBM to the GPi, it will be of interest to model the motor BG loop as well.

Tables continues on next page

Alzheimer's disease (AD)	NBM Fornix	Similar to PDD and DLB, AD patients have also enrolled in trials of NBM DBS; early results demonstrating safety, increased cortical glucose metabolism, and potentially some disease stabilization after 1 year follow up (Kuhn et al., 2014). Additionally, trials are exploring the efficacy of DBS of the fornix. Open label data at 1 year (n=6) suggest "possible improvements and/or slowing in the rate of cognitive decline… in some patients" (Laxton et al., 2010), as well as increased functional connectivity in "two orthogonal networks" (frontal-temporal-parietal-striatal-thalamic network and a frontal-temporal-parietal-occipital- hippocampal network) (Smith et al., 2012).
Major Depressive Disorder (MDD)	SCC NAcc ITP MFB	The SCC has been repeatedly implicated in the pathophysiology of depression, and is an area of convergence of white matter tracts projecting to the brainstem, hypothalamus, and insula, as well as OFC, PFC and ACC. SCC DBS reduced hyperactivity in the target in responsive patients (Mayberg et al., 2005), with patients doing better when their electrodes intersected forceps minor and uncinate fasciculus, as well as the cingulum bundle, and projections to subcortical nuclei (Riva-Posse et al., 2014). One hypothesised circuit of interest would model the dynamics between the PFC, SCC, ACC and ventral striatum, and the effect of SCC DBS.

Table 13.1 Diseases for which DBS has been used (to varying degrees of success), and the circuit dynamics that would be interesting to model ON and OFF stimulation. Abbreviations: STN = Subthalamic nucleus, GPi = globus pallidus interna, Vim = thalamic ventralis intermedius, PPN = pedunculopontine nucleus, NAcc = nucleus accumbens, ITP = inferior thalamic peduncle, AIC = anterior limb of internal capsule, CM-Pf = centromedian-parafascicular thalamus, NBM = nucleus basalis of Meynert, SCC = subcallosal cingulate area, MFB = medial forebrain bundle. For review of DBS in psychiatry see (Lozano and Lipsman, 2013)

14 Conclusions

> *Remember that all models are wrong; the practical question is how wrong do they have to be to not be useful*
> George Box & Norman Draper, Empirical Model Building and Response Surfaces, 1987.

14.1 Advances in the field

Experiments presented in this thesis demonstrate:

1. **Functional MRI is both safe and feasible in patients with implanted DBS hardware under certain MRI protocols.** I demonstrate that so long as the sequence energy deposition is kept low (<0.4 W/Kg), scanning at 1.5T using either the head-transmit/receive coil, or the body-transmit coil with a multi-channel head receive coil produces <1°C heating in the DBS system, complying with international safety recommendations for intra-cranial heating. Furthermore, we did not observe significant differences in heating under different DBS conditions during routine fMRI sequences, suggesting that studies contrasting DBS conditions should not be confounded by electrode temperature. Additionally, measurements of DBS IPG output did not suggest that scanning produced any disruption to the programmed stimulation settings, or induced additional components that posed any danger to the patient, or significant confounds in fMRI studies. *Importantly* however, while these results enabled the safe collection of data in subsequent experiments, the generalizability to other centres of these *in vitro* experiments remains limited, and I stress again that centres seeking to collect fMRI data in implanted patients must ensure to collect onsite *in vitro* data with their scanning

protocol. Finally, DBS fMRI presents a number of technical limitations that must be considered in the experimental design; not all regions of the brain can be recorded from, and future experiments should be tailored to this important limitation. This material is presented in Chapter 9.

2. **During voluntary movements, STN DBS increases regional BOLD response most potently in M1 and the cerebellum.** Increased responses in the insula cortex and thalamus were additionally reported, however later experiments using an optimised protocol suggest that interactions are most marked in the aforementioned regions. These findings are supported by results previously reported in the PET literature, and highlight that modulation of BG produce changes in both cortical and cerebellar motor processing. We did not observe any statistically significant decreases in regional responses under therapeutic STN DBS. This material is presented in Chapters 7 & 10.
3. **Modelling STN DBS as a modulator of extrinsic effective connectivity suggests that DBS has consistent effects on the BG during both movement and resting sessions.** These effects include increasing the effective connection strength of the (1) direct pathway, supporting rate-based models of BG pathway function and PD, (2) cortico-striatal pathway, specifically the M1-putamen connection in these studies, (3) thalamic output to the cortex (M1 in these experiments). In contrast, DBS decreases the response of the STN to afferent signals from the hyperdirect pathway, and the indirect pathway (acknowledging that this latter pathway was considerably simplified in this work). In addition, the thalamic response to STN activity was similarly reduced by therapeutic stimulation. In relating these changes to observed changes in motor symptoms, when considering models only including

the BG motor loop at rest, I demonstrate that the strength of the direct and hyperdirect pathways, as well as the indirect pathway afferents to the STN have significant predictive capacity on contralateral motor impairment. Unfortunately, subsequent modelling including cerebellar dynamics (and fewer observations) failed to reproduce these predictive relationships; larger studies are required to confirm my initial observations. This material is presented in Chapters 8, 10 & 11.

4. **During movement, STN DBS additionally modulates cortico-cerebellar dynamics.** Finally, during performance of voluntary movements, I demonstrate that STN DBS additionally modulates integration within the cortico-cerebellar loop; specifically in this case, increasing the cerebellar response to afferents from M1. This highlights the role of cerebellum in the production of voluntary movements in PD, and potentially reflects a normalisation of task-dependent functional integration, although further studies with control cohorts would be required to test this hypothesis. During resting sessions, we did not observe significant modulatory effects on cortical-cerebellar dynamics, suggesting that these modulatory effects are state-dependent, whereas modulatory effects on the BG are independent of task or cognitive state. This material is presented in Chapters 10 & 11.

14.2 Concluding remarks

This thesis poses questions of functional integration; in other words, does connectivity change under STN DBS, can it be characterised in a group of patients, and is it related to the clinical improvements observed? The scientific rationale for the study of connectivity in clinical cohorts has recently been reviewed by (Rowe, 2010). To summarise, phenotypes

observed in neurological diseases are not solely caused by focal lesions to a specific node. Function is dependent on the integration of specialised nodes, thus neurology (and psychiatry) is the result of both *nodal lesions* and what we will term *lesions of coupling*. Biologically, lesions of coupling might result from impaired neurotransmitter function (or receptor function), or subtle structural changes in cortical architecture that alters the function of the canonical microcircuit. Interestingly, neurodegenerative conditions and dementias often involve loss of neuromodulatory neurotransmitters such as DA, acetylcholine and noradrenaline, all of which have been hypothesised to alter neural gain in some form, i.e. responsiveness to afferent drive (Chance et al., 2002; Eldar et al., 2013; Friston et al., 2012; Servan-Schreiber et al., 1990). Studying connectivity (both functional and effective) may even be more sensitive to pathology than regional activity alone (Rowe, 2010; Rowe et al., 2007). The advantage of the effective connectivity methods employed herein, as opposed to examining correlations in functional data is that the direction of influence can be characterised, and the superadded effect of DBS on this influence can be estimated. Furthermore, working within this framework tends to remove speculation often voiced in the conclusions of neuroimaging studies. For example, a number of studies have documented changes in cortical response following either STN DBS or dopaminergic medications (Grafton et al., 2006; Hughes et al., 2010), and subsequently infer that these changes are likely caused by downstream changes in BG output, given the anatomy. Under the DCM framework, prior beliefs such as the well-characterised structural and functional anatomy are embedded in the scientific question, allowing the experimenter to specifically pose simple model selection questions such as *is the thalamo-cortical output modulated by the intervention?* These methodological concepts are not new; in fact, some of the earliest applications of similar modelling techniques were in PD patients receiving pallidotomies.

In that case, surgery was shown to attenuate pallido-thalamic and thalamo-cortical connectivity (specifically to the mesial frontal motor areas), as well as changes upstream from the lesion (Grafton et al., 1994).

In this thesis, I present an additional perspective on the mechanism of action of STN DBS in PD at the systems level, casting DBS as a modulator of extrinsic effective connectivity. I believe further study into the effects of DBS on functional integration in both PD patients, and those with other neurological or psychiatric conditions, will enable characterisation of its distributed effects, and perhaps one day, rational development of this therapy, based on the dynamics of a diseased brain network, and the effects DBS has on said dynamics.

However, it is always worth remembering that all models are wrong. What I have presented in this thesis is an attempt to distil an extremely complex system that produces complicated behaviours into a graph of a handful of nodes and edges that the literature has shown to be important in PD pathogenesis and DBS efficacy. Obviously, these experiments make a number of simplifying assumptions, however, returning to the quote I placed at the beginning of this Chapter, *is the presented modelling wrong enough to not be considered useful?* My opinion, unsurprisingly, is no. However, I look forward to further work, from both myself, and from others, which challenges and refines the ideas presented herein.

15Bibliography

Abosch, A., Kapur, S., Lang, A.E., Hussey, D., Sime, E., Miyasaki, J., Houle, S., Lozano, A.M., 2003. Stimulation of the Subthalamic Nucleus in Parkinson's Disease Does Not Produce Striatal Dopamine Release. Neurosurgery 53, 1095–1105.

Ackermans, L., Duits, A., van der Linden, C., Tijssen, M., Schruers, K., Temel, Y., Kleijer, M., Nederveen, P., Bruggeman, R., Tromp, S., van Kranen-Mastenbroek, V., Kingma, H., Cath, D., Visser-Vandewalle, V., 2011. Double-blind clinical trial of thalamic stimulation in patients with Tourette syndrome. Brain 134, 832–44.

Ahlskog, J.E., Muenter, M.D., 2001. Frequency of levodopa-related dyskinesias and motor fluctuations as estimated from the cumulative literature. Mov. Disord. 16, 448–58.

Ahmari, S.E., Spellman, T., Douglass, N.L., Kheirbek, M.A., Simpson, H.B., Deisseroth, K., Gordon, J.A., Hen, R., 2013. Repeated cortico-striatal stimulation generates persistent OCD-like behavior. Science 340, 1234–9.

Albin, R.L., Young, A.B., Penney, J.B., 1989. The functional anatomy of basal ganglia disorders. Trends Neurosci. 12, 366–75.

Alexander, G.E.G.E., DeLong, M.R.R., Strick, P.L.L., 1986. Parallel organization of functionally segregated circuits linking basal ganglia and cortex. Annu. Rev. Neurosci. 9, 357–81.

Andersson, J.L., Hutton, C., Ashburner, J., Turner, R., Friston, K., 2001. Modeling geometric deformations in EPI time series. Neuroimage 13, 903–19.

Antoniades, C.A., Buttery, P., FitzGerald, J.J., Barker, R.A., Carpenter, R.H.S., Watts, C., 2012. Deep brain stimulation: eye movements reveal anomalous effects of electrode placement and stimulation. PLoS One 7, e32830.

Arai, N., Yokochi, F., Ohnishi, T., Momose, T., Okiyama, R., Taniguchi, M., Takahashi, H., Matsuda, H., Ugawa, Y., 2008. Mechanisms of unilateral STN-DBS in patients with Parkinson's disease : a PET study. J. Neurol. 255, 1236–43.

Arantes, P.R., Cardoso, E.F., Barreiros, M. a, Teixeira, M.J., Gonçalves, M.R., Barbosa, E.R., Sukwinder, S.S., Leite, C.C., Amaro, E., 2006. Performing functional magnetic resonance imaging in patients with Parkinson's disease treated with deep brain stimulation. Mov. Disord. 21, 1154–62.

Asanuma, K., Tang, C., Ma, Y., Dhawan, V., Mattis, P., Edwards, C., Kaplitt, M.G., Feigin, A., Eidelberg, D., 2006. Network modulation in the treatment of Parkinson's disease. Brain 129, 2667–78.

Aström, M., Tripoliti, E., Hariz, M.I., Zrinzo, L.U., Martinez-Torres, I., Limousin, P., Wårdell, K., 2010. Patient-specific model-based investigation of speech intelligibility and movement during deep brain stimulation. Stereotact. Funct. Neurosurg. 88, 224–33.

Attwell, D., Buchan, A.M., Charpak, S., Lauritzen, M., Macvicar, B. a, Newman, E. a, 2010a. Glial and neuronal control of brain blood flow. Nature 468, 232–43.

Attwell, D., Buchan, A.M., Charpak, S., Lauritzen, M., Macvicar, B. a, Newman, E. a, 2010b. Glial and neuronal control of brain blood flow. Nature 468, 232–43.

Attwell, D., Iadecola, C., 2002. The neural basis of functional brain imaging signals. Trends Neurosci. 25, 621–5.

Attwell, D., Laughlin, S.B., 2001. An energy budget for signaling in the grey matter of the brain. J. Cereb. Blood Flow Metab. 21, 1133–45.

Azevedo, E., Santos, R., Freitas, J., Rosas, M.-J., Gago, M., Garrett, C., Rosengarten, B., 2010. Deep brain stimulation does not change neurovascular coupling in non-motor visual cortex: an autonomic and visual evoked blood flow velocity response study. Parkinsonism Relat. Disord. 16, 600–3.

Baker, K.B., Tkach, J. a, Nyenhuis, J. a, Phillips, M., Shellock, F.G., Gonzalez-Martinez, J., Rezai, A.R., 2004. Evaluation of specific absorption rate as a dosimeter of MRI-related implant heating. J. Magn. Reson. Imaging 20, 315–20.

Baker, K.B., Tkach, J., Hall, J.D., Nyenhuis, J. a., Shellock, F.G., Rezai, A.R., 2005. Reduction of Magnetic Resonance Imaging-related Heating in Deep Brain Stimulation Leads Using a Lead Management Device. Neurosurgery 57, 392–397.

Baker, K.B., Tkach, J.A., Phillips, M.D., Rezai, A.R., 2006. Variability in RF-induced heating of a deep brain stimulation implant across MR systems. J. Magn. Reson. Imaging 24, 1236–42.

Bastos, A.M.M., Usrey, W.M.M., Adams, R.A. a, Mangun, G.R.R., Fries, P., Friston, K.J.J., 2012. Canonical Microcircuits for Predictive Coding. Neuron 76, 695–711.

Baudrexel, S., Witte, T., Seifried, C., von Wegner, F., Beissner, F., Klein, J.C., Steinmetz, H., Deichmann, R., Roeper, J., Hilker, R., 2011. Resting state fMRI reveals increased subthalamic nucleus-motor cortex connectivity in Parkinson's disease. Neuroimage 55, 1728–38.

Behrens, T.E.J., Johansen-Berg, H., Woolrich, M.W., Smith, S.M., Wheeler-Kingshott, C. a M., Boulby, P.A., Barker, G.J., Sillery, E.L., Sheehan, K., Ciccarelli, O., Thompson, A.J., Brady, J.M., Matthews, P.M., 2003. Non-invasive mapping of connections between human thalamus and cortex using diffusion imaging. Nat. Neurosci. 6, 750–757.

Benabid, A.L., Pollak, P., Louveau, A., Henry, S., de Rougemont, J., 1987. Combined (thalamotomy and stimulation) stereotactic surgery of the VIM thalamic nucleus for bilateral Parkinson disease. Appl. Neurophysiol. 50, 344–6.

Benazzouz, a, Gross, C., Féger, J., Boraud, T., Bioulac, B., 1993. Reversal of rigidity and improvement in motor performance by subthalamic high-frequency stimulation in MPTP-treated monkeys. Eur. J. Neurosci. 5, 382–9.

Benazzouz, A., Gao, D., Ni, Z., Benabid, A.L., 2000a. High frequency stimulation of the STN influences the activity of dopamine neurons in the rat. Neuroreport 11, 1593–1596.

Benazzouz, A., Gao, D.M., Ni, Z.G., Piallat, B., Bouali-Benazzouz, R., Benabid, A.L., 2000b. Effect of high-frequency stimulation of the subthalamic nucleus on the neuronal activities of the substantia nigra pars reticulata and ventrolateral nucleus of the thalamus in the rat. Neuroscience 99, 289–95.

Bergman, H., Wichmann, T., DeLong, M.R., 1990. Reversal of experimental parkinsonism by lesions of the subthalamic nucleus. Science 249, 1436–8.

Bernasconi, C., König, P., 1999. On the directionality of cortical interactions studied by structural analysis of electrophysiological recordings. Biol. Cybern. 81, 199–210.

Beurrier, C., Bioulac, B., Audin, J., Hammond, C., 2001. High-frequency stimulation produces a transient blockade of voltage-gated currents in subthalamic neurons. J. Neurophysiol. 85, 1351–6.

Bhidayasiri, R., Bronstein, J.M., Sinha, S., Krahl, S.E., Ahn, S., Behnke, E.J., Cohen, M.S., Frysinger, R., Shellock, F.G., 2005. Bilateral neurostimulation systems used for deep brain stimulation: in vitro study of MRI-related heating at 1.5 T and implications for clinical imaging of the brain. Magn. Reson. Imaging 23, 549–55.

Birn, R.M., 2012. The role of physiological noise in resting-state functional connectivity. Neuroimage 62, 864–70.

Biswal, B., DeYoe, E.A., Hyde, J.S., 1996. Reduction of physiological fluctuations in fMRI using digital filters. Magn. Reson. Med. 35, 107–113.

Biswal, B., Yetkin, F.Z., Haughton, V.M., Hyde, J.S., 1995. Functional connectivity in the motor cortex of resting human brain using echo-planar MRI. Magn. Reson. Med. 34, 537–41.

Boertien, T., Zrinzo, L., Kahan, J., Jahanshahi, M., Hariz, M., Mancini, L., Limousin, P., Foltynie, T., 2011. Functional imaging of subthalamic nucleus deep brain stimulation in Parkinson's disease. Mov. Disord. 26, 1835–43.

Bostan, A.C., Dum, R.P., Strick, P.L., 2010. The basal ganglia communicate with the cerebellum. Proc. Natl. Acad. Sci. U. S. A. 107, 8452–8456.

Boulant, J.A., 1998. Hypothalamic Neurons: Mechanisms of Sensitivity to Temperature a. Ann. N. Y. Acad. Sci. 856, 108–115.

Bourne, S.K., Eckhardt, C. a, Sheth, S. a, Eskandar, E.N., 2012. Mechanisms of deep brain stimulation for obsessive compulsive disorder: effects upon cells and circuits. Front. Integr. Neurosci. 6, 29.

Braak, H., Tredici, K. Del, Rüb, U., de Vos, R. a. ., Jansen Steur, E.N.., Braak, E., 2003. Staging of brain pathology related to sporadic Parkinson's disease. Neurobiol. Aging 24, 197–211.

Bradberry, T.J., Metman, L.V., Contreras-Vidal, J.L., van den Munckhof, P., Hosey, L.A., Thompson, J.L.W., Schulz, G.M., Lenz, F., Pahwa, R., Lyons, K.E., Braun, A.R., 2012. Common and unique responses to dopamine agonist therapy and deep brain stimulation in Parkinson's disease: an H(2)(15)O PET study. Brain Stimul. 5, 605–15.

Brittain, J.-S., Brown, P., 2014. Oscillations and the basal ganglia: motor control and beyond. Neuroimage 85 Pt 2, 637–47.

Brittain, J.-S., Sharott, A., Brown, P., 2014. The highs and lows of beta activity in cortico-basal ganglia loops. Eur. J. Neurosci. 39, 1951–9.

Brooks, J.C.W., Faull, O.K., Pattinson, K.T.S., Jenkinson, M., 2013. Physiological noise in brainstem FMRI. Front. Hum. Neurosci. 7, 623.

Brown, P., Mazzone, P., Oliviero, A., Altibrandi, M.G., Pilato, F., Tonali, P.A., Di Lazzaro, V., 2004. Effects of stimulation of the subthalamic area on oscillatory pallidal activity in Parkinson's disease. Exp. Neurol. 188, 480–490.

Brown, P., Oliviero, A., Mazzone, P., Insola, A., Tonali, P., Di Lazzaro, V., 2001. Dopamine dependency of oscillations between subthalamic nucleus and pallidum in Parkinson's disease. J. Neurosci. 21, 1033–8.

Brunenberg, E.J.L., Moeskops, P., Backes, W.H., Pollo, C., Cammoun, L., Vilanova, A., Janssen, M.L.F., Visser-Vandewalle, V.E.R.M., ter Haar Romeny, B.M., Thiran, J.-P., Platel, B., 2012. Structural and resting state functional connectivity of the subthalamic nucleus: identification of motor STN parts and the hyperdirect pathway. PLoS One 7, e39061.

Büchel, C., Friston, K.J., 1997. Modulation of connectivity in visual pathways by attention: cortical interactions evaluated with structural equation modelling and fMRI. Cereb. Cortex 7, 768–778.

Buckholtz, J.W.W., Meyer-Lindenberg, A., 2012. Psychopathology and the human connectome: toward a transdiagnostic model of risk for mental illness. Neuron 74, 990–1004.

Bullmore, E., Sporns, O., 2009. Complex brain networks: graph theoretical analysis of structural and functional systems. Nat. Rev. Neurosci. 10, 186–98.

Burns, R.S., Chiueh, C.C., Markey, S.P., Ebert, M.H., Jacobowitz, D.M., Kopin, I.J., 1983. A primate model of parkinsonism: selective destruction of dopaminergic neurons in the pars compacta of the substantia nigra by N-methyl-4-phenyl-1,2,3,6-tetrahydropyridine. Proc. Natl. Acad. Sci. U. S. A. 80, 4546–50.

Butson, C.R., Cooper, S.E., Henderson, J.M., McIntyre, C.C., 2007. Patient-specific analysis of the volume of tissue activated during deep brain stimulation. Neuroimage 34, 661–70.

Buxhoeveden, D.P., Casanova, M.F., 2002. The minicolumn hypothesis in neuroscience. Brain 125, 935–51.

Buxton, R.B., Wong, E.C., Frank, L.R., 1998. Dynamics of blood flow and oxygenation changes during brain activation: the balloon model. Magn. Reson. Med. 39, 855–64.

Carmichael, D.W., Pinto, S., Limousin-Dowsey, P., Thobois, S., Allen, P.J., Lemieux, L., Yousry, T., Thornton, J.S., 2007. Functional MRI with active, fully implanted, deep brain stimulation systems: safety and experimental confounds. Neuroimage 37, 508–17.

Carpenter, M.B., Strominger, N.L., 1967. Efferent fibers of the subthalamic nucleus in the monkey. A comparison of the efferent projections of the subthalamic nucleus, substantia nigra and globus pallidus. Am. J. Anat. 121, 41–72.

Catalan, M.J., Ishii, K., Honda, M., Samii, A., Hallett, M., 1999. A PET study of sequential finger movements of varying length in patients with Parkinson's disease. Brain 122, 483–495.

Cavanagh, J.F., Wiecki, T. V, Cohen, M.X., Figueroa, C.M., Samanta, J., Sherman, S.J., Frank, M.J., 2011. Subthalamic nucleus stimulation reverses mediofrontal influence over decision threshold. Nat. Neurosci. 14, 1462–7.

Ceballos-Baumann, A.O., Boecker, H., Bartenstein, P., von Falkenhayn, I., Riescher, H., Conrad, B., Moringlane, J.R., Alesch, F., 1999. A positron emission tomographic study of subthalamic nucleus stimulation in Parkinson disease: enhanced movement-related activity of motor-association cortex and decreased motor cortex resting activity. Arch. Neurol. 56, 997–1003.

Chabardès, S., Polosan, M., Krack, P., Bastin, J., Krainik, A., David, O., Bougerol, T., Benabid, A.L., 2012. Deep brain stimulation for obsessive-compulsive disorder: subthalamic nucleus target. World Neurosurg. 80, S31.e1–8.

Chance, F.S., Abbott, L.F., Reyes, A.D., 2002. Gain modulation from background synaptic input. Neuron 35, 773–82.

Cilia, R., Marotta, G., Landi, A., Isaias, I.U., Mariani, C.B., Vergani, F., Benti, R., Sganzerla, E., Pezzoli, G., Antonini, A., 2009. Clinical and cerebral activity changes induced by subthalamic nucleus stimulation in advanced Parkinson's disease: a prospective case-control study. Clin. Neurol. Neurosurg. 111, 140–6.

Cilia, R., Siri, C., Marotta, G., Gaspari, D., 2007. Brain networks underlining verbal fluency decline during STN-DBS in Parkinson's disease: an ECD-SPECT study. Park. & Relat. 13, 290–4.

Collins, C.M., Smith, M.B., Turner, R., 2004. Model of local temperature changes in brain upon functional activation. J. Appl. Physiol. 97, 2051–2055.

Cotzias, G.C., Van Woert, M.H., Schiffer, L.M., 1967. Aromatic amino acids and modification of parkinsonism. N. Engl. J. Med. 276, 374–9.

Crick, F., Koch, C., 1998. Constraints on cortical and thalamic projections: the no-strong-loops hypothesis. Nature 391, 245–50.

Daunizeau, J., David, O., Stephan, K.E., 2011. Dynamic causal modelling: a critical review of the biophysical and statistical foundations. Neuroimage 58, 312–22.

Daunizeau, J., Lemieux, L., Vaudano, a E., Friston, K.J., Stephan, K.E., 2012a. An electrophysiological validation of stochastic DCM for fMRI. Front. Comput. Neurosci. 6, 103.

Daunizeau, J., Stephan, K.E., Friston, K.J., 2012b. Stochastic dynamic causal modelling of fMRI data: should we care about neural noise? Neuroimage 62, 464–81.

David, O., Guillemain, I., Saillet, S., Reyt, S., Deransart, C., Segebarth, C., Depaulis, A., 2008. Identifying neural drivers with functional MRI: an electrophysiological validation. PLoS Biol. 6, 2683–97.

David, O., Harrison, L., Friston, K.J., 2005. Modelling event-related responses in the brain. Neuroimage 25, 756–70.

David, O., Kiebel, S.J., Harrison, L.M., Mattout, J., Kilner, J.M., Friston, K.J., 2006. Dynamic causal modeling of evoked responses in EEG and MEG. Neuroimage 30, 1255–72.

David, O., Maess, B., Eckstein, K., Friederici, A.D., 2011. Dynamic causal modeling of subcortical connectivity of language. J. Neurosci. 31, 2712–7.

De Hemptinne, C., Ryapolova-Webb, E.S., Air, E.L., Garcia, P.A., Miller, K.J., Ojemann, J.G., Ostrem, J.L., Galifianakis, N.B., Starr, P.A., 2013. Exaggerated phase-amplitude coupling in the primary motor cortex in Parkinson disease. Proc. Natl. Acad. Sci. U. S. A. 110, 4780–5.

De Solages, C., Hill, B.C., Koop, M.M., Henderson, J.M., Bronte-Stewart, H., 2010. Bilateral symmetry and coherence of subthalamic nuclei beta band activity in Parkinson's disease. Exp. Neurol. 221, 260–6.

Deco, G., Jirsa, V.K., McIntosh, A.R., 2011. Emerging concepts for the dynamical organization of resting-state activity in the brain. Nat. Rev. Neurosci. 12, 43–56.

Deichmann, R., Gottfried, J.., Hutton, C., Turner, R., 2003. Optimized EPI for fMRI studies of the orbitofrontal cortex. Neuroimage 19, 430–441.

DeLong, M.R., 1990. Primate models of movement disorders of basal ganglia origin. Trends Neurosci. 13, 281–5.

Deniau, J.-M., Degos, B., Bosch, C., Maurice, N., 2010. Deep brain stimulation mechanisms: beyond the concept of local functional inhibition. Eur. J. Neurosci. 32, 1080–91.

Deuschl, G., Schade-Brittinger, C., Krack, P., Volkmann, J., Schäfer, H., Bötzel, K., Daniels, C., Deutschländer, A., Dillmann, U., Eisner, W., Gruber, D., Hamel, W., Herzog, J., Hilker, R., Klebe, S., Kloss, M., Koy, J., Krause, M., Kupsch, A., Lorenz, D., Lorenzl, S., Mehdorn, H.M., Moringlane, J.R., Oertel, W., Pinsker, M.O., Reichmann, H., Reuss, A., Schneider, G.-H., Schnitzler, A., Steude, U., Sturm, V., Timmermann, L., Tronnier, V., Trottenberg, T., Wojtecki, L., Wolf, E., Poewe, W., Voges, J., 2006. A randomized trial of deep-brain stimulation for Parkinson's disease. N. Engl. J. Med. 355, 896–908.

Devlin, J.T., Russell, R.P., Davis, M.H., Price, C.J., Wilson, J., Moss, H.E., Matthews, P.M., Tyler, L.K., 2000. Susceptibility-induced loss of signal: comparing PET and fMRI on a semantic task. Neuroimage 11, 589–600.

Diedrichsen, J., Balsters, J.H., Flavell, J., Cussans, E., Ramnani, N., 2009. A probabilistic MR atlas ot the human Cerebellum. Neuroimage 46, 39–46.

Dorval, A.D., Russo, G.S., Hashimoto, T., Xu, W., Grill, W.M., Vitek, J.L., 2008. Deep brain stimulation reduces neuronal entropy in the MPTP-primate model of Parkinson's disease. J. Neurophysiol. 100, 2807–18.

Douglas, R.J., Martin, K.A., 1991. A functional microcircuit for cat visual cortex. J. Physiol. 440, 735–769.

Eickhoff, S.B., Stephan, K.E., Mohlberg, H., Grefkes, C., Fink, G.R., Amunts, K., Zilles, K., 2005. A new SPM toolbox for combining probabilistic cytoarchitectonic maps and functional imaging data. Neuroimage 25, 1325–35.

Eidelberg, D., Moeller, J.R., Dhawan, V., Spetsieris, P., Takikawa, S., Ishikawa, T., Chaly, T., Robeson, W., Margouleff, D., Przedborski, S., 1994. The metabolic topography of parkinsonism. J. Cereb. Blood Flow Metab. 14, 783–801.

Einevoll, G.T., Kayser, C., Logothetis, N.K., Panzeri, S., 2013. Modelling and analysis of local field potentials for studying the function of cortical circuits. Nat. Rev. Neurosci. 14, 770–85.

Eldar, E., Cohen, J.D., Niv, Y., 2013. The effects of neural gain on attention and learning. Nat. Neurosci. 16, 1146–53.

Esposito, F., Tessitore, A., Giordano, A., De Micco, R., Paccone, A., Conforti, R., Pignataro, G., Annunziato, L., Tedeschi, G., 2013. Rhythm-specific modulation of the sensorimotor network in drug-naive patients with Parkinson's disease by levodopa. Brain 136, 710–25.

Etgen, T., Winbeck, K., Conrad, B., Sander, D., 2003. Hemiballism with insular infarction as first manifestation of Takayasu's arteritis in association with chronic hepatitis B. J. Neurol. 250, 226–9.

Eusebio, A., Cagnan, H., Brown, P., 2012. Does suppression of oscillatory synchronisation mediate some of the therapeutic effects of DBS in patients with Parkinson's disease? Front. Integr. Neurosci. 6, 47.

Eusebio, Thevathasan, W., Doyle Gaynor, L., Pogosyan, A., Bye, E., Foltynie, T., Zrinzo, L., Ashkan, K., Aziz, T., Brown, P., 2011a. Deep brain stimulation can suppress pathological synchronisation in parkinsonian patients. J. Neurol. Neurosurg. Psychiatry 82, 569–73.

Eusebio, Thevathasan, W., Doyle Gaynor, L., Pogosyan, A., Bye, E., Foltynie, T., Zrinzo, L., Ashkan, K., Aziz, T., Brown, P., 2011b. Deep brain stimulation can suppress pathological synchronisation in parkinsonian patients. J. Neurol. Neurosurg. Psychiatry 82, 569–73.

Farrar, D.E., Glauber, R.R., 1967. Multicollinearity in Regression Analysis: The Problem Revisited. Rev. Econ. Stat. 49, 92–107.

Fasano, A., Romito, L.M., Daniele, A., Piano, C., Zinno, M., Bentivoglio, A.R., Albanese, A., 2010. Motor and cognitive outcome in patients with Parkinson's disease 8 years after subthalamic implants. Brain 133, 2664–76.

Fearnley, J.M., Lees, A.J., 1991. Ageing and Parkinson's disease: substantia nigra regional selectivity. Brain 114 (Pt 5), 2283–301.

Felleman, D.J., Van Essen, D.C., 1991. Distributed hierarchical processing in the primate cerebral cortex. Cereb. Cortex 1, 1–47.

Finelli, D.A., Rezai, A.R., Ruggieri, P.M., Tkach, J.A., Nyenhuis, J.A., Hrdlicka, G., Sharan, A., Gonzalez-Martinez, J., Stypulkowski, P.H., Shellock, F.G., 2002. MR imaging-related heating of deep brain stimulation electrodes: in vitro study. AJNR. Am. J. Neuroradiol. 23, 1795–802.

Follett, K. a, Weaver, F.M., Stern, M., Hur, K., Harris, C.L., Luo, P., Marks, W.J., Rothlind, J., Sagher, O., Moy, C., Pahwa, R., Burchiel, K., Hogarth, P., Lai, E.C., Duda, J.E., Holloway, K., Samii, A., Horn, S., Bronstein, J.M., Stoner, G., Starr, P.A., Simpson, R., Baltuch, G., De Salles, A., Huang, G.D., Reda, D.J., 2010. Pallidal versus subthalamic deep-brain stimulation for Parkinson's disease. N. Engl. J. Med. 362, 2077–91.

Foltynie, T., Hariz, M.I., 2010. Surgical management of Parkinson's disease. Expert Rev. Neurother. 10, 903–14.

Foltynie, T., Zrinzo, L., Martinez-Torres, I., Tripoliti, E., Petersen, E., Holl, E., Aviles-Olmos, I., Jahanshahi, M., Hariz, M., Limousin, P., 2011. MRI-guided STN DBS in Parkinson's disease without microelectrode recording: efficacy and safety. J. Neurol. Neurosurg. Psychiatry 82, 358–63.

Forstmann, B.U., Keuken, M.C., Jahfari, S., Bazin, P.-L., Neumann, J., Schäfer, A., Anwander, A., Turner, R., 2012. Cortico-subthalamic white matter tract strength predicts interindividual efficacy in stopping a motor response. Neuroimage 60, 370–5.

Fox, M.D., Greicius, M., 2010. Clinical applications of resting state functional connectivity. Front. Syst. Neurosci. 4, 19.

Fox, M.D., Raichle, M.E., 2007. Spontaneous fluctuations in brain activity observed with functional magnetic resonance imaging. Nat. Rev. Neurosci. 8, 700–11.

Fox, P.T., Raichle, M.E., 1986. Focal physiological uncoupling of cerebral blood flow and oxidative metabolism during somatosensory stimulation in human subjects. Proc. Natl. Acad. Sci. U. S. A. 83, 1140–4.

Fox, P.T., Raichle, M.E., Mintun, M.A., Dence, C., 1988. Nonoxidative glucose consumption during focal physiologic neural activity. Science 241, 462–4.

Frank, M.J., Samanta, J., Moustafa, A. a, Sherman, S.J., 2007. Hold your horses: impulsivity, deep brain stimulation, and medication in parkinsonism. Science 318, 1309–12.

Frankemolle, A.M.M., Wu, J., Noecker, A.M., Voelcker-Rehage, C., Ho, J.C., Vitek, J.L., McIntyre, C.C., Alberts, J.L., 2010. Reversing cognitive-motor impairments in Parkinson's disease patients using a computational modelling approach to deep brain stimulation programming. Brain 133, 746–61.

Fransson, P., 2005. Spontaneous low-frequency BOLD signal fluctuations: an fMRI investigation of the resting-state default mode of brain function hypothesis. Hum. Brain Mapp. 26, 15–29.

Friston, K., 2008. Neurophysiology: the brain at work. Curr. Biol. 18, R418–20.

Friston, K., 2009. Causal modelling and brain connectivity in functional magnetic resonance imaging. PLoS Biol. 7, e33.

Friston, K., Daunizeau, J., Stephan, K.E., 2013a. Model selection and gobbledygook: response to Lohmann et al. Neuroimage 75, 275–8; discussion 279–81.

Friston, K., Moran, R., Seth, A.K., 2013b. Analysing connectivity with Granger causality and dynamic causal modelling. Curr. Opin. Neurobiol. 23, 172–178.

Friston, K., Stephan, K., Li, B., Daunizeau, J., 2010. Generalised Filtering. Math. Probl. Eng. 2010, 1–34.

Friston, K.J., 1994. Functional and effective connectivity in neuroimaging: A synthesis. Hum. Brain Mapp. 2, 56–78.

Friston, K.J., 2002. Bayesian estimation of dynamical systems: an application to fMRI. Neuroimage 16, 513–30.

Friston, K.J., 2011. Functional and Effective Connectivity: A Review. Brain Connect. 1, 13–36.

Friston, K.J., Buechel, C., Fink, G.R., Morris, J., Rolls, E., Dolan, R.J., 1997. Psychophysiological and modulatory interactions in neuroimaging. Neuroimage 6, 218–29.

Friston, K.J., Frith, C.D., Liddle, P.F., Dolan, R.J., Lammertsma, A.A., Frackowiak, R.S., 1990. The relationship between global and local changes in PET scans. J. Cereb. Blood Flow Metab. 10, 458–66.

Friston, K.J., Harrison, L., Penny, W., 2003. Dynamic causal modelling. Neuroimage 19, 1273–1302.

Friston, K.J., Holmes, A.P., Poline, J.B., Grasby, P.J., Williams, S.C., Frackowiak, R.S., Turner, R., 1995. Analysis of fMRI time-series revisited. Neuroimage 2, 45–53.

Friston, K.J., Holmes, A.P., Worsley, K.J., Poline, J.-P.P., Frith, C.D., Frackowiak, R.S.J., 1994a. Statistical parametric maps in functional imaging: A general linear approach. Hum. Brain Mapp. 2, 189–210.

Friston, K.J., Jezzard, P., Turner, R., 1994b. Analysis of functional MRI time-series. Hum. Brain Mapp. 1, 153–171.

Friston, K.J., Kahan, J., Razi, A., Stephan, K.E., Sporns, O., 2014. On nodes and modes in resting state fMRI. Neuroimage.

Friston, K.J., Li, B., Daunizeau, J., Stephan, K.E., 2011. Network discovery with DCM. Neuroimage 56, 1202–21.

Friston, K.J., Mechelli, a, Turner, R., Price, C.J., 2000. Nonlinear responses in fMRI: the Balloon model, Volterra kernels, and other hemodynamics. Neuroimage 12, 466–77.

Friston, K.J., Shiner, T., FitzGerald, T., Galea, J.M., Adams, R., Brown, H., Dolan, R.J., Moran, R., Stephan, K.E., Bestmann, S., 2012. Dopamine, affordance and active inference. PLoS Comput. Biol. 8, e1002327.

Friston, K.J., Williams, S., Howard, R., Frackowiak, R.S., Turner, R., 1996. Movement-related effects in fMRI time-series. Magn. Reson. Med. 35, 346–55.

Gallay, M.N., Jeanmonod, D., Liu, J., Morel, A., 2008. Human pallidothalamic and cerebellothalamic tracts: anatomical basis for functional stereotactic neurosurgery. Brain Struct. Funct. 212, 443–63.

Garcia, B.G., Neely, M.D., Deutch, A.Y., 2010. Cortical regulation of striatal medium spiny neuron dendritic remodeling in parkinsonism: modulation of glutamate release reverses dopamine depletion-induced dendritic spine loss. Cereb. Cortex 20, 2423–32.

Garraux, G., Bahri, M. a, Lemaire, C., Degueldre, C., Salmon, E., Kaschten, B., 2011. Brain energization in response to deep brain stimulation of subthalamic nuclei in Parkinson's disease. J. Cereb. Blood Flow Metab. 31, 1612–22.

Geday, J., Østergaard, K., Johnsen, E., Gjedde, A., 2009. STN-stimulation in Parkinson's disease restores striatal inhibition of thalamocortical projection. Hum. Brain Mapp. 30, 112–21.

Georgi, J.-C., Stippich, C., Tronnier, V.M., Heiland, S., 2004. Active deep brain stimulation during MRI: a feasibility study. Magn. Reson. Med. 51, 380–8.

Georgopoulos, a., Schwartz, a., Kettner, R., 1986. Neuronal population coding of movement direction. Science (80-.). 233, 1416–1419.

Gillies, A., Willshaw, D., Li, Z., 2002. Subthalamic-pallidal interactions are critical in determining normal and abnormal functioning of the basal ganglia. Proc. Biol. Sci. 269, 545–551.

Gleason, C.A., Kaula, N.F., Hricak, H., Schmidt, R. a, Tanagho, E.A., 1992. The effect of magnetic resonance imagers on implanted neurostimulators. Pacing Clin. Electrophysiol. 15, 81–94.

Glickstein, S.B., Ilch, C.P., Reis, D.J., Golanov, E. V., 2001. Stimulation of the subthalamic vasodilator area and fastigial nucleus independently protects the brain against focal ischemia. Brain Res. 912, 47–59.

Glover, G.H., Li, T.Q., Ress, D., 2000. Image-based method for retrospective correction of physiological motion effects in fMRI: RETROICOR. Magn. Reson. Med. 44, 162–7.

Goebel, R., Roebroeck, A., Kim, D.S., Formisano, E., 2003. Investigating directed cortical interactions in time-resolved fMRI data using vector autoregressive modeling and Granger causality mapping. Magn. Reson. Imaging 21, 1251–1261.

Goense, J.B.M., Logothetis, N.K., 2008. Neurophysiology of the BOLD fMRI signal in awake monkeys. Curr. Biol. 18, 631–40.

Golanov, E. V, Christensen, J.R., Reis, D.J., 2001. Neurons of a limited subthalamic area mediate elevations in cortical cerebral blood flow evoked by hypoxia and excitation of neurons of the rostral ventrolateral medulla. J. Neurosci. 21, 4032–4041.

Golombeck, M. a, Thiele, J., Dössel, O., 2002. Magnetic resonance imaging with implanted neurostimulators: numerical calculation of the induced heating. Biomed. Tech. (Berl). 47 Suppl 1, 660–3.

Gradinaru, V., Mogri, M., Thompson, K.R., Henderson, J.M., Deisseroth, K., 2009. Optical deconstruction of parkinsonian neural circuitry. Science 324, 354–9.

Grafton, S.T., Sutton, J., Couldwell, W., Lew, M., Waters, C., 1994. Network analysis of motor system connectivity in Parkinson's disease: Modulation of thalamocortical interactions after pallidotomy. Hum. Brain Mapp. 2, 45–55.

Grafton, S.T., Turner, R.S., Desmurget, M., Bakay, R., Delong, M., Vitek, J., Crutcher, M., 2006. Normalizing motor-related brain activity: subthalamic nucleus stimulation in Parkinson disease. Neurology 66, 1192–9.

Granger, C., 1969. Investigating causal relations by econometric models and cross-spectral methods. Econom. J. Econom. Soc. 37, 424–438.

Gratwicke, J., Kahan, J., Zrinzo, L., Hariz, M., Limousin, P., Foltynie, T., Jahanshahi, M., 2013. The nucleus basalis of Meynert: A new target for deep brain stimulation in dementia? Neurosci. Biobehav. Rev. 37, 2676–88.

Green, S.B., 1991. How many subjects does it take to do a regression-analysis. Multivariate Behav. Res. 26, 499–510.

Guatteo, E., Chung, K.K.H., Bowala, T.K., Bernardi, G., Mercuri, N.B., Lipski, J., 2005. Temperature sensitivity of dopaminergic neurons of the substantia nigra pars compacta: involvement of transient receptor potential channels. J. Neurophysiol. 94, 3069–80.

Hacker, C.D., Perlmutter, J.S., Criswell, S.R., Ances, B.M., Snyder, A.Z., 2012. Resting state functional connectivity of the striatum in Parkinson's disease. Brain 135, 3699–711.

Haegelen, C., Verin, M., Broche, B.A., Prigent, F., Jannin, P., Gibaud, B., Morandi, X., 2005. Does subthalamic nucleus stimulation affect the frontal limbic areas? A single-

photon emission computed tomography study using a manual anatomical segmentation method. Surg. Radiol. Anat. 27, 389–94.

Hamani, C., Saint-Cyr, J. a, Fraser, J., Kaplitt, M., Lozano, A.M., 2004. The subthalamic nucleus in the context of movement disorders. Brain 127, 4–20.

Hammond, C., Ammari, R., Bioulac, B., Garcia, L., 2008. Latest view on the mechanism of action of deep brain stimulation. Mov. Disord. 23, 2111–21.

Hammond, C., Bergman, H., Brown, P., 2007. Pathological synchronization in Parkinson's disease: networks, models and treatments. Trends Neurosci. 30, 357–64.

Hardman, C.D., Henderson, J.M., Finkelstein, D.I., Horne, M.K., Paxinos, G., Halliday, G.M., 2002. Comparison of the basal ganglia in rats, marmosets, macaques, baboons, and humans: volume and neuronal number for the output, internal relay, and striatal modulating nuclei. J. Comp. Neurol. 445, 238–55.

Hariz, M.I., Blomstedt, P., Zrinzo, L., 2010. Deep brain stimulation between 1947 and 1987: the untold story. Neurosurg. Focus 29, E1.

Harris, R.J., 1985. A primer of multivariate statistics, 2nd ed. ed. Academic Press, New York.

Hashimoto, T., Elder, C.M., Okun, M.S., Patrick, S.K., Vitek, J.L., 2003. Stimulation of the subthalamic nucleus changes the firing pattern of pallidal neurons. J. Neurosci. 23, 1916–23.

Haslinger, B., Kalteis, K., Boecker, H., Alesch, F., Ceballos-Baumann, A.O., 2005. Frequency-correlated decreases of motor cortex activity associated with subthalamic nucleus stimulation in Parkinson's disease. Neuroimage 28, 598–606.

Haynes, W.I. a, Haber, S.N., 2013. The organization of prefrontal-subthalamic inputs in primates provides an anatomical substrate for both functional specificity and integration: implications for Basal Ganglia models and deep brain stimulation. J. Neurosci. 33, 4804–14.

Helmich, R.C., Janssen, M.J.R., Oyen, W.J.G., Bloem, B.R., Toni, I., 2011. Pallidal dysfunction drives a cerebellothalamic circuit into Parkinson tremor. Ann. Neurol. 69, 269–81.

Henderson, J.M., 2012. "Connectomic surgery": diffusion tensor imaging (DTI) tractography as a targeting modality for surgical modulation of neural networks. Front. Integr. Neurosci. 6, 15.

Henderson, J.M., Tkach, J., Phillips, M., Baker, K., Shellock, F.G., Rezai, A.R., 2005. Permanent neurological deficit related to magnetic resonance imaging in a patient with implanted deep brain stimulation electrodes for Parkinson's disease: case report. Neurosurgery 57, E1063; discussion E1063.

Henson, R., 2004. Analysis of fMRI Timeseries, in: Ashburner, J., Friston, K., Penny, W. (Eds.), Human Brain Function. Academic Press.

Henson, R., 2007. Efficient experimental design for fMRI, in: Statistical Parametric Mapping: The Analysis of Functional Brain Images. Academic Press, pp. 193–210.

Henze, D.A., Borhegyi, Z., Csicsvari, J., Mamiya, A., Harris, K.D., Buzsáki, G., 2000. Intracellular features predicted by extracellular recordings in the hippocampus in vivo. J. Neurophysiol. 84, 390–400.

Hershey, T., Revilla, F.J., Wernle, a R., McGee-Minnich, L., Antenor, J. V, Videen, T.O., Dowling, J.L., Mink, J.W., Perlmutter, J.S., 2003. Cortical and subcortical blood flow effects of subthalamic nucleus stimulation in PD. Neurology 61, 816–21.

Herzog, J., Weiss, P.H., Assmus, A., Wefer, B., Seif, C., Braun, P.M., Herzog, H., Volkmann, J., Deuschl, G., Fink, G.R., 2006. Subthalamic stimulation modulates cortical control of urinary bladder in Parkinson's disease. Brain 129, 3366–75.

Hesselmann, V., Sorger, B., Girnus, R., Lasek, K., Maarouf, M., Wedekind, C., Bunke, J., Schulte, O., Krug, B., Lackner, K., Sturm, V., 2004. Intraoperative functional MRI as a new approach to monitor deep brain stimulation in Parkinson's disease. Eur. Radiol. 14, 686–90.

Hilker, R., Portman, a T., Voges, J., Staal, M.J., Burghaus, L., van Laar, T., Koulousakis, a, Maguire, R.P., Pruim, J., de Jong, B.M., Herholz, K., Sturm, V., Heiss, W.-D., Leenders, K.L., 2005. Disease progression continues in patients with advanced Parkinson's disease and effective subthalamic nucleus stimulation. J. Neurol. Neurosurg. Psychiatry 76, 1217–21.

Hilker, R., Voges, J., Ghaemi, M., Lehrke, R., Rudolf, J., Koulousakis, A., Herholz, K., Wienhard, K., Sturm, V., Heiss, W.-D., 2003. Deep brain stimulation of the subthalamic nucleus does not increase the striatal dopamine concentration in parkinsonian humans. Mov. Disord. 18, 41–8.

Hilker, R., Voges, J., Thiel, a, Ghaemi, M., Herholz, K., Sturm, V., Heiss, W.-D., 2002. Deep brain stimulation of the subthalamic nucleus versus levodopa challenge in Parkinson's disease: measuring the on- and off-conditions with FDG-PET. J. Neural Transm. 109, 1257–64.

Hilker, R., Voges, J., Weber, T., Kracht, L.W., Roggendorf, J., Baudrexel, S., Hoevels, M., Sturm, V., Heiss, W.D., 2008. STN-DBS activates the target area in Parkinson disease: an FDG-PET study. Neurology 71, 708–13.

Hilker, R., Voges, J., Weisenbach, S., Kalbe, E., Burghaus, L., Ghaemi, M., Lehrke, R., Koulousakis, A., Herholz, K., Sturm, V., Heiss, W.-D., 2004. Subthalamic nucleus stimulation restores glucose metabolism in associative and limbic cortices and in cerebellum: evidence from a FDG-PET study in advanced Parkinson's disease. J. Cereb. Blood Flow Metab. 24, 7–16.

Hill, K.K., Campbell, M.C., McNeely, M.E., Karimi, M., Ushe, M., Tabbal, S.D., Hershey, T., Flores, H.P., Hartlein, J.M., Lugar, H.M., Revilla, F.J., Videen, T.O., Earhart, G.M., Perlmutter, J.S., 2013. Cerebral blood flow responses to dorsal and ventral STN DBS correlate with gait and balance responses in Parkinson's disease. Exp. Neurol. 241, 105–12.

Hirano, S., Asanuma, K., Ma, Y., Tang, C., Feigin, A., Dhawan, V., Carbon, M., Eidelberg, D., 2008. Dissociation of metabolic and neurovascular responses to levodopa in the treatment of Parkinson's disease. J. Neurosci. 28, 4201–9.

Holgado, A.J.N., Terry, J.R., Bogacz, R., 2010. Conditions for the generation of beta oscillations in the subthalamic nucleus-globus pallidus network. J. Neurosci. 30, 12340–52.

Holl, E.M., Petersen, E.A., Foltynie, T., Martinez-Torres, I., Limousin, P., Hariz, M.I., Zrinzo, L., 2010. Improving targeting in image-guided frame-based deep brain stimulation. Neurosurgery 67, 437–47.

Hoshi, E., Tremblay, L., Féger, J., Carras, P.L., Strick, P.L., 2005. The cerebellum communicates with the basal ganglia. Nat. Neurosci. 8, 1491–1493.

HPA, 2008. Protection of Patients and Volunteers Undergoing MRI Procedures: Advice from the Health Protection Agency (RCE-7).

Hughes, A.J., Daniel, S.E., Kilford, L., Lees, A.J., 1992. Accuracy of clinical diagnosis of idiopathic Parkinson's disease: a clinico-pathological study of 100 cases. J. Neurol. Neurosurg. Psychiatry.

Hughes, L.E., Barker, R.A., Owen, A.M., Rowe, J.B., 2010. Parkinson's disease and healthy aging: Independent and interacting effects on action selection. Hum. Brain Mapp. 31, 1886–1899.

Hutton, C., Bork, A., Josephs, O., Deichmann, R., Ashburner, J., Turner, R., 2002. Image distortion correction in fMRI: A quantitative evaluation. Neuroimage 16, 217–40.

Iannetti, G.D., Wise, R.G., 2007. BOLD functional MRI in disease and pharmacological studies: room for improvement? Magn. Reson. Imaging 25, 978–88.

Jahanshahi, M., Jenkins, I.H., Brown, R.G., Marsden, C.D., Passingham, R.E., Brooks, D.J., 1995. Self-initiated versus externally triggered movements. I. An investigation using measurement of regional cerebral blood flow with PET and movement-related potentials in normal and Parkinson's disease subjects. Brain 118 (Pt 4, 913–33.

Jansen, B.H., Rit, V.G., 1995. Electroencephalogram and visual evoked potential generation in a mathematical model of coupled cortical columns. Biol. Cybern. 73, 357–66.

Jech, R., Mueller, K., Urgošík, D., Sieger, T., Holiga, Š., Růžička, F., Dušek, P., Havránková, P., Vymazal, J., Růžička, E., 2012. The Subthalamic Microlesion Story in Parkinson's Disease: Electrode Insertion-Related Motor Improvement with Relative Cortico-Subcortical Hypoactivation in fMRI. PLoS One 7, e49056.

Jech, R., Urgosík, D., Tintera, J., Nebuzelský, A., Krásenský, J., Liscák, R., Roth, J., Růzicka, E., 2001. Functional magnetic resonance imaging during deep brain stimulation: a pilot study in four patients with Parkinson's disease. Mov. Disord. 16, 1126–32.

Jezzard, P., Balaban, R.S., 1995. Correction for geometric distortion in echo planar images from B0 field variations. Magn. Reson. Med. 34, 65–73.

Kahan, J., Foltynie, T., 2013. Understanding DCM: ten simple rules for the clinician. Neuroimage 83, 542–9.

Kahan, J., Mancini, L., Urner, M., Friston, K., Hariz, M., Holl, E., White, M., Ruge, D., Jahanshahi, M., Boertien, T., Yousry, T., Thornton, J.S., Limousin, P., Zrinzo, L., Foltynie, T., 2012. Therapeutic subthalamic nucleus deep brain stimulation reverses cortico-thalamic coupling during voluntary movements in Parkinson's disease. PLoS One 7, e50270.

Kahan, J., Urner, M., Moran, R., Flandin, G., Marreiros, A., Mancini, L., White, M., Thornton, J., Yousry, T., Zrinzo, L., Hariz, M., Limousin, P., Friston, K., Foltynie, T., 2014. Resting state functional MRI in Parkinson's disease: the impact of deep brain stimulation on "effective" connectivity. Brain 137, 1130–44.

Kainz, W., Neubauer, G., Uberbacher, R., Alesch, F., Chan, D.D., 2002. Temperature measurement on neurological pulse generators during MR scans. Biomed. Eng. Online 1, 2.

Karimi, M., Golchin, N., Tabbal, S.D., Hershey, T., Videen, T.O., Wu, J., Usche, J.W.M., Revilla, F.J., Hartlein, J.M., Wernle, a R., Mink, J.W., Perlmutter, J.S., 2008. Subthalamic nucleus stimulation-induced regional blood flow responses correlate with improvement of motor signs in Parkinson disease. Brain 131, 2710–9.

Kass, R.E., Raftery, A.E., 1995. Bayes Factors. J. Am. Stat. Assoc., Journal of the Americaln Statistical Association 90, 773–795.

Kemp, J.M., Powell, T.P., 1971. The connexions of the striatum and globus pallidus: synthesis and speculation. Philos. Trans. R. Soc. Lond. B. Biol. Sci. 262, 441–457.

Keuken, M.C., Bazin, P.-L., Schäfer, A., Neumann, J., Turner, R., Forstmann, B.U., 2013. Ultra-high 7T MRI of structural age-related changes of the subthalamic nucleus. J. Neurosci. 33, 4896–900.

Kiebel, S.J., Holmes, A.P., 2004. The general linear model, in: Ashburner, J., Friston, K., Penny, W. (Eds.), Human Brain Function. Academic Press.

Kitai, S.T., Deniau, J.M., 1981. Cortical inputs to the subthalamus: intracellular analysis. Brain Res. 214, 411–5.

Kiyatkin, E.A., 2007. Physiological and pathological brain hyperthermia. Prog. Brain Res. 162, 219–43.

Ko, J.H., Mure, H., Tang, C.C., Ma, Y., Dhawan, V., Spetsieris, P., Eidelberg, D., 2013. Parkinson's disease: increased motor network activity in the absence of movement. J. Neurosci. 33, 4540–9.

Krack, P., Batir, A., Van Blercom, N., Chabardes, S., Fraix, V., Ardouin, C., Koudsie, A., Limousin, P.D., Benazzouz, A., LeBas, J.F., Benabid, A.-L., Pollak, P., 2003. Five-year follow-up of bilateral stimulation of the subthalamic nucleus in advanced Parkinson's disease. N. Engl. J. Med. 349, 1925–34.

Kravitz, A. V, Freeze, B.S., Parker, P.R.L., Kay, K., Thwin, M.T., Deisseroth, K., Kreitzer, A.C., 2010. Regulation of parkinsonian motor behaviours by optogenetic control of basal ganglia circuitry. Nature 466, 622–6.

Kress, G.J., Yamawaki, N., Wokosin, D.L., Wickersham, I.R., Shepherd, G.M.G., Surmeier, D.J., 2013. Convergent cortical innervation of striatal projection neurons. Nat. Neurosci. 1–4.

Kugel, H., Bremer, C., Püschel, M., Fischbach, R., Lenzen, H., Tombach, B., Van Aken, H., Heindel, W., 2003. Hazardous situation in the MR bore: induction in ECG leads causes fire. Eur. Radiol. 13, 690–4.

Kühn, A. a, Kempf, F., Brücke, C., Gaynor Doyle, L., Martinez-Torres, I., Pogosyan, A., Trottenberg, T., Kupsch, A., Schneider, G.-H., Hariz, M.I., Vandenberghe, W., Nuttin, B., Brown, P., 2008. High-frequency stimulation of the subthalamic nucleus suppresses oscillatory beta activity in patients with Parkinson's disease in parallel with improvement in motor performance. J. Neurosci. 28, 6165–73.

Kuhn, J., Hardenacke, K., Lenartz, D., Gruendler, T., Ullsperger, M., Bartsch, C., Mai, J.K., Zilles, K., Bauer, A., Matusch, A., Schulz, R.-J., Noreik, M., Bührle, C.P., Maintz, D., Woopen, C., Häussermann, P., Hellmich, M., Klosterkötter, J., Wiltfang, J., Maarouf, M., Freund, H.-J., Sturm, V., 2014. Deep brain stimulation of the nucleus basalis of Meynert in Alzheimer's dementia. Mol. Psychiatry.

Künzle, H., 1975. Bilateral projections from precentral motor cortex to the putamen and other parts of the basal ganglia. An autoradiographic study in Macaca fascicularis. Brain Res. 88, 195–209.

Künzle, H., 1978. An autoradiographic analysis of the efferent connections from premotor and adjacent prefrontal regions (areas 6 and 9) in macaca fascicularis. Brain. Behav. Evol. 15, 185–234.

Kurth, F., Zilles, K., Fox, P.T., Laird, A.R., Eickhoff, S.B., 2010. A link between the systems: functional differentiation and integration within the human insula revealed by meta-analysis. Brain Struct. Funct. 214, 519–34.

Kwong, K., Belliveau, J., Chesler, D., Goldberg, I., Weisskoff, R., Poncelet, B., Kennedy, D., Hoppel, B., Cohen, M., Turner, R., 1992. Dynamic magnetic resonance imaging of human brain activity during primary sensory stimulation. Proc Natl Acad Sci U S A 89, 5675–5679.

Lai, H.-Y., Younce, J.R., Albaugh, D.L., Kao, Y.-C.J., Shih, Y.-Y.I., 2014. Functional MRI reveals frequency-dependent responses during deep brain stimulation at the subthalamic nucleus or internal globus pallidus. Neuroimage 84, 11–8.

Lambert, C., Lutti, A., Helms, G., Frackowiak, R., Ashburner, J., 2013. Multiparametric brainstem segmentation using a modified multivariate mixture of Gaussians. NeuroImage. Clin. 2, 684–94.

Lambert, C., Zrinzo, L., Nagy, Z., Lutti, A., Hariz, M., Foltynie, T., Draganski, B., Ashburner, J., Frackowiak, R., 2012. Confirmation of functional zones within the human subthalamic nucleus: patterns of connectivity and sub-parcellation using diffusion weighted imaging. Neuroimage 60, 83–94.

Lanciego, J.L., Luquin, N., Obeso, J. a, 2012. Functional neuroanatomy of the basal ganglia. Cold Spring Harb. Perspect. Med. 2, a009621.

Laxton, A.W., Tang-Wai, D.F., McAndrews, M.P., Zumsteg, D., Wennberg, R., Keren, R., Wherrett, J., Naglie, G., Hamani, C., Smith, G.S., Lozano, A.M., 2010. A phase I trial of deep brain stimulation of memory circuits in Alzheimer's disease. Ann. Neurol. 68, 521–34.

Le Jeune, F., Péron, J., Grandjean, D., Drapier, S., Haegelen, C., Garin, E., Millet, B., Vérin, M., 2010. Subthalamic nucleus stimulation affects limbic and associative circuits: a PET study. Eur. J. Nucl. Med. Mol. Imaging 37, 1512–20.

Leblois, A., Boraud, T., Meissner, W., Bergman, H., Hansel, D., 2006. Competition between feedback loops underlies normal and pathological dynamics in the basal ganglia. J. Neurosci. 26, 3567–83.

Lehéricy, S., Benali, H., Van de Moortele, P.-F., Pélégrini-Issac, M., Waechter, T., Ugurbil, K., Doyon, J., 2005. Distinct basal ganglia territories are engaged in early and advanced motor sequence learning. Proc. Natl. Acad. Sci. U. S. A. 102, 12566–12571.

Lévesque, J.-C., Parent, A., 2005. GABAergic interneurons in human subthalamic nucleus. Mov. Disord. 20, 574–84.

Levy, R., Ashby, P., Hutchison, W.D., Lang, A.E., Lozano, A.M., Dostrovsky, J.O., 2002. Dependence of subthalamic nucleus oscillations on movement and dopamine in Parkinson's disease. Brain 125, 1196–209.

Li, B., Daunizeau, J., Stephan, K.E., Penny, W., Hu, D., Friston, K., 2011. Generalised filtering and stochastic DCM for fMRI. Neuroimage 58, 442–57.

Li, D., Zuo, C., Guan, Y., Zhao, Y., Shen, J., Zan, S., Sun, B., 2006. FDG-PET study of the bilateral subthalamic nucleus stimulation effects on the regional cerebral metabolism in advanced Parkinson disease. Acta Neurochir. Suppl. 99, 51–4.

Li, Q., Ke, Y., Chan, D.C.W., Qian, Z.-M., Yung, K.K.L., Ko, H., Arbuthnott, G.W., Yung, W.-H., 2012. Therapeutic deep brain stimulation in Parkinsonian rats directly influences motor cortex. Neuron 76, 1030–41.

Li, S., Arbuthnott, G.W., Jutras, M.J., Goldberg, J. a, Jaeger, D., 2007. Resonant antidromic cortical circuit activation as a consequence of high-frequency subthalamic deep-brain stimulation. J. Neurophysiol. 98, 3525–37.

Ligot, N., Krystkowiak, P., Simonin, C., Goldman, S., Peigneux, P., Van Naemen, J., Monclus, M., Lacroix, S.F., Devos, D., Dujardin, K., Delmaire, C., Bardinet, E., Delval, A., Delliaux, M., Defebvre, L., Yelnik, J., Blond, S., Destée, A., De Tiège, X., 2011. External globus pallidus stimulation modulates brain connectivity in Huntington's disease. J. Cereb. Blood Flow Metab. 31, 41–6.

Limousin, P., Greene, J., Pollak, P., Rothwell, J., Benabid, A.L., Frackowiak, R., 1997. Changes in cerebral activity pattern due to subthalamic nucleus or internal pallidum stimulation in Parkinson's disease. Ann. Neurol. 42, 283–91.

Limousin, P., Krack, P., Pollak, P., Benazzouz, A., Ardouin, C., Hoffmann, D., Benabid, A.L., 1998. Electrical stimulation of the subthalamic nucleus in advanced Parkinson's disease. N. Engl. J. Med. 339, 1105–11.

Limousin, P., Pollak, P., Benazzouz, A., Hoffmann, D., Le Bas, J.F., Broussolle, E., Perret, J.E., Benabid, A.L., 1995. Effect of parkinsonian signs and symptoms of bilateral subthalamic nucleus stimulation. Lancet 345, 91–5.

Little, S., Brown, P., 2012. What brain signals are suitable for feedback control of deep brain stimulation in Parkinson's disease? Ann. N. Y. Acad. Sci. 1265, 9–24.

Little, S., Pogosyan, A., Neal, S., Zavala, B., Zrinzo, L., Hariz, M., Foltynie, T., Limousin, P., Ashkan, K., FitzGerald, J., Green, A.L., Aziz, T.Z., Brown, P., 2013. Adaptive deep brain stimulation in advanced Parkinson disease. Ann. Neurol. 74, 449–57.

Litvak, V., Jha, A., Eusebio, A., Oostenveld, R., Foltynie, T., Limousin, P., Zrinzo, L., Hariz, M.I., Friston, K., Brown, P., 2011. Resting oscillatory cortico-subthalamic connectivity in patients with Parkinson's disease. Brain 134, 359–74.

Logothetis, N.K., 2003. The underpinnings of the BOLD functional magnetic resonance imaging signal. J. Neurosci. 23, 3963–71.

Logothetis, N.K., 2008. What we can do and what we cannot do with fMRI. Nature 453, 869–78.

Logothetis, N.K., Pauls, J., Augath, M., Trinath, T., Oeltermann, a, 2001. Neurophysiological investigation of the basis of the fMRI signal. Nature 412, 150–7.

Logothetis, N.K., Wandell, B. a, 2004. Interpreting the BOLD signal. Annu. Rev. Physiol. 66, 735–69.

Lohmann, G., Erfurth, K., Müller, K., Turner, R., 2012. Critical comments on dynamic causal modelling. Neuroimage 59, 2322–9.

Lohmann, G., Margulies, D.S., Horstmann, A., Pleger, B., Lepsien, J., Goldhahn, D., Schloegl, H., Stumvoll, M., Villringer, A., Turner, R., 2010. Eigenvector centrality mapping for analyzing connectivity patterns in fMRI data of the human brain. PLoS One 5, e10232.

Lokkegaard, a, Werdelin, L.M., Regeur, L., Karlsborg, M., Jensen, S.R., Brødsgaard, E., Madsen, F.F., Lonsdale, M.N., Friberg, L., 2007. Dopamine transporter imaging and the effects of deep brain stimulation in patients with Parkinson's disease. Eur. J. Nucl. Med. Mol. Imaging 34, 508–16.

Lowe, M.J., Mock, B.J., Sorenson, J.A., 1998. Functional connectivity in single and multislice echoplanar imaging using resting-state fluctuations. Neuroimage 7, 119–32.

Lozano, A.M.M., Lipsman, N., 2013. Probing and Regulating Dysfunctional Circuits Using Deep Brain Stimulation. Neuron 77, 406–424.

Lund, T.E., 2001. fcMRI--mapping functional connectivity or correlating cardiac-induced noise? Magn. Reson. Med. 46, 628–9.

Lyoo, C.H., Aalto, S., Rinne, J.O., Lee, K.O., Oh, S.H., Chang, J.W., Lee, M.S., 2007. Different cerebral cortical areas influence the effect of subthalamic nucleus stimulation on parkinsonian motor deficits and freezing of gait. Mov. Disord. 22, 2176–82.

Mallet, L., Polosan, M., Jaafari, N., Baup, N., Welter, M.-L., Fontaine, D., du Montcel, S.T., Yelnik, J., Chéreau, I., Arbus, C., Raoul, S., Aouizerate, B., Damier, P., Chabardès, S., Czernecki, V., Ardouin, C., Krebs, M.-O., Bardinet, E., Chaynes, P., Burbaud, P., Cornu, P., Derost, P., Bougerol, T., Bataille, B., Mattei, V., Dormont, D., Devaux, B., Vérin, M., Houeto, J.-L., Pollak, P., Benabid, A.-L., Agid, Y., Krack, P., Millet, B., Pelissolo, A., 2008. Subthalamic nucleus stimulation in severe obsessive-compulsive disorder. N. Engl. J. Med. 359, 2121–2134.

Mallet, N., Pogosyan, A., Sharott, A., Csicsvari, J., Bolam, J.P., Brown, P., Magill, P.J., 2008. Disrupted dopamine transmission and the emergence of exaggerated beta oscillations in subthalamic nucleus and cerebral cortex. J. Neurosci. 28, 4795–806.

Marreiros, a C., Kiebel, S.J., Friston, K.J., 2008. Dynamic causal modelling for fMRI: a two-state model. Neuroimage 39, 269–78.

Marreiros, A.C., Cagnan, H., Moran, R.J., Friston, K.J., Brown, P., 2012. Basal ganglia-cortical interactions in Parkinsonian patients. Neuroimage 66C, 301–310.

Martinez-Torres, I., Hariz, M.I., Zrinzo, L., Foltynie, T., Limousin, P., 2009. Improvement of tics after subthalamic nucleus deep brain stimulation. Neurology 72, 1787–9.

Maurice, N., Thierry, A.-M., Glowinski, J., Deniau, J.-M., 2003. Spontaneous and evoked activity of substantia nigra pars reticulata neurons during high-frequency stimulation of the subthalamic nucleus. J. Neurosci. 23, 9929–9936.

Mayberg, H.S., Lozano, A.M., Voon, V., McNeely, H.E., Seminowicz, D., Hamani, C., Schwalb, J.M., Kennedy, S.H., 2005. Deep brain stimulation for treatment-resistant depression. Neuron 45, 651–60.

McIntosh, A.R., Gonzalez-Lima, F., 1994. Structural equation modeling and its application to network analysis in functional brain imaging. Hum. Brain Mapp. 2, 2–22.

McIntyre, C.C., Hahn, P.J., 2010. Network perspectives on the mechanisms of deep brain stimulation. Neurobiol. Dis. 38, 329–37.

McIntyre, C.C., Mori, S., Sherman, D.L., Thakor, N. V, Vitek, J.L., 2004a. Electric field and stimulating influence generated by deep brain stimulation of the subthalamic nucleus. Clin. Neurophysiol. 115, 589–95.

McIntyre, C.C., Savasta, M., Kerkerian-Le Goff, L., Vitek, J.L., 2004b. Uncovering the mechanism(s) of action of deep brain stimulation: activation, inhibition, or both. Clin. Neurophysiol. 115, 1239–48.

McLntosh, a. R., Gonzalez-Lima, F., 1994. Structural equation modeling and its application to network analysis in functional brain imaging. Hum. Brain Mapp. 2, 2–22.

Medtronic, 2010. MRI Guidelines.

Meissner, W., Leblois, A., Hansel, D., Bioulac, B., Gross, C.E., Benazzouz, A., Boraud, T., 2005. Subthalamic high frequency stimulation resets subthalamic firing and reduces abnormal oscillations. Brain 128, 2372–82.

Merola, A., Rizzi, L., Zibetti, M., Artusi, C.A., Montanaro, E., Angrisano, S., Lanotte, M., Rizzone, M.G., Lopiano, L., 2013. Medical therapy and subthalamic deep brain stimulation in advanced Parkinson's disease: a different long-term outcome? J. Neurol. Neurosurg. Psychiatry.

Mikos, a, Bowers, D., Noecker, a M., McIntyre, C.C., Won, M., Chaturvedi, A., Foote, K.D., Okun, M.S., 2011. Patient-specific analysis of the relationship between the volume of tissue activated during DBS and verbal fluency. Neuroimage 54 Suppl 1, S238–46.

Min, H.-K., Hwang, S.-C., Marsh, M.P., Kim, I., Knight, E., Striemer, B., Felmlee, J.P., Welker, K.M., Blaha, C.D., Chang, S.-Y., Bennet, K.E., Lee, K.H., 2012. Deep brain stimulation induces BOLD activation in motor and non-motor networks: An fMRI comparison study of STN and EN/GPi DBS in large animals. Neuroimage 63, 1408–20.

Miyachi, S., Hikosaka, O., Miyashita, K., Kárádi, Z., Rand, M.K., 1997. Differential roles of monkey striatum in learning of sequential hand movement. Exp. Brain Res. 115, 1–5.

Moran, a, Bergman, H., Israel, Z., Bar-Gad, I., 2008. Subthalamic nucleus functional organization revealed by parkinsonian neuronal oscillations and synchrony. Brain 131, 3395–409.

Moran, Mallet, N., Litvak, V., Dolan, R.J., Magill, P.J., Friston, K.J., Brown, P., 2011a. Alterations in brain connectivity underlying beta oscillations in Parkinsonism. PLoS Comput. Biol. 7, e1002124.

Moran, R., Pinotsis, D.A., Friston, K., 2013. Neural masses and fields in dynamic causal modeling. Front. Comput. Neurosci. 7, 57.

Moran, R.J., Stephan, K.E., Seidenbecher, T., Pape, H.-C., Dolan, R.J., Friston, K.J., 2009. Dynamic causal models of steady-state responses. Neuroimage 44, 796–811.

Moran, Symmonds, M., Stephan, K.E., Friston, K.J., Dolan, R.J., 2011b. An in vivo assay of synaptic function mediating human cognition. Curr. Biol. 21, 1320–5.

Mountcastle, V.B., 1997. The columnar organization of the neocortex. Brain 120 (Pt 4, 701–22.

Mueller, K., Jech, R., Schroeter, M.L., 2013. Deep-brain stimulation for Parkinson's disease. N. Engl. J. Med. 368, 482–3.

Mure, H., Hirano, S., Tang, C.C., Isaias, I.U., Antonini, A., Ma, Y., Dhawan, V., Eidelberg, D., 2011. Parkinson's disease tremor-related metabolic network: characterization, progression, and treatment effects. Neuroimage 54, 1244–53.

Nagaoka, T., Katayama, Y., Kano, T., Kobayashi, K., Oshima, H., Fukaya, C., Yamamoto, T., 2007. Changes in glucose metabolism in cerebral cortex and cerebellum correlate with tremor and rigidity control by subthalamic nucleus stimulation in Parkinson's disease: a positron emission tomography study. Neuromodulation 10, 206–15.

Nambu, a, Takada, M., Inase, M., Tokuno, H., 1996. Dual somatotopical representations in the primate subthalamic nucleus: evidence for ordered but reversed body-map transformations from the primary motor cortex and the supplementary motor area. J. Neurosci. 16, 2671–83.

Nambu, A., 2005. A new approach to understand the pathophysiology of Parkinson's disease. J. Neurol. 252 Suppl , IV1–IV4.

Nambu, A., Tokuno, H., Hamada, I., Kita, H., Imanishi, M., Akazawa, T., Ikeuchi, Y., Hasegawa, N., 2000. Excitatory cortical inputs to pallidal neurons via the subthalamic nucleus in the monkey. J. Neurophysiol. 84, 289–300.

Nambu, A., Tokuno, H., Takada, M., 2002. Functional significance of the cortico-subthalamo-pallidal "hyperdirect" pathway. Neurosci. Res. 43, 111–7.

Ni, Z., Pinto, A.D., Lang, A.E., Chen, R., 2010. Involvement of the cerebellothalamocortical pathway in Parkinson disease. Ann. Neurol. 68, 816–24.

Nilsson, M.H., Patel, M., Rehncrona, S., Magnusson, M., Fransson, P.-A., 2013. Subthalamic deep brain stimulation improves smooth pursuit and saccade performance in patients with Parkinson's disease. J. Neuroeng. Rehabil. 10, 33.

Nimura, T., Yamaguchi, K., Ando, T., Shibuya, S., Oikawa, T., Nakagawa, A., Shirane, R., Itoh, M., Tominaga, T., 2005. Attenuation of fluctuating striatal synaptic dopamine levels in patients with Parkinson disease in response to subthalamic nucleus stimulation: a positron emission tomography study. J. Neurosurg. 103, 968–73.

Norris, D.G., 2012. Spin-echo fMRI: The poor relation? Neuroimage.

Odekerken, V.J.J., van Laar, T., Staal, M.J., Mosch, A., Hoffmann, C.F.E., Nijssen, P.C.G., Beute, G.N., van Vugt, J.P.P., Lenders, M.W.P.M., Contarino, M.F., Mink, M.S.J., Bour, L.J., van den Munckhof, P., Schmand, B. a, de Haan, R.J., Schuurman, P.R., de Bie, R.M. a, 2013. Subthalamic nucleus versus globus pallidus bilateral deep brain stimulation for advanced Parkinson's disease (NSTAPS study): a randomised controlled trial. Lancet Neurol. 12, 37–44.

Ogawa, S., Lee, T.M., Kay, a R., Tank, D.W., 1990a. Brain magnetic resonance imaging with contrast dependent on blood oxygenation. Proc. Natl. Acad. Sci. U. S. A. 87, 9868–72.

Ogawa, S., Lee, T.M., Nayak, A.S., Glynn, P., 1990b. Oxygenation-sensitive contrast in magnetic resonance image of rodent brain at high magnetic fields. Magn. Reson. Med. 14, 68–78.

Parent, A., Hazrati, L.N., 1995a. Functional anatomy of the basal ganglia. I. The cortico-basal ganglia-thalamo-cortical loop. Brain Res. Brain Res. Rev. 20, 91–127.

Parent, A., Hazrati, L.N., 1995b. Functional anatomy of the basal ganglia. II. The place of subthalamic nucleus and external pallidum in basal ganglia circuitry. Brain Res. Brain Res. Rev. 20, 128–54.

Park, H.-J., Friston, K., 2013. Structural and Functional Brain Networks: From Connections to Cognition. Science (80-.). 342, 1238411–1238411.

Park, S.M., Nyenhuis, J. a., Smith, C.D., Lim, E.J., Foster, K.S., Baker, K.B., Hrdlicka, G., Rezai, a. R., Ruggieri, P., Sharan, a., Shellock, F.G., Stypulkowski, P.H., Tkach, J., 2003. Gelled versus nongelled phantom material for measurement of MRI-induced temperature increases with bioimplants. IEEE Trans. Magn. 39, 3367–3371.

Paschali, A., Constantoyannis, C., Angelatou, F., Vassilakos, P., 2013. Perfusion brain SPECT in assessing motor improvement after deep brain stimulation in Parkinson's disease. Acta Neurochir. (Wien). 155, 497–505.

Paul, G., Reum, T., Meissner, W., Marburger, A., Sohr, R., Morgenstern, R., Kupsch, A., 2000. High frequency stimulation of the subthalamic nucleus influences striatal dopaminergic metabolism in the naive rat. Neuroreport 11, 441–444.

Pauling, L., Coryell, C.D., 1936. The Magnetic Properties and Structure of Hemoglobin, Oxyhemoglobin and Carbonmonoxyhemoglobin. Proc. Natl. Acad. Sci. 22, 210–216.

Payoux, P., Remy, P., Damier, P., Miloudi, M., Loubinoux, I., Pidoux, B., Gaura, V., Rascol, O., Samson, Y., Agid, Y., 2004. Subthalamic nucleus stimulation reduces abnormal motor cortical overactivity in Parkinson disease. Arch. Neurol. 61, 1307–13.

Penny, W.D., Stephan, K.E., Daunizeau, J., Rosa, M.J., Friston, K.J., Schofield, T.M., Leff, A.P., 2010. Comparing families of dynamic causal models. PLoS Comput. Biol. 6, e1000709.

Penny, W.D., Stephan, K.E., Mechelli, a, Friston, K.J., 2004. Comparing dynamic causal models. Neuroimage 22, 1157–72.

Penny, W.D., Trujillo-Barreto, N.J., Friston, K.J., 2005. Bayesian fMRI time series analysis with spatial priors. Neuroimage 24, 350–62.

Perlmutter, J.S., Mink, J.W., 2006. Deep brain stimulation. Annu. Rev. Neurosci. 29, 229–57.

Phillips, M.D., Baker, K.B., Lowe, M.J., Tkach, J.A., Cooper, S.E., Kopell, B.H., Rezai, A.R., 2006. Parkinson disease: pattern of functional MR imaging activation during deep brain stimulation of subthalamic nucleus--initial experience. Radiology 239, 209–16.

Pinto, S., Thobois, S., Costes, N., Le Bars, D., Benabid, A.-L., Broussolle, E., Pollak, P., Gentil, M., 2004. Subthalamic nucleus stimulation and dysarthria in Parkinson's disease: a PET study. Brain 127, 602–15.

Poldrack, R. a, 2006. Can cognitive processes be inferred from neuroimaging data? Trends Cogn. Sci. 10, 59–63.

Poline, J.-B., Kherif, F., Penny, W., 2004. Contrasts and Classical Inference, in: Ashburner, J., Friston, K., Penny, W. (Eds.), Human Brain Function. Academic Press.

Pollo, C., Villemure, J.-G., Vingerhoets, F., Ghika, J., Maeder, P., Meuli, R., 2004. Magnetic resonance artifact induced by the electrode Activa 3389: an in vitro and in vivo study. Acta Neurochir. (Wien). 146, 161–4.

Pourfar, M., Tang, C., Lin, T., Dhawan, V., Kaplitt, M.G., Eidelberg, D., 2009. Assessing the microlesion effect of subthalamic deep brain stimulation surgery with FDG PET. J. Neurosurg. 110, 1278–82.

Quiroga-Varela, a, Walters, J.R., Brazhnik, E., Marin, C., Obeso, J. a, 2013. What basal ganglia changes underlie the parkinsonian state? The significance of neuronal oscillatory activity. Neurobiol. Dis. 58, 242–8.

Rajput, A.H., Rozdilsky, B., Rajput, A., 1991. Accuracy of clinical diagnosis in parkinsonism--a prospective study. Can. J. Neurol. Sci. 18, 275–278.

Rascol, O., Brooks, D.J., Korczyn, A.D., De Deyn, P.P., Clarke, C.E., Lang, A.E., 2000. A five-year study of the incidence of dyskinesia in patients with early Parkinson's disease who were treated with ropinirole or levodopa. 056 Study Group. N. Engl. J. Med. 342, 1484–91.

Rascol, O., Sabatini, U., Fabre, N., Brefel, C., Loubinoux, I., Celsis, P., Senard, J.M., Montastruc, J.L., Chollet, F., 1997. The ipsilateral cerebellar hemisphere is overactive during hand movements in akinetic parkinsonian patients. Brain 120, 103–110.

Redgrave, P., Rodriguez, M., Smith, Y., Rodriguez-Oroz, M.C., Lehericy, S., Bergman, H., Agid, Y., DeLong, M.R., Obeso, J.A., 2010. Goal-directed and habitual control in the basal ganglia: implications for Parkinson's disease. Nat. Rev. Neurosci. 11, 760–72.

Rees, G., Friston, K., Koch, C., 2000. A direct quantitative relationship between the functional properties of human and macaque V5. Nat. Neurosci. 3, 716–723.

Rezai, a R., Lozano, a M., Crawley, a P., Joy, M.L., Davis, K.D., Kwan, C.L., Dostrovsky, J.O., Tasker, R.R., Mikulis, D.J., 1999. Thalamic stimulation and functional magnetic resonance imaging: localization of cortical and subcortical activation with implanted electrodes. Technical note. J. Neurosurg. 90, 583–90.

Rezai, A.R., Baker, K.B., Tkach, J.A., Phillips, M., Hrdlicka, G., Sharan, A.D., Nyenhuis, J., Ruggieri, P., Shellock, F.G., Henderson, J., 2005. Is magnetic resonance imaging safe for patients with neurostimulation systems used for deep brain stimulation? Neurosurgery 57, 1056–62; discussion 1056–62.

Rezai, A.R., Finelli, D., Nyenhuis, J.A., Hrdlicka, G., Tkach, J., Sharan, A., Rugieri, P., Stypulkowski, P.H., Shellock, F.G., 2002. Neurostimulation Systems for Deep Brain Stimulation : In Vitro Evaluation of Magnetic Resonance Imaging – Related Heating at 1 . 5 Tesla. J. Magn. Reson. Imaging 250, 241–250.

Riva-Posse, P., Choi, K.S., Holtzheimer, P.E., McIntyre, C.C., Gross, R.E., Chaturvedi, A., Crowell, A.L., Garlow, S.J., Rajendra, J.K., Mayberg, H.S., 2014. Defining Critical White Matter Pathways Mediating Successful Subcallosal Cingulate Deep Brain Stimulation for Treatment-Resistant Depression. Biol. Psychiatry.

Rodriguez-Oroz, M.C., Jahanshahi, M., Krack, P., Litvan, I., Macias, R., Bezard, E., Obeso, J.A., 2009. Initial clinical manifestations of Parkinson's disease: features and pathophysiological mechanisms. Lancet Neurol. 8, 1128–39.

Roebroeck, A., Formisano, E., Goebel, R., 2005. Mapping directed influence over the brain using Granger causality and fMRI. Neuroimage 25, 230–42.

Rothwell, J., 1994. Control of Human Voluntary Movement, Second edi. ed. Chapman & Hall, London.

Rouzaire-Dubois, B., Scarnati, E., 1985. Bilateral corticosubthalamic nucleus projections: an electrophysiological study in rats with chronic cerebral lesions. Neuroscience 15, 69–79.

Rowe, J., Stephan, K.E., Friston, K., Frackowiak, R., Lees, A., Passingham, R., 2002. Attention to action in Parkinson's disease: impaired effective connectivity among frontal cortical regions. Brain 125, 276–89.

Rowe, J.B., 2010. Connectivity Analysis is Essential to Understand Neurological Disorders. Front. Syst. Neurosci. 4, 1–13.

Rowe, J.B., Hughes, L.E., Barker, R.A., Owen, A.M., 2010. Dynamic causal modelling of effective connectivity from fMRI: Are results reproducible and sensitive to Parkinson's disease and its treatment? Neuroimage 52, 1015–1026.

Rowe, J.B., Sakai, K., Lund, T.E., Ramsøy, T., Christensen, M.S., Baare, W.F.C., Paulson, O.B., Passingham, R.E., 2007. Is the prefrontal cortex necessary for establishing cognitive sets? J. Neurosci. 27, 13303–13310.

Salcman, M., Moriyama, E., Elsner, H.J., Rossman, H., Gettleman, R.A., Neuberth, G., Corradino, G., 1989. Cerebral blood flow and the thermal properties of the brain: a preliminary analysis. J. Neurosurg. 70, 592–598.

Santaniello, S., Gale, J.T., Montgomery, E.B., Sarma, S. V, 2012. Reinforcement mechanisms in putamen during high frequency STN DBS: A point process study. Conf. Proc. IEEE Eng. Med. Biol. Soc. 2012, 1214–7.

Scherfler, C., Esterhammer, R., Nocker, M., Mahlknecht, P., Stockner, H., Warwitz, B., Spielberger, S., Pinter, B., Donnemiller, E., Decristoforo, C., Virgolini, I., Schocke, M., Poewe, W., Seppi, K., 2013. Correlation of dopaminergic terminal dysfunction and microstructural abnormalities of the basal ganglia and the olfactory tract in Parkinson's disease. Brain 136, 3028–37.

Schuepbach, W.M.M.M.M., Rau, J., Knudsen, K., Volkmann, J., Krack, P., Timmermann, L., Hälbig, T.D.D., Hesekamp, H., Navarro, S.M.M., Meier, N., Falk, D., Mehdorn, M., Paschen, S., Maarouf, M., Barbe, M.T.T., Fink, G.R.R., Kupsch, A., Gruber, D., Schneider, G.-H.G.-H., Seigneuret, E., Kistner, A., Chaynes, P., Ory-Magne, F., Brefel Courbon, C., Vesper, J., Schnitzler, A., Wojtecki, L., Houeto, J.-L.J.-L., Bataille, B., Maltête, D., Damier, P., Raoul, S., Sixel-Doering, F., Hellwig, D., Gharabaghi, A., Krüger, R., Pinsker, M.O.O., Amtage, F., Régis, J.-M.J.-M., Witjas, T., Thobois, S., Mertens, P., Kloss, M., Hartmann, A., Oertel, W.H.H., Post, B., Speelman, H., Agid, Y., Schade-Brittinger, C., Deuschl, G., 2013. Neurostimulation for Parkinson's Disease with Early Motor Complications. N. Engl. J. Med. 368, 610–622.

Seghier, M.L., Friston, K.J., 2013. Network discovery with large DCMs. Neuroimage 68, 181–91.

Sergio, L.E., Hamel-Pâquet, C., Kalaska, J.F., 2005. Motor cortex neural correlates of output kinematics and kinetics during isometric-force and arm-reaching tasks. J. Neurophysiol. 94, 2353–78.

Servan-Schreiber, D., Printz, H., Cohen, J.D., 1990. A network model of catecholamine effects: gain, signal-to-noise ratio, and behavior. Science 249, 892–895.

Sestini, S., Ramat, S., Formiconi, A.R., Ammannati, F., Sorbi, S., Pupi, A., 2005. Brain networks underlying the clinical effects of long-term subthalamic stimulation for Parkinson's disease: a 4-year follow-up study with rCBF SPECT. J. Nucl. Med. 46, 1444–54.

Sestini, S., Scotto di Luzio, A., Ammannati, F., De Cristofaro, M.T.R., Passeri, A., Martini, S., Pupi, A., 2002. Changes in regional cerebral blood flow caused by deep-brain stimulation of the subthalamic nucleus in Parkinson's disease. J. Nucl. Med. 43, 725–32.

Sharan, a, Rezai, a R., Nyenhuis, J. a, Hrdlicka, G., Tkach, J., Baker, K., Turbay, M., Rugieri, P., Phillips, M., Shellock, F.G., 2003. MR safety in patients with implanted deep brain stimulation systems (DBS). Acta Neurochir. Suppl. 87, 141–5.

Shepherd, G.M.G., 2013. Corticostriatal connectivity and its role in disease. Nat. Rev. Neurosci. 14, 278–91.

Sherman, S.M., Guillery, R.W., 1998. On the actions that one nerve cell can have on another: distinguishing "drivers" from "modulators". Proc. Natl. Acad. Sci. U. S. A. 95, 7121–7126.

Shimamoto, S.A., Ryapolova-Webb, E.S., Ostrem, J.L., Galifianakis, N.B., Miller, K.J., Starr, P.A., 2013. Subthalamic nucleus neurons are synchronized to primary motor cortex local field potentials in Parkinson's disease. J. Neurosci. 33, 7220–33.

Shrivastava, D., Abosch, A., Hughes, J., Goerke, U., DelaBarre, L., Visaria, R., Harel, N., Vaughan, J.T., 2012. Heating induced near deep brain stimulation lead electrodes during magnetic resonance imaging with a 3 T transceive volume head coil. Phys. Med. Biol. 57, 5651–65.

Sidiropoulos, C., Walsh, R., Meaney, C., Poon, Y.Y., Fallis, M., Moro, E., 2013. Low-frequency subthalamic nucleus deep brain stimulation for axial symptoms in advanced Parkinson's disease. J. Neurol. 260, 2306–11.

Silberstein, P., Pogosyan, A., Kühn, A. a, Hotton, G., Tisch, S., Kupsch, A., Dowsey-Limousin, P., Hariz, M.I., Brown, P., 2005. Cortico-cortical coupling in Parkinson's disease and its modulation by therapy. Brain 128, 1277–91.

Smith, G.S., Laxton, A.W., Tang-Wai, D.F., McAndrews, M.P., Diaconescu, A.O., Workman, C.I., Lozano, A.M., 2012. Increased cerebral metabolism after 1 year of deep brain stimulation in Alzheimer disease. Arch. Neurol. 69, 1141–8.

Spetsieris, P.G., Eidelberg, D., 2011. Scaled subprofile modeling of resting state imaging data in Parkinson's disease: methodological issues. Neuroimage 54, 2899–914.

Spiegel, J., Fuss, G., Backens, M., Reith, W., Magnus, T., Becker, G., Moringlane, J.-R., Dillmann, U., 2003. Transient dystonia following magnetic resonance imaging in a patient with deep brain stimulation electrodes for the treatment of Parkinson disease. Case report. J. Neurosurg. 99, 772–4.

Sporns, O., 2014. Contributions and challenges for network models in cognitive neuroscience. Nat. Neurosci. 17, 652–60.

Stefani, A., Lozano, A.M., Peppe, A., Stanzione, P., Galati, S., Tropepi, D., Pierantozzi, M., Brusa, L., Scarnati, E., Mazzone, P., 2007. Bilateral deep brain stimulation of the pedunculopontine and subthalamic nuclei in severe Parkinson's disease. Brain 130, 1596–607.

Stefurak, T., Mikulis, D., Mayberg, H., Lang, A.E., Hevenor, S., Pahapill, P., Saint-Cyr, J., Lozano, A., 2003. Deep brain stimulation for Parkinson's disease dissociates mood and motor circuits: a functional MRI case study. Mov. Disord. 18, 1508–16.

Stein, E., Bar-Gad, I., 2013. β oscillations in the cortico-basal ganglia loop during parkinsonism. Exp. Neurol. 245, 52–9.

Stephan, K.E., Penny, W.D., Daunizeau, J., Moran, R.J., Friston, K.J., 2009a. Bayesian model selection for group studies. Neuroimage 46, 1004–17.

Stephan, K.E., Penny, W.D., Moran, R.J., den Ouden, H.E.M., Daunizeau, J., Friston, K.J., 2010. Ten simple rules for dynamic causal modeling. Neuroimage 49, 3099–109.

Stephan, K.E., Tittgemeyer, M., Knösche, T.R., Moran, R.J., Friston, K.J., 2009b. Tractography-based priors for dynamic causal models. Neuroimage 47, 1628–38.

Strafella, A.P., Dagher, A., Sadikot, A.F., 2003a. Cerebral blood flow changes induced by subthalamic stimulation in Parkinson's disease. Neurology 60, 1039–42.

Strafella, A.P., Sadikot, A.F., Dagher, A., 2003b. Subthalamic deep brain stimulation does not induce striatal dopamine release in Parkinson's disease. Neuroreport 14, 1287–1289.

Surmeier, D.J., Ding, J., Day, M., Wang, Z., Shen, W., 2007. D1 and D2 dopamine-receptor modulation of striatal glutamatergic signaling in striatal medium spiny neurons. Trends Neurosci. 30, 228–35.

Tanei, T., Kajita, Y., Nihashi, T., Kaneoke, Y., Takebayashi, S., Nakatsubo, D., Wakabayashi, T., 2009. Changes in regional blood flow induced by unilateral subthalamic nucleus stimulation in patients with Parkinson's disease. Neurol. Med. Chir. (Tokyo). 49, 507–13.

Tatsch, K., Poepperl, G., 2013. Nigrostriatal dopamine terminal imaging with dopamine transporter SPECT: an update. J. Nucl. Med. 54, 1331–8.

Taylor Webb, J., Ferguson, M.A., Nielsen, J.A., Anderson, J.S., 2013. BOLD granger causality reflects vascular anatomy. PLoS One 8.

Temperli, P., Ghika, J., Villemure, J.-G., Burkhard, P.R., Bogousslavsky, J., Vingerhoets, F.J.G., 2003. How do parkinsonian signs return after discontinuation of subthalamic DBS? Neurology 60, 78–81.

Terman, D., Rubin, J.E., Yew, A.C., Wilson, C.J., 2002. Activity patterns in a model for the subthalamopallidal network of the basal ganglia. J. Neurosci. 22, 2963–2976.

Thobois, S., Dominey, P., Fraix, V., Mertens, P., Guenot, M., Zimmer, L., Pollak, P., Benabid, A.-L., Broussolle, E., 2002. Effects of subthalamic nucleus stimulation on actual and imagined movement in Parkinson's disease : a PET study. J. Neurol. 249, 1689–98.

Thobois, S., Fraix, V., Savasta, M., Costes, N., Pollak, P., Mertens, P., Koudsie, a, Le Bars, D., Benabid, a L., Broussolle, E., 2003. Chronic subthalamic nucleus stimulation and striatal D2 dopamine receptors in Parkinson's disease--A [(11)C]-raclopride PET study. J. Neurol. 250, 1219–23.

Thobois, S., Hotton, G.R., Pinto, S., Wilkinson, L., Limousin-Dowsey, P., Brooks, D.J., Jahanshahi, M., 2007. STN stimulation alters pallidal-frontal coupling during response selection under competition. J. Cereb. Blood Flow Metab. 27, 1173–84.

Travis, K.A., Bockholt, H.J., Zardetto-Smith, A.M., Johnson, A.K., 1995. In vitro thermosensitivity of the midline thalamus. Brain Res. 686, 17–22.

Tronnier, V.M., Staubert, A., Hähnel, S., Sarem-Aslani, A., 1999. Magnetic resonance imaging with implanted neurostimulators: an in vitro and in vivo study. Neurosurgery 44, 118–25; discussion 125–6.

Tryba, A.K., Ramirez, J.-M., 2004. Hyperthermia modulates respiratory pacemaker bursting properties. J. Neurophysiol. 92, 2844–52.

Tuch, D.S., Wedeen, V.J., Dale, A.M., George, J.S., Belliveau, J.W., 2001. Conductivity tensor mapping of the human brain using diffusion tensor MRI. Proc. Natl. Acad. Sci. U. S. A. 98, 11697–11701.

Tziortzi, A.C., Haber, S.N., Searle, G.E., Tsoumpas, C., Long, C.J., Shotbolt, P., Douaud, G., Jbabdi, S., Behrens, T.E.J., Rabiner, E.A., Jenkinson, M., Gunn, R.N., 2014. Connectivity-based functional analysis of dopamine release in the striatum using diffusion-weighted MRI and positron emission tomography. Cereb. Cortex 24, 1165–77.

Uitti, R.J., Tsuboi, Y., Pooley, R.A., Putzke, J.D., Turk, M.F., Wszolek, Z.K., Witte, R.J., Wharen, R.E., 2002. Magnetic resonance imaging and deep brain stimulation. Neurosurgery 51, 1423–28; discussion 1428–31.

Urner, M., Schwarzkopf, D.S., Friston, K., Rees, G., 2013. Early visual learning induces long-lasting connectivity changes during rest in the human brain. Neuroimage 77, 148–156.

Vafaee, M.S., ØStergaard, K., Sunde, N., Gjedde, a, Dupont, E., Cumming, P., 2004. Focal changes of oxygen consumption in cerebral cortex of patients with Parkinson's disease during subthalamic stimulation. Neuroimage 22, 966–74.

Vedam-Mai, V., van Battum, E.Y., Kamphuis, W., Feenstra, M.G.P., Denys, D., Reynolds, B. a, Okun, M.S., Hol, E.M., 2012. Deep brain stimulation and the role of astrocytes. Mol. Psychiatry 17, 124–31, 115.

Volonté, M. a, Garibotto, V., Spagnolo, F., Panzacchi, a, Picozzi, P., Franzin, a, Giovannini, E., Leocani, L., Cursi, M., Comi, G., Perani, D., 2012. Changes in brain glucose metabolism in subthalamic nucleus deep brain stimulation for advanced Parkinson's disease. Parkinsonism Relat. Disord. 18, 770–4.

Vulliemoz, S., Carmichael, D.W., Rosenkranz, K., Diehl, B., Rodionov, R., Walker, M.C., McEvoy, A.W., Lemieux, L., 2011. Simultaneous intracranial EEG and fMRI of interictal epileptic discharges in humans. Neuroimage 54, 182–90.

Walker, R.H., Moore, C., Davies, G., Dirling, L.B., Koch, R.J., Meshul, C.K., 2012. Effects of subthalamic nucleus lesions and stimulation upon corticostriatal afferents in the 6-hydroxydopamine-lesioned rat. PLoS One 7, e32919.

Wang, J., Ma, Y., Huang, Z., Sun, B., Guan, Y., Zuo, C., 2010. Modulation of metabolic brain function by bilateral subthalamic nucleus stimulation in the treatment of Parkinson's disease. J. Neurol. 257, 72–8.

Weinberger, M., Mahant, N., Hutchison, W.D., Lozano, A.M., Moro, E., Hodaie, M., Lang, A.E., Dostrovsky, J.O., 2006. Beta oscillatory activity in the subthalamic nucleus and its relation to dopaminergic response in Parkinson's disease. J. Neurophysiol. 96, 3248–56.

Weiskopf, N., Hutton, C., Josephs, O., Deichmann, R., 2006. Optimal EPI parameters for reduction of susceptibility-induced BOLD sensitivity losses: A whole-brain analysis at 3??T and 1.5??T. Neuroimage 33, 493–504.

Welter, M.-L., Houeto, J.-L., Bonnet, A.-M., Bejjani, P.-B., Mesnage, V., Dormont, D., Navarro, S., Cornu, P., Agid, Y., Pidoux, B., 2004. Effects of high-frequency stimulation on subthalamic neuronal activity in parkinsonian patients. Arch. Neurol. 61, 89–96.

Welter, M.-L., Schüpbach, M., Czernecki, V., Karachi, C., Fernandez-Vidal, S., Golmard, J.-L., Serra, G., Navarro, S., Welaratne, A., Hartmann, A., Mesnage, V., Pineau, F., Cornu, P., Pidoux, B., Worbe, Y., Zikos, P., Grabli, D., Galanaud, D., Bonnet, A.-M., Belaid, H., Dormont, D., Vidailhet, M., Mallet, L., Houeto, J.-L., Bardinet, E., Yelnik, J., Agid, Y., 2014. Optimal target localization for subthalamic stimulation in patients with Parkinson disease. Neurology 82, 1352–61.

Whittier, J.R., Mettler, F.A., 1949. Studies on the subthalamus of the rhesus monkey; anatomy and fiber connections of the subthalamic nucleus of Luys. J. Comp. Neurol. 90, 281–317.

Wu, D.H., Lewin, J.S., Duerk, J.L., 1997. Inadequacy of motion correction algorithms in functional MRI: Role of susceptibility-induced artifacts. J. Magn. Reson. Imaging 7, 365–370.

Wu, T., Hallett, M., 2013. The cerebellum in Parkinson's disease. Brain 136, 696–709.

Wu, T., Wang, L., Chen, Y., Zhao, C., Li, K., Chan, P., 2009. Changes of functional connectivity of the motor network in the resting state in Parkinson's disease. Neurosci. Lett. 460, 6–10.

Wu, T., Wang, L., Hallett, M., Chen, Y., Li, K., Chan, P., 2011. Effective connectivity of brain networks during self-initiated movement in Parkinson's disease. Neuroimage 55, 204–15.

Wylie, G.R., Genova, H., DeLuca, J., Chiaravalloti, N., Sumowski, J.F., 2014. Functional magnetic resonance imaging movers and shakers: does subject-movement cause sampling bias? Hum. Brain Mapp. 35, 1–13.

Xu, W., Russo, G.S., Hashimoto, T., Zhang, J., Vitek, J.L., 2008. Subthalamic nucleus stimulation modulates thalamic neuronal activity. J. Neurosci. 28, 11916–24.

Yelnik, J., Bardinet, E., Dormont, D., Malandain, G., Ourselin, S., Tandé, D., Karachi, C., Ayache, N., Cornu, P., Agid, Y., 2007. A three-dimensional, histological and deformable atlas of the human basal ganglia. I. Atlas construction based on immunohistochemical and MRI data. Neuroimage 34, 618–38.

Yin, H.H., Knowlton, B.J., 2006. The role of the basal ganglia in habit formation. Nat. Rev. Neurosci. 7, 464–476.

Yu, H., Sternad, D., Corcos, D.M., Vaillancourt, D.E., 2007. Role of hyperactive cerebellum and motor cortex in Parkinson's disease. Neuroimage 35, 222–233.

Yugeta, A., Terao, Y., Fukuda, H., Hikosaka, O., Yokochi, F., Okiyama, R., Taniguchi, M., Takahashi, H., Hamada, I., Hanajima, R., Ugawa, Y., 2010. Effects of STN stimulation on the initiation and inhibition of saccade in Parkinson disease. Neurology 74, 743–8.

Zhao, Y., Sun, B., Li, D., Wang, Q., 2004. Effects of bilateral subthalamic nucleus stimulation on resting-state cerebral glucose metabolism in advanced Parkinson's disease. Chin. Med. J. (Engl). 117, 1304–8.

Zrinzo, L., Yoshida, F., Hariz, M.I., Thornton, J., Foltynie, T., Yousry, T. a, Limousin, P., 2011. Clinical safety of brain magnetic resonance imaging with implanted deep brain stimulation hardware: large case series and review of the literature. World Neurosurg. 76, 164–72.